Final Report for Research Project

LONG TERM BRIDGE MAINTENANCE MONITORING DEMONSTRATION ON A MOVABLE BRIDGE

A framework for structural health monitoring of movable bridges

F. Necati Catbas, Ph.D., P.E.
Associate Professor, Principal Investigator

Dr. Mustafa Gul, Dr. Ricardo Zaurin, H. Burak Gokce, Thomas Terrell, Taha Dumlupinar, Daniel Maier, Research Team

Civil, Environmental and Construction Engineering Department
University of Central Florida
4000 Central Florida Boulevard, PO Box 162450, Orlando, Florida 32816
Tel: 407-823-3743 and Fax: 407-823-3315

A Report on a Research Project Sponsored by
Florida Department of Transportation
Contract No.: BD-548-23
Marcus Ansley, P.E., Project Manager, FDOT

June 2010

DISCLAIMER

The opinions, findings, and conclusions expressed in this publication are those of the authors and not necessarily those of the State of Florida Department of Transportation.

UNIT CONVERSION TABLE

To convert from	To	Multiply by
inch	centimeter	2.54
square inch	square centimeter	6.4516
kip	kiloNewton (kN)	4.44747
kip/sq.in.	(ksi) kN/sq.m (kPa)	6,894.28
kip-foot	kN-meter	1.3556
btu	joule	1,055
btu/hr	watt	0.2931
degrees Fahrenheit – 32	degrees celcius	0.5555
lb/cu.in.	kgs./cu.m	27,680
btu/sq.ft./min.	watts/sq.in.	0.122

TECHNICAL REPORT DOCUMENTATION PAGE

1. Report No.	2. Government Accession No.	3. Recipient's Catalog No.
4. Title and Subtitle Long Term Bridge Maintenance Monitoring Demonstration on a Movable Bridge *A Framework for Structural Health Monitoring of Movable Bridges*		5. Report Date June 2010 6. Performing Organization Code University of Central Florida
7. Author(s) F. Necati Catbas, Mustafa Gul, Ricardo Zaurin, H. Burak Gokce, Thomas Terrell, Taha Dumlupinar, Daniel Maier		8. Performing Organization Report No.
9. Performing Organization Name and Address University of Central Florida Civil, Environmental and Construction Engineering Department Engineering Bldg Room 211 Orlando, FL 32816		10. Work Unit No. (TRAIS) 11. Contract or Grant No. BD548-23
12. Sponsoring Agency Name and Address Florida Department of Transportation Research Center, MS 30 605 Suwannee Street Tallahassee, FL 32310		13. Type of Report and Period Covered Final Report April 2007 – June 2010 14. Sponsoring Agency Code FDOT
15. Supplementary Notes		

16. Abstract

Movable bridges are unique structures with particular maintenance and repair needs. According to FDOT Engineers, the resulting rehabilitation and repairs cost much more than of a fixed bridge per square feet basis. The inspection and maintenance needs make movable bridges ideal candidates for demonstrating Structural Health Monitoring (SHM), or more specifically for this project, Bridge Health Monitoring for maintenance purposes. SHM can be defined as the measurement of a structure's operating and loading environment through use of a sensing system to track and evaluate incidents, anomalies, damage and deterioration.

The objective of this project was to design, develop and implement a structural health monitoring system on a representative movable bridge located in FDOT District 4 for condition assessment mainly for maintenance purposes, detecting anomalies and evaluation of the bridge performance. The selected movable bridge, which was a representative bridge in terms of geometry and age, was the West-bound span of two parallel spans on Sunrise Boulevard in Ft. Lauderdale. The researchers designed, developed and successfully implemented a comprehensive structural health monitoring system for the critical structural, mechanical and electrical components using approximately 200+ sensors along with effective analysis methods for condition evaluation and maintenance purposes.

Following the implementation of the monitoring system, the bridge was monitored continuously to establish operating conditions under vehicular traffic, environmental effects, and routine operation of the bridge for vehicular and marine traffic. Data was collected for a period of time to set baseline levels as well as to explore input-response relationships for the components of the bridge. In addition, certain deficiency (damage) scenarios in terms of mechanical and structural alterations were implemented in collaboration with FDOT Engineers in order to establish thresholds for conditions that require attention for repair and maintenance. These structural and mechanical deficiencies were successfully detected by the specialized data analysis methods that were developed for various sensor data and video images. In addition to the monitoring data, a truck load test was conducted to obtain data for the bridge structural responses, which were also employed to verify the finite element (FE) model of the bridge. This FE model was then used to determine the load rating of the bridge, and this is important for decision-making on the safe load carrying capacity of existing bridges. The load ratings showed that the main girders, floor beams and stringers of the bridge can safely carry load levels that are highly unlikely to happen on this bridge with three AASHTO design trucks side by side for creating the most critical load placement simultaneously.

The findings of this monitoring project have excellent potential for developing improved knowledge on performance and degradation, better design methods and performance predictive models, and advanced management decision making tools for maintenance and operation. It should be noted that the existing system has been developed in parallel to efforts of the Federal Highway Administration (FHWA) Advanced Exploratory Research Program, therefore, it has a potential to have a broader impact.

17. Key Word Structural Health Monitoring, movable bridges, maintenance, sensors, data acquisition, FEM, load test, load rating	18. Distribution Statement		
19. Security Classif. (of this report) Unclassified	20. Security Classif. (of this page) Unclassified	21. No. of Pages 186	22. Price NA

Form DOT F 1700.7 (8-72) Reproduction of completed page authorized

ACKNOWLEDGEMENTS

This project is made possible through the support of the Florida Department of Transportation (FDOT), and the guidance, suggestions and feedback of the FDOT central office and district engineers Messrs. Marcus Ansley, Angel Rodriguez and Richard Kerr were very instrumental in the development of this project with their continuous input. Mr. John Danielson provided critical input and support at different stages of the project. Mr. Duane Robertson from the FDOT Materials Laboratory at Gainesville provided legacy data for the Sunrise Bridge. The bridge tenders at the Sunrise Bridge were also very helpful.

Mr. Marcus Ansley provided invaluable feedback to develop a monitoring framework throughout the project, supported our technical and field test requests, and also gave his review for the report.

Special thanks are due Mr. Alberto Sardinas (from FDOT District 4) for sharing his experience on movable bridges, his interest and support throughout the project. His help and interest have been very critical for the execution of several tasks of this project.

The support from the Federal Highway Administration Advanced Exploratory Program has been invaluable for the completion of this project. For this, we are grateful to Drs. Hamid Ghasemi and Steve Chase for their support.

The authors would like to acknowledge the field support from Dr. Kirk Grimmelsman for his time and effort at the initial stages of the project. Prof. Dan Frangopol has contributed greatly in the area of reliability and uncertainty evaluation. Mr. Bill Bauer was also very instrumental for our field studies.

Last but not least is our team members, in no particular order: Ozerk Sazak, Don Harper, Dr. Yunus Dere, Dr Il-Bum Kwon, Daron Holt, MJ Levi, Dustin Forsyth and Nancy Holt. All of these individuals made important contributors to the development work presented in this report and they are greatly appreciated.

In memory of

Marcus H. “Marc” Ansley, P.E.

his contributions to Florida’s bridge engineering will always be remembered...

PREFACE

The report describes and presents the background, methodology, and results of a research project conducted by University of Central Florida researchers and funded by the Florida Department of Transportation.

EXECUTIVE SUMMARY

Background

The 98 movable bridges owned and operated by the Florida Department of Transportation (FDOT) represent one of the largest populations of movable bridges in the U.S. These complex structures utilize machinery to open a portion of the bridge, which allows for passage of waterborne traffic. Movable bridges are unique bridges with particular maintenance and repair needs. According to FDOT Engineers, the resulting rehabilitation and repairs can cost roughly 100 times more than of a fixed bridge per square feet basis. Condition assessment and decision making of bridges including the movable bridges currently rely on visual inspections and simplified analysis techniques despite some of the limitations. In addition, the effectiveness of the maintenance for different structural and mechanical components carried out by bridge contractors need to be objectively evaluated by the FDOT maintenance engineers. The inspection and maintenance needs make movable bridges ideal candidates for demonstrating Structural Health Monitoring (SHM), or more specifically for this project, Bridge Health Monitoring for maintenance purposes. SHM can be defined as the measurement of a structure's operating and loading environment through use of a sensing system to track and evaluate incidents, anomalies, damage and deterioration. SHM utilizes advanced technology to capture the critical inputs and responses of a structural system in order to understand the root causes of problems as well as to track responses to predict future behavior. A properly designed SHM system can improve bridge safety, enhance efficiency and enable effective and low cost maintenance through instrumentation, sensing, data collection and processing, use of analytical methods, and specialized algorithms for condition evaluation.

Objective and Scope

The objective of this project was to design, develop and implement a structural health monitoring system on a representative movable bridge located in FDOT District 4 for condition assessment, mainly for maintenance purposes, detecting anomalies and

evaluation of the bridge performance. The selected representative movable bridge was the West-bound span of two parallel spans on Sunrise Boulevard in Ft. Lauderdale, which was constructed in 1989. It has double bascule leaves with a total span length of 117 ft and a width of 53.5 ft, carrying three traffic lanes. Each leaf is 70-ft long and 40-ft wide. The bridge opens about 10 to 15 times a day. To the best of the authors' literature search, the monitoring design was one of the first and most comprehensive monitoring implementation, where critical structural, mechanical and electrical components were considered simultaneously with such variety of sensing technologies and evaluation methods. Following the implementation of the monitoring system, the bridge was monitored continuously to establish operating conditions under vehicular traffic, environmental effects, and routine operation of the bridge for vehicular and marine traffic. Data was collected for a period of time to set baseline levels, as well as to explore input-response relationships for the components of the bridge. In addition, certain deficiency (damage) scenarios in terms of mechanical and structural alterations were developed in collaboration with FDOT Engineers in order to establish thresholds for conditions that require attention for repair and maintenance. This comprehensive monitoring system provides an excellent opportunity to understand the optimum monitoring strategies and to prepare a refined monitoring framework in such a way that it could be implemented system-wide. It should also be mentioned that these technologies, methods and strategies that are demonstrated in this project are not limited to movable bridge monitoring.

Project Tasks

The project consisted of six main tasks. Prior to conducting these tasks, the researchers conducted an extensive literature search, made field visits and held numerous meetings to identify the specific structural, mechanical and electrical operations and associated issues and problems. Consequently, the first task of the project was to conduct a market survey appropriate for the specific sensing needs, data acquisition systems and other peripherals, purchase equipment and conduct investigative laboratory studies. The researchers, in collaboration with consultants from mechanical and electrical engineering disciplines, identified proven and promising sensors for field implementation. A series of

laboratory studies were conducted to develop and test hardware and software, such as sensor characteristics, DAQ (Data Acquisition) programs, cable connectors, and noise levels.

The second task of the project was to finalize the instrumentation design by evaluating the inspection and maintenance records, getting feedback from FDOT and project consultants as well as using the finite element model of the bridge. With the active participation of FDOT engineers and consultants, several field visits and meetings were conducted for the finalization of the instrumentation.

The third task of the project was the laboratory preparation and field installation of the finalized instrumentation. The installation of the sensors and associated pre-laboratory preparation was an intensive and important task that was completed by the research team. The research team also undertook the installation of the sensors, cabling system, cabinets and data acquisition systems at the bridge. The field work was carried out with assistance from the FDOT District 4 personnel in terms of coordination with the Coast Guard, providing management of traffic and snooper trucks.

The fourth task of the project was data collection, analysis and reporting. As part of the long-term monitoring, data was collected continuously on every single opening and during rush hours. It should be noted here that the monitoring system is still collecting data at the time of writing this report. The data collected from the monitoring system through routine monitoring, as well as from the damage scenarios, were employed for developing and demonstrating methodologies to identify mechanical and structural alterations. The researchers first developed methods and tools to efficiently analyze the data in order to have valuable information to be extracted in a timely manner and interpreted easily by engineers. Various algorithms were investigated by the researchers and then the most effective ones were employed to provide meaningful information about the condition of the structure. Excellent results were obtained using the methodologies developed for structural and mechanical monitoring of critical components of the movable bridge. This task also allows refining the extensive monitoring system for a practical and cost-effective monitoring design (e.g. fewer sensors than what was considered for this research project) for system-wide implementation to the movable bridge population.

The fifth task of the project was to use the monitoring data for finite element simulations. As part of this task, truck load tests were carried out at the bridge in collaboration with FDOT Structures Research Office and District 4. The data from truck load tests were used to determine the stress levels on various critical structural elements of the bridge. Acquired data from continuous monitoring and the truck load tests were used by the researchers to further verify the finite element model of the bridge. The field-calibrated model was then used for several simulations, such as calculating the operating and inventory load rating of the bridge. The load rating, under extreme and highly unlikely load configurations, established the safe load carrying capacity of the Sunrise Bridge, which is a representative bridge for the movable bridge population in terms of geometry, condition and age.

The sixth and final task of the project was documentation and submission of the final report.

Findings and Results

The researchers designed, developed and successfully implemented a comprehensive structural health monitoring system for the critical structural, mechanical and electrical components using approximately 200+ sensors. This instrumentation plan was developed based on the critical issues that are observed at movable bridges and that are particularly important for maintenance practices. Some of the critical conditions were simulated at the bridge in collaboration with the FDOT engineers. These problems and alterations (damage scenarios) are live load shoe shim removal, span lock shim removal, rack and pinion bolt and grease removal, open gear grease removal, and gearbox oil reduction. All of these conditions or damage scenarios are critical and need to be determined to mitigate worse problems and breakdowns that may require additional time and funds for repair and replacement. The operation of the bridge with these conditions was monitored and compared with the data collected from long term monitoring of the same components. The monitoring data were analyzed using novel data analysis techniques for effective condition evaluation.

As part of the data analysis methods, the researchers developed a cross correlation based method for structural assessment, which successfully detected the Live Load Shoe

and Span Lock damage scenarios. This method identifies changes efficiently, and it can also help to evaluate the effectiveness of the maintenance. Moreover, it helps to develop a refined instrumentation plan. As for the monitoring of the mechanical components, the researchers developed two specific data analysis methods for assessment. The first methodology uses computer vision edge detection techniques to identify if open gear lubrication is adequate. This method was demonstrated using data collected for approximately 3 months, which included proper lubrication data from a month, inadequate lubrication for a month, and one month after maintenance.

The gearbox and rack-pinion damage scenarios require a different approach using the vibration data from the opening-closing of the bridge. This second methodology uses Artificial Neural Networks (ANN) and employs descriptive statistics of opening data to identify damage scenarios corresponding to a change in gear box oil levels and grease removal from the rack and pinion. This method allows for effective decision making through reduction of analyzed data sets to "0 and 1" values, corresponding to healthy (undamaged) or unhealthy (damaged) condition. The damage scenarios that were implemented at the gearbox and rack-pinion were successfully identified using the approach developed and presented in the report.

The data collected from continuous monitoring, as well as the load test, were used to update a detailed FE model and to calculate the design load ratings of the bridge. The researchers compared the FE model with dynamic tests results for the global frequencies for FE model verification purposes. In addition, the opening and closing of the leaves were simulated and compared with the experimental counterparts. Data from operating traffic under transit RTA bus and structural data from the load test were employed to verify the FE model. This model was then used to determine the load rating of the bridge, which is important for decision-making on the safe load carrying capacity of existing bridges. The load rating of the main girders of the Sunrise Bridge, which is a representative bridge for the bascule bridge population in Florida, was evaluated using the field calibrated FE model. The inventory load rating for the fracture-critical main girders was calculated as 1.17, and the operating load rating was found to be 1.52 for flexure. The load ratings showed that the main girders of the bridge can safely carry load

levels that are highly unlikely to happen on this bridge with three AASHTO design trucks side by side for creating the most critical load placement simultaneously.

Studies for exploring the long term environmental effects on structural and mechanical components were conducted. Daily strain variation due to temperature were observed to be in the order of 20 microstrain during the summer season and 40 microstrain during the winter season. The strain cycle due to temperature was below truck induced strains under regular traffic and therefore, the observed temperature strains were within acceptable range. However, it is important to monitor over long term, especially for temperature effects on span locks when the bridge is to be opened. The total monitoring duration for this project was less a year after the design and implementation of the monitoring system where it would be desirable to establish at least a yearly cycle due to environmental effects. Moreover, long term monitoring can also provide important information about the effects of the temperature variations on the bridge balance and seating of different girders. For the mechanical components, preliminary long term monitoring studies showed that there was an interaction between the friction numbers and environmental effects. The effects of wind speed and barometric pressure on mechanical friction were also analyzed but these environmental effects were not as significant as temperature and humidity. The most critical environmental effect for mechanical friction was observed to be due to temperature changes; however, humidity was also observed to have some effect, but the correlation of friction to temperature was seen to be higher than the correlation to humidity. As for the bridge operation, change in mechanical friction may be an indicator of a need for maintenance. With better understanding the causes of the changes, maintenance can be done more effectively and timely.

Recommendations

Despite the successful implementation of an SHM system on a movable bridge and current findings, there is currently only limited long term data. It would be desirable to have a one to two year cycle after the completion of the installation of the monitoring system to accumulate sufficiently long term data to establish performance. In addition, the comprehensive monitoring system generated data that needs additional treatment and

evaluation. Given the presence of the current system, an excellent opportunity exists to conduct and refine analysis methods that can be employed for system-wide implementation. It is our sincere belief that the technologies, approaches and methods developed and successfully demonstrated in this project have the potential to be implemented for effective monitoring of bridges for improved inspections and condition-based maintenance. The findings in this monitoring project have also excellent potential for developing improved knowledge on performance and degradation, better design methods and performance predictive models, and advanced management decision making tools for maintenance and operation. Continued monitoring and collection of data from a sufficiently long cycle would allow for calibrating and fine tuning methods and investigation of cause-and-effect. Further exploration of sensor data and damage cases, improvement to programming and communication systems, and monitoring based fatigue evaluation can be carried out by taking advantage of the existing system. Further research will also allow for the design and implementation of a compact monitoring system for system-wide application. It should be noted that the existing system has been developed in parallel to efforts of the Federal Highway Administration (FHWA) Advanced Exploratory Research Program, therefore, it has a potential to have a broader impact.

TABLE OF CONTENTS

DISCLAIMER ii
UNIT CONVERSION TABLE iii
TECHNICAL REPORT DOCUMENTATION PAGE iv
ACKNOWLEDGEMENTS v
PREFACE vii
EXECUTIVE SUMMARY viii
TABLE OF CONTENTS xv
LIST OF FIGURES xix
1. INTRODUCTION 1
1.1. Background 1
1.2. Issues Related to Movable Bridges 1
1.3. Problem Statement 2
1.4. Structural Health Monitoring and Application to Movable Bridges for Maintenance 3
1.5. Project Objectives 4
1.6. Organization of the Report 5
2. DESIGN OF MONITORING SYSTEM 6
2.1. Design Considerations 6
2.1.1. Electrical Motors 6
2.1.2. Gear Boxes 7
2.1.3. Drive Shafts 8
2.1.4. Open Gears/Racks 9
2.1.1. Trunnions 10
2.1.2. Live Load Shoes 11
2.1.3. Span Locks 12
2.1.4. Main Girders, Floor Beams, and Stringers 14
2.2. Instrumentation Plan 16
2.2.1. System Configuration 16
2.2.2. Monitoring Strategy 16
2.2.2.1. Mechanical and Electrical Components 17
2.2.2.2. Structural Components 18
2.2.3. East Leaf Instrumentation Plan Summary 20
2.2.4. West Leaf Instrumentation Plan Summary 21
2.2.5. East Leaf Mechanical Instrumentation Plan Summary 22
2.2.6. West Leaf Mechanical Instrumentation Plan Summary 23
2.3. Sensors 24
2.4. Data Acquisition Systems (DAQs) 25
2.4.1. DAQ for High Speed Measurements 27
2.4.2. DAQ for Slow Speed Events 29
2.4.3. Weather Station DAQ 31
2.4.4. Video Camera System 32
2.4.5. Wireless Router 32
2.4.6. GPS Synchronization 33

2.5. Remote Access 33
2.6. Data Archiving 34
2.6.1. Programming the DAQs 34
3. FIELD WORK AND PREPARATIONS 36
3.1. Field Implementation and Challenges 36
3.2. Cabling, Connector, and Cabinet Design 37
3.3. Cabling 37
3.3.1. Design Considerations and Alternatives 37
3.3.2. Selected Product Specifications 38
3.3.3. Lab Preparation 39
3.3.4. Quality Control 39
3.4. Sensor-Cable Connection 39
3.4.1. Design Considerations and Alternatives 39
3.4.2. Selected Product Specifications 40
3.4.2.1. Lab Preparation 41
3.4.2.2. Quality Control 42
3.4.3. Cabinets 42
3.4.3.1. Side Cabinet Junction Boxes 43
3.4.3.2. Side Junction Box Interior Configuration 44
3.4.3.3. Lab Preparation 44
3.4.3.4. NI Terminal Block Lab Preparation 45
3.5. Lab Studies for Trouble Shooting 45
3.5.1. Overview 45
3.5.2. Testing of Monitoring Components 47
3.6. Sensor Installation 52
3.7. Cabinet Installation 54
3.8. Weather Station and Traffic Camera Installation 55
4. NUMERICAL STUDIES 56
4.1. FE Modeling of Sunrise Bridge 56
4.1.1. Mesh Sensitivity Analysis 57
4.1.2. Equivalent Deck Analysis 58
4.2. Finite Element Model Development of the Entire Structure 59
4.3. FE Model Verification 62
4.3.1. Global Verification with Dynamic Data 62
4.3.2. Local Verification 64
5. CONTROLLED STATIC AND MOVING TRUCK LOAD TEST 69
5.1. Objectives of the Load Tests 69
5.2. Test Design and Execution 69
5.2.1. Trucks and Testing Configurations 70
5.2.2. Execution of the Tests 73
5.3. Correlation with Finite Element Model 74
5.4. Load Rating 80
5.4.1. Overview 80
5.5. Types 81
5.6. General Equation 81
5.7. Load Rating with Finite Element Model 82

5.7.1. Dead and Live Load Modeling 83
5.7.2. Design-Load Rating 85
5.8. Load Rating with Experimental Data 87
5.9. Summary of the Results 89
6. DATA ANALYSIS APPROACHES FOR MAINTENANCE AND OPERATION 91
6.1. Introduction 91
6.2. Overview of Data from Different Components 92
6.2.1. Mechanical and Electrical 92
6.2.2. Structural 97
6.3. Data Quality Control 103
6.3.1. Visual Checks 103
6.3.2. Sensor Cross Correlation 105
6.3.3. Finite Element Model (FEM)-based Verification 108
6.4. Possible Methods for Data Analysis in this Study 108
6.4.1. Statistical Methods 108
6.4.2. Image and Video Analysis 109
6.4.3. Time Domain Analysis 110
6.4.4. Frequency Domain Analysis 111
6.4.5. Artificial Neural Networks 112
6.5. Application of Data Analysis Methods for Main Components 115
6.5.1. Mechanical and Electrical Components 115
6.5.2. Structural Components 116
7. FIELD TESTS WITH ARTIFICIALLY INDUCED DAMAGE AND LONG TERM MONITORING 121
7.1. Objectives of the Tests and Monitoring 121
7.2. Damage Scenarios 121
7.2.1. Structural Alterations and Simulated Damage 121
7.2.1.1. Live Load Shoe (LLS) Shim Removal 121
7.2.1.2. Span Lock (SL) Shims Removal 123
7.2.2. Mechanical Alterations and Simulated Damage 124
7.2.2.1. Gear Box Oil Removal 124
7.2.2.2. Open Gear Lubrication Removal 125
7.2.2.3. Rack and Pinnion Bolt Removal 126
7.2.2.4. Shaft Bolt Removal 127
7.3. Data Analysis to Detect Damage and Establish Triggers 128
7.3.1. Identification of Structural Alterations at Live Load Shoe and Span Lock 128
7.3.2. Review of Results for Structural Alterations at Live Load Shoe and Span Lock 136
7.3.3. Mechanical Alterations - Gearbox Oil and Open Gear Grease Removal . 137
7.3.3.1. Artificial Neural Network (ANN) Framework 138
7.3.3.2. Best Neural Network Model 140
7.3.4. Mechanical Alterations - Open Gear Lubrication Removal 141
7.3.5. Review of Results for Mechanical Alterations 144
7.4. Long Term Monitoring of Critical Components 145
7.4.1. Friction Number 145

7.5. Structural Response due to Environmental Traffic Induced Effects 150
7.5.1. Temperature Effects 151
7.5.2. Traffic Effects 152
8. SUMMARY, CONCLUSIONS AND RECOMMENDATIONS 156
8.1. Brief Summary 156
8.2. Conclusions and Findings 158
8.3. Recommendations 160
9. REFERENCES 163
10. APPENDIX 174
10.1. Sensor Characteristics Definitions 174
10.2. File Name Structure 174
10.3. Cabling Design Alternatives 175
10.4. Cable Segment Labels 176
10.5. Connector Design Alternatives 177
10.6. Connector Individual Components 178
10.7. Internal Components of Side Junction Boxes 178
10.8. Oil Sample Test 183
10.9. CR1000 Code 185

LIST OF FIGURES

Figure 1: Sunrise Bridge in Ft. Lauderdale, Florida....5
Figure 2: Some of the Mechanical/Electrical System of Representative Movable Bridge .6
Figure 3: Electrical Motor....7
Figure 4: Gear Box and Attached Drive Shaft....8
Figure 5: Open Gear and Rack and Pinion (Diagram- Patton 2006) 10
Figure 6: Trunnion....11
Figure 7: Live Load Shoe (sketch adapted from Christa McAuliffe Bridge construction plans) 12
Figure 8: Span Lock 13
Figure 9: Span Lock Components (sketch adapted from Christa McAuliffe Bridge construction plans) 13
Figure 10: Main Girders in Open Position....14
Figure 11: Some of the Monitored Bridge Components....16
Figure 12: Some of the Monitored Bridge Components (East Leaf) 20
Figure 13: Some of the Monitored Bridge Components (West Leaf)....21
Figure 14: Some of the Monitored Bridge Components (East Leaf Mechanical)....22
Figure 15: Some of the Monitored Bridge Components (West Leaf Mechanical) 23
Figure 16: Scheme Used for Data Transmission....26
Figure 17: Layout of Individual DAQ Components 27
Figure 18: SCXI 1001 Chassis 28
Figure 19: SCXI - 1520 Module (left), 1314 Terminal Block (center), 1531 Module (right)....28
Figure 20: SCXI - 1102 Module (left), 1303 Terminal block (right)....29
Figure 21: Power and Wiring Panel of CR1000 (http://www.campbellsci.com/cr1000)..30
Figure 22: Vibrating Wire Interface of CR1000 30
Figure 23: AM16/32B Multiplexer of CR1000....30
Figure 24: Location and Connections of CR1000 Data Acquisition in the Cabinet 31
Figure 25: D-Link WBR-2310 Wireless Router....32
Figure 26: Trimble Resolution T GPS Timing Receiver 33
Figure 27: Belden Cable 1079a and 1080a....38
Figure 28: Lab Prepared Wire Tips: The Cable After Cutting (Left), Cable After Preparing the Ends and Labeling (Right)....39
Figure 29: Harting Han Industrial Connector 40
Figure 30: Sensor Group Installation (Left) and Cable Connected Installation (Right) 41
Figure 31: Installed Connector Secure on the Bottom Flange of the Main Girder 41
Figure 32: Different Views of the Connector 42
Figure 33: Sensor Group Ready for Bridge Installation 42
Figure 34: East Leaf Cabinet 43
Figure 35: Interior View of Side Junction Box (Left) and Lab Prepared Junction Box Panel (Right)....44
Figure 36: Cable Entries to DIN Rail on Side Junction Box Panel....45
Figure 37: Lab Prepared NI Terminal Block and Completed NI Terminal Blocks Ready for Field Installation....45

Figure 38: Experiment Sensor Layout 46
Figure 39: Beam and Sensor Locations 46
Figure 40: Loading Plates (Left), Installed Strain Gages (Center) and Accelerometer (Right) 47
Figure 41: Acceleration Data from the Laboratory Test 47
Figure 42: Typical Tilt Data (Left) and Tiltmeter on the Beam (Right) 48
Figure 43: Ampmeter Data and Ampmeter 48
Figure 44: Different Views of the Connector 49
Figure 45: Acceleration Data from Connector Test (with Connector) 49
Figure 46: Strain Data from Connector Test (Raw Data for Evaluation) 50
Figure 47: Grey Cable (Left), Black Cable (Center), Sensor Wire (Right) 50
Figure 48: Constant Voltage Data 51
Figure 49: Outdoor Testing of Wireless Connection and GPS Synchronization 51
Figure 50: Sensor Installation Under the Bridge 52
Figure 51: Installed Sensors at the Girder, Specially Designed Connectors, Vibrating Wire and High-speed Strain Gages 53
Figure 52: Accelerometers at the Gear Box and Strain Rosettes at the Drive Shaft 53
Figure 53: Strain Gage Installation Steps Under the Bridge: Grinding, Welding and Painting 53
Figure 54: Close View of the Vibrating Wire and Dynamic Strain Gages Before and After Painting 54
Figure 55: Tiltmeter Installation at the Span Lock Room 54
Figure 56: Moving the Cabinets with Snooper Truck 54
Figure 57: Cabinet Location and Different Views 55
Figure 58: Installation of the Weather Station and Traffic Camera 55
Figure 59: Setting of the Weather Station Direction with a Compass 55
Figure 60: Sunrise Blvd. Bridge (Left) and Created FE Model (Right) 57
Figure 61: Coarse Mesh of the Main Girder 57
Figure 62: Dense Mesh of the Main Girder 58
Figure 63: Mesh Sensitivity Analysis for the Main Girder 58
Figure 64: Orthotropic Deck (Left) and Homogenous Steel Plate Deck Model (Right) 59
Figure 65: Construction Plans of Sunrise Blvd. Bridge 60
Figure 66: Main Girders, Floor Beams and Stringers of a Single Leaf 61
Figure 67: Final Sunrise Blvd. Bridge FE model 61
Figure 68: FE Model First Three Mode Shapes and Corresponding Frequencies 62
Figure 69: Ambient Acceleration Data from West South Main Girder of the Bridge 63
Figure 70: East South Main Girder Live Load Shoe Strain Gage Location 65
Figure 71: Opening and Closing Strains at ES3 (Experimental and Analytical) 65
Figure 72: East North Main Girder Live Load Shoe Strain Gage Location 66
Figure 73: Typical RTA Bus and Basic Properties 67
Figure 74: The Effect of Typical RTA Bus on EN3 (Experimental and Analytical) 68
Figure 75: Selected Load Testing Truck Load Configuration 70
Figure 76: Static Load Test: Lane 1 (Right Lane) Test Configuration 71
Figure 77: Crawl Test: Lane 1, 2, and 3 Testing Configurations 72
Figure 78: Dynamic Load Test: Lane 1, 2, and 3 Testing Configurations 73
Figure 79: Static Load Test Sample Data Set 74

Figure 80: Representative Diagram of FE Model Load Truck 74
Figure 81: FE Model and Experimental Strain Comparison of LC-6 on Right Lane 75
Figure 82: FE Model and Experimental Strain Comparison of LC-6 on Middle Lane 76
Figure 83: FE Model and Experimental Strain Comparison of LC-6 on Left Lane 76
Figure 84: FE Model and Experimental Strain Comparison of LC-7 on Right Lane 77
Figure 85: FE Model and Experimental Strain Comparison of LC-7 on Middle Lane 77
Figure 86: FE Model and Experimental Strain Comparison of LC-7 on Left Lane 78
Figure 87: FE Model and Experimental Strain Comparison of LC-8 on Right Lane 78
Figure 88: FE Model and Experimental Strain Comparison of LC-8 on Middle Lane 79
Figure 89: FE Model and Experimental Strain Comparison of LC-8 on Left Lane 79
Figure 90: Members and Section Locations Used for Load Rating 83
Figure 91: HL-93 Load Cases Applied to Bridge 84
Figure 92: Main Girder Locations A, B, and C 85
Figure 93: Mechanical Room 92
Figure 94: Electrical Motor and the Horizontal and Vertical Acccelerometers on the Drive Shaft Side (Left) and Sample Data from the Accelerometer (Right) 93
Figure 95: Motor Ampmeter (Left) and Sample Data from the Ampmeter (Right) 93
Figure 96: Gearbox and Accelerometer Installed (Left) and Sample Data from One of the Accelerometers (Right) 94
Figure 97: Gearbox Microphone (Left) and Sample Data from the Microphone (Right) .94
Figure 98: Rack and Pinnion and the Accelerometer on it (Left) Sample Data from the Accelerometer (Right) 95
Figure 99: Shaft and Rosette on it (Left) and Sample Data from the Rosette (Right) 95
Figure 100: Trunnion and Tiltmeter on it (Left) and Sample Data from the Tiltmeter (Right) 96
Figure 101: Span Lock and Pressure Gages on it (Left) and Sample Data from the Pressure Gage (Right) 96
Figure 102: Sample Data from East South Main Girder Accelerometers 97
Figure 103: Sample Data from East South Main Girder LLS Strain Rosettes 98
Figure 104: Sample Data from East North Main Girder LLS Strain Gages 98
Figure 105: Real Time Video Image Around t=70 Seconds 99
Figure 106: Sample Data from West South Main Girder Tip Strain Gages 99
Figure 107: Sample Data from West Main Girder Tip Tiltmeters 100
Figure 108: Sample Data from East South Middle Floor Beam 101
Figure 109: Sample Data from East North Middle Stringer 101
Figure 110: Sample Data from Wind Speed, Wind Direction, Humidity and Barometric Pressure 102
Figure 111: Sample Data from Vibrating Wire Strain and Temperature Readings 103
Figure 112: Example of a Non-working or “Dead” Sensor 104
Figure 113: Example of a Non-working Sensor Registering Noise 105
Figure 114: Example of a Non-working Sensor Drifting 105
Figure 115: West Leaf Middle Span Floor Beam Top-Bottom Strain Correlation 106
Figure 116: North West Middle Span Main Girder Top Sensor Raw and Filtered Data 107
Figure 117: Close View North West Middle Span Main Girder Top Sensor Filtered Data 108
Figure 118: The Components of a Monitoring Framework with Computer Vision 110

Figure 119: Summary of CMIF Method 112
Figure 120: Single Hidden Layer Feedforward Neural Networks 113
Figure 121: Daily Maximum and Minimum Strain for Each Data Set from Bottom Flange of East South Stringer 116
Figure 122: West South Main Girder Neighbor Location Scatter Plot 118
Figure 123: Symmetric Location Scatter Plot 118
Figure 124: Different Location Scatter Plot 119
Figure 125: Strain Comparison After RMS 119
Figure 126: Live Load Shoe (LLS) and the Shim Removal Operation by FDOT Contractors (sketch adapted from Christa McAuliffe Bridge construction plans) 122
Figure 127: LLS with Shims and Without Shims 122
Figure 128: Typical Span Lock (SL) 123
Figure 129: Lock Bar, Receiver and Hydraulic Unit (sketch adapted from Christa McAuliffe Bridge construction plans) 124
Figure 130: FDOT Contractors Removing Some of the Shims from the SL 124
Figure 131: Removal of the Oil from the Gearbox 125
Figure 132: Removal of Open Gear Grease 126
Figure 133: Rack and Pinnion Bolt Removal 127
Figure 134: Removal of the bolts 127
Figure 135: Strain Gage Locations on the Bridge 128
Figure 136: WN3 Top & Bottom Strain Correlations 129
Figure 137: EN2 Top & Bottom Strain Correlations 130
Figure 138: WS3 & WN3 Strain Correlations 130
Figure 139: WS3 & EN3 Strain Correlations 132
Figure 140: WS3 & ES3 Strain Correlations 132
Figure 141: WS1 & EN1 Strain Correlations 133
Figure 142: WN3 & EN3 Strain Correlations 134
Figure 143: WN3 & ES3 Strain Correlations 134
Figure 144: EN3 & ES3 Strain Correlations 135
Figure 145: WS1-F & WS2-F Strain Correlations 135
Figure 146: WS1-F & ES1-F Strain Correlations 136
Figure 147: Sensors on Gearbox and Rack and Pinion with Corresponding Sample Acceleration Data 138
Figure 148: Open Gear with Proper Lubrication and with Lack of Lubrication 142
Figure 149: Selecting the Area of Interest for Detection Purposes 142
Figure 150: Implementation of Edge Detection Techniques for Detection Grease for with and without Proper Lubrication 143
Figure 151: Monitoring and Tracking Lubrication Index (LI) Over Long Term 144
Figure 152: Strain Rosette on the Drive Shaft 146
Figure 153: West Leaf North Shaft SR2 Open/Closing Torque 10/22/2009 4:30PM 147
Figure 154: West Leaf South Shaft SR2 Open/Closing Torque 10/22/2009 4:30PM 147
Figure 155: West Leaf FDOT Archived Open/Closing Torque 10/01/2008 148
Figure 156 – Friction Number Trend from 10/15/09 to 11/15/09 149
Figure 157 – West Leaf Open/Closing Operation Corresponding Temperature Trend 10/15/09 to 11/15/09 149
Figure 158: Strain–Temperature Relation for Tip Location 151

Figure 159: Strain–Temperature Relation for Main Girder Location 152
Figure 160: Weekly Strain Data from Live Load Shoe Location 153
Figure 161: Three Months Daily Maximum Strain Histogram 154
Figure 162: Extreme Values Histogram with Fitted Distribution 155
Figure 163: Cable Alternatives, a) Individual 1-2 Pair Shielded, b) Multiconductor Twisted Pair, c) Multiconductor Twisted Pair Individually Shielded..... 176
Figure 164: Military Style Connector (Not Selected for Use)..... 177
Figure 165: Strain Relief for Main Cables..... 179

1. INTRODUCTION

1.1. Background

Bridges are one of the most critical components of transportation systems, and therefore, ensuring their continuous operation is of utmost importance for safe and efficient transportation. Long term performance of bridges depends on many parameters, including the operational and environmental effects and the effectiveness of the maintenance operations. Periodic visual bridge inspections are required and collected by each State Department of Transportation. This inspection data is then reported to the Federal Highway Administration (FHWA) through the National Bridge Inventory Standards (NBIS). Visual inspection has been the traditional inspection method, yet it has some inherent drawbacks. A study conducted by the Federal Highway Administration's NDE Center on the accuracy of visual inspection of short-to-medium span bridges concluded that at least 56% of the bridges given an average condition rating were done incorrectly (Turner-Fairbank Research Center, 2005). In addition to visual inspection, a complementary approach using currently cost-effective and maturing monitoring technologies has been discussed in many forums, such as annual Transportation Research Board (TRB) meetings. While these monitoring technologies have still been explored, it has been accepted that a thorough understanding of the performance and behavior of a bridge requires extensive analysis, modeling and test results. Consequently, Structural Health Monitoring (SHM) applications have gained a considerable attention as an objective methodology to evaluate the condition and performance of the structures. In Florida, movable bridges were deemed to be ideal candidates for the implementation and demonstration of monitoring technologies in order to evaluate the performance of structural, mechanical and electrical components of movable bridges for proactive assessment and maintenance purposes. Movable bridges have unique design, operation and maintenance considerations as summarized in the following section.

1.2. Issues Related to Movable Bridges

The Florida Department of Transportation owns and operates one of the largest number of movable bridges in the U.S. The 98 movable bridges in Florida are complex structures utilizing machinery to move a portion of the structure back and forth between two alternate positions in a controlled manner, allowing for the passage of both land and

waterborne traffic. Movable bridges are commonly used over waterways, especially in flat terrain regions. The main advantage of this type of structure is that the bridge can be constructed with little vertical clearance, avoiding the expense of high piers and long approaches. Mechanical and electrical components fuse with the structural elements, creating a very unique type of structure, often referred to as kinetic architecture. The majority of the movable bridges in Florida are of the bascule type, having interior spans, called "leaves", that rotate upward and away from the centerline of the waterway providing clear passage. Although the moving condition of a movable bridge brings a lot of advantages, it is also the main reason for significant drawbacks and problems associated with the operation and performance (Aktan et al, 2001).

Movable bridge rehabilitation and maintenance costs are considerably higher than that of a fixed bridge. Deterioration is a concern since they are located over waterways, and often close to the coast, which constitute conditions suitable for corrosion, causing section losses. Deterioration and damage is also observed due to moving parts, friction, wear and tear of the structural and mechanical components. Fatigue can be a problem due to the reversal or the fluctuation of stresses as the spans open and close. If there are breakdowns, these cause problems for both land and maritime traffic. Maintenance costs associated with the operation system and mechanical parts require special expertise, and may cause extensive repair work. Finally, difficulty in repair works is an issue for movable bridges. A malfunction of any component can cause an unexpected failure of bridge operation. Electrical and mechanical problems may require experts and may be difficult and time consuming to fix.

1.3. Problem Statement

A Bridge Maintenance Monitoring System (BMMS) was developed and demonstrated for a District 4 movable bridge. Routine maintenance, repair and operation are particular challenges for movable bridges because of their unique design and operation. The maintenance costs are often high. The goal of the project was to demonstrate the application of monitoring on an actual movable bridge in Florida, providing a complete framework for maintenance evaluation. The BMMS will generate flags and warnings to indicate a worsening condition (e.g. gear box lubrication deterioration) with respect to pre-established conditions and thresholds. Methods and

procedures to monitor structural, electrical and mechanical components were developed as part of the project. A future use of such a monitoring system is that bridge owners and maintenance contractors can connect into the BMMS for real-time asset management. Bridge owners may use flags and warnings as a mechanism to monitor/assess maintenance performance. The data may be used by the contractors in scheduling preventive maintenance to maximize the service life of the equipment and the structure. In addition, the root causes of the structural and mechanical problems can be determined, and future designs can be improved using the information generated from BMMS. The technology for monitoring such structures is called Structural Health Monitoring (SHM) and a brief review is provided in the following section.

1.4. Structural Health Monitoring and Application to Movable Bridges for Maintenance

Structural Health Monitoring (SHM) is conducted for condition assessment of different types of structures including aerospace, mechanical and civil structures. Though the earliest SHM applications were in aerospace engineering, mechanical and civil applications have gained momentum in the last few decades.

Different definitions of SHM can be found in the engineering literature. For example, Aktan et al. (2000) defined SHM as follows; “SHM is the measurement of the operating and loading environment and the critical responses of a structure to track and evaluate the symptoms of operational incidents, anomalies, and/or deterioration or damage indicators that may affect operation, serviceability, or safety and reliability.” Another definition was given by Farrar et al. (1999) and Sohn et al. (2001) where the researchers stated that “SHM is a statistical pattern recognition process to implement a damage detection strategy for aerospace, civil and mechanical engineering infrastructure and it is composed of four portions: (1) operational evaluation, (2) data acquisition, fusion and cleansing, (3) feature extraction, and (4) statistical model development.”

The starting point of an SHM system may be considered as the sensing and data acquisition step. The properties of the data acquisition system and the sensor network are rather application specific. The number and types of the sensors, as well as the data processing methods, have a direct effect on the accuracy and the reliability of the monitoring process. The data collected during an SHM process generally includes the

response of the structure at different locations and information about the environmental and operational conditions. The measurements related to the structural response may include strain, displacement, acceleration, rotation and others. On the other hand, data related to environmental and operational conditions may include temperature, humidity and wind speed and direction measurements.

With the recent technological advances and reduced cost of sensing technologies, large amounts of data can be acquired easily with different types of sensors. As a result, data analysis methodologies are to be developed for effectively extracting information from large amounts of data in a timely fashion. In addition to the analysis of experimental data, interpretation might require modeling and simulation where the analytical and numerical results may be combined or compared with experimental findings. Finally, information extracted from the data is used for decision-making about the safety, reliability, maintenance, operation and future performance of the structure.

1.5. Project Objectives

The main objectives of the project presented in this report are to design, develop and implement a monitoring system on an FDOT movable bridge for evaluation of maintenance practices. After the implementation of the monitoring system, data will be collected for a sufficiently long time period to set a threshold for remedial actions. Certain deficiency (damage) scenarios can be developed in collaboration with FDOT engineers in order to set thresholds as well. Ultimately, the monitoring system will be refined and the data will be analyzed in such a way that it could be implemented system-wide.

As a result, the monitoring system is designed and implemented on a representative bridge in District 4 in Ft. Lauderdale, Florida. The selected representative movable span is the West-bound span of two parallel spans on Sunrise Boulevard in Ft. Lauderdale. This span was constructed in 1989. It has double bascule leaves with a total span length of 117 ft and a width of 53.5 ft, carrying three traffic lanes. Each leaf is 70-ft long and 40-ft wide. The bridge can be opened every 30 minutes when requested. Depending on the boat traffic, the bridge opens usually about 10 to 15 times a day. Details about the Sunrise Bridge will be given in later sections.

Figure 1: Sunrise Bridge in Ft. Lauderdale, Florida

1.6. Organization of the Report

The organization of the report is as follows.

In *Chapter 2*, the issues related to movable bridges are discussed along with the proposed monitoring methods and applications. Design of the monitoring system and instrumentation plan are also discussed in this chapter.

In *Chapter 3*, different components of the monitoring system such as the data acquisition system, sensors and cabling are detailed.

In *Chapter 4*, the numerical studies conducted are discussed, including development and verification of the FE model.

In *Chapter 5*, the executed truck load tests are discussed, and load rating calculations are shown for the Sunrise Boulevard Bridge.

In *Chapter 6*, sample data from each sensor is shown and data analysis approaches are described.

In *Chapter 7*, the artificially induced damage scenarios are described, application of new methods are shown, and preliminary long term monitoring data results are presented.

In *Chapter 8*, a summary, conclusions and recommendations are discussed.

2. DESIGN OF MONITORING SYSTEM

2.1. Design Considerations

For static structures, monitoring of structural components is usually the only concern for maintenance, safety and operation; however, for movable bridges, the monitoring of mechanical and electrical components is equally important. Bridge opening and closing operations induce additional stresses on the structural and mechanical components of movable bridges due to mechanical and dynamic forces. Therefore, a properly designed monitoring system for a movable bridge should consider all structural, mechanical, and electrical components of the particular bridge. For this reason, the most common types of machinery and related problems were investigated and considered, in order to provide a monitoring solution to detect these problems, track their development, and plan for corrective action before failure. These and other site specific issues were collected from a series of kick-off group meetings and communications with bridge engineers, FDOT officials and consultants. In this section, the specific electrical, mechanical and structural components and elements identified as critical components will be discussed. Selected monitoring devices will be described, followed by further details of the final instrumentation. Figure 2 provides an overview of some of the mechanical and electrical components for each leaf of the bridge.

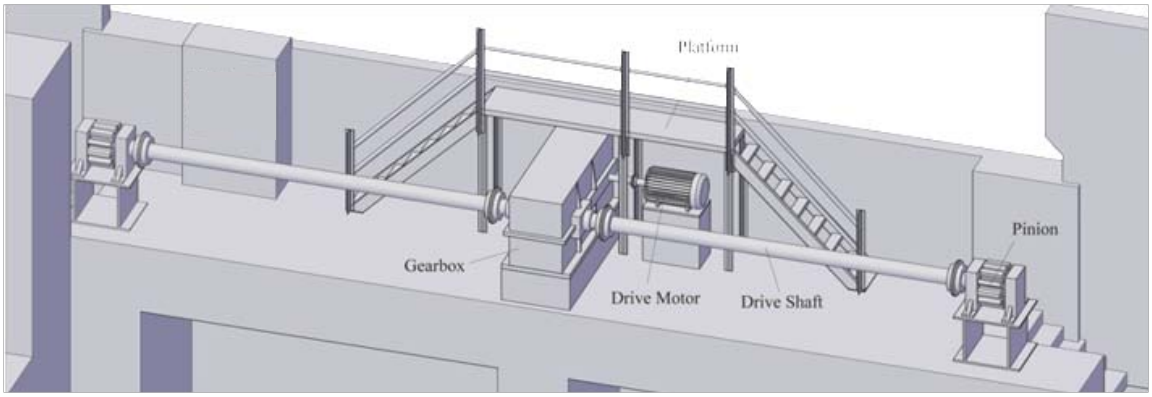

Figure 2: Some of the Mechanical/Electrical System of Representative Movable Bridge

2.1.1. Electrical Motors

The electrical motors (Figure 3) generate the torque required for the opening and closing of the bridge. Some of the indicators of improper function are high amperage,

high temperature, vibration and high revolution speed. Therefore, it was decided that the monitoring system would include ampmeters to measure the amperage levels for each one of the electric motor phases, accelerometers to measure the vibration on the motor during opening and closings, and infrared temperature sensors to check the temperature of the electrical motor.

Figure 3: Electrical Motor

2.1.2. Gear Boxes

The gear boxes contain the assembly that transmits the torque generated by the motor to the shafts (Figure 4). When the gear boxes experience deterioration, or lack of lubrication, some change in the vibration and sound characteristics during operation should be noted. Abnormal vibration is an indicator of wear in the gears. Oil viscosity is also an important parameter for proper functioning of the gear box. Considering these issues, the monitoring system included accelerometers to measure the vibration on the gear box during openings and closings. Furthermore, microphones were also included within the gear box vicinity to determine the acoustic print corresponding to normal/abnormal lubrication.

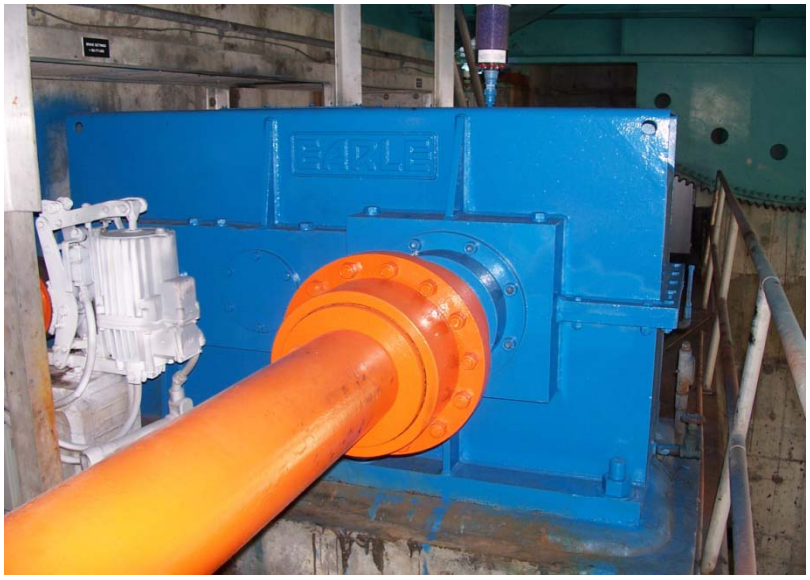

Figure 4: Gear Box and Attached Drive Shaft

2.1.3. Drive Shafts

The shaft is the connecting element between the motor and the pinion, and it is responsible for transmitting the required power for opening and closing operations. Its condition is directly related to the structural integrity and functioning of the movable bridge. Any unanticipated distress on the shaft will indicate either degradation on the shaft, motor, gears, rack, or overloading of the bridge during operation.

The drive shafts can be monitored for the total torque, friction of the system, as well as for the center of weight, by means of a balance test, which is a common method for detecting changes in the opening/closing operation. During the test, torsional strain measurements are made using strain rosettes mounted on the shaft. The torque on the drive shafts can be determined from these torsional strain measurements using the procedure given by Malvern et al. (1982) which is discussed in detail in Chapter-7. The measured torque is generally assumed to be the resultant of the torques due to the unbalanced leaf load and friction in the mechanical system. During opening and closing, even a perfectly tuned and maintained leaf is expected to show some friction, however, disruption to alignment of leaves or any part of the mechanical system would increase the friction. The balance test provides critical information on both the balance of the leaf and

the friction present in the mechanical system. Based on this information, recommendations can be made concerning balancing and/or lubrication of components.

The balance test does not require any intrusion or alteration. It is currently being performed for all movable bridges in Florida, with similar measurements performed successfully in the past. The current procedure, however, is conducted only intermittently and requires a team from the State Materials Office to drive to the bridge, instrument the bridge one leaf per day, collect data, calculate the friction number, and submit a recommendation.

To monitor the shafts continuously, the monitoring system included strain rosettes at both shafts on each leaf. The instrumentation of both shafts enables a comparison of data, providing better motor performance and serving as an indicator of shaft condition/deterioration. The implemented monitoring system is capable of performing a balance test for each opening/closing operation. This continuous monitoring offers numerous advantages. Tracking of the torque and friction number with time can help to apply corrective/preventive maintenance on time, establish power/imbalance relationships and prevent failures of motor, shaft, gear box and trunnion. Savings in technical labor and repairs are anticipated benefits of the system.

2.1.4. Open Gears/Racks

The open gears are the main gears, which are part of the leaf main girder and receive the torque from the rack and pinion assembly (Figure 5). Excessive strain, out-of-plane rotation and misalignment are common problems for open gears. Another concern is loading sequence problems, which mean that the drive shafts begin rotation in delayed sequence. This has an adverse effect on the condition of the open gears, usually by causing impact loading. Routine maintenance is required on the gear teeth. Unless they are kept lubricated at all times, wear and corrosion due to grinding of the rack and the pinion will occur.

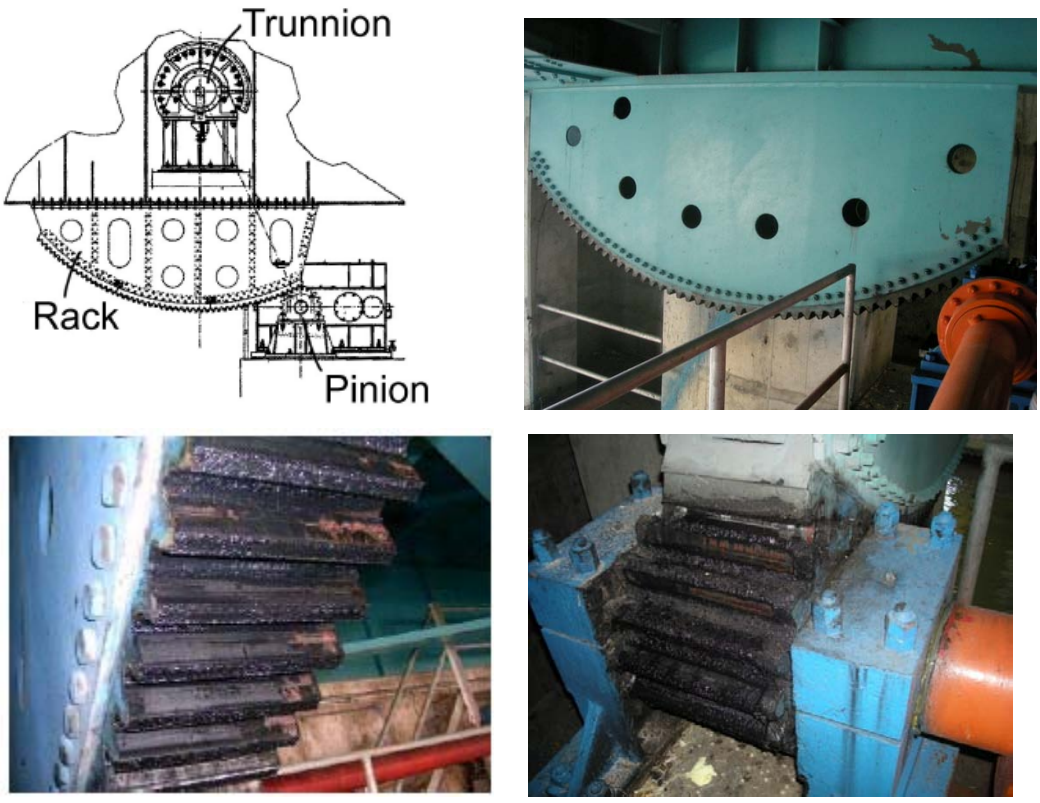

Figure 5: Open Gear and Rack and Pinion (Diagram- Patton 2006)

To monitor the condition and maintenance needs of the open gears and rack and pinions, accelerometers installed to the Rack and Pinion base to check the vibrations were included in the instrumentation plan. A firewire camera was also decided to be installed facing the open gear for employment of computer vision algorithms to detect the corroded and/or non lubricated areas, as discussed in later parts of this text.

2.1.1. Trunnions

Trunnions (Figure 6) are the pivot points of the leaves. The alignment of the trunnion is critical to prevent premature wear of the trunnion bearings and to reduce out-of-plane web distortions that introduce fatigue damage. Misalignment in the trunnion axis can cause additional load on the trunnion-hub assembly and distress on the main girder plate, causing distortions, and eventually web buckling. Trunnion misalignment is also a major cause of wobble that can result in mismatch of the leaf tips, disturbing regular operation (Malvern et al. 1982; Besterfield et al. 2001; Koglin 2003; Patton 2006).

Figure 6: Trunnion

Based on the meetings with FDOT maintenance engineers, it was concluded that trunnion lubrication is a major factor for opening/closing operation friction previously discussed. For these reasons, the instrumentation plan contains strain rosette gages to calculate the shear values in the trunnion area, and microphones are included to catch any unexpected acoustic data. Tiltmeters were also included in the design of the instrumentation to measure the opening and closing angles, which are necessary measurements of the balance test.

2.1.2. Live Load Shoes

Live load shoes (LLS), shown in Figure 7, are support blocks that the girders rest on while in the closed position. The live load shoes are located forward of the trunnions and hold the main girder up. Cracking and wear are rarely seen on the live load shoe, but operational problems, such as a loss of contact, are of the major concern. If misaligned or improperly balanced, the bridge may not fully sit on the live load shoe. In that case, the dead load and traffic load are transferred to the gears and shafts, which cause damage on mechanical assemblies. Small gaps also lead to the girders pounding on the live load shoes, which results in further misalignment, additional stresses, fatigue damage and excessive wear.

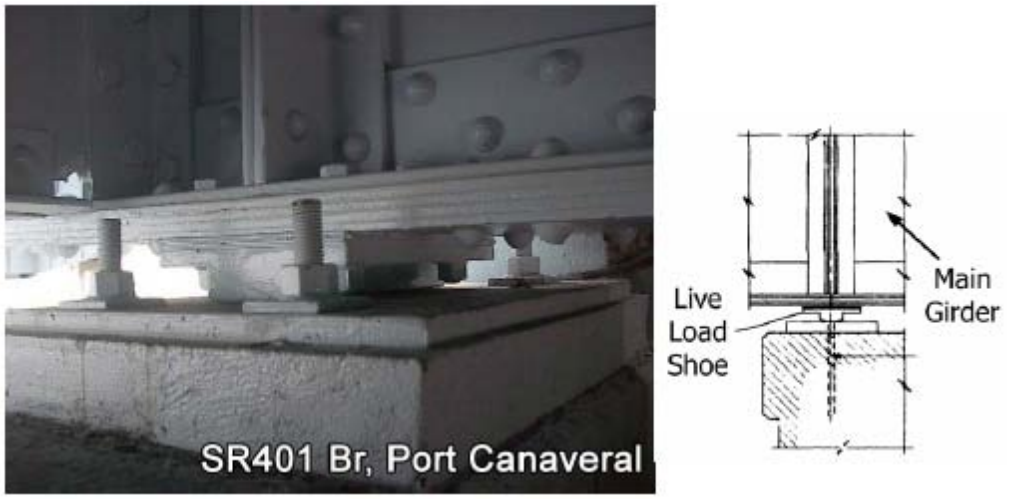

Figure 7: Live Load Shoe (sketch adapted from Christa McAuliffe Bridge construction plans)

Therefore, it was decided that strain rosette gages would be installed at the LLS area to record the critical shear values in the web of the main girder adjacent to the live load shoe. Instrumentation of the LLS area also included accelerometers for measurement of vibrations and to detect impact loading due to pounding.

2.1.3. Span Locks

Span locks tie the tip ends of the two cantilevered bascule leaves together and force the leaves to deflect equally and prevent a discontinuity in the deck as traffic crosses the span. The span locks consist of a rectangular lock bar supported by a pair of guides on one leaf that engages a single receiver on the opposite leaf. During operation, the lock bar slides across bronze shoes mounted in the rectangular guide and receiver housings. Lock bars are driven or retracted directly using a hydraulic linear actuator.

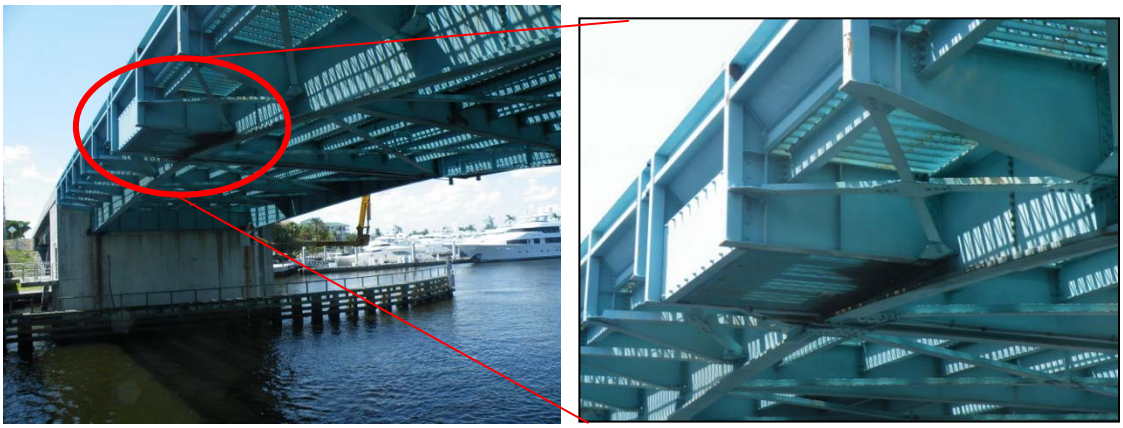

Figure 8: Span Lock

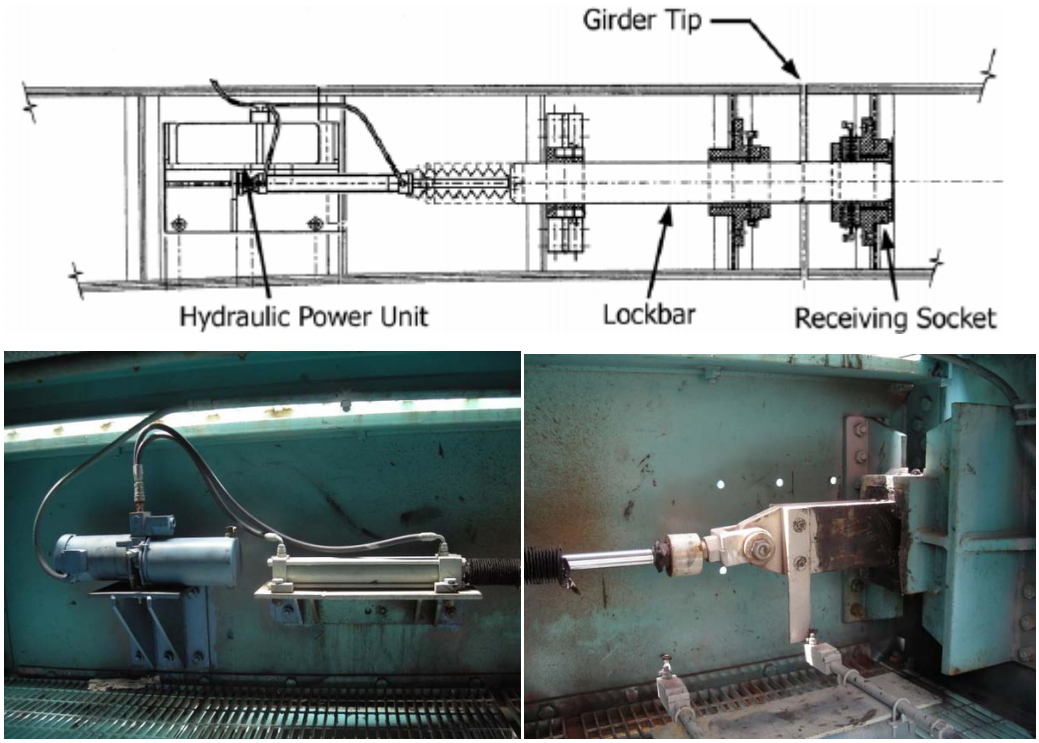

Figure 9: Span Lock Components (sketch adapted from Christa McAuliffe Bridge construction plans)

Span locks are one of the members that fail the most. Deterioration or incorrect operation can cause failure, which disrupts function of the bridge. Based on the discussions with bridge engineers, it was decided to install two pressure gages at each span lock to measure the hydraulic pressure of the span lock to detect any leak or other

anomalies with the pressure applied to span locks. Strain rosette gages were also included in the instrumentation of the span lock to check the excessive stress on the lock bar receiver. Finally, tiltmeters were installed to check the alignment of both leaves.

2.1.4. Main Girders, Floor Beams, and Stringers

Main girders and floor beams form the main frame of the spans. They are made from both rolled and built-up sections with welded plates. Corrosion is a main concern on the bridge girders, floor beams, and stringers, especially on exposed surfaces. Corrosion leads to section loss and reduced capacity. Any misalignment, bending, or deformation can cause increased strain on the structure. Deformation or thermal effects can cause misalignment of the girders, leading to operation malfunction. The selected sensor layout provides the distribution of stresses on the girders and is expected to provide information regarding damage and deterioration for preventive maintenance purposes.

Figure 10: Main Girders in Open Position

Bascule bridges are slender and lightweight, and are significantly affected by strong wind forces, especially when they are open. In addition to wind, ambient temperature and structural member temperatures need to be monitored. Past studies have shown that

temperature differentials can cause considerably higher stresses than stresses induced by vehicular traffic (Catbas and Aktan 2002). Therefore, the instrumentation plan consisted of a weather station to measure wind speed, wind direction, temperature, humidity, and rain quantity, duration and intensity. Wind monitoring can be used for determining the input load on the structure caused by air currents. Measured wind speed and direction can also be useful during hurricane-strength winds, indicating excessive force on the girders.

After several discussions and careful investigations, it was decided that the instrumentation plan of the main girders would include tiltmeters, accelerometers, dynamic strain gages, vibrating wire strain gages, and strain rosettes at various locations. The tiltmeters provide information about the angle of rotation at the tip of the span. The tiltmeter readings serve two functions: checking the leveling between girders on both sides for alignment during opening/closing and ensuring that the tips are in correct position for the locking maneuver. Accelerometers register the vibrations caused by environmental effects and vehicular traffic. Analysis of the vibration data might also indicate if there is change in structural system such as due to imbalance or due to span lock failure.

Investigations of the finite element model (Chapter-4) for the bridge revealed that connection between the trunnion and girder is a critical area where stress concentrations occur. This area was selected to be monitored because its damage can result in complete malfunction and require extensive repair. Strain rosettes on the center of the web panel were included in the monitoring system to measure shear stresses. Dynamic and vibrating wire strain gages were also decided to be installed on the top and bottom flanges at separate critical locations to measure stresses caused by bending. The dynamic (high speed) strain gages measure traffic induced strain and the vibrating wire strain gages collect slow speed temperature and strain data due to temperature induced stresses.

The behavior of select floor beams and stringers was monitored with dynamic strain gages and vibrating wire strain gages, which were installed on the top and bottom flanges. Finally, a video camera was included in the monitoring system as a complementary element to collect and correlate vehicular traffic data with other sensor readings and to inform bridge owners about accidents and suspicious activities.

2.2. Instrumentation Plan

2.2.1. System Configuration

After considering the issues related to movable bridges and several meetings with FDOT bridge engineers, maintenance engineers and consultants, the instrumentation plan was developed to monitor the most critical electrical, mechanical, and structural components. The final instrumentation plan consists of an array of 160 sensors, which add up to 200+ channels. The monitored structural components include main girders, floor beams, stringers, and live load shoes. As for the mechanical and electrical components, the electrical motor, gear box, shafts, open gear, rack and pinion and trunnions are monitored with various sensors. It should be mentioned that the instrumentation plan for system-wide applications is expected to be reduced significantly to an optimum level based on the findings of this current research. In addition, this study explores the performance of different sensors and their signals such as pressure or images for detecting anomalies and sudden changes in signal characteristics..

Figure 11: Some of the Monitored Bridge Components

2.2.2. Monitoring Strategy

A summary of the individual monitored components and associated installed sensors is provided in the following sections. This section is organized to provide a quick reference for type and location of the sensors, along with the purpose of the application. At the time of this writing, all sensors and hardware are still installed and data collection

continues. Therefore, present tense form will be used when describing the location of sensors, data collection, and operation of the SHM system.

2.2.2.1. Mechanical and Electrical Components

Electrical Motors

- Ampmeters were installed to measure the amperage values for each one of the electric motor phases.
- Accelerometers were installed to measure the vibration on the motor during opening and closings.
- IR Temperature sensors were installed to check the temperature of the motor during opening and closing.

Gear Boxes

- Accelerometers were installed to check and track the vibration on the gear box during openings and closings.
- Microphones were attached within gear box vicinity to determine the acoustic print corresponding to normal/abnormal lubrication.

Shafts

- Strain rosette gages were installed on the shafts to determine the opening and closing torque.

Rack and Pinion

- Accelerometers were also installed to the Rack and Pinion base to check the vibrations.

Open Gears

- Fire wire camera was installed to process the images to find the corroded and/or non lubricated areas.

Trunnions

- Tiltmeters were installed to measure the opening closing angles.
- Microphones were installed to catch the unexpected acoustic data.
- Strain rosette gages were installed to calculate the shear values in the trunnion area.

Live Load Shoe

- Strain rosette gages were installed to record the critical shear values.
- Accelerometers were installed for the vibrations in the live load shoe areas.

Span Lock Area

- Pressure gages were installed to measure the hydraulic pressure of the span lock.
- Strain rosette gages were installed to check the excessive stress on the lock bar receiver.
- Tiltmeters were installed to check the alignment of both leaves.

2.2.2.2. Structural Components

Main Girders

- Dynamic strain gages were installed; one (1) on the top and one (1) on the bottom flanges, at separate critical locations to measure the traffic induced strain.
- Vibrating wire strain gages (VWSG) installed the same as the dynamic strain gages; one (1) on the top and one (1) on the bottom flanges, at separate critical locations to collect slow speed temperature and strain data continuously.
- Strain rosettes were installed at the center of the web to record critical shear values at the LLS area
- Accelerometers were installed to measure vertical (twelve sensors) and horizontal (four sensors) acceleration.
- Tilt meters were installed at the tip of each main girder to measure the angle of inclination during opening-closing operation.

Floor Beams

- Dynamic strain gages were installed; one (1) on the top and one (1) on the bottom flanges, at separate critical locations to measure the traffic induced strain.
- Vibrating wire strain gages (VWSG) installed the same as the dynamic strain gages; one (1) on the top and one (1) on the bottom flanges, at separate critical locations to collect slow speed temperature and strain data continuously.

Stringers

- Dynamic strain gages were installed; one (1) on the top and one (1) on the bottom flanges, at separate critical locations to measure the traffic induced strain.
- Vibrating wire strain gages (VWSG) were installed at the same locations as the dynamic strain gages; one (1) on the top and one (1) on the bottom flanges, at separate critical locations to collect slow speed temperature and strain data continuously.

Graphical representations of the instrumentation plan are also provided in the following sections.

2.2.3. East Leaf Instrumentation Plan Summary

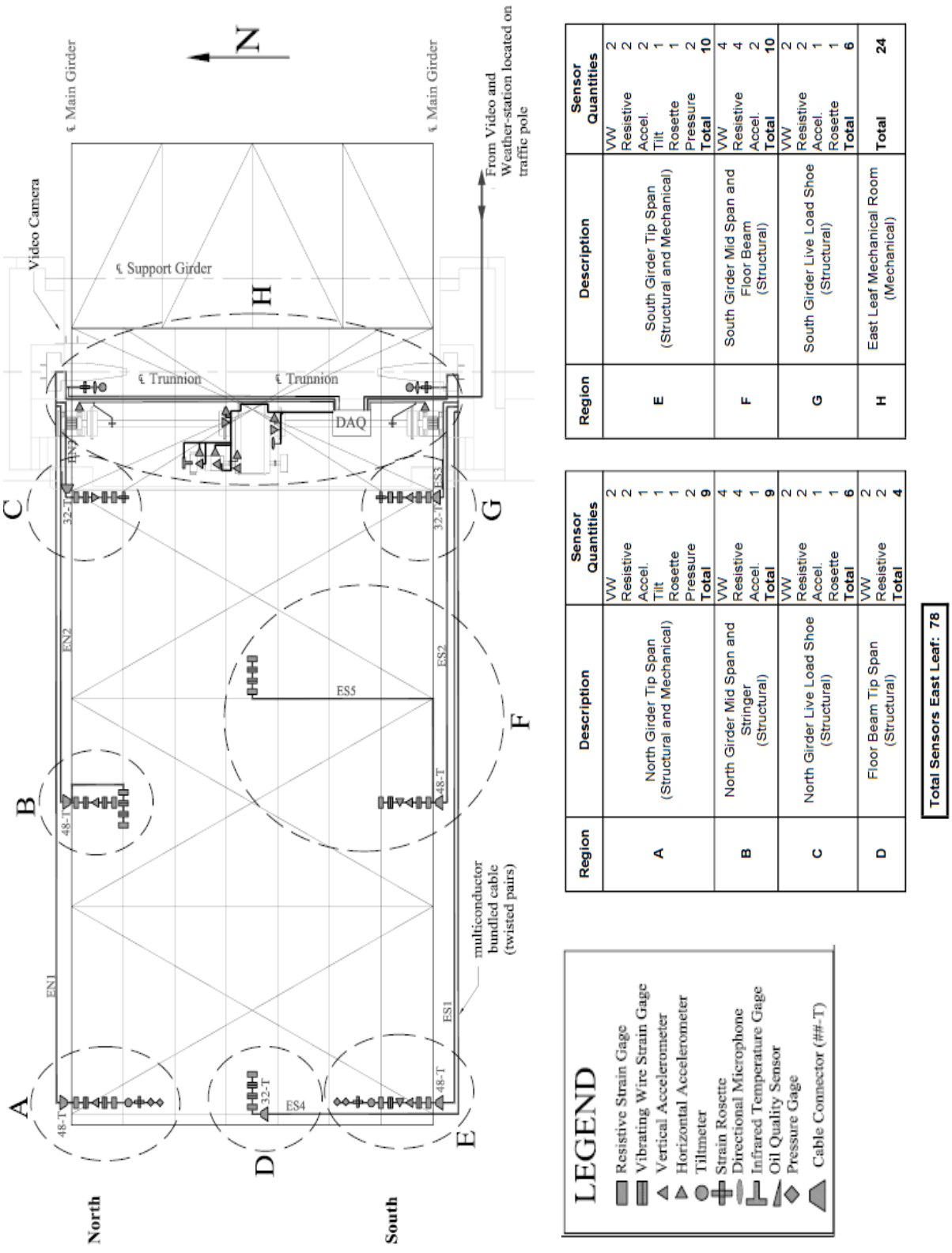

Region	Description	Sensor Quantities	
A	North Girder Tip Span (Structural and Mechanical)	VW	2
		Resistive	2
		Accel.	1
		Tilt	1
		Rosette	1
		Pressure	2
		Total	**9**
B	North Girder Mid Span and Stringer (Structural)	VW	4
		Resistive	4
		Accel.	1
		Total	**9**
C	North Girder Live Load Shoe (Structural)	VW	2
		Resistive	2
		Accel.	1
		Rosette	1
		Total	**6**
D	Floor Beam Tip Span (Structural)	VW	2
		Resistive	2
		Total	**4**

Region	Description	Sensor Quantities	
E	South Girder Tip Span (Structural and Mechanical)	VW	2
		Resistive	2
		Accel.	2
		Tilt	1
		Rosette	1
		Pressure	2
		Total	**10**
F	South Girder Mid Span and Floor Beam (Structural)	VW	4
		Resistive	4
		Accel.	2
		Total	**10**
G	South Girder Live Load Shoe (Structural)	VW	2
		Resistive	2
		Accel.	1
		Rosette	1
		Total	**6**
H	East Leaf Mechanical Room (Mechanical)	**Total**	**24**

Total Sensors East Leaf: 78

Figure 12: Some of the Monitored Bridge Components (East Leaf)

2.2.4. West Leaf Instrumentation Plan Summary

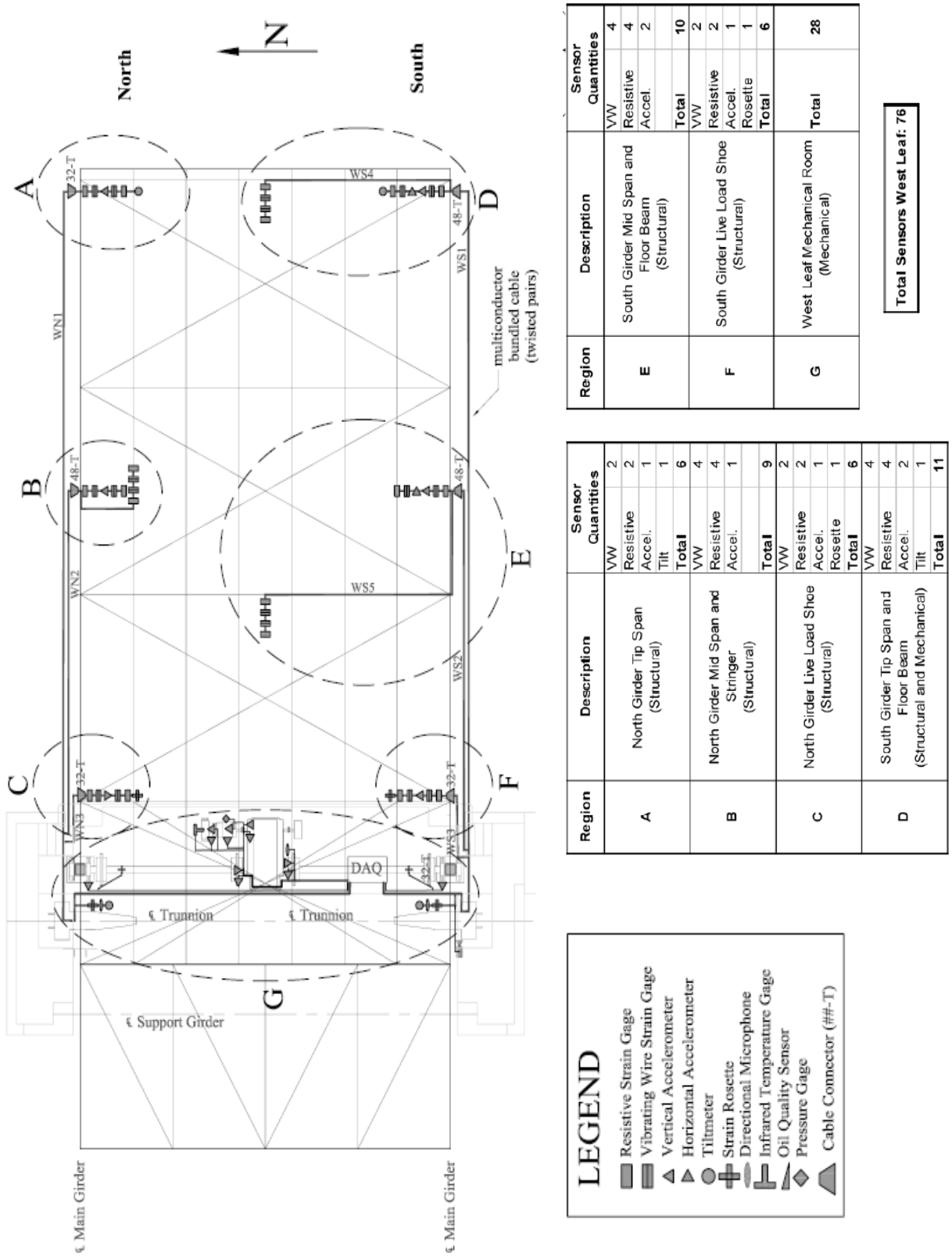

Region	Description	Sensor Quantities	
A	North Girder Tip Span (Structural)	VW	2
		Resistive	2
		Accel.	1
		Tilt	1
		Total	**6**
B	North Girder Mid Span and Stringer (Structural)	VW	4
		Resistive	4
		Accel.	1
		Total	**9**
C	North Girder Live Load Shoe (Structural)	VW	2
		Resistive	2
		Accel.	1
		Rosette	1
		Total	**6**
D	South Girder Tip Span and Floor Beam (Structural and Mechanical)	VW	4
		Resistive	4
		Accel.	2
		Tilt	1
		Total	**11**

Region	Description	Sensor Quantities	
E	South Girder Mid Span and Floor Beam (Structural)	VW	4
		Resistive	4
		Accel.	2
		Total	**10**
F	South Girder Live Load Shoe (Structural)	VW	2
		Resistive	2
		Accel.	1
		Rosette	1
		Total	**6**
G	West Leaf Mechanical Room (Mechanical)	**Total**	**28**

Total Sensors West Leaf: 76

Figure 13: Some of the Monitored Bridge Components (West Leaf)

2.2.5. East Leaf Mechanical Instrumentation Plan Summary

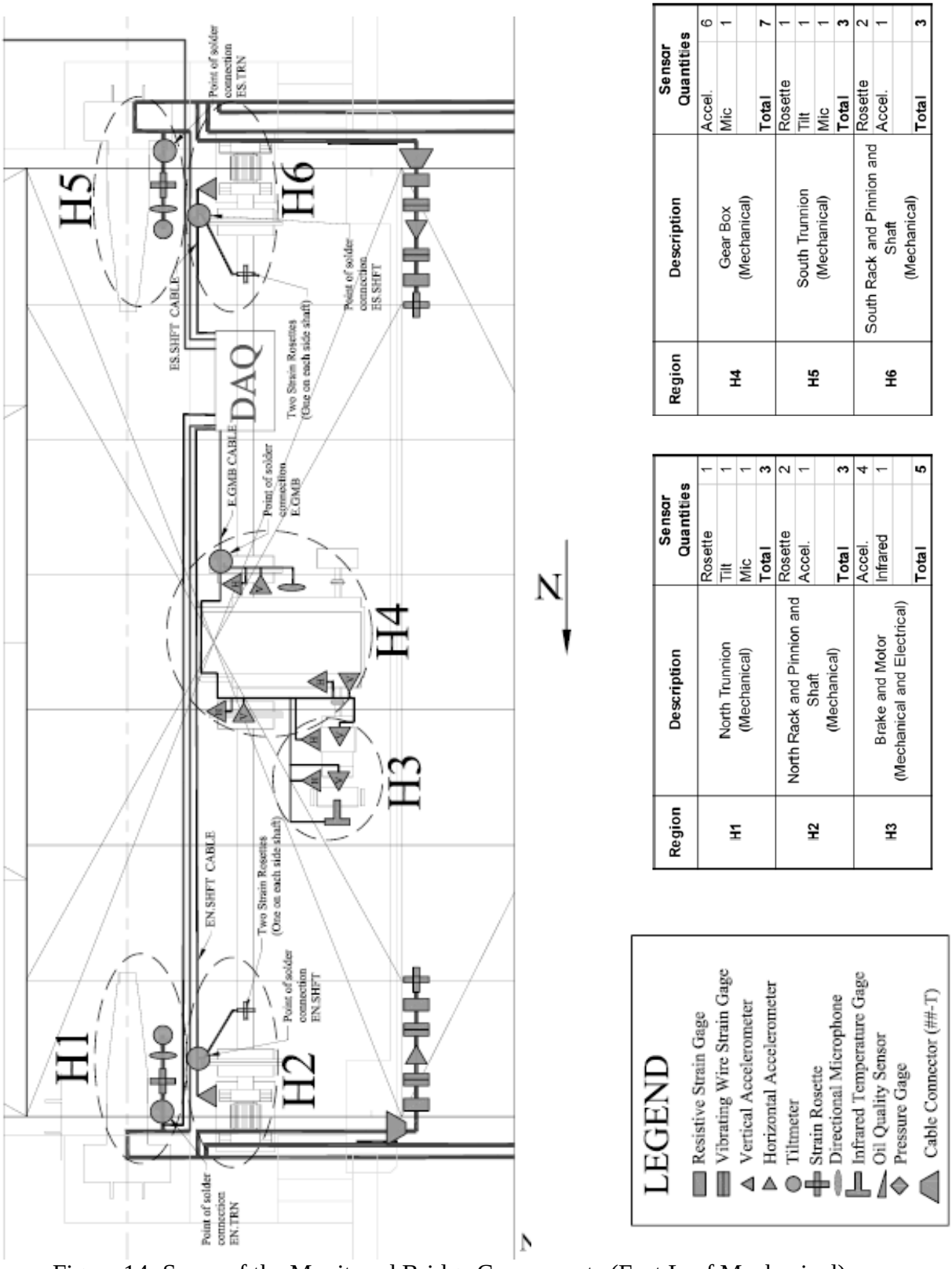

Region	Description	Sensor Quantities	
H1	North Trunnion (Mechanical)	Rosette	1
		Tilt	1
		Mic	1
		Total	**3**
H2	North Rack and Pinnion and Shaft (Mechanical)	Rosette	2
		Accel.	1
		Total	**3**
H3	Brake and Motor (Mechanical and Electrical)	Accel.	4
		Infrared	1
		Total	**5**

Region	Description	Sensor Quantities	
H4	Gear Box (Mechanical)	Accel.	6
		Mic	1
		Total	**7**
H5	South Trunnion (Mechanical)	Rosette	1
		Tilt	1
		Mic	1
		Total	**3**
H6	South Rack and Pinnion and Shaft (Mechanical)	Rosette	2
		Accel.	1
		Total	**3**

Figure 14: Some of the Monitored Bridge Components (East Leaf Mechanical)

2.2.6. West Leaf Mechanical Instrumentation Plan Summary

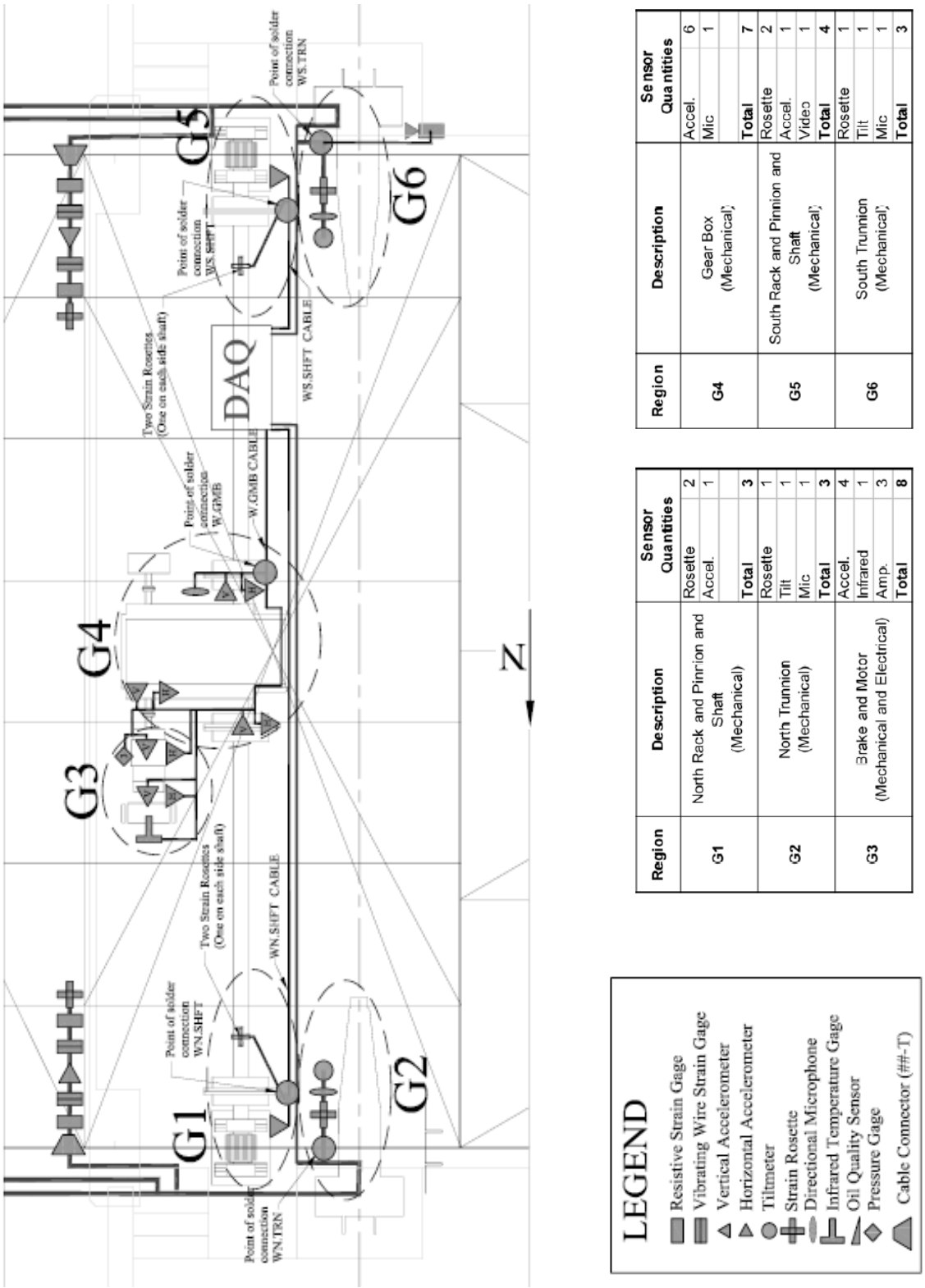

Region	Description	Sensor Quantities	
G1	North Rack and Pinnion and Shaft (Mechanical)	Rosette	2
		Accel.	1
		Total	**3**
G2	North Trunnion (Mechanical)	Rosette	1
		Tilt	1
		Mic	1
		Total	**3**
G3	Brake and Motor (Mechanical and Electrical)	Accel.	4
		Infrared	1
		Amp.	3
		Total	**8**

Region	Description	Sensor Quantities	
G4	Gear Box (Mechanical)	Accel.	6
		Mic	1
		Total	**7**
G5	South Rack and Pinnion and Shaft (Mechanical)	Rosette	2
		Accel.	1
		Video	1
		Total	**4**
G6	South Trunnion (Mechanical)	Rosette	1
		Tilt	1
		Mic	1
		Total	**3**

Figure 15: Some of the Monitored Bridge Components (West Leaf Mechanical)

2.3. Sensors

The current installation consists of an array of 160 channels/sensors as follows:

Dynamic strain gages: A total of 36 Hitec-weldable-dynamic strain gages have been deployed on main girders, floor beams, and stringers; collecting data at a rate of 250Hz. Low pass filters and averaging every 25 data points were employed to minimize noise and to reduce to size of the data sets for an effective rate, respectively.

Strain Rosettes: A total of 22 Hitec sensors were installed and located at the following areas: Four (4) are placed on girders at the live-load shoe locations to correlate with traffic loads, Another two (2) are located at the receiving encasing for the span locks, Eight (8) at the trunnions vicinities for studying the shear on these critical regions, and Eight (8) at the main shafts to correlate with tiltmeters and monitor the torque/balance on each opening/closing operation.

Vibrating wire strain gages (VWSG): A total of 36 VWSG from Geokon were installed, collecting temperature and strain continuously every 15 min. The sampling at 15 minutes deemed sufficient to capture the temperature-induced stresses with an effective rate.

Accelerometers: A total of 40 PCB accelerometers collecting at 250 Hz were installed. A total of 16, Eight (8) on the girders of each leaf, are installed to measure vertical (12) and Horizontal (4) acceleration. Another 6 are placed on each one of the gear boxes and another 4 on the electric motors to monitor their performance. Also, 2 are placed on each rack and pinion base for detecting excessive vibration.

Tiltmeters (8 uniaxial Tuff tiltmeters): A total of eight (8) uniaxial Tuff tiltmeters were installed. Four (4) are located at the trunnion regions to correlate with the torque and calculate the friction/balance of the bridge, and another four (4 are placed at the tip of each girder for checking the alignment of both leaves.

Microphones: A total of six (6) PCB microphones are installed. Four (4) are located at the trunnion regions to detect any unexpected acoustic data and another two (2) are attached within the gear box vicinity to determine the acoustic print corresponding to normal/abnormal lubrication.

Pressure gages: Four (4) TPS sensors were placed at the spanlock hydraulic system for detecting problems related with alignment between the spanlock bar and the receiver.

Infrared Temperature sensors: Two (2) noncontact IT Omega transmitters were in charge of measuring anomalies on the motor brakes.

Amperage meters sensors: Three (3) current sensors were placed to monitor the amperage consumption of the west leaf motor during the opening/closing operations.

Table 1 shows the overall sensor quantities for this project. The current installation consists of an array of 160 channels/sensors. These sensors were installed to monitor structural, mechanical and electrical components of the bridge. In addition, a weather station to monitor the environmental factors was also installed.

Table 1: Summary of the Sensors

Sensor type	**Structural Sensors**	**Mechanical and Electrical Sensors**	**Total**
High-speed Strain Gage	36	0	36
Vibrating Wire Strain	36	0	36
Strain Rosette	6	16	22
Tiltmeter	4	4	8
Accelerometer	16	24	40
Pressure Gage	0	4	4
Microphone	0	6	6
Infrared Temperature	0	2	2
Video Camera	1	1	2
Ampmeter	0	3	6
Weather Station	1	0	1
Total	**100**	**60**	**160**

2.4. Data Acquisition Systems (DAQs)

The data acquisition system (DAQ) is a critical component of SHM and is related to the acquisition of the data, which includes data collection, signal processing, synchronization, digitization and storage. The data from the sensors is transmitted by cable connection (in wired DAQ) to the data acquisition unit. The goal is to have the data

to be received uncorrupted without time delay or loss of information. Signal conditioning is usually necessary to improve the quality of the signals, and most data acquisition systems are equipped with signal conditioning components.

In the current application, since the two leaves of the movable bridge are physically separated from each other, wireless communication was needed to ensure data transmission between the leaves of the bridge, and two GPS units were used for synchronization. Figure 16 shows the scheme used for the data transmission. An overall summary of the DAQ with the installed sensors is given in Figure 17.

The data acquisition equipment was installed in permanent protective and temperature-humidity-controlled-enclosures located in both machinery rooms at each side of the bridge. The sensors were connected by weatherproof cables. The above components will be discussed in further detail in subsequent sections.

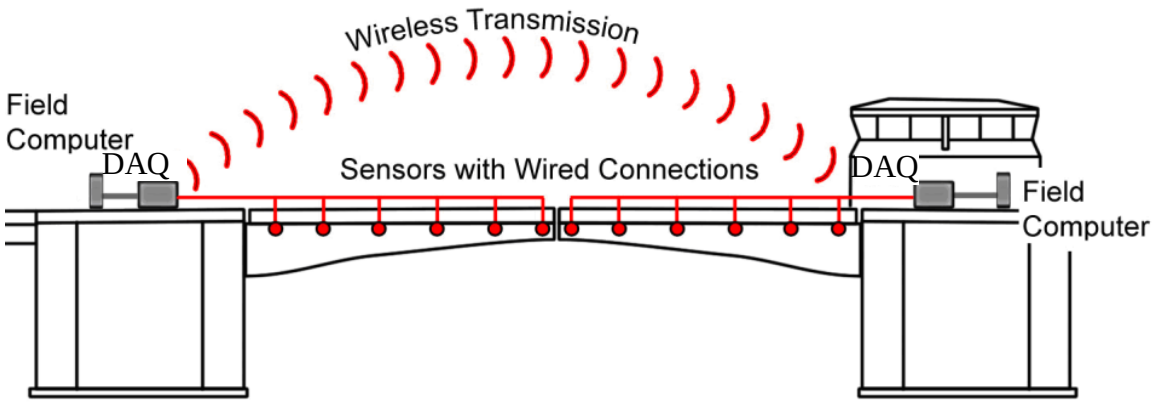

Figure 16: Scheme Used for Data Transmission

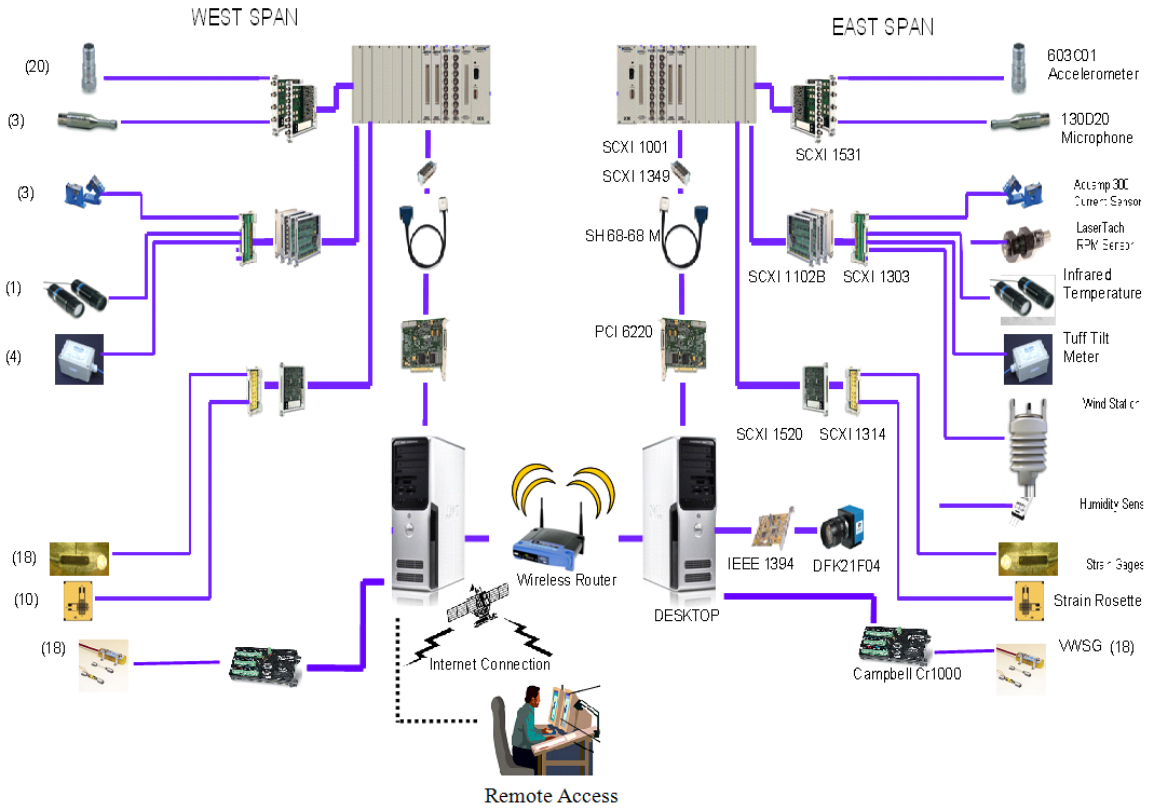

Figure 17: Layout of Individual DAQ Components

The DAQ is controlled by two personal computers; one on each leaf. A DSL Internet connection and router are located on the East leaf. A wireless router is connected to the router, providing a hardwire Internet connection to the east leaf computer and a wireless internet connection for the West leaf computer. Data collection and processing on each leaf are handled by two systems. All the dynamic sensors are connected to one of the two National Instruments SCXI 1001 signal conditioning chassis with its corresponding modules: SCXI 1520, SCXI 1102B, SCXI 1531; for strain, voltage and acceleration respectively. The vibrating wire strain gages are controlled by one of two CR1000 units by Campbell Scientific.

2.4.1. DAQ for High Speed Measurements

The individual components comprising the installed National Instrument system are provided below. The following specifications are based on the product information provided by National Instruments website (www.ni.com).

Chassis

The SCXI-1001 is a rugged, low-noise chassis that holds the 12 SCXI modules. This chassis, shown in Figure 18, powers the SCXI modules, as well as handles all timing, trigger, and signal routing between the digitizer and SCXI modules.

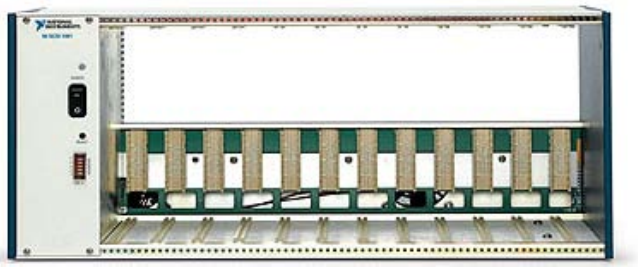

Figure 18: SCXI 1001 Chassis

Modules

The SCXI-1520 module is an eight-channel module for interfacing with strain-gage bridges and other Wheatstone-bridge based sensors (Figure 19-left). Terminal block SCXI 1314 provides interface between the module and sensors (Figure 19-center). The National Instruments SCXI-1531, shown in Figure 19-right is a signal conditioning module for Integrated Electronic Piezoelectric (IEPE) compatible accelerometers and microphones. Each of the eight input channels includes a programmable AC instrumentation amplifier, 4-pole Bessel low pass filter, and excitation current source. The NI SCXI-1531 offers simultaneous sampling to preserve inter-channel phase relationships. This module also offers parallel-mode operation for faster scanning rates and BNC connectors to simplify signal connection.

Figure 19: SCXI - 1520 Module (left), 1314 Terminal Block (center), 1531 Module (right)

The National Instruments SCXI-1102 (Figure 20-left) is designed for high-accuracy thermocouple measurements. The SCXI-1102 also can acquire milivolt, volt and 0 to 20 milliamp current input signals. Each of the 32 analog input channels includes an instrumentation amplifier and a 2 Hz low pass filter. The SCXI-1303 (Figure 20-right) is a terminal block for use with the SCXI-1102B modules and includes isothermal construction that minimizes errors caused by thermal gradients between terminals and the cold-junction sensor. The SCXI-1303 also includes circuitry for open-thermocouple detection as well as automatic ground referencing for floating (non-grounded) thermo-couples.

Figure 20: SCXI - 1102 Module (left), 1303 Terminal block (right)

2.4.2. DAQ for Slow Speed Events

CR1000 Data Acquisition and Components

CR1000 by Campbell Scientific is used to collect slow speed vibrating wire strain gage data. The components of the CR1000 are the power station, wiring panel, multiplexer and vibrating wire interface. The wiring panel provides terminals for connecting sensors, power and communications devices. In case of power loss, a lithium battery backs up the CR1000 clock, program, and memory. Figure 21 shows the CR1000 power station connected to the wiring panel. Through a RS-232 type of connection, the data acquisition system can be connected to the computer.

Figure 21: Power and Wiring Panel of CR1000 (http://www.campbellsci.com/cr1000)

Vibrating-wire gages have been used extensively in civil engineering applications due to their long-term stability. The AVW200 vibrating-wire interface (Figure 22) is used to reduce noise and improve accuracy of the vibrating-wire measurements.

Figure 22: Vibrating Wire Interface of CR1000

Multiplexers are the critical links between the gages and the data acquisition systems. The AM16/32B multiplexer has the capability to work more efficiently with the AVW200-series vibrating wire interfaces, and also allows the data acquisition to measure more sensors. In Figure 23, a 32 channel AM16/32B multiplexer is shown.

Figure 23: AM16/32B Multiplexer of CR1000

The CR1000 requires a program to be sent to its memory for direct measurement, pre-processing, and data storage operations. Programs can be created with CRBASIC Editor

and are sent with *Logger-Net* support software. The fundamental elements of CRBASIC include: variables, constants, common instructions and special instructions. These four elements must be properly placed within the program structure for the program to work.

In this project, four multiplexers (two for each leaf) were placed, and a total of 36 channels were used for each multiplexer. The 36 channels are equivalent to 18 vibrating wire strain gages because each strain gage is reading both strain and temperature at the same time. In Figure 24, the location and connections of CR1000 data acquisition in the cabinet are shown.

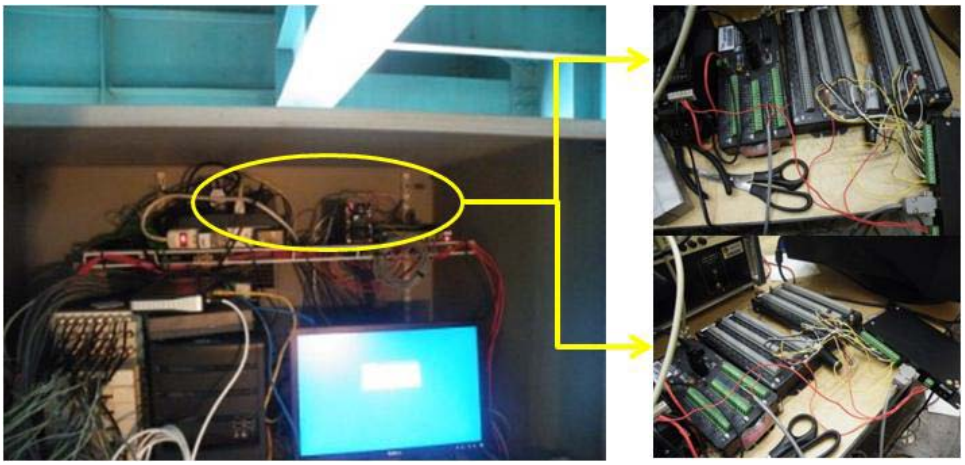

Figure 24: Location and Connections of CR1000 Data Acquisition in the Cabinet

2.4.3. Weather Station DAQ

One (1) Orion 420 multi-channel weather station from Columbia Weather Systems was installed and provides weather monitoring for correlation with all the other measurements. A single sensor module provides measurements of: ultrasonic wind direction and speed, rain amount, intensity, and duration, temperature, relative humidity, and barometric pressure. The specifications of the system are shown in Table 2.

An included weatherproof enclosure provides preliminary data processing and houses the AC power supply with +24 VDC output, AC power filer and suppressor, two (2) RS-232 to 4-20mA converters, and a sensor terminal block. The sensor cable connects to the sensor terminal block and a series of multiconductor cables relay the data to the NI system, where it is further processed.

Table 2: Orion 420 Weather Station Specifications

Sensor	Range	Accuracy	Resolution
Temperature	-60 to 140°F	±0.5°F at 68°F	0.1°F
Barometric Pressure	17.50 to 32.5 InHg	±0.015 InHg at +32 to 86°F	0.01 InHg
Wind Speed	0 - 115 mph	±0.7 mph	1 mph
Wind Direction	0 -360°	±2°	1°
Relative Humidity	0 -100 %RH	±3%RH	1%RH
Rainfall	cumulative	±5%	0.01 in.

2.4.4. Video Camera System

Two (2) FireWire cameras collect video stream data at a rate of 15 Hz. One is dedicated to monitor the live bridge traffic and the other is used to detect corrosion on the open gears. Both cameras are connected directly to the computers through FireWire connections. Interfacing is done through the developed LabVIEW program where computer vision techniques are used.

2.4.5. Wireless Router

Communication and transmittal of data between the two separated data acquisition systems is accomplished through a D-Link WBR-2310 wireless router (Figure 25), which is a combined 4-port switch plus range booster type G router. For security, this network is password protected.

Figure 25: D-Link WBR-2310 Wireless Router

2.4.6. GPS Synchronization

As stated before, one of the main challenges of designing the data acquisition system for a bascule type movable bridge is the data transmission and synchronization. First, both computers were coarse-grained synchronized by using a standard Network Time Protocol (NPT). This NTP continuously measures the wireless network latency between both computers located at each side of the bridge, compensating in real time the subrogated slave computer to the master. This procedure served a preliminary synchronization, with the timing offset in the order of 10 milliseconds.

Because of the high-speed data, further refining in the synchronization was needed. The desired synchronization was achieved by using a Trimble Resolution T Global Positioning System (GPS) timing receiver at each side (Figure 26). The receiver is a full 12-channel, parallel tracking, embeddable GPS receiver designed to provide precise GPS or UTC (Coordinated Universal Time) time, which is needed for synchronization. These GPS timing receivers, not only provides location information, but also supply a global time reference, accurate up to a few micro seconds. Every second, each GPS outputs a pulse whose leading edge is synchronized. These signals were captured simultaneously with other sensor data and embedded within the data files. By matching pulses on both computers, desired synchronization was achieved.

Figure 26: Trimble Resolution T GPS Timing Receiver

2.5. Remote Access

A Digital Subscriber Line (DSL) Internet connection was established at the East side of the bridge. This connection was terminated in a wireless access point. The West side gained connection to this access point by using a standard 802.11 PCI wireless card. A static IP address was required to ensure a consistent Internet presence. For the initial

phase, standard Microsoft Remote Desktop is used to communicate and fully control both computers.

2.6. Data Archiving

The internal data collection process and file archiving are unique for each of the two systems; National Instrument and Campbell Scientific; and detailed below.

2.6.1. Programming the DAQs

All slow speed vibrating wire strain gage data was collected through one of the two Campbell Scientific systems. The program was adjusted to collect data, which included the strain and temperature data for every 15 minutes. The reason for slow speed data collection is to see the daily, weekly, monthly and seasonally temperature effects on the structure. More discussion about vibrating wire data can be seen in Chapter-7.

All high speed sensor data, as well as the traffic and open gear video, was collected through one of the two National Instrument systems. A LabVIEW program was developed to collect and save the high speed data. All data was saved in the hard disk of the computer corresponding to each DAQ in order to minimize the error due to wireless transmission. Then, periodically all data was uploaded to a remote server. For redundancy purposes, the data sets also kept on each hard disk. Initially, the following data collection regime was in use:

Scheduled Data Collection

Three pre-scheduled time slots, corresponding to peak hours of operation, were selected for data collection. Scheduled data collection was not carried at the top of hours because the bridge is generally opening and closing at those times, and therefore, operational events would not be saved. Therefore, the following times were selected for data collection: (1) From *9:10:00 A.M.* to *9:15:00 A.M*, (2) From *1:10:00 P.M.* to *1:15:00 P.M*, (3) From *5:10:00 P.M.* to *5:15:00 P.M*.

On Demand Data Collection

In addition to the automated scheduled data collection, data can be collected manually through the LabVIEW program any time it is needed and the data is then saved to the hard disks after the on-demand collection. This procedure can be also done remotely using an established Microsoft Remote Desktop Connection.

Trigger Based Data Collection

Based on the normal operational responses, a trigger based data collection mechanism can be activated. Triggering thresholds can be defined for different sensors, and data can be saved once those limits are reached. The software includes triggers for each one of the dynamic strain gages. Every time an extraordinary strain is detected, the data will be saved for all the sensors.

Opening/Closing Operation

Every time the bridge opens/closes, the DAQ saves the data corresponding to all dynamic sensors. The pedestrian gates on the bridge are used as triggers for capturing these events.

File Structure

An automated file naming system is in place to prevent confusion and speed post processing of the data. For details regarding the file naming convention please refer to Appendix 10.2. It is important to note that when the collection trigger is coming from a structural sensor, only the files corresponding to strain, acceleration and traffic video data are saved. A separate file, named EVENTS.lvm, logs the name of all recorded events and indicates the date, time, and triggering event that cause it. This facilitates extraction of information by sorting the data files in several ways. It is also useful for automated data analysis.

3. FIELD WORK AND PREPARATIONS

3.1. Field Implementation and Challenges

As mentioned in the above sections, the movable bridge under consideration was instrumented with various sensors. The instrumentation plan was developed by the researchers considering the feedback of FDOT bridge engineers and practitioners who have accumulated experience with the issues related to movable bridges. The technical challenges associated with field implementation of a structural health monitoring program for bridges are commonly related to installation, operation, and maintenance of the various components of the monitoring system. The main components generally include the sensors and data acquisition hardware, power and communication systems, cabling, connectors and enclosures. Ideally, a structural health monitoring system should be designed to operate accurately and reliably, with minimal maintenance for the entire duration for which the bridge will be monitored. Meeting this standard requires careful consideration of the following issues and incorporating some degree of flexibility and redundancy into the system during the initial design of the system.

In addition to the technical challenges described above, there are also many significant issues to consider that are generally more non-technical in nature, but no less critical for ensuring the success of a project. These challenges are commonly associated with communication and coordination between the various parties involved in such projects, safety, access and security, logistics, scheduling, and weather related issues. One of the main issues in real life SHM applications is the challenges to be overcome during field implementation. These challenges may include organizational, operational, technical and practical issues. Especially for a movable bridge application, like the one mentioned here, there are special considerations and coordination required, such as informing the Coast Guard for marine traffic regulations. During normal operation, the movable bridge is opened every half and full hour if requested by boat owners. However, the bridge cannot be opened often during instrumentation of the bridge, since the snooper truck is on the bridge, and it is not very practical to open the bridge every 30 minutes. Therefore, the Coast Guard should be informed in advance about the fieldwork, so that they can announce the change in the opening hours. Since the bridge must still be opened

and closed during the sensor installation, the installation time and requirements, such as clearing the bridge, must be carefully considered during the field operations.

In this chapter, the selected and installed cabling, connectors, and enclosures will be discussed. Design considerations and alternatives, selected product specifications, and laboratory preparation will be discussed for each. The design considerations and alternatives consider the above discussed technical and logistical challenges and the available product options. Based on these considerations, the selected product will be described. Laboratory preparation of the SHM hardware was a critical and time consuming process. The details of this preparation process will be described, as well as the quality control measures which were executed. Following this will be a discussion of the numerous laboratory tests performed to establish a baseline of sensor data for sensors such as strain gages, accelerometers, tiltmeters, etc. using various cable configurations. Lastly, the installation of the sensors, cabinets, weather station and traffic camera will be discussed.

3.2. Cabling, Connector, and Cabinet Design

Structural Health Monitoring (SHM) of large structures involves much more than simply connecting various sensors directly to a data acquisition (DAQ). The large distance between groups of sensors and the DAQ system creates a wiring issue, which is, relaying the signal from the sensors to DAQ effectively. Simply extending the individual sensor wires becomes drastically inefficient with larger sensor groups and increased distances. Therefore, use of a multiconductor cable facilitates transmitting sensor signals to the DAQ. In this project, large connectors were used to connect sensor groups together. Using the same connectors, the sensor cables were connected into one of the many multiconductor cables. Moreover, an environmentally controlled cabinet on each leaf was designed and manufactured to house the computer and hardware. The sections below will address the design considerations, available alternatives, and selected product specifications relating to the multiconductor cables, connectors, and cabinets.

3.3. Cabling

3.3.1. Design Considerations and Alternatives

Durability and reliability are of extreme importance for the design of different elements in a long-term SHM project, and therefore warrant high consideration as

controlling parameters in design decisions. The environmental impact on cabling installed at a location such as Ft. Lauderdale is quite important. Therefore, the selected product was a Belden multiconductor Twisted Pair Individually Shielded cable with PVC outer jacket, which offered the required durability; including protection from environmental and electrical interference. Testing revealed that signal quality was better as a result of the pairs being individually shielded and grounded, and the PVC outer jacket was rated for outdoor use and sunlight and oil resistive; providing confidence for long-term use in a harsh environment. Other cabling alternatives were individual 1-2 pair shielded/grounded cables and multiconductor twisted pair cable; however, both of these alternatives were determined to be insufficient for our application. Please refer to Appendix 10.3 for more information regarding the cabling design alternatives.

3.3.2. Selected Product Specifications

The quantity of sensor channels needed at each sensor group, or node, determined the selection of the number of twisted pairs needed for our project. 16-Pair (Belden Product 1079a) and 24-Pair (Belden Product 1079a) cables were selected since they offered the optimal configuration for the current application. Please see Appendix 10.3 for more information about the cable properties.

Figure 27: Belden Cable 1079a and 1080a

3.3.3. Lab Preparation

The selected cables were delivered in 500 and 1000 foot spools. Before the cable could be installed on the bridge the following tasks were executed: (1) Measurement and cutting cable to proper length segments, (2) Labeling and re-bundling of each cable (Refer to Appendix 10.4), (3) Cable ends preparation, which included the removal of a small length of outer jacket, determination and labeling of each twisted pair, and wire stripping and tinning of each wire. Figure 28 below shows the ends of one of the cables after execution of the above steps.

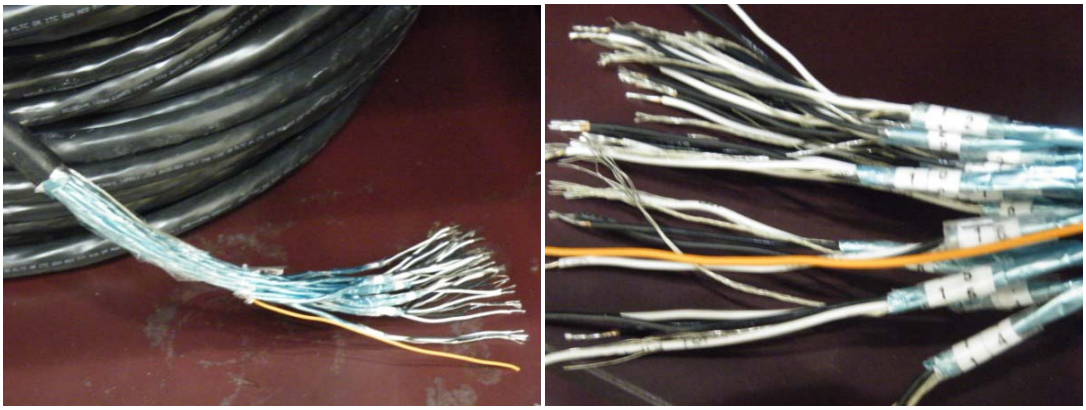

Figure 28: Lab Prepared Wire Tips: The Cable After Cutting (Left), Cable After Preparing the Ends and Labeling (Right)

3.3.4. Quality Control

The selected Belden cable products contain only black and white twisted pairs. To differentiate between pairs the pair number has been printed on the outside of each individual wire. As a result, quick pair differentiation was not possible. Therefore, new larger and weather resistant number labels were added to each pair, as seen in Figure 28**,** in order to speed field installation time and prevent field errors. After relabeling of the pairs, each wire's continuity was tested to ensure that the labels had been applied appropriately at each end of the cable.

3.4. Sensor-Cable Connection

3.4.1. Design Considerations and Alternatives

For the sensor installation on a movable bascule bridge, the connection point between each group of sensors was determined to be a highly critical design consideration. In

addition, the installation duration was limited due to opening and closing of the bridge as well as the availability of the snooper trucks. As a result, the following design options for this connection were analyzed: pre-connecting sensors to the cables in the lab, girder installed junction box enclosures, military style connectors, and industrial connectors. For a detailed comparison of the alternatives please refer to Appendix 10.5.

3.4.2. Selected Product Specifications

Upon analysis of the design options, the Harting brand Han industrial connector product was selected. This product provided the best time critical and quality controlled solution to the sensor/main cable connection.

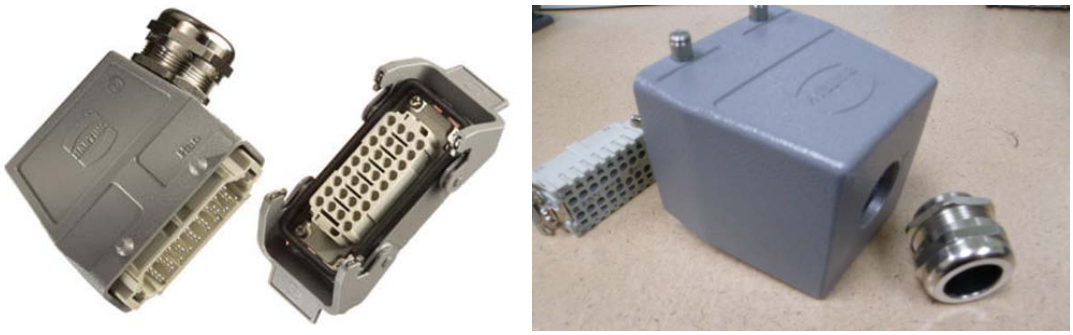

Figure 29: Harting Han Industrial Connector

The Harting Han industrial connectors have both male and female parts, with each of these actually composed of four (4) distinct components: the outer weather-proof housing, the internal electrical connector, the opening reducer, and the cable gland. The two different main cable sizes (24-pair & 16-pair) resulted in an increase in the variation of required connector components. A summary of the components contained in each complete connection (both halves) and associated product names are provided in Appendix 10.6.

The use of connectors enabled a critical option during the installation procedure; the opportunity to install the sensor group and main cable at separate times. Upon completion of both individual installations, each half of the connector was quickly connected together and locked with a watertight seal by two snap connectors.

Figure 30: Sensor Group Installation (Left) and Cable Connected Installation (Right)

The relatively small profile of each connector enabled it to rest on the bottom flanges of the girders and be held in place with two C-clamps. As seen in Figure 31, this installation method on the bottom flange of the main girder proved to be both efficient during installation and secure during bridge openings.

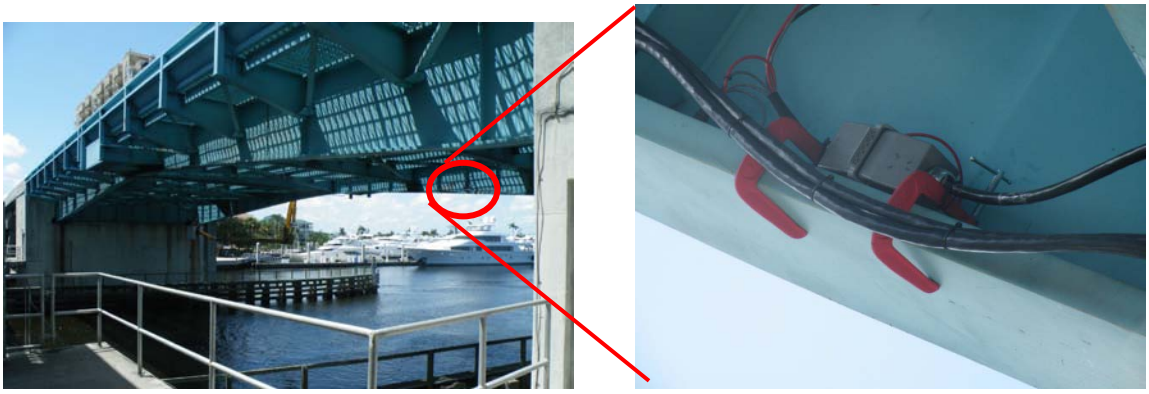

Figure 31: Installed Connector Secure on the Bottom Flange of the Main Girder

3.4.2.1. Lab Preparation

Due to the variety of components ordered, the first step prior to field installation was the assembly of each connector with proper components. The connectors are of two different types, cage clamp and crimp terminal. The crimp terminal type required that each incoming and outgoing wire have a crimp contact installed with the use of a specialized crimping tool. The wire bundle for each cable was then fed through the cable gland, reducer, and outer housing. The crimp terminals were then installed into the crimp terminal type connectors with another specialized tool. The cage clamp connectors had the appropriate wires installed into each slot with a flat head screwdriver. Finally, the

connectors were fitted back into the outer housings and secured (Figure 32). To ensure quick field installation each sensor group, with attached connector halve, was packaged in a box and labeled.

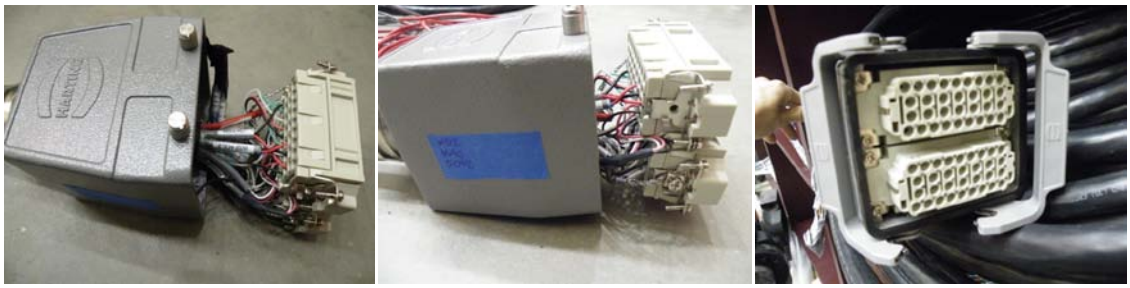

Figure 32: Different Views of the Connector

Figure 33: Sensor Group Ready for Bridge Installation

3.4.2.2. Quality Control

A quality control test was conducted to make certain that the appropriate individual wire and connector connections had been made. Since there were a large number of connectors and thousands of wires, it was not efficient to check all the wires. Therefore, a random sampling process was developed to check a number of pairs from each connector. Each selected pair was tested for continuity between connector terminal and cable end. Consequently, these preliminary quality control tests convinced the researchers that a reliable cable-connector system was created.

3.4.3. Cabinets

The DAQ systems for each leaf are housed in environmentally controlled cabinets. Each cabinet consists of 3 major components of cabinet enclosure to house the data acquisitions and computer, four legs to hold the cabinet and two side junction boxes to sort the individual pairs of the main cables. Based on a market search, the researchers

decided to custom design a cabinet for their specific purposes and prepare the inside panels themselves in a cost-effective manner. Cabinet fabrication was commissioned by ProMark Engineered Systems Inc. Dimensions of the water resistive steel cabinet, without the junction boxes, is 30” x 30” x 48”. Since the computer and the data acquisition would increase the inside temperature, an air conditioner system was installed on the back side of the cabinet.

Figure 34: East Leaf Cabinet

3.4.3.1. Side Cabinet Junction Boxes

A side junction box was attached to the end sides of each cabinet. The side junction boxes served as a junction point for the main cables and the pre-wired NI Terminal block cables. This junction was necessary because each main cable contains the pairs for various sensors, which needed to be installed in different terminal blocks. Therefore, these side junction boxes served as organizers for this separation. The Hoffman hinged cover NEMA type 3R enclosure was the product selected because it was designed for electrical instrumentation and to protect against falling rain. The dimensions of the junction boxes are 30” x 30” x 8”, and galvanized steel material was used. Please refer to Appendix 10.7 for a detailed list of the various products internal to each side junction box.

3.4.3.2. Side Junction Box Interior Configuration

The main cables enter the side junction boxes from the bottom and were held in place by strain reliefs (see Appendix 10.7 for details). The individual pairs from the main cables were sorted in the slotted cable sorters and terminate at the appropriate terminal block along DIN rails. The individual lab pre-installed NI cables left the adjacent side of the terminal block and were sorted by another slotted cable sorter. These wires then traveled through one of the holes connecting the side junction box to the cabinet. The cable then entered the proper NI terminal block and was connected to the appropriate channel (Figure 35-left).

Figure 35: Interior View of Side Junction Box (Left) and Lab Prepared Junction Box Panel (Right)

3.4.3.3. Lab Preparation

The interior components of the side junction boxes were installed on the provided removable back panels. Figure 35-right shows a completed back panel ready for installation into the appropriate junction box. Configuration of the DIN rail mounted terminal blocks was designed for a stagger, or tiered, layout of the main cables which can be seen in (Figure 36).

Figure 36: Cable Entries to DIN Rail on Side Junction Box Panel

3.4.3.4. NI Terminal Block Lab Preparation

Each sensor channel must be connected to the appropriate NI terminal block channel. The SCXI 1531, SCXI 1303 and SCXI 1314 all house channels in a screw-down metal enclosure. Therefore, the connections of the NI terminal block cables to the appropriate NI terminal block channel were done in the lab. Figure 37 shows a terminal block with its cover off and NI terminal blocks and their cables ready for field installation.

Figure 37: Lab Prepared NI Terminal Block and Completed NI Terminal Blocks Ready for Field Installation

3.5. Lab Studies for Trouble Shooting

3.5.1. Overview

In this part of the report, the authors are aiming to present the laboratory studies conducted to develop and test hardware and software such as sensor characteristics, DAQ

programs, cable connectors, and noise levels. The preliminary laboratory studies were essential to explore the noise levels in the cable and the connection settings of each sensor. Therefore, laboratory tests were conducted on a simple beam. The main purpose of the laboratory studies was to establish a baseline of sensor data for sensors, such as strain gages, accelerometers, tiltmeters, etc., using various cable configurations.

The test setup design was as follows (Figure 38): Two symmetrical sensor layouts of tilt meters were installed at the support locations whereas the strain gages (3) and accelerometers (3) were installed at middle of the beam on the top flange. Using this kind of configurations on the same beam allowed for comparison of different hardware setups (see Testing below). Loading and unloading of the beam with approximately 300lb took place during each test, and both averaged data and raw data were saved. The beam can be seen in Figure 38 and Figure 39.

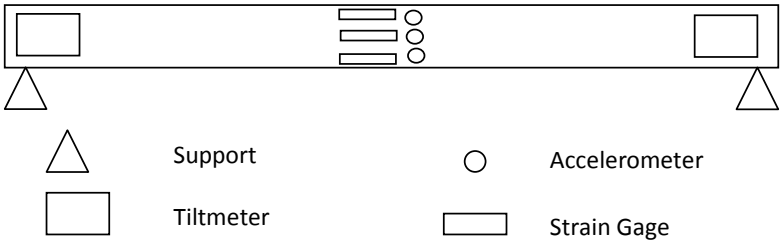

Figure 38: Experiment Sensor Layout

Figure 39: Beam and Sensor Locations

3.5.2. Testing of Monitoring Components

In this step, each sensor was tested individually to fully understand the connection settings and the reading values.

- Strain and Acceleration Test: A simple test was conducted on a laboratory beam. The test procedure involved loading the beam with 300 lb at the one third locations with plates (Figure 40 a) and collecting strain data. Due to the loading, the vibration on the beam was also collected. The strain gage and accelerometer plots can be seen in Figure 40.

Figure 40: Loading Plates (Left), Installed Strain Gages (Center) and Accelerometer (Right)

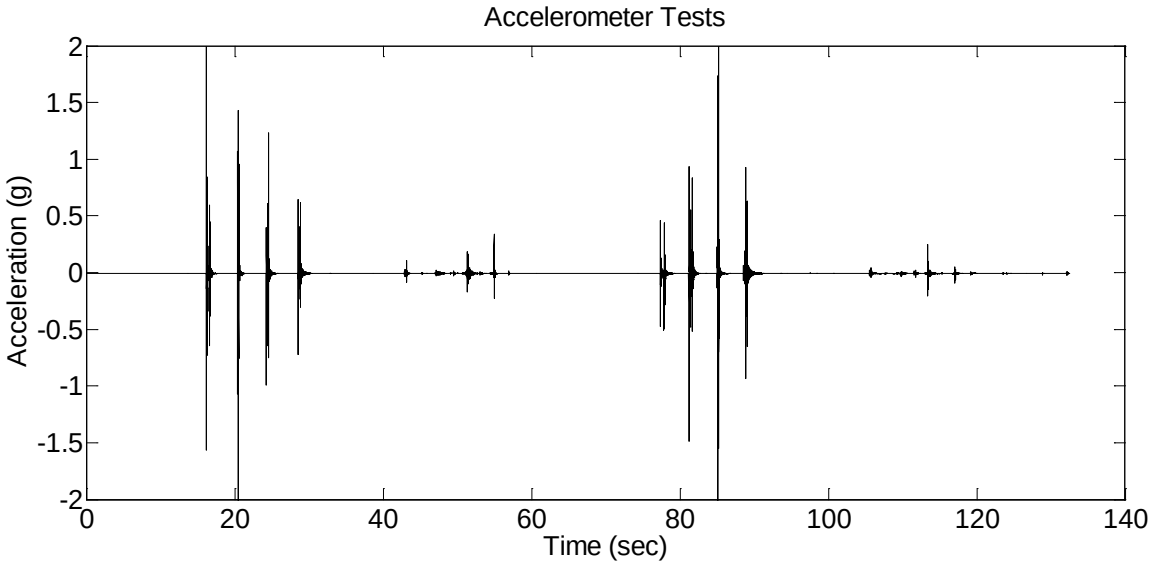

Figure 41: Acceleration Data from the Laboratory Test

- Tiltmeter Test: Tiltmeters were tested using the described beam test setup in a tiltmeter test. Testing resulted in detection and collection of data containing small rotation values. Therefore, for demonstration purposes, Figure 42 shows representative tilt data and the tiltmeter used.

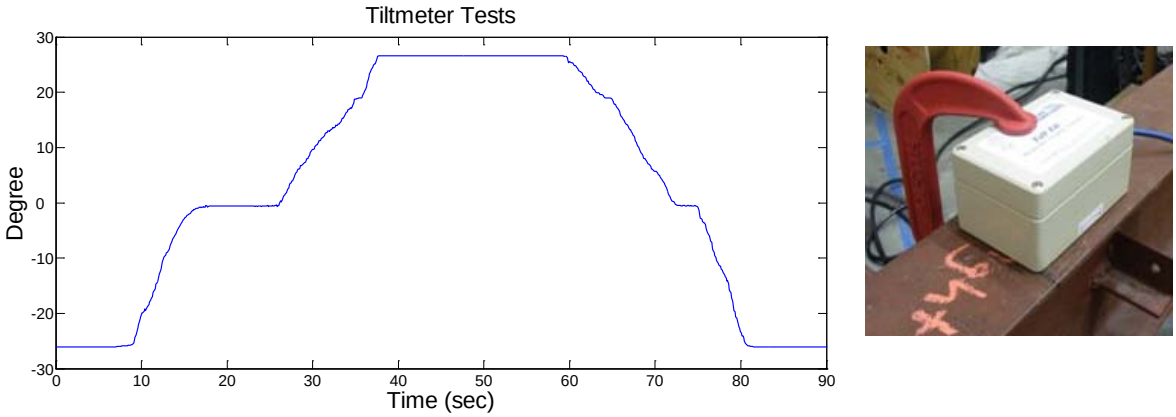

Figure 42: Typical Tilt Data (Left) and Tiltmeter on the Beam (Right)

- Ampmeter Test: For the ampmeter tests, a basic power outlet cable and a heat gun connected to this power cable were used. The test procedure was as follows: first heat gun was off; then, the heat gun was operating at level-1, and finally heat gun was operating at level-2 and finally turned off. In Figure 43, the ampmeter and its data can be seen. The reading values were also checked with an external ampmeter.

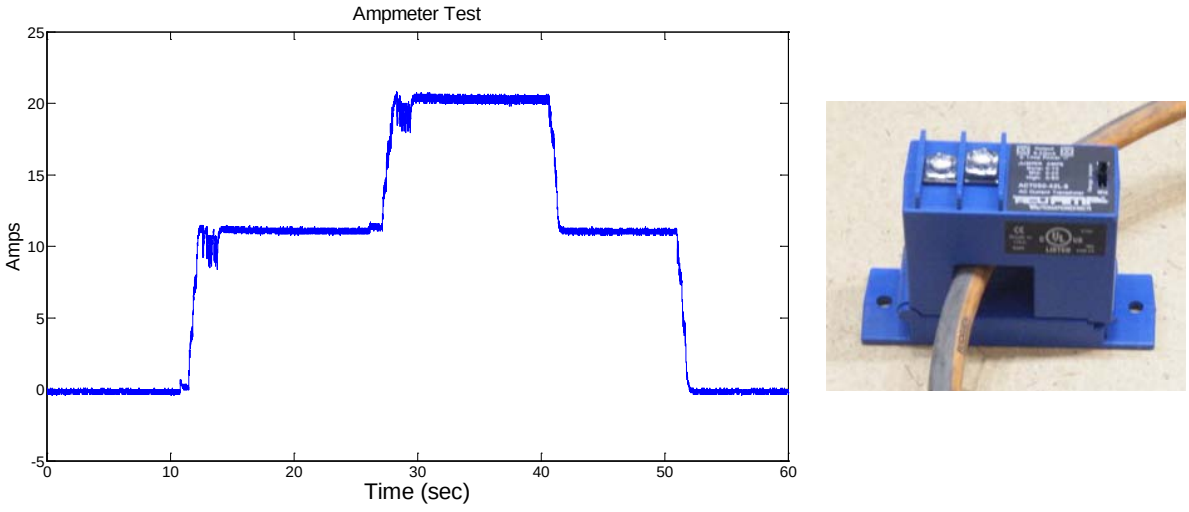

Figure 43: Ampmeter Data and Ampmeter

- Connector Test: To identify the noise source at the field, a 150 ft multiconductor cable segment was tested in the structures laboratory, with and without the connector (shown in Figure 44) installed. Acceleration and strain data was collected using the beam test setup. Figure 45 shows the acceleration plot and Figure 46 shows the strain plot, each with the connector installed. From comparison of the two testing configurations, it was observed that the connectors have a minimal noise impact, and quality of the signal is not affected by the use of the connector.

Figure 44: Different Views of the Connector

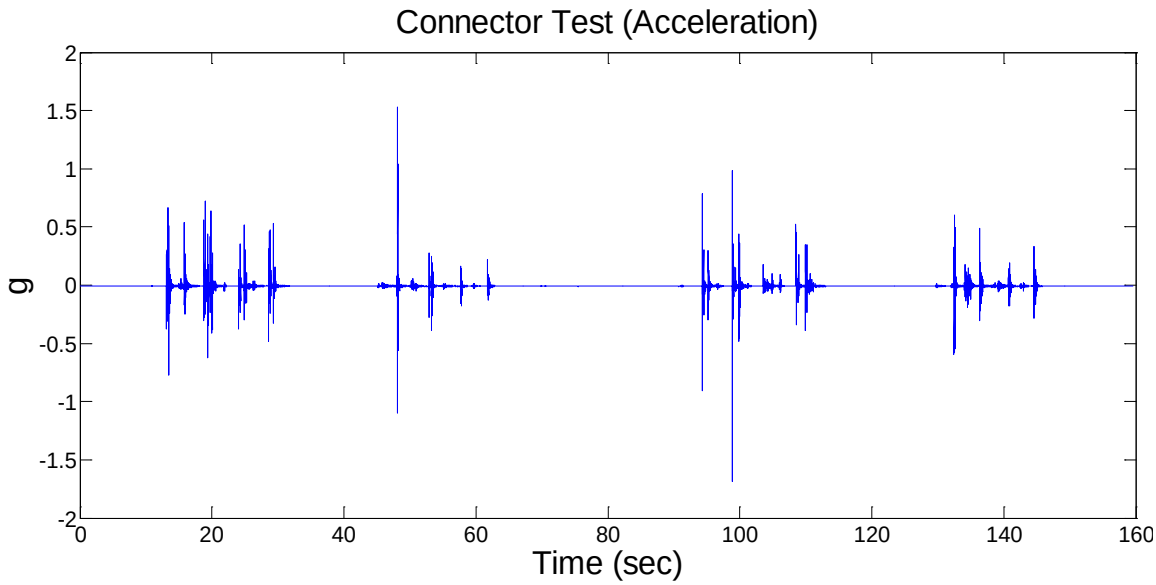

Figure 45: Acceleration Data from Connector Test (with Connector)

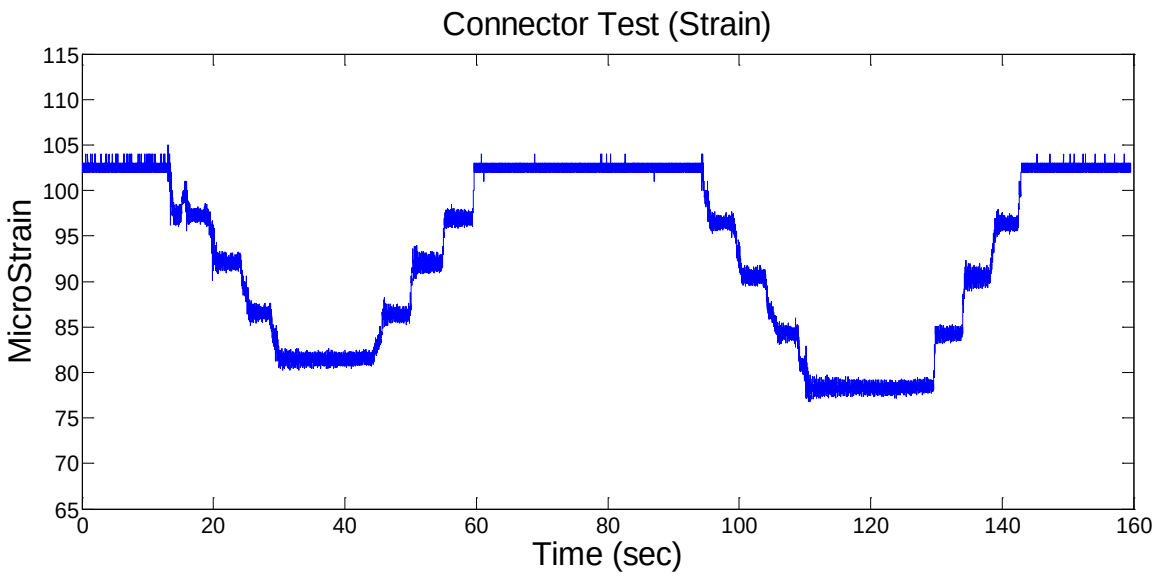

Figure 46: Strain Data from Connector Test (Raw Data for Evaluation)

In addition, the researchers conducted several tests to minimize the noise in the signals. Two filters (100 Hz and 60 Hz) and grounding the cable were employed to reduce the noise level. Totally, 13 tests were conducted on the laboratory beam, which had three strain gages and three accelerometers in the middle span (Figure 38). There were two main setups due to the cables. In the first cable setup, a 30 ft black cable, 150 ft black cable, and a 30 ft sensor wire were compared. In the second cable setup, a 30 ft black cable, a 20 ft grey cable, and sensor wire were compared (Figure 47). In each test, the variables were as follows: power cord nearby, grounding, excitation value, and cable bundled or straight.

Figure 47: Grey Cable (Left), Black Cable (Center), Sensor Wire (Right)

After the laboratory tests preliminary field data was also investigated from the East-North leaf of the Sunrise Blvd. Bridge. For this reason, 4 different data sets were collected. The differences between data sets are the filter values. These studies showed that the noise values were decreased after application of the 100 Hz and 60 Hz filters. It should be noted that the field test includes cable grounding, because in the sensor tests section, it was mentioned that the grounding has an important effect on the noise value.

- Noise Level Tests: In the noise level voltage tests, the National Instrument (NI) system was used to apply a constant voltage to the cable, and this voltage was read from another NI card. From Figure 48 it is seen that although 100 milivolt is applied the readings has 1% error, which is in an acceptable range.

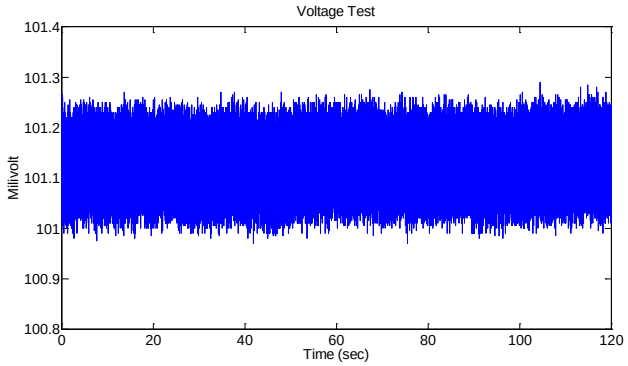

Figure 48: Constant Voltage Data

Before the field trip for the data acquisition system installation, the two computers and National Instrument systems were setup to test communications and simulate the two separate DAQ systems of the bridge. With this test, the wireless connection and synchronization of the systems were evaluated (Figure 49).

Figure 49: Outdoor Testing of Wireless Connection and GPS Synchronization

3.6. Sensor Installation

The sensors on the structural elements were installed with the help of a snooper truck to reach the underneath locations (Figure 50). Figure 51 shows an example picture, showing the installed sensors, such as vibrating wire strain gage, dynamic strain gage, strain rosette and accelerometer, at the live load shoe area. Furthermore, Figure 51 also shows a top view of some of the sensors and a specially designed connector on the bottom flange. Finally, Figure 52 shows the instrumentation with an accelerometer and a rosette gage at the gear box of the mechanical parts. The installation procedure for strain gages and rosette gages was as follows (Figure 53): (1) Grind a small surface area with a grinder, (2) Weld the gages by using Micro-dot welder, (3) Paint the sensors against rust. In Figure 54, a close view of the vibrating wire and dynamic sensors can be seen before and after painting. On the other hand, the installation procedure for accelerometer and tiltmeter was as follows: (1) Grind the surface, (2) Epoxy the gage, (3) Paint the sensor against rust. The tiltmeter installation in the span lock room is shown in Figure 55. Lastly, ampmeters, infrared temperature sensors and microphones were directly installed with epoxy or c-clamps.

Figure 50: Sensor Installation Under the Bridge

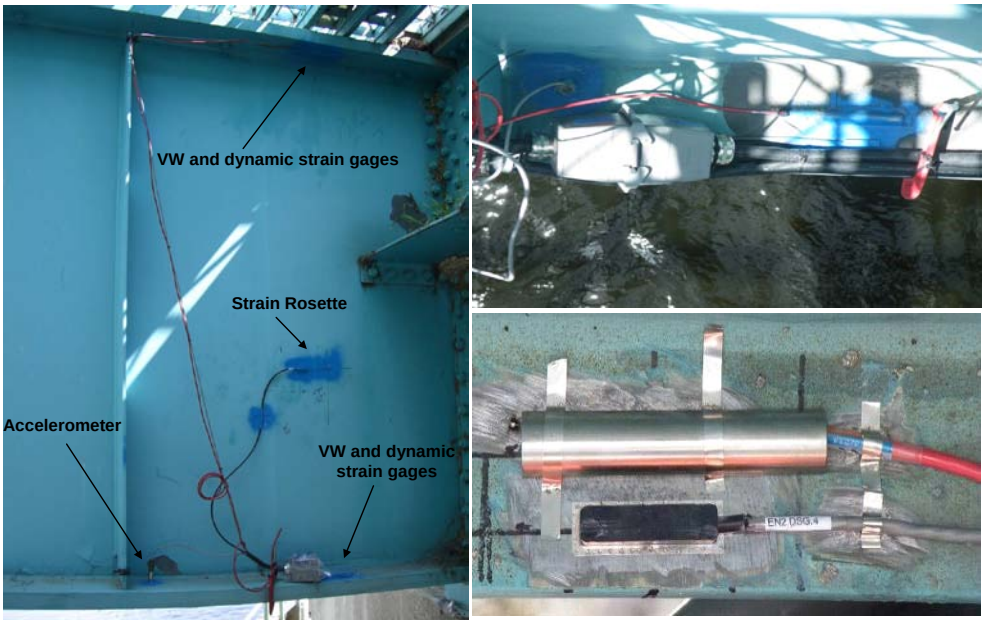

Figure 51: Installed Sensors at the Girder, Specially Designed Connectors, Vibrating Wire and High-speed Strain Gages

Figure 52: Accelerometers at the Gear Box and Strain Rosettes at the Drive Shaft

Figure 53: Strain Gage Installation Steps Under the Bridge: Grinding, Welding and Painting

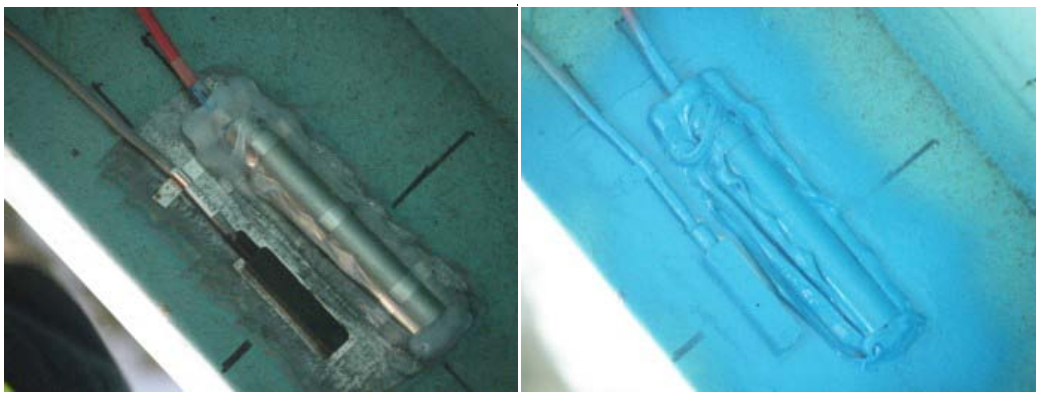

Figure 54: Close View of the Vibrating Wire and Dynamic Strain Gages Before and After Painting

Figure 55: Tiltmeter Installation at the Span Lock Room

3.7. Cabinet Installation

The cabinets were lowered down to mechanical rooms with the help of a snooper truck (Figure 56). In the mechanical room, first their legs were installed to the ground with high strength bolts, and then the cabinets were put on top of them and connected to the legs. Finally the air conditioner was attached to the back of the cabinet (Figure 56).

Figure 56: Moving the Cabinets with Snooper Truck

Figure 57: Cabinet Location and Different Views

3.8. Weather Station and Traffic Camera Installation

The weather station and the traffic camera were installed on top of the traffic light pole on the east north bound of the movable bridge. A lift truck was used for installation (Figure 58). During the installation, the camera view angle and the weather station direction were also set (Figure 59). After these operations, the cables of these systems were run through pipes which were attached to the median side of the bridge.

Figure 58: Installation of the Weather Station and Traffic Camera

Figure 59: Setting of the Weather Station Direction with a Compass

4. NUMERICAL STUDIES

Finite element modeling is used to simulate the behavior of complex systems and overcome experimental limitations in analyzing and predicting the performance of structures. However, even with a good knowledge of the system details and component properties, precise results reflecting the actual behavior are often difficult to obtain. As a result, experimental results from the structure should be used to correctly parameterize the model, thereby to get an accurate simulation of the system behavior.

In this chapter, FE modeling of the Sunrise Blvd. Bridge is carried out. The finite element libraries of modern general-purpose structural analysis software such as SAP2000 offer various options for 3D FE modeling of bridges. Development of a FE model requires attention to the underlying equations for the elements defined to represent structural components. Appropriate finite elements should be used to construct a model with a behavior as similar as possible to the actual structure. Also, discretization, connections, and constraints of the elements are also important for matching the geometric requirements. A thorough inspection and verification stage is crucial to ensure the model has the intended behavior.

In performing SHM on movable bridges, it is especially important that a reliable FE model is developed for various purposes, which can be listed as follows: to develop a sensor instrumentation plan, to establish a structural response level and aid in the selection of sensors, to check and compare sensor readings, to perform a load rating, to have a model for various simulations such as loading cases, repairs, damage and deterioration scenarios. For these purposes, a FE model of the Sunrise Blvd. Bridge was created.

4.1. FE Modeling of Sunrise Bridge

The main objective of this chapter is to present the development of a linear elastic FE model of the Sunrise Blvd. Bridge. The bridge was modeled using SAP2000 software, geometrically representing all critical elements, such that the developed model characterizes the actual bridge as close as possible at local and global levels. The Sunrise Blvd. Bridge and created model can be seen in Figure 60. Information for the bridge can be seen in Figure 60.

For the development of the model, first, one of the main girders was developed by using different mesh sizes to obtain the one giving best performance with a reasonable computation time. Then, the girder was replicated to the other side. The two girders were connected to each other with floor and secondary beams using rigid links. After the equivalent deck was placed, one leaf of the bridge FE model was created. Finally, the leaf was replicated to other side and span lock connections were created to obtain the final bridge model.

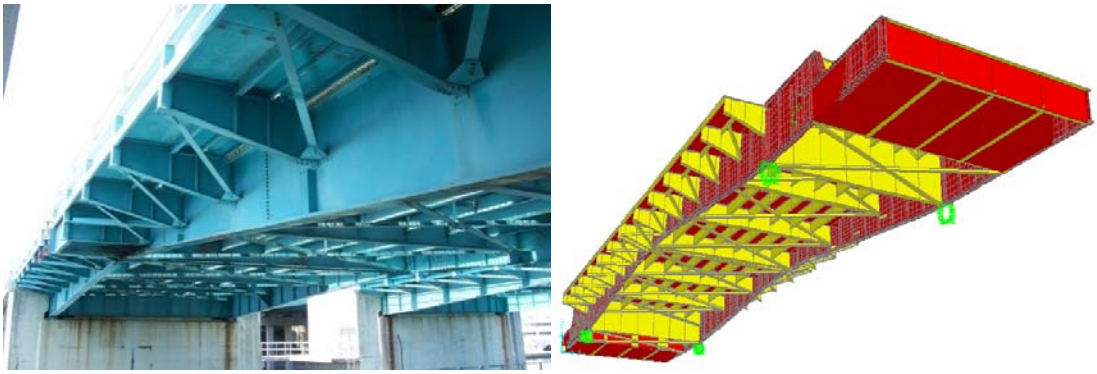

Figure 60: Sunrise Blvd. Bridge (Left) and Created FE Model (Right)

Table 3: Sunrise Boulevard Bridge Information

Bridge ID (NB Span)	Construction Date	No. of Lanes	Span Length (ft)	Deck Width (ft)	FDOT District ID	ADT
860467	1989	3	117	53.3	4	16,000

4.1.1. Mesh Sensitivity Analysis

A mesh sensitivity analysis was conducted on one leaf of the main girder. The main reason for conducting this analysis was to determine a mesh configuration that would yield accurate results without compromising computational efficiency.

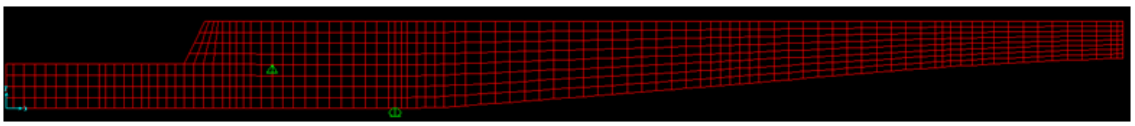

Figure 61: Coarse Mesh of the Main Girder

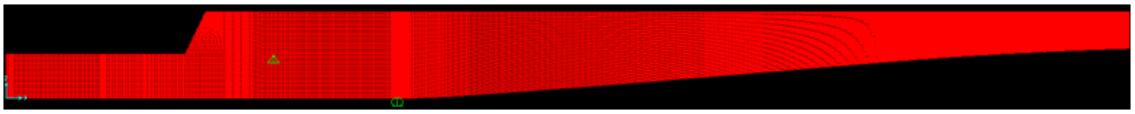

Figure 62: Dense Mesh of the Main Girder

Five different mesh configurations were selected, ranging from 2,300 – 576,500 elements, and two of these configurations can be seen in Figure 61 and Figure 62. The dead load deflection at the tip of the girder was used as the measure of sensitivity. The graphical results for each mesh size configuration from dead load tip deflection analyses can be found in Figure 63. It was concluded that a mesh density of approximately 14400 elements could be used in developing the full-scale finite element models. This conclusion is based on the fact that the absolute error between the least and most dense mesh cases was 0.75% in terms of tip deflection. Therefore, by taking the model creation and computational time in consideration, the course mesh is selected.

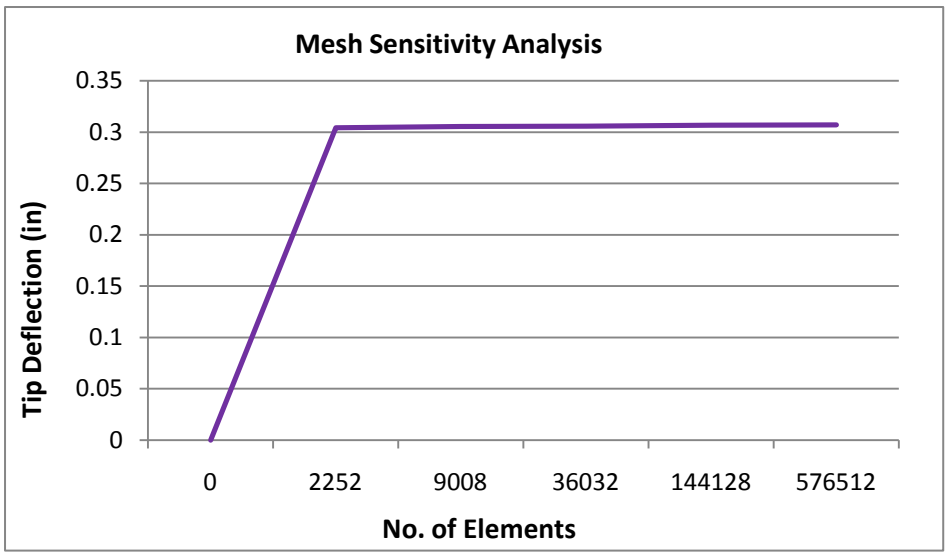

Figure 63: Mesh Sensitivity Analysis for the Main Girder

4.1.2. Equivalent Deck Analysis

Due to the complexity of the deck geometry (Figure 64-Left) on the actual bridge, an equivalent deck was used for the FE models in this study as detailed in a previous report by the authors. The thickness of the deck was calculated based on the field data results as

a parameter for sensitivity for the correlation of model and field data (Catbas et al, 2007). The field data shows that the top flange and bottom flange strain values are close to each other, meaning the neutral axis of the composite section is close to the neutral axis of the main girder alone. In other words, the deck is not fully contributing to the system stiffness. The dead load due to the orthotropic deck is included in the model. The homogenous steel deck (Figure 64-Right) was modeled using a single homogenous steel plate of 0.025 in. thickness and a mass of 17 psf is applied to the nodes of the deck (http://www.idsi.org/open_steel_grid.php).

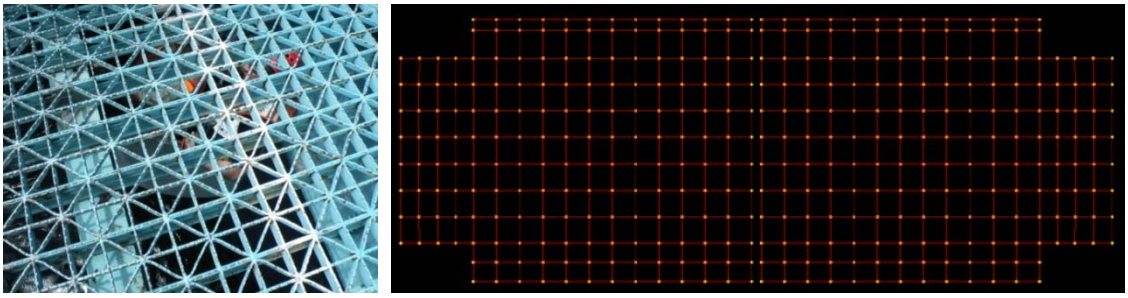

Figure 64: Orthotropic Deck (Left) and Homogenous Steel Plate Deck Model (Right)

4.2. Finite Element Model Development of the Entire Structure

FE Model design and construction was conducted in a systematic manner. Construction plans and details of the Sunrise Bridge (Figure 65) were closely studied prior to FE modeling to ensure a proper modeling of the superstructure. The main components of the bridge superstructure are critical, and were modeled accurately for the local behavior of the deck and secondary beams, as well as the global behavior. In the construction of the FE model, symmetry played a major role for the syntax through which the geometry was created. The first main component of the bridge that was constructed was a single main girder. Once this was created meshing was conducted based on results from the mesh sensitivity analysis. Once the girder was discretized and material properties were assigned, the girder and associated properties were mirrored to create the second main girder of the first leaf. The girders are composed of 4-node quadrilateral elements (approximately 14400 elements per one main girder). To finalized girder construction boundary conditions were imposed at the trunnion and live load shoe locations.

The second main component of the system to be created was the secondary beams, sidewalk and roadway brackets, and diagonal bracing. These components were composed of frame elements. Frame elements were used instead of shells to reduce the complexity and computation time of the model, however, while doing this, some geometric discontinuities between frame-to-frame and frame-to-shell connections developed. This problem was rectified by connecting discontinuous elements with rigid links (multi-point constraints) at the centroids of the frame elements. A single leaf with can be seen in Figure 66.

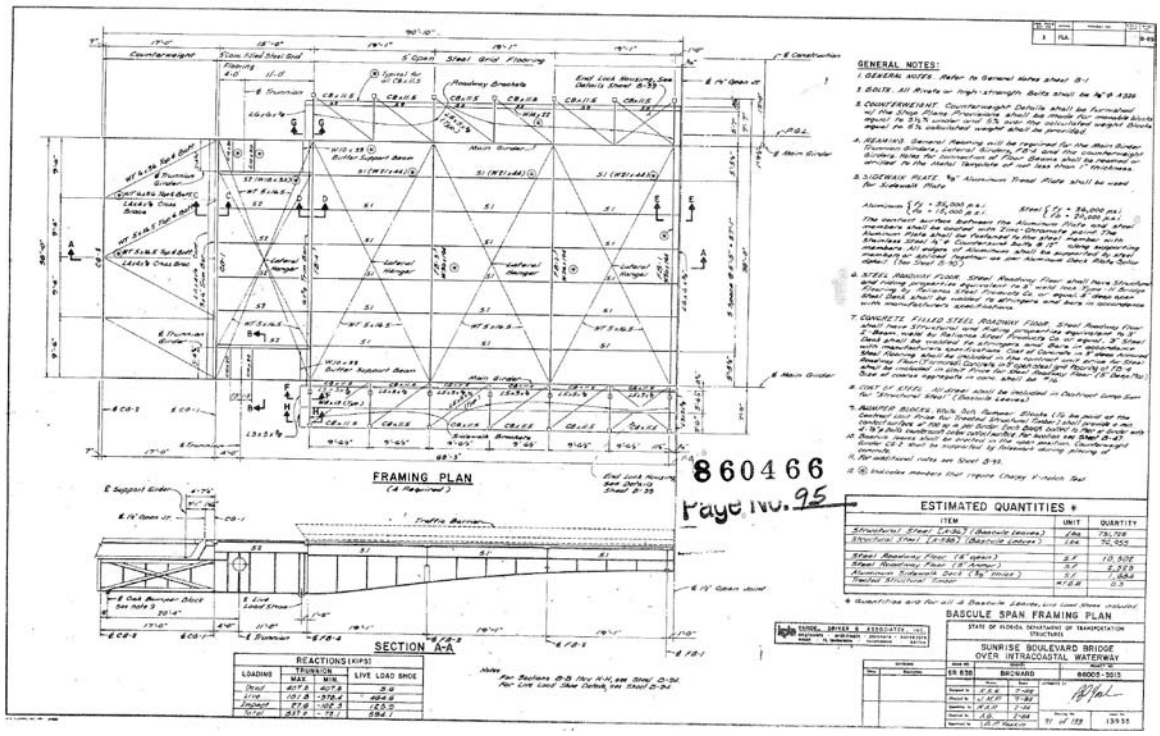

Figure 65: Construction Plans of Sunrise Blvd. Bridge

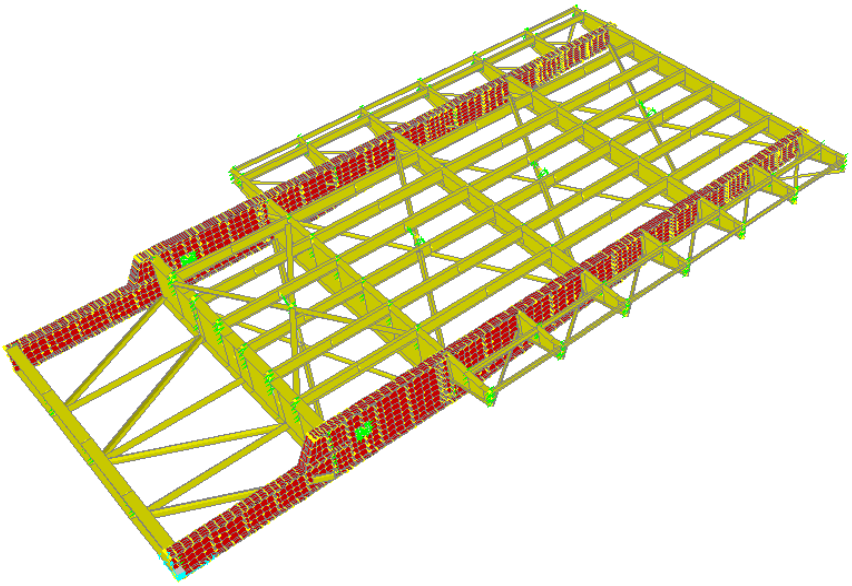

Figure 66: Main Girders, Floor Beams and Stringers of a Single Leaf

Once all secondary beams (both geometry and mesh) were created, the deck for the first leaf of the bridge was constructed. The properties of the deck that were found from the preliminary analysis discussed earlier were employed. The deck was modeled using 4-node quadrilateral elements and connected to the main girders and secondary beams using rigid links. To finalize the completion of the first leaf of the bridge, 8–node brick solid elements were created to model the concrete counterweight.

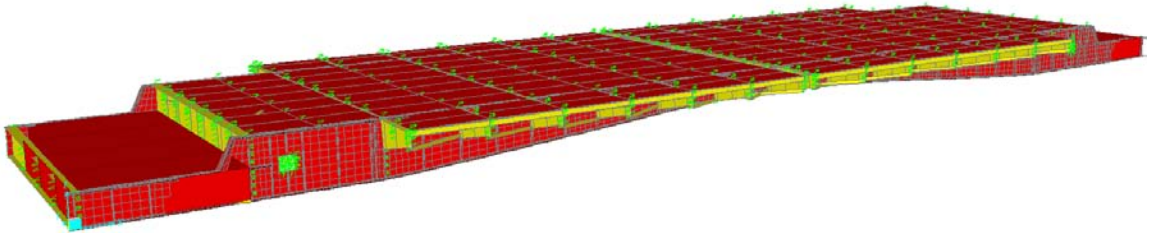

Figure 67: Final Sunrise Blvd. Bridge FE model

After the completion of the full first leaf, the geometry, elements, material properties, and boundary conditions were mirrored about the transverse centerline of the bridge to create the second leaf. The last step in the model construction was the addition of the span locks. These were modeled using multi-point constraints that were free to extend in the longitudinal direction of the bridge and constrained in transverse and vertical

translation assuming a proper functioning span lock. The final model can be seen in Figure 67, whereas Table 4 shows the FE model parameters.

Table 4: FE Model Parameters

FE Model Parameters	
Shells (Q4)	34,240
Frames	518
Rigid Links	1,106
Solids	8
D.O.F.	211,488

4.3. FE Model Verification

4.3.1. Global Verification with Dynamic Data

This section discusses the comparison of the FEM model with monitoring data. Figure 68 shows the first three mode shapes and frequencies for FE model of Sunrise Blvd Bridge.

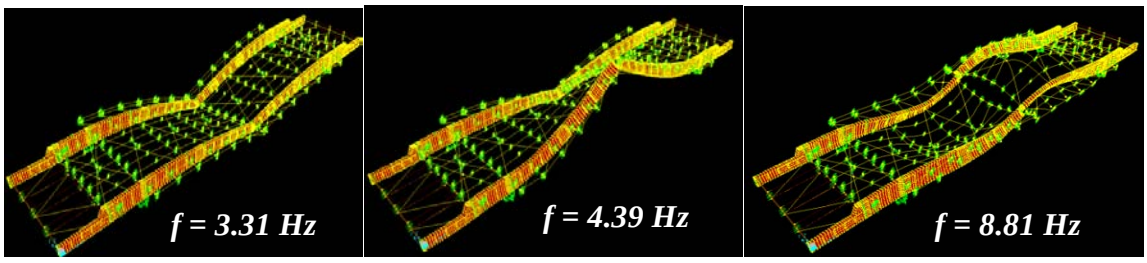

Figure 68: FE Model First Three Mode Shapes and Corresponding Frequencies

The verification of the model using field data was first carried out for the global dynamic properties. This stage was for identifying major issues, such as problems with boundary conditions, continuity conditions, or total mass and its distribution. Ambient vibration test data from accelerometers were collected using 16 sensors that are located at critical locations of the bridge in both vertical and horizontal directions. Based on the preliminary FE analysis results, these sensors can adequately capture the dynamic behavior of the bridge. Sample data sets from the West South main girder are shown in Figure 69.

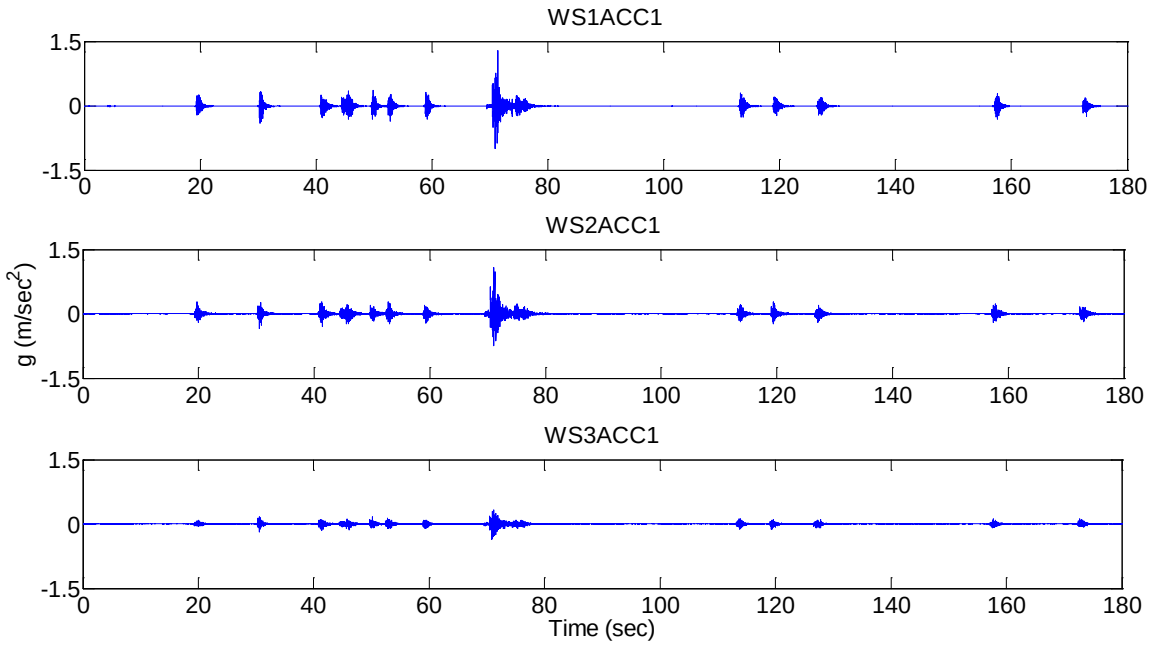

Figure 69: Ambient Acceleration Data from West South Main Girder of the Bridge

The first three natural frequencies of the bridge were identified through an ambient vibration data analysis. In this study, a Complex Mode Indicator Function (CMIF) based modal parameter estimation technique was used, along with the Random Decrement (RD) technique. First, the ambient vibration data was averaged by using RD to obtain un-scaled free response data. Then, the modal parameters were identified with CMIF using the un-scaled free responses. A detailed discussion about the methodology is beyond the scope of this study, and more information can be found in (Catbas et al, 2010). The modal parameters identified from the field data and the first three modes of the FE model are presented in Table 5. The comparison of the dynamic results shows that the FE model can capture the global behavior of the structure quite satisfactorily. The model can be calibrated and further improved to obtain a better match with the field data, however this was not investigated in the current phase of the study, as the current correlation was deemed quite satisfactory. These results also verified the consistency of the field data, although it is noted, that data quality can be improved with future investigations with higher resolution sensors, improved cabling, connections, higher dynamic range data acquisition systems with dedicated A/D converters, etc. After checking the global

dynamic behavior of the model, localized comparisons were conducted by using strain data as explained in the next sections.

Table 5: FE Model and Field Data Modal Frequency Results

Mode #	Field Data (Hz)	FE Model (Hz)
1	3.54	3.42
2	5.13	4.57
3	9.28	9.09

4.3.2. Local Verification

After the global verification of the FE model another important part was the local verification, which had two main steps. The first step was the operational verification, which considered the strain changes due to the dead load of the structure during the opening and closing of the leaves. The second step was the traffic induced strain comparison with the help of the traffic camera.

As for the first local behavior comparison, the strains developed at the live load shoe area during opening and closing were compared for field and FE model data. The location of this sensor was the East South main girder live load shoe (ES3), and it is shown in Figure 70. Figure 71 shows data collected during the opening and closing of the bridge at the East South main girder live load shoe (ES3). The corresponding strain variation for the upper flange was 164 microstrains, whereas it was 127 microstrains for lower flange. Then, opening and closing were also simulated in FE model, and the strains developed for each case were recorded, as shown in the right side of Figure 71. The strain variation for the upper flange was 156 microstrains which was 5% different from the experimental data. While for the lower flange, it was 132 microstrains, which was 4% different from the experimental data. These results again indicated that FE model agrees well with experimental data for this simulation.

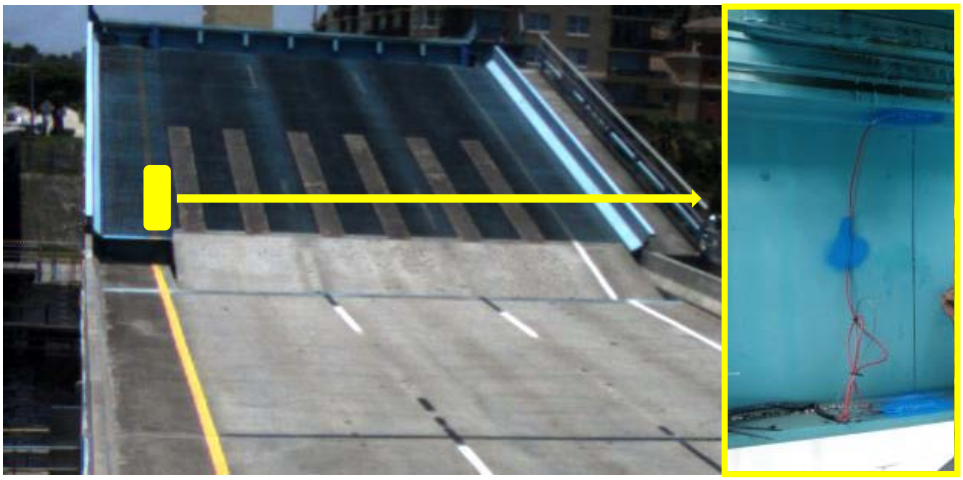

Figure 70: East South Main Girder Live Load Shoe Strain Gage Location

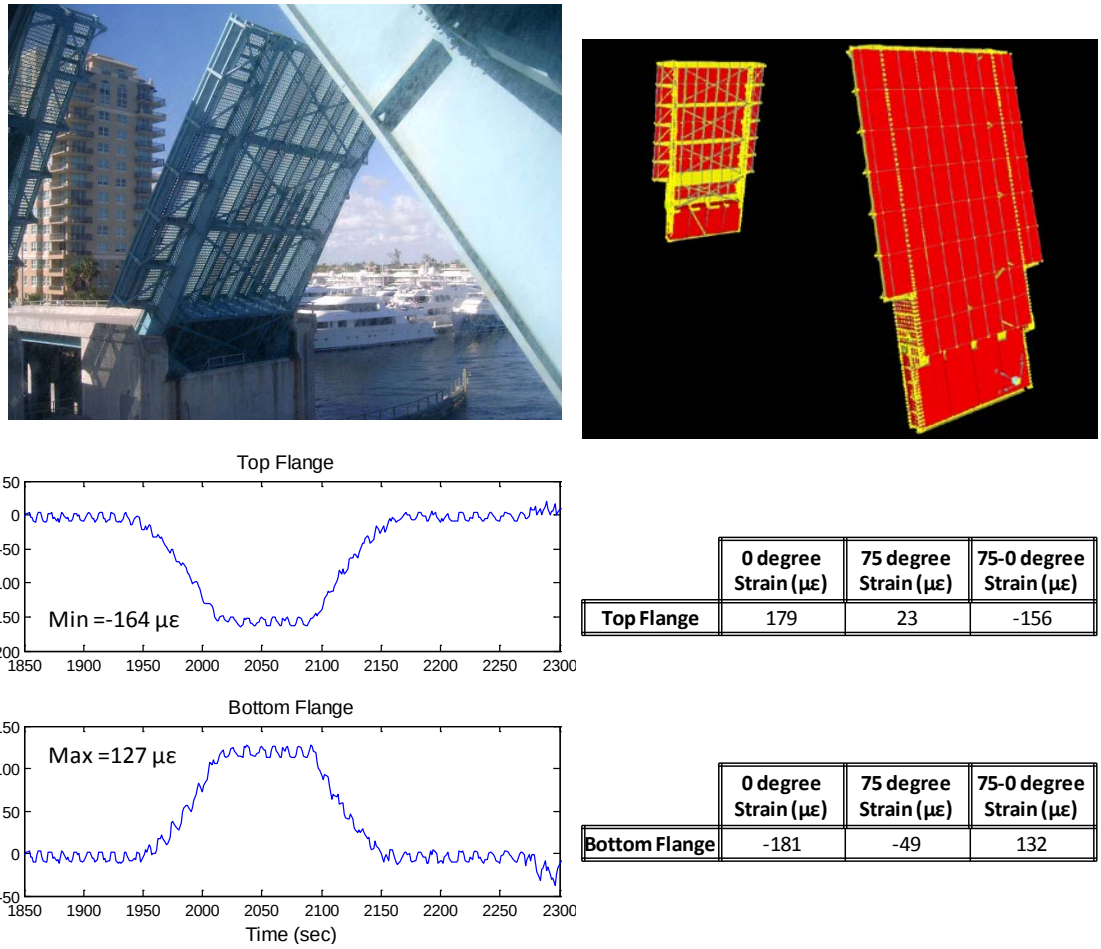

	0 degree Strain (με)	75 degree Strain (με)	75-0 degree Strain (με)
Top Flange	179	23	-156

	0 degree Strain (με)	75 degree Strain (με)	75-0 degree Strain (με)
Bottom Flange	-181	-49	132

Figure 71: Opening and Closing Strains at ES3 (Experimental and Analytical)

As for the second local behavior comparison, traffic induced strain data was collected at different locations including the live load shoes, span locks, floor beams and different sections of the main girders. Here, the data coming from the live load shoes (support area) is presented since the effect of the traffic loading is mostly the highest in these locations. The location of this sensor is the East North main girder live load shoe and shown in Figure 72.

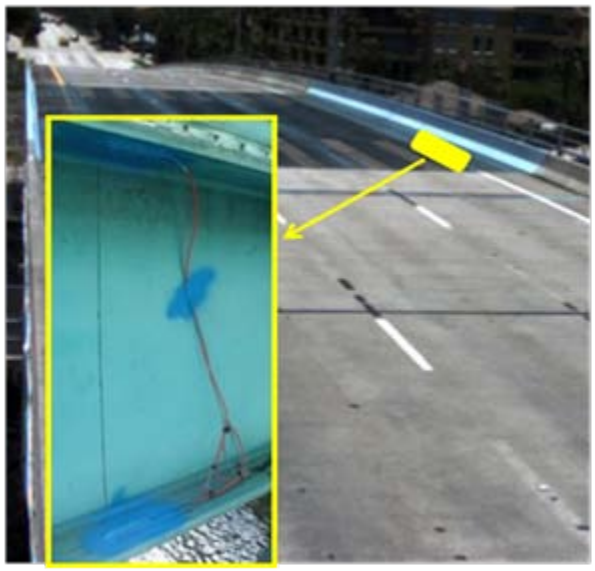

Figure 72: East North Main Girder Live Load Shoe Strain Gage Location

To complete the strain comparison, the video images were used to find a pre-defined vehicle. A Riverside Transit Agency (RTA) bus was utilized for this study. A detailed discussion of using the RTA bus was presented by the authors at TRB meeting in 2010 (Catbas et al, 2010). The properties of the bus were identified and were incorporated in the FE model to simulate the behavior of the model under this vehicle. The drawing of the bus and its basic properties are shown in Figure 73.

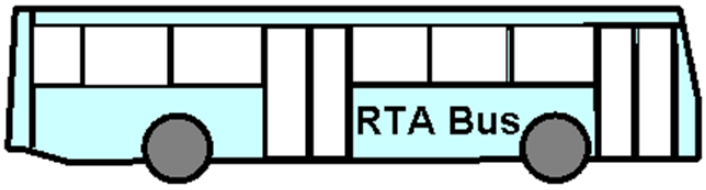

Overall Vehicle Length	40ft 7in
Overall Vehicle Width	8ft 6in
Front Axle to Front Bumper	7ft 7in
Rear Axle to Rear Bumper	10ft 3in

Vehicle Gross Weight	40600lbs
Weight at Front Axle	14600lbs
Weight at Rear Axle	26000lbs
Note: Gross includes passengers	

Figure 73: Typical RTA Bus and Basic Properties

The effect of the RTA bus was simulated in the FE model by applying point loads corresponding to the wheels of the bus as illustrated in Figure 74. The left part of Figure 74 shows the bus crossing the bridge, and the right part of Figure 74 shows the response of the simulated RTA bus using the FE model. It should be noted that the x-axis for the left side of the figure is time in seconds and for the right side of the figure is in meters. A good consistency between the response of the FE model and real structure was observed. The maximum response developed for the upper flange was 57 microstrains, while the calculated strain in FE model for the same flange was 60 microstrains. Similarly, the maximum response developed for the lower flange was -64 microstrains, while the calculated strain in FE model for the same flange was -65 microstrains. The difference between the measured and calculated strain for upper flange was 5% and for the lower flange was 1%. These results indicated that generated FE model is in good agreement with actual bridge data for localized strain measurements as well.

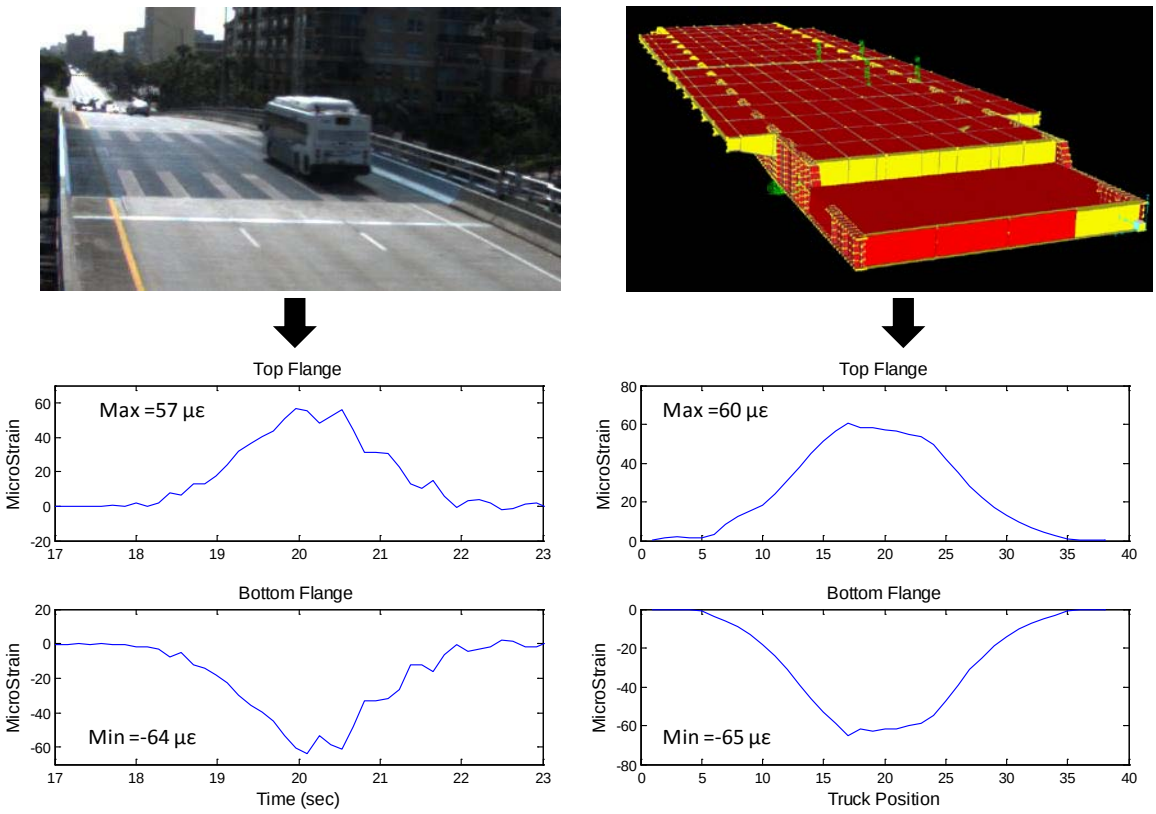

Figure 74: The Effect of Typical RTA Bus on EN3 (Experimental and Analytical)

These preliminary studies, which include global and local comparisons, showed that the nominal FE model was acceptable for other simulations such as load rating, repair, and rehabilitation. Therefore, this model will also be used for Load Rating calculations in Chapter 5.

5. CONTROLLED STATIC AND MOVING TRUCK LOAD TEST

5.1. Objectives of the Load Tests

Load tests are commonly employed to better understand the performance of new bridges compared to design predictions. In addition, these tests are also conducted to achieve a better understanding of the bridges response under known loading conditions, and to validate and/or calibrate Finite Element Model (FEM) results. These models can be used for load rating also. In regard to load ratings, load tests can be used to verify both component and system performance under a known live load and to provide an alternative evaluation methodology to analytically computing the load rating of a bridge as given in AASHTO Manual.

For this project, both static and dynamic load tests were performed in collaboration with FDOT Engineers. The primary objectives of the static diagnostic load tests executed in this project were to establish stress levels on various structural elements of the bridge, to validate the FEM, and to obtain load rating of the bridge using the FEM. In general terms, these tests were conducted by recording measurements of known loads, and their corresponding effects on critical bridge members, and comparing these measured load effects with analytical model computed values. More details of this procedure will be presented in following sections. The dynamic load tests can be used to determine the dynamic load allowance and live load stress ranges under crawl speed crossing of the bridge. In addition, these tests can also be used in a manner similar to vibration tests, where the dynamic characteristics, such as frequencies of vibration, mode shapes, and damping can be determined.

5.2. Test Design and Execution

Details regarding the specifications of the load test vehicle used in testing, loading configuration of the truck, load cases with pre-determined placements, and data collection considerations will be discussed in the following. The load testing design process should ensure not only proper collection of data and smooth testing execution, but also the safety of the bridge, personnel, and public.

5.2.1. Trucks and Testing Configurations

The load truck selected for load testing was provided by FDOT Structures Laboratory in Tallahassee and operated by FDOT personnel. The UCF team coordinated the truckload test with FDOT engineers and personnel before and during the execution of the tests. The data collection was carried out with the monitoring system that was already in place. The load test truck has a variety of loading configuration to fit the needs of each particular bridge. For this project, a full truck loading configuration with concrete block loading was selected. A twenty-four (24) block load was selected with a total vehicle weight of 96.7 kips (Figure 75).

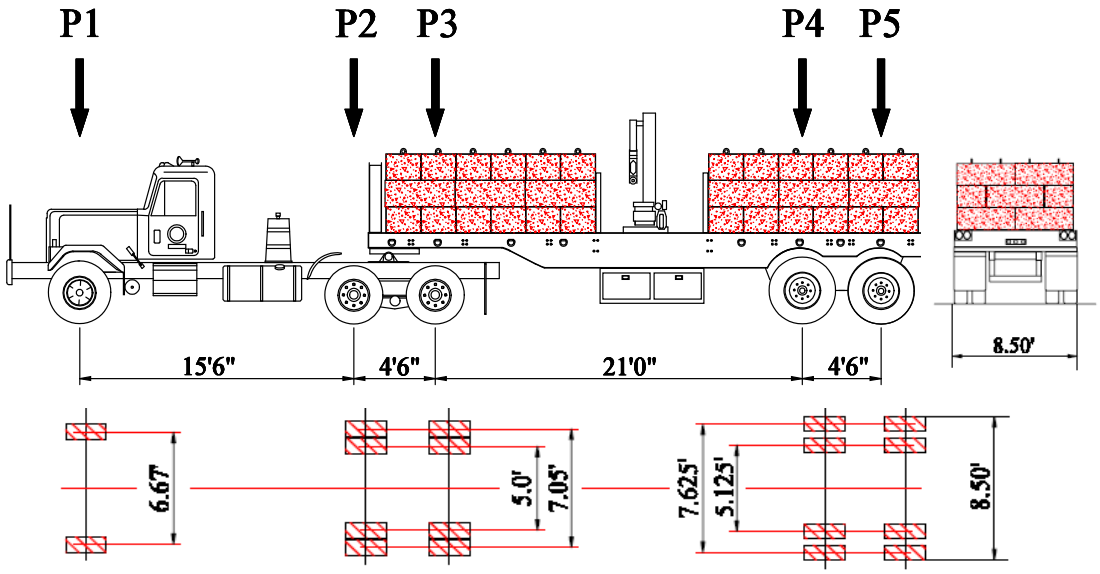

Description of Loads	Front Axle P1 (Kips)	Front Tandem		Rear Tandem	
		P2 (Kips)	P3 (Kips)	P4 (Kips)	P5 (Kips)
24 Blocks	11.60	19.51	19.51	23.04	23.04

Figure 75: Selected Load Testing Truck Load Configuration

The FE model was utilized to verify that truck load tests would not create any nonlinear effect by yielding the structure. At the same time, the load level had to be selected that the loaded truck load would be sufficiently high to ensure reliable measurements. As a result, the FE model played an important role in the design of the load levels and patterns to safely and accurately test the bridge.

Three separate load tests were performed: a static load test, a crawl speed load test, and a dynamic load test, in order to capture the bridge behavior in a comprehensive manner and create a database for possible studies, such as influence line generation, dynamic allowance factors, and more reliable calibration of analytical models. The Sunrise Bridge Northern leaves (West bound bridge) were considered for load testing. The following notation is used: Right Lane-Lane 1, Middle Lane-Lane 2, and Left Lane-Lane 3. Details of the executed test configurations are presented below.

Static Load Test

The static load test was designed to ensure that the test load be placed at a variety of locations to ensure measurement of the response in all critical bridge members. Three separate static test configurations were executed two times each: Lane-1: (11 Load Cases), Lane-2: (11 Load Cases), and Lane-3: (11 Load Cases).

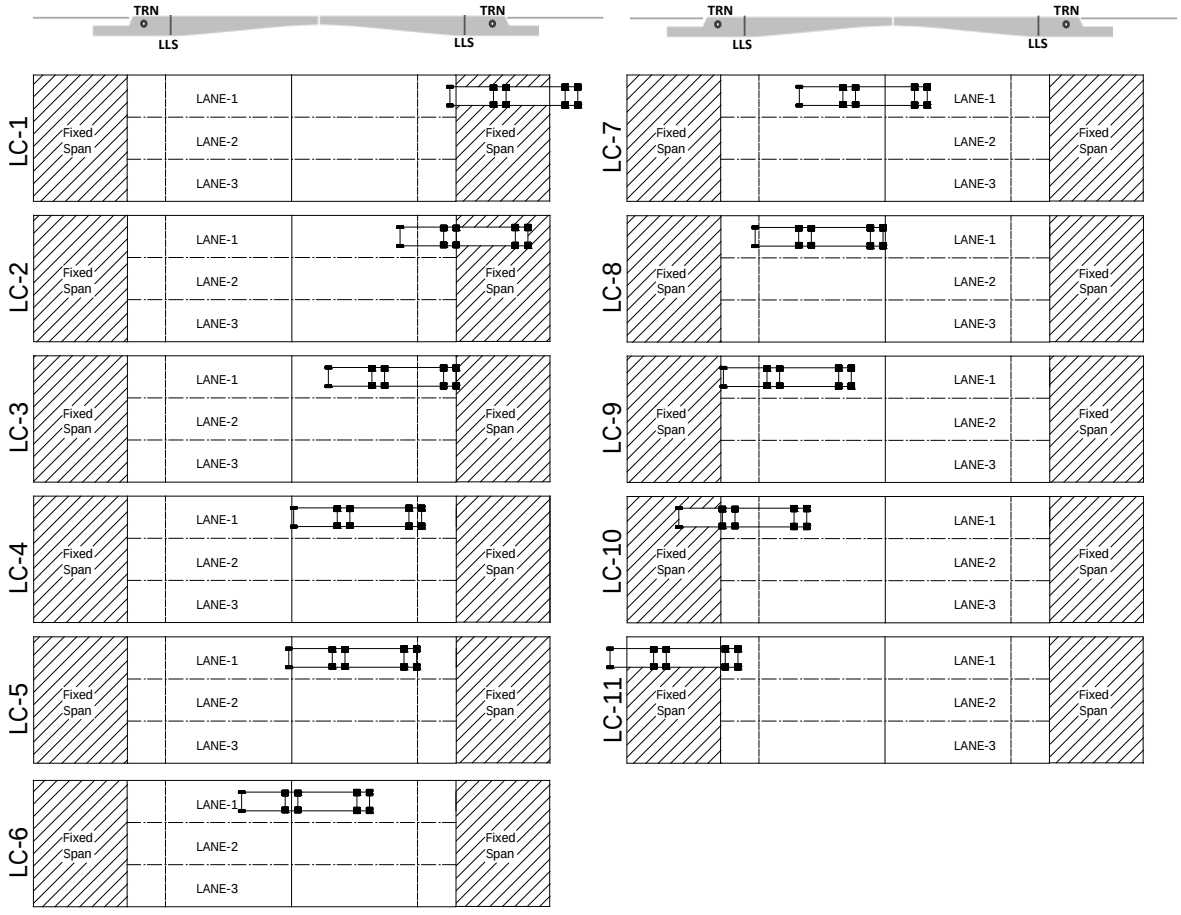

Figure 76: Static Load Test: Lane 1 (Right Lane) Test Configuration

The eleven (11) static load positions shown in Figure 76 were selected to correspond to unique load placements.

Crawl Speed Load Test

The crawl speed load test was designed to ensure that each of the design lanes experienced separate vehicle loading. The three separate static test configurations executed two times each were: Lane-1: Crawl, Lane-2: Crawl, and Lane-3: Crawl.

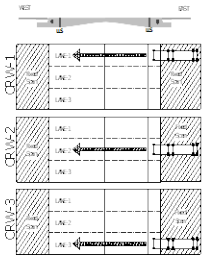

Figure 77: Crawl Test: Lane 1, 2, and 3 Testing Configurations

Dynamic Load Test (Using 2x4 & Front Axles on the Bridge):

Three separate dynamic test configurations were executed two times each: Lane-1: Dynamic, Lane-2: Dynamic, and Lane-3: Dynamic as shown in the following:

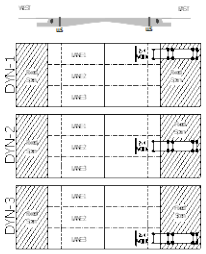

Figure 78: Dynamic Load Test: Lane 1, 2, and 3 Testing Configurations

5.2.2. Execution of the Tests

All load tests were executed from 9:00 PM, Friday, December 11, 2009 through 3:00 AM, Saturday, December 12, 2009. These times were selected to cause a minimal traffic impact.

Data was collected and recorded during load testing through synchronized correspondence with team members located at the DAQ cabinets and members who were on the bridge. Shown below, in Figure 79 is an example of the strain measurements recorded from a location along the main girder.

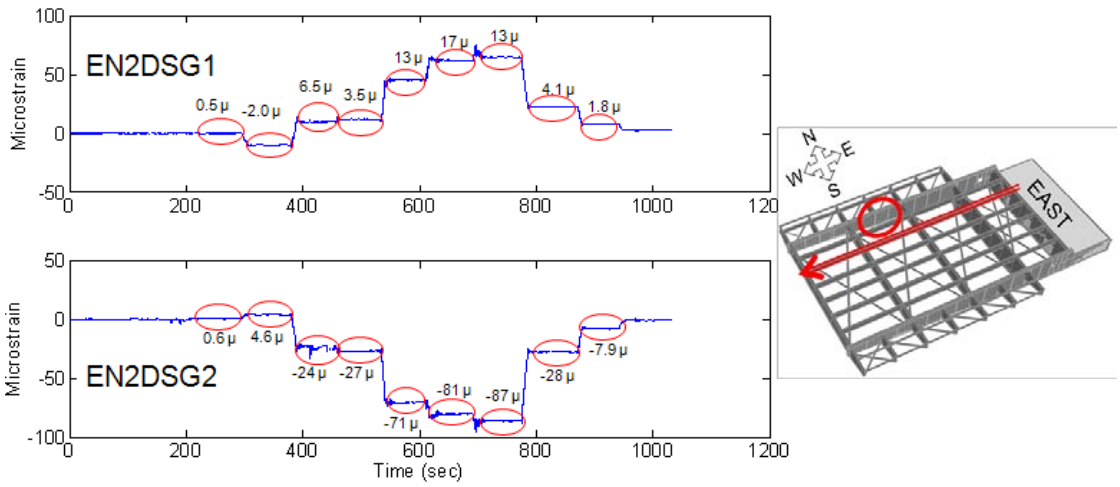

Figure 79: Static Load Test Sample Data Set

5.3. Correlation with Finite Element Model

One of the main objectives of load testing in this project was to provide additional data for the verification of the FE model and data for calculating design load ratings based on experimental studies. The first step of this process was to compare experimental data with the analytical counterparts. First, the strain readings along the main girders were selected for comparison purposes. The FE model previously discussed was loaded with the load test truck, with load placements corresponding to the load cases (Figure 80).

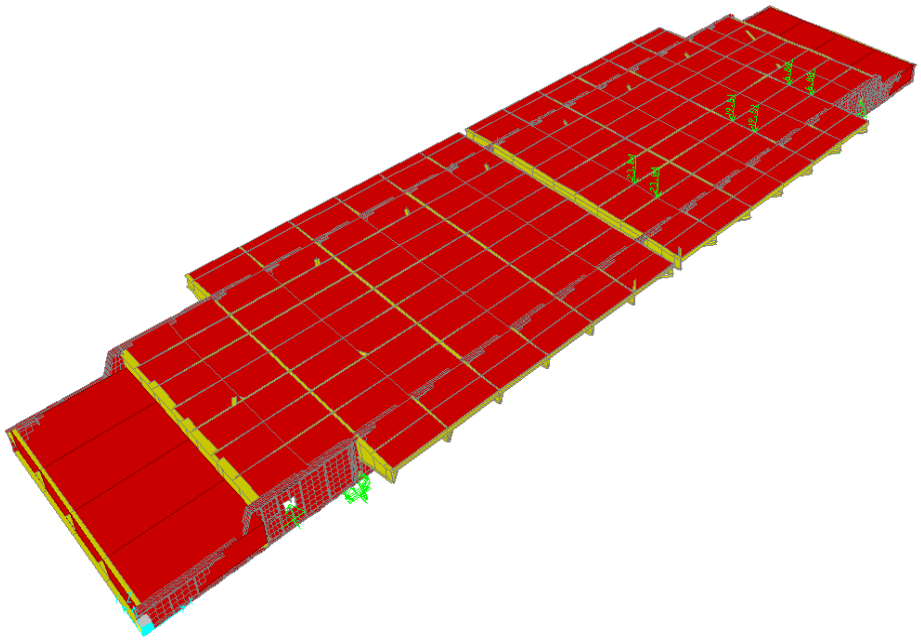

Figure 80: Representative Diagram of FE Model Load Truck

As in the dead load cases during opening and closing of the bridge, as well as the RTA bus loading, comparison of analytical and experimental strain values corresponding to the same static load test cases revealed that the FE model was quite reasonably representing the actual bridge response. The main girders of bascule bridges exhibit cantilever beam characteristics due to the counterweight near the live load shoe and a span lock connection at the leaf tips. Therefore, the internal stresses in the main girders are a maximum at the live load shoe locations and decrease to a minimum at the leaf tip locations. The stresses at each location along the main girder were determined for both the FE model load truck cases and the experimental load truck cases. Comparison of these results for the three most critical loading configurations (LC-6, LC-7 and LC-8, for each lane) are shown in following figures. Figure 81, Figure 82, and Figure 83 are for LC-6 in the right, middle, and left lanes, respectively. Figure 84, Figure 85, and Figure 86 are for LC-7 in the right, middle, and left lanes, respectively. While Figure 87, Figure 88, and Figure 89 are for LC-8 in the right, middle, and left lanes, respectively.

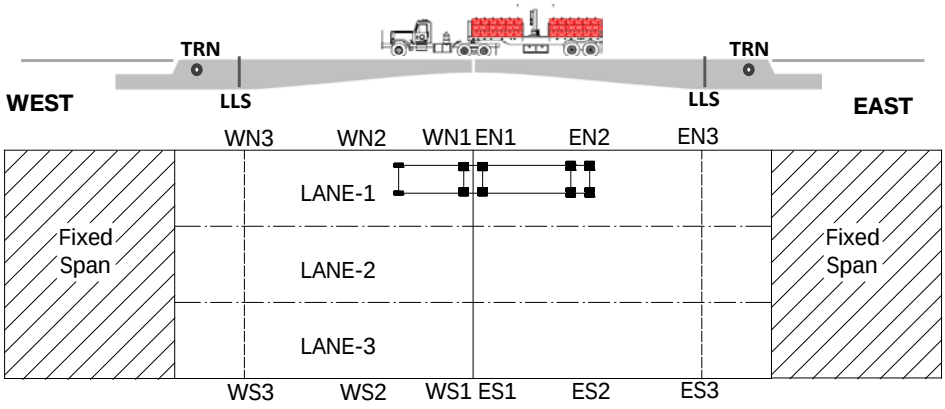

Sensor	*FE*	*Exp*	*Sensor*	*FE*	*Exp*	*Sensor*	*FE*	*Exp*	*Sensor*	*FE*	*Exp*
ES1DSG1	1	NA	EN1DSG1	-2	13	WS1DSG1	1	-1	WN1DSG1	1	-2
ES1DSG2	-4	-2.9	EN1DSG2	-5	-11	WS1DSG2	-10	-22	WN1DSG2	-5	NA
ES2DSG1	23	23	EN2DSG1	46	44	WS2DSG1	29	32	WN2DSG1	72	63
ES2DSG2	-35	-39	EN2DSG2	-70	-71	WS2DSG2	-44	-41	WN2DSG2	-108	-85
ES3DSG1	49	54	EN3DSG1	152	132	WS3DSG1	40	NA	WN3DSG1	117	105
ES3DSG2	-52	-55	EN3DSG2	-161	-136	WS3DSG2	-46	-42	WN3DSG2	-136	-118

Figure 81: FE Model and Experimental Strain Comparison of LC-6 on Right Lane

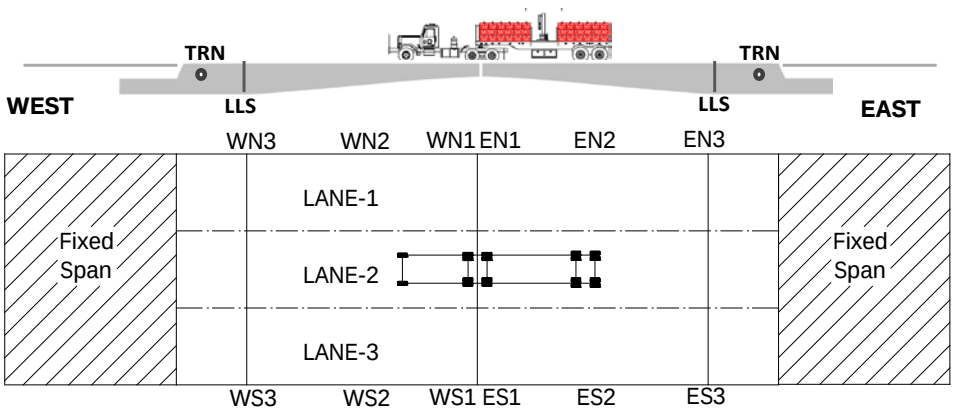

Sensor	*FE*	*Exp*	*Sensor*	*FE*	*Exp*	*Sensor*	*FE*	*Exp*	*Sensor*	*FE*	*Exp*
ES1DSG1	-1	NA	EN1DSG1	1	11	WS1DSG1	1	-6	WN1DSG1	1	-1
ES1DSG2	-10	-10	EN1DSG2	-4	-4	WS1DSG2	-14	-25	WN1DSG2	-8	NA
ES2DSG1	45	46	EN2DSG1	29	28	WS2DSG1	64	63	WN2DSG1	40	40
ES2DSG2	-63	-62	EN2DSG2	-45	-47	WS2DSG2	-92	-75	WN2DSG2	-60	-56
ES3DSG1	125	107	EN3DSG1	75	77	WS3DSG1	98	NA	WN3DSG1	61	65
ES3DSG2	-133	-116	EN3DSG2	-79	-80	WS3DSG2	-114	-94	WN3DSG2	-70	-71

Figure 82: FE Model and Experimental Strain Comparison of LC-6 on Middle Lane

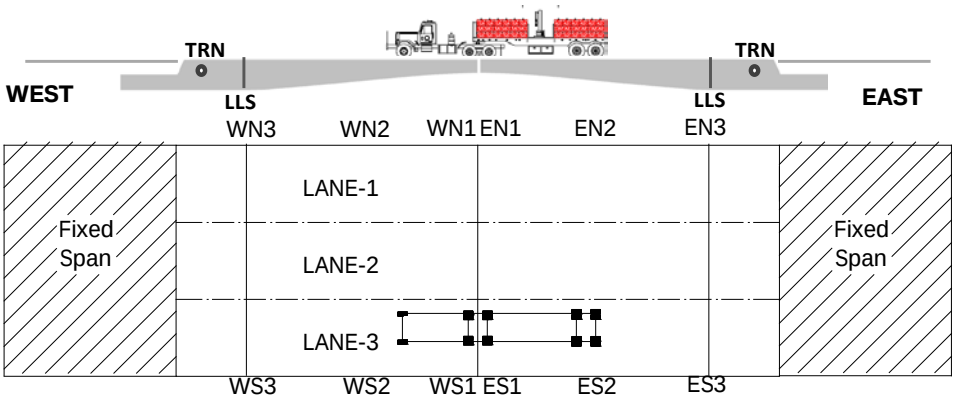

Sensor	*FE*	*Exp*	*Sensor*	*FE*	*Exp*	*Sensor*	*FE*	*Exp*	*Sensor*	*FE*	*Exp*
ES1DSG1	-5	NA	EN1DSG1	1	2.3	WS1DSG1	3	-11	WN1DSG1	3	5
ES1DSG2	2	-4	EN1DSG2	-4	5.5	WS1DSG2	-11	-23	WN1DSG2	-7	NA
ES2DSG1	50	66	EN2DSG1	15	9.8	WS2DSG1	88	94	WN2DSG1	16	13
ES2DSG2	-73	-79	EN2DSG2	-23	-23	WS2DSG2	-125	-107	WN2DSG2	-27	-22
ES3DSG1	179	159	EN3DSG1	23	18	WS3DSG1	136	NA	WN3DSG1	21	24
ES3DSG2	-190	-183	EN3DSG2	-22	-21	WS3DSG2	-158	-146	WN3DSG2	-22	-17

Figure 83: FE Model and Experimental Strain Comparison of LC-6 on Left Lane

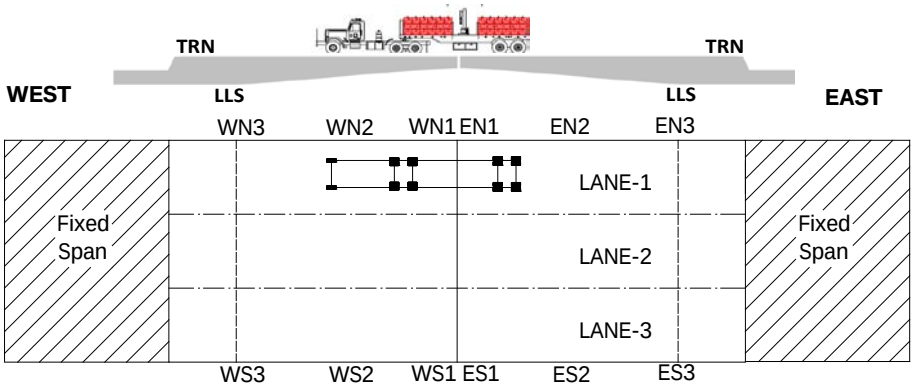

Sensor	*FE*	*Exp*	*Sensor*	*FE*	*Exp*	*Sensor*	*FE*	*Exp*	*Sensor*	*FE*	*Exp*
ES1DSG1	2	NA	EN1DSG1	-15	17	WS1DSG1	1	-3	WN1DSG1	-4	-14
ES1DSG2	-5	-2	EN1DSG2	-7	-21	WS1DSG2	-8	-16	WN1DSG2	-7	NA
ES2DSG1	28	30	EN2DSG1	65	61	WS2DSG1	25	25	WN2DSG1	54	54
ES2DSG2	-39	-40	EN2DSG2	-87	-81	WS2DSG2	-40	-40	WN2DSG2	-88	-76
ES3DSG1	45	49	EN3DSG1	136	122	WS3DSG1	46	NA	WN3DSG1	141	116
ES3DSG2	-49	-53	EN3DSG2	-146	-133	WS3DSG2	-52	-47	WN3DSG2	-164	-128

Figure 84: FE Model and Experimental Strain Comparison of LC-7 on Right Lane

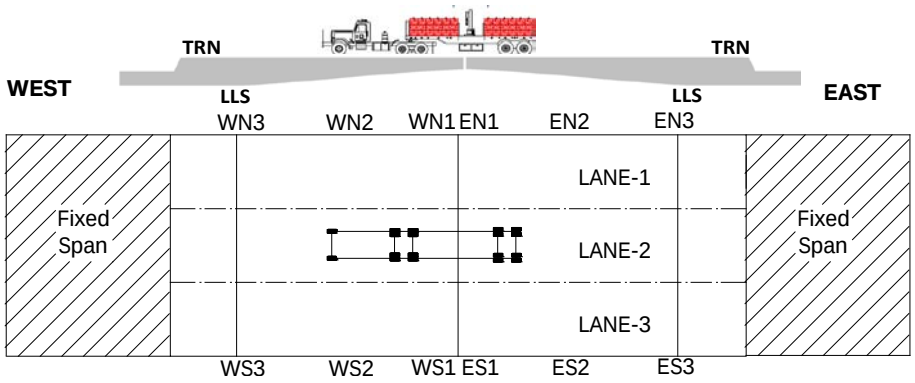

Sensor	*FE*	*Exp*	*Sensor*	*FE*	*Exp*	*Sensor*	*FE*	*Exp*	*Sensor*	*FE*	*Exp*
ES1DSG1	2	NA	EN1DSG1	2	13	WS1DSG1	-1	-10	WN1DSG1	-1	-5
ES1DSG2	-17	-15	EN1DSG2	-5	-5	WS1DSG2	-9	-8	WN1DSG2	-6	NA
ES2DSG1	59	59	EN2DSG1	37	37	WS2DSG1	51	62	WN2DSG1	33	32
ES2DSG2	-76	-70	EN2DSG2	-52	-52	WS2DSG2	-77	-69	WN2DSG2	-52	-50
ES3DSG1	113	97	EN3DSG1	69	74	WS3DSG1	117	NA	WN3DSG1	72	75
ES3DSG2	-122	-112	EN3DSG2	-74	-77	WS3DSG2	-136	-103	WN3DSG2	-79	-75

Figure 85: FE Model and Experimental Strain Comparison of LC-7 on Middle Lane

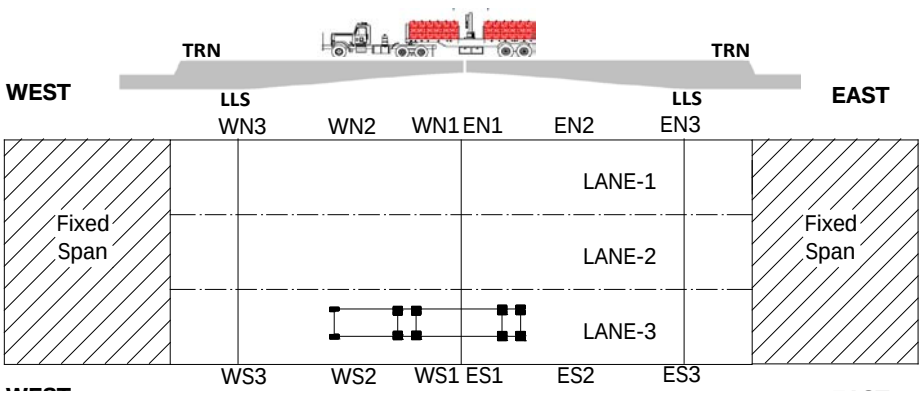

Sensor	*FE*	*Exp*	*Sensor*	*FE*	*Exp*	*Sensor*	*FE*	*Exp*	*Sensor*	*FE*	*Exp*
ES1DSG1	-3	NA	EN1DSG1	2	3	WS1DSG1	-5	-13	WN1DSG1	2	3
ES1DSG2	-11	-9	EN1DSG2	-7	-6	WS1DSG2	-2	4	WN1DSG2	-6	NA
ES2DSG1	83	92	EN2DSG1	17	13	WS2DSG1	67	85	WN2DSG1	15	11
ES2DSG2	-101	-97	EN2DSG2	-25	-23	WS2DSG2	-99	-95	WN2DSG2	-26	-22
ES3DSG1	158	145	EN3DSG1	22	15	WS3DSG1	170	NA	WN3DSG1	23	27
ES3DSG2	-170	-170	EN3DSG2	-22	-21	WS3DSG2	-192	-168	WN3DSG2	-24	-18

Figure 86: FE Model and Experimental Strain Comparison of LC-7 on Left Lane

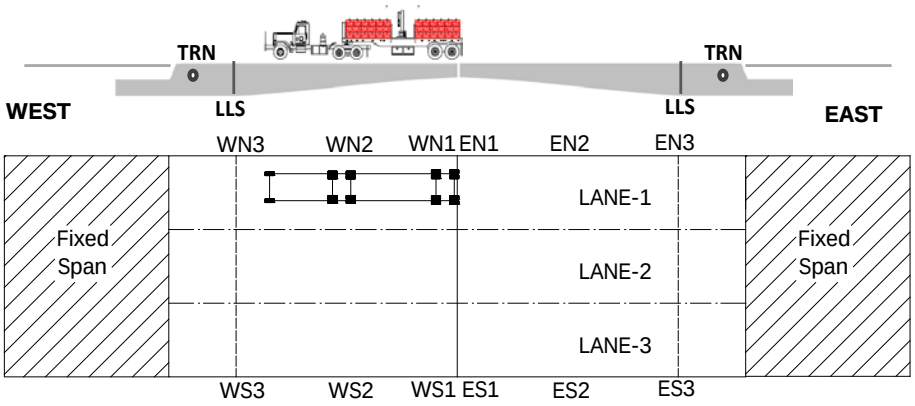

Sensor	*FE*	*Ex.*	*Sensor*	*FE*	*Exp*	*Sensor*	*FE*	*Exp*	*Sensor*	*FE*	*Exp*
ES1DSG1	5	NA	EN1DSG1	15	12	WS1DSG1	-3	-14	WN1DSG1	-11	-28
ES1DSG2	-8	-1	EN1DSG2	-14	-15	WS1DSG2	-8	-15	WN1DSG2	6	NA
ES2DSG1	31	32	EN2DSG1	81	61	WS2DSG1	20	20	WN2DSG1	41	42
ES2DSG2	-41	-38	EN2DSG2	-102	-87	WS2DSG2	-36	-37	WN2DSG2	-73	-69
ES3DSG1	35	35	EN3DSG1	102	94	WS3DSG1	49	NA	WN3DSG1	155	125
ES3DSG2	-39	-39	EN3DSG2	-111	-102	WS3DSG2	-54	-48	WN3DSG2	-178	-132

Figure 87: FE Model and Experimental Strain Comparison of LC-8 on Right Lane

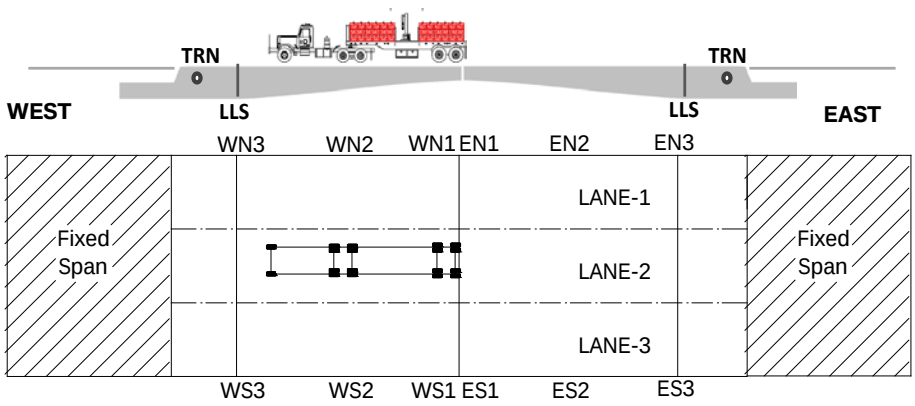

Sensor	*FE*	*Exp*	*Sensor*	*FE*	*Exp*	*Sensor*	*FE*	*Exp*	*Sensor*	*FE*	*Exp*
ES1DSG1	*5*	*NA*	*EN1DSG1*	*7*	*6*	*WS1DSG1*	*-9*	*-29*	*WN1DSG1*	*-5*	*-19*
ES1DSG2	*-10*	*-11*	*EN1DSG2*	*-10*	*-3*	*WS1DSG2*	*-7*	*-6*	*WN1DSG2*	*-8*	*NA*
ES2DSG1	*69*	*63*	*EN2DSG1*	*43*	*38*	*WS2DSG1*	*40*	*42*	*WN2DSG1*	*26*	*26*
ES2DSG2	*-87*	*-71*	*EN2DSG2*	*-56*	*-53*	*WS2DSG2*	*-66*	*-61*	*WN2DSG2*	*-46*	*-46*
ES3DSG1	*85*	*72*	*EN2DSG3*	*53*	*56*	*WS2DSG3*	*127*	*NA*	*WN1DSG1*	*77*	*80*
ES3DSG2	*-93*	*-86*	*EN3DSG2*	*-58*	*-59*	*WS3DSG2*	*-145*	*-106*	*WN3DSG2*	*-83*	*-78*

Figure 88: FE Model and Experimental Strain Comparison of LC-8 on Middle Lane

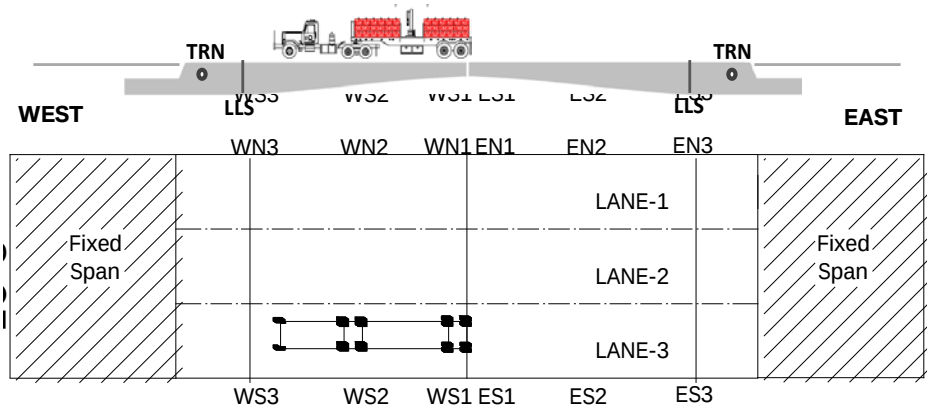

Sensor	*FE*	*Exp*	*Sensor*	*FE*	*Exp*	*Sensor*	*FE*	*Exp*	*Sensor*	*FE*	*Exp*
ES1DSG1	5	NA	EN1DSG1	-1	-1	WS1DSG1	-14	-14	WN1DSG1	2	3
ES1DSG2	-15	-17	EN1DSG2	-7	7	WS1DSG2	14	15	WN1DSG2	-7	NA
ES2DSG1	95	95	EN2DSG1	18	12	WS2DSG1	47	62	WN2DSG1	13	10
ES2DSG2	-117	-103	EN2DSG2	-25	-21	WS2DSG2	-74	-74	WN2DSG2	-24	-22
ES3DSG1	118	110	EN3DSG1	19	24	WS3DSG1	188	NA	WN3DSG1	24	31
ES3DSG2	-132	-131	EN3DSG2	-20	-15	WS3DSG2	-211	-174	WN3DSG2	-24	-19

Figure 89: FE Model and Experimental Strain Comparison of LC-8 on Left Lane

In the above figure(s), the distribution of stresses along the main girder is shown. At the live load shoe locations, the critical locations for bending stresses, the FEM and experimental strain results showed a reasonable level of correlation. These results indicated that the FEM was in good agreement with the actual bridge localized strain measurements. There are some variations, especially at the high stress locations, which can be attributed to finite element mesh size, load discretization on the FE model, and uncertainties on load placement to create the highest load. In addition, the stiffness contribution from the orthotropic deck system is not uniform, as seen in the FE model development. While these can be further refined to obtain a close correlation, the current model was successful in representing the measured behavior and mostly slightly conservative where there are variations.

5.4. Load Rating

5.4.1. Overview

Load rating of a bridge is the process of determining the safe live load carrying capacity of a new or existing vehicular bridge. Load ratings represent a quantitative measure of identifying the need for load posting and/or bridge strengthening, as well as in making overweight-vehicle permit decisions. The final load rating represents the rating of the weakest point of the weakest member within the bridge. The National Bridge Inspection Standards (NBIS) requires the state highway departments to inspect, prepare reports and determine/update the load ratings for all bridges. The load rating process is a component of the inspection process which is conducted in a regular inspection cycle or if any relevant changes in bridge condition occur. There are four ratings methods: Allowable stress rating (ASR), Load Factor Rating (LFR), Load and Resistance Factor Rating (LRFR), and Load Testing. In this project, the AASHTO *Guide Manual for Condition Evaluation and Load and Resistance Factor Rating (LRFR) of Highway Bridges* (hereafter *the Manual*) is used. It should be noted that load testing is used with the LRFR method in this project and this procedure is outlined in Chapter 8 of the Manual. The Florida Department of Transportation (FDOT) requires that the load ratings for existing bridges be performed using the LF, load test, or the LRFR methods. Much like the LRFD formulations for limit states, the LFRD method includes factors, which will be determined based on the load rating procedure and bridge specifications.

5.5. Types

Load ratings can be subdivided into 3 load-rating procedures: Design load rating (first level evaluation), legal load rating (second level evaluation), and permit load rating (third level evaluation). Depending on the load rating needed, it may not be necessary to perform each of the load rating procedures. For comprehensive purposes each of the 3 load-rating procedures will be briefly described, however, the design load ratings are the only ones provided in this report.

The design load rating assesses the performance of existing bridges utilizing the LRFD design HL-93 loading. It can serve as a screening process to identify bridges that should be load rated for legal loads. The design load rating can be performed at one of two levels: Inventory and/or Operating Level. The, higher level, inventory level design load rating is performed at the same design level reliability adopted for new bridges. A bridge that passes the design load check at the Inventory level will have a satisfactory load rating for all legal loads. The operating level design load rating is performed at a lower reliability which is comparable to the Operating level reliability inherent in past load-rating practices.

The legal load rating is a second level rating and is for bridges that do not have sufficient capacity under the design-load rating. Legal load rating establishes whether there is a need for load posting or strengthening. It determines the safe load capacity of a bridge for the AASHTO family of legal loads and State legal loads, using safety and serviceability criteria considered appropriate for evaluation.

The permit load rating checks the safety and serviceability of bridges in the review of permit applications for the passage of vehicles above the legally established weight limits. Since this is a third level rating it should only be applied to bridges having sufficient capacity for AASHTO legal loads.

5.6. General Equation

The load rating is expressed as a single rating factor, RF. The following equation from *the Manual* may be used in determining the load rating of each component or connection subject to a single force effect:

where “C” is the factored load carrying capacity, “DC” is the dead load of structural components, “DW” is the dead load of the wearing surface, “P” is a dead load concentrated at single point, “LL” is the live load effect, “IM” is the impact factor, and “γ”s are the safety factors. The load factors change according to the type of load rating, i.e., inventory load rating or operating load rating.

5.7. Load Rating with Finite Element Model

The most common method for determining a load rating for a bridge is through an analytical method utilizing a simple model. Examples using the most common, beam-line analysis method, are available in the literature. These simple model methods, while varied, commonly result in conservative load ratings. If these theoretical rating calculations result in a required posting of the bridge or restriction to permit vehicles, more accurate 3D models may be developed. For this project, a complex FEM had already been developed and therefore was the ideal model for determining theoretical load ratings. Using this FEM, an analysis was made to determine the inventory and operating level load ratings for the bridge. This procedure will be described below and these load rating values will updated based on experimental load test data.

The general equation for determining the load rating was expressed previously (see Eqn. 1). In simplified terms, the rating factor can be thought of as being composed of three terms: Capacity, Dead Load Demand, and Live Load Demand. The design-load rating was calculated for all of the most critical components of the bridge to determine the weakest/governing element. Due to symmetry, only the sections of one leaf were analyzed. In addition, the West South main girder consistently showed the largest strain values during application of lane loads, therefore, only the West South (WS) main girder and associated load ratings will be shown. The 11 critical element sections which were used to compute the load rating were: the LLS area on the main girder, the main girder at the center floor beam (FB) intersection, the main girder at the tip FB intersection, the mid-span point of the tip and center floor beams, and the mid-span points of 6 of the center stringers. Figure 90 shows the members and section locations used for computation of the load ratings. Therefore, the capacities, dead load effects, and live load effects were determined at these locations to compute load ratings.

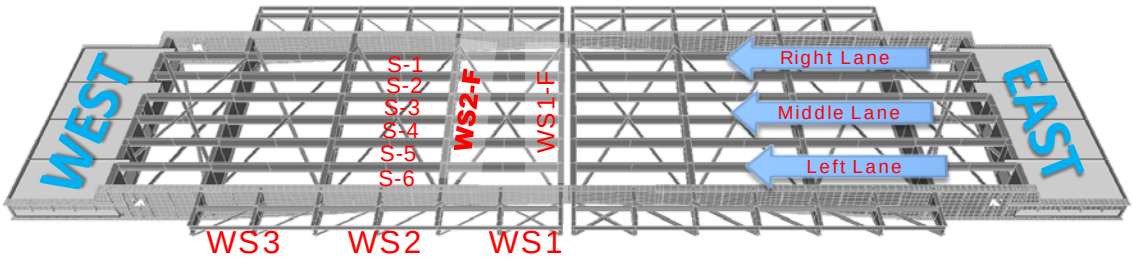

Figure 90: Members and Section Locations Used for Load Rating

5.7.1. Dead and Live Load Modeling

The procedure for calculating the design-load rating using a FEM is similar to standard analytical methods. The main difference is that strain values from the critical locations are used to determine dead load and live load effects. For the design-load rating, the HL-93 load was applied to the FEM. It should be noted that, unlike traditional beam-line methods, application of the HL-93 load to a FEM is not as prescribed in nature. In the beam-line method, the typical loading for a flexure critical member is 1-Dimensional, and is the superposition of a 0.64 kip/ft design lane load and a HS-20 truck. In the case of a FEM, application of these loads is 3-Dimensional in nature, and therefore a method for representing the AASHTO defined loads must be selected. Based on private discussions with consulting bridge engineers, it is also seen that implementation of truck loads on FE modes vary from case to case, and based on the assumptions and justifications. In this study, three FEM loading configurations were selected. AASHTO allows for more accurate loading configurations to be used when more advanced modeling methods are used. Therefore, it was determined that representation of multiple design trucks on the FEM were to be considered. The three truck design loaded configuration provided the highest loading, although the likelihood of three trucks side-by-side, for the most critical loading, is the lowest. The transverse cross-section of the deck (Figure 91) shows the location of the lanes and axle position for the three HL-93 design truck loading cases selected for determination of design-load ratings.

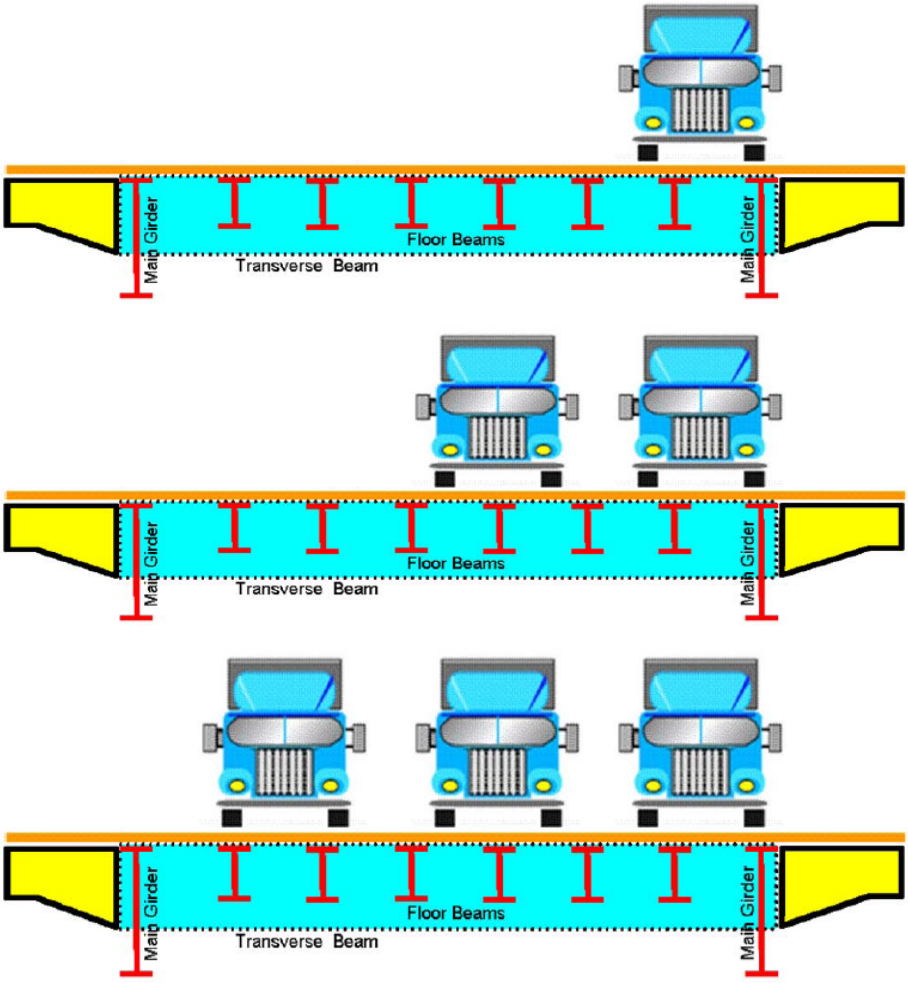

Figure 91: HL-93 Load Cases Applied to Bridge

Axle loads were defined as individual point loads corresponding to the HS-20 truck, as described in the AASHTO code. The yield strength of the steel was taken as 36.0 ksi and a dynamic impact factor of 33% was used for both inventory and operating ratings.

Since the main girder is tapered, the critical truck configuration was not easy to locate. As a result, a moving load simulation was conducted to determine the load ratings as a function of truck location. It was seen that the cross-section at the live load shoe (Location-C) was more critical than the sections at Location-A and Location-B due to cantilever type configuration of the movable bridges (Figure 92). Location-A, Location-B and Location-C are the same for each of the four main girders.

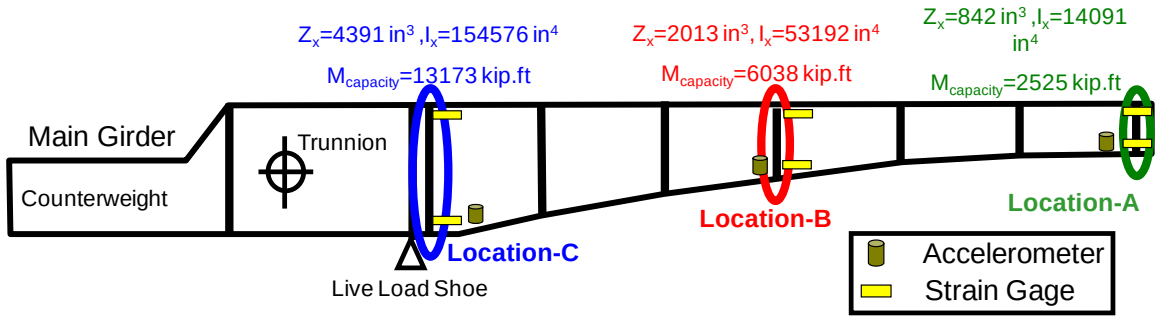

Figure 92: Main Girder Locations A, B, and C

5.7.2. Design-Load Rating

For steel bridges the Manual requires that the Strength I and Service II load combinations be checked for design loading. In this study Strength I limit state governs, and therefore will be the only combination shown. The process for calculating the design-load rating will be shown for the main girder at the LLS location with the loading case of the HL-93 loaded on the left lane only. However, the load ratings for the other sections and HL-93 on the left and middle lanes, as well as HL-93 on all lanes were also computed. Since the main girders were modeled as shell elements the main girder load rating calculations first required conversion of strain values to internal moments, which was not necessary for the floor beams and stringers.

First, the maximum dead load strain value at Location C was found and converted to a dead load moment demand using a combination of the stress-strain relationship. The equation for the normal stress of a beam in pure bending is shown below (Eqn. 2). It should be noted that pure bending in this case is a conservative assumption by taking the largest strain of the girder for the dead load and live load demands.

_____

where ε = maximum strain value, I = moment of inertia, E = modulus of elasticity of steel, and c = d/2. Inserting the values at location C and solving yields:

_____ __

Similarly, the maximum live load strain value at Location C was found and converted to a live load moment demand using Eqn. 4.

The capacity of the section at Location C was calculated based on the ultimate moment capacity, which can be obtained by multiplication of the yield strength (F_y) and plastic section modulus (Z_x).

The applicable load factors from the *Manual* Table 6-1 are summarized below.

Table 6: Applicable Load Factors

Load Factor (γ)	**Design Live Load**		**Permit LL**
	Inventory	**Operating**	
DC	1.25	1.25	1.25
LL+IM	1.75	1.35	1.15

Inventory Level

Since the current condition of the bridge is not known, a good or satisfactory condition, $\varphi_c = 1.0$, was assumed. The system factor for the main girders and floor beams was selected from the Manual Table 6-3 as $\varphi_s = 0.85$, due to the each leaf having only two girders and welded members. A system factor of 1.0 was used for the stringers. Solving Eqn. 1 for the Flexure rating factor:

Since this inventory RF >1 then the bridge will have a satisfactory load rating for all legal loads.

Operating Level

Using the operating level load factors and solving Eqn. 1 for the Flexure rating factor:

This same procedure was done for the other critical locations and the results are shown below. The main girder section at the LLS (WS3) had the minimum load ratings, and therefore, this location will be used as the governing load rating location for the bridge.

Table 7: FEM Load Ratings Summary for 3 Loading Cases

Location	Inventory Load Rating (HL-93 All Lanes)	Operating Load Rating (HL-93 All Lanes)
Main Girder-WS3	***1.17***	***1.52***
Main Girder-WS2	1.59	2.06
Main Girder-WS1	4.88	6.33
Floor Beam-WS1-F	1.83	2.37
Floor Beam-WS2-F	2.36	3.06
Stringers-S1	2.56	3.32
Stringers-S2	2.33	3.02
Stringers-S3	4.03	5.23
Stringers-S4	2.64	3.42
Stringers-S5	2.38	3.08
Stringers-S6	2.49	3.23

This same procedure was done for the HL-93 in left and middle lanes, as well as HL-93 in all lanes (Figure 91) and the results are shown below.

Table 8: FEM Load Ratings Summary for 3 Loading Cases

Loading Case (Main Girder-WS3)	FEM Design Load Rating	
	Inventory	Operating
HL-93 Left Lane	2.32	3.00
HL-93 Left + Middle Lanes	1.36	1.76
HL-93 All Lanes	1.17	1.52

5.8. Load Rating with Experimental Data

In this section, a procedure given in the *Manual* will be described along with its objectives and drawbacks. Assessment of the differences between predicted and measured responses is a major part of diagnostic testing. Based on this comparison the analytically calculated load rating can be modified. The *Manual* equation used to modify the calculated load rating following a diagnostic test is:

where RF_T = the load-rating factor for the live-load capacity based on the load test result, RF_c = the rating factor based on calculations prior to incorporating test results, K = adjustment factor resulting from comparison of measured test behavior with the analytical model. The adjustment factor, K, is given by:

where: K_b accounts for the understanding of the load tests results when compared with those predicted by theory (in this case K_b =1.0) and K_a is provided by the general expression:

—

where: ε_T = maximum member strain measured during the load test and ε_c = corresponding calculated strain due to the test vehicle, at its position on the bridge which produced ε_T.

Since K_b =1.0, the adjustment factor K is dependent upon the relationship between ε_T = maximum member strain measured during the load test and ε_c = corresponding calculated strain due to the test vehicle, at its position on the bridge which produced ε_T. The value of ε_T was selected from a graphical representation of the raw data from the load test left lane loading case. The maximum strain value was on the bottom flange at Location C of the East South girder, ε_T = -183 με. The corresponding calculated strain due to the test vehicle, at its position on the bridge which produced ε_T was ε_c = -190 με. The value K_a can then be calculated from:

———

The adjustment factor, K is then:

The analytically determined design-load ratings were then adjusted based on the results of the load testing by multiplying the adjustment factor K by the previously determined load ratings. A comparison of these results is summarized in the table below.

Table 9- Experimental Adjusted Load Ratings

Loading Case (Main Girder-WS3)	Experimentally Adjusted FEM Design Load Rating	
	Inventory	Operating
HL-93 Left Lane	2.41	3.11
HL-93 Left + Middle Lanes	1.41	1.83
HL-93 All Lanes	1.21	1.58

The main drawback of this approach is that it does not fully consider the uncertainties of experimentally measuring strain along a small gage length and scaling analytical results with respect to this measurement.

5.9. Summary of the Results

While it is often true that the real structure offers more live load capacity than that is calculated based on theory and a model, caution should be used when applying a K factor to adjust analytically determined load ratings. It can be seen from the above calculations that the adjustment to the analytical load rating is based solely on a single ratio of experimental vs. analytical strain values from the critical location on the structure. Both stress and strain, however, are localized in nature; capable of varying greatly in short distances. Therefore, it is possible that the critical location yields a very non-conservative, large, K factor, while the rest of the structure yield conservative, small, K factors. The experimental strain measurement is also highly dependent on placement and installation of the strain gage. With this said, a more accurate representation of the load rating would likely be achieved through using all of the experimentally collected data to further calibrate a FEM, and then use this model to determine load ratings. In this study, both procedures were conducted, and all locations demonstrated good correspondence of FEM and experimental strain values. As a result, the calculated K factor from the critical location was quite small and had little impact on the adjustment of the load rating. This is shown in Table 10. Based on these results, the Sunrise Bridge has an acceptable load rating at inventory level, even with all three lanes loaded with a HL-93 design load. It is the author's opinion that the FEM Design Load Rating values are to be used for the Sunrise Bridge. Based on the load rating results of Sunrise Bridge, which is a

representative bridge in terms of geometry and condition, it should be also concluded that such bridges provide sufficient live load carrying capacity, even for the highly unlikely 3 lanes simultaneously loaded with the most critical truck loading cases, when they are maintained properly, deterioration is minimized, and all boundary and continuity conditions function as expected.

Table 10- Experimental Adjusted Load Ratings vs. FEM Load Ratings Comparison

Loading Case (Main Girder-WS3)	**FEM Design Load Rating**		**Experimentally Adjusted FEM Design Load Rating**	
	Inventory	**Operating**	**Inventory**	**Operating**
HL-93 Left Lane	2.32	3.00	2.41	3.11
HL-93 Left + Middle Lanes	1.36	1.76	1.41	1.83
HL-93 All Lanes	1.17	1.52	1.21	1.58

6. DATA ANALYSIS APPROACHES FOR MAINTENANCE AND OPERATION

6.1. Introduction

The monitoring of the Sunrise Bridge is quite comprehensive in the sense that structural, mechanical and electrical components were instrumented with a variety of different sensors as discussed in the previous sections. Therefore, a suite of different data analysis methodologies should be employed to extract the most useful information about the maintenance, load carrying capacity and safety of the bridge. One of the critical objectives of the monitoring was to develop methods and approaches for monitoring of maintenance operations. With appropriate measurements, it was important to develop methods that can provide information for the engineers. The information extracted from the bridge should be easy to interpret by the bridge owners, as well as robust, as demonstrated by field tests. As a result, a number of different data analysis methods have been developed and demonstrated for these purposes, for different monitored components. As for the monitoring strategy, threshold levels indicating pre-established limits for each component during normal operation should be defined. Then, the data should be analyzed with different methods to obtain the performance features, which should be compared with the threshold values. The methods that were investigated, developed and implemented to track the performance and possible damage/deterioration of the movable bridge are discussed in this chapter.

The data analysis in the context of system identification is the process of creating the characteristics and the properties of a mathematical model of a system by using a set of inputs and outputs. It has been widely used in various numbers of disciplines and subjects. Two types of identification approaches can be employed according to the models that are being used: parametric (physics based) methods and non-parametric (data-driven) methods. Parametric methods generally assume that a physics-based *a priori* model representing the system is known. These models can be created in time domain or frequency domain. The aim of such methods is usually to compute the unknown parameters of this model. These parameters are mostly related to physical quantities such as mass, damping and stiffness of the system. Correlation of the changes in these parameters with the condition of the structure has been an active research area

for the last a few decades in the context of SHM and damage detection. Non-parametric methods, on the other hand, make use of mathematical models of the system, without relating these models to the physical characteristics of the system. Some of the most common non-parametric methods include time series modeling and Artificial Neural Networks (ANN).

In this chapter, the researchers review some of these parametric and non-parametric methods that were used to analyze the data from different parts of the movable bridge. Backgrounds of these methods are discussed along with examples of data from different components.

6.2. Overview of Data from Different Components

6.2.1. Mechanical and Electrical

The components in the machinery room were instrumented by various sensors. The most important components were the gearbox, motor, rack and pinnion, shaft, open gear and trunnion. Locations of some of these components are schematically shown in the figure below. In this section, some sample data will be displayed for each component.

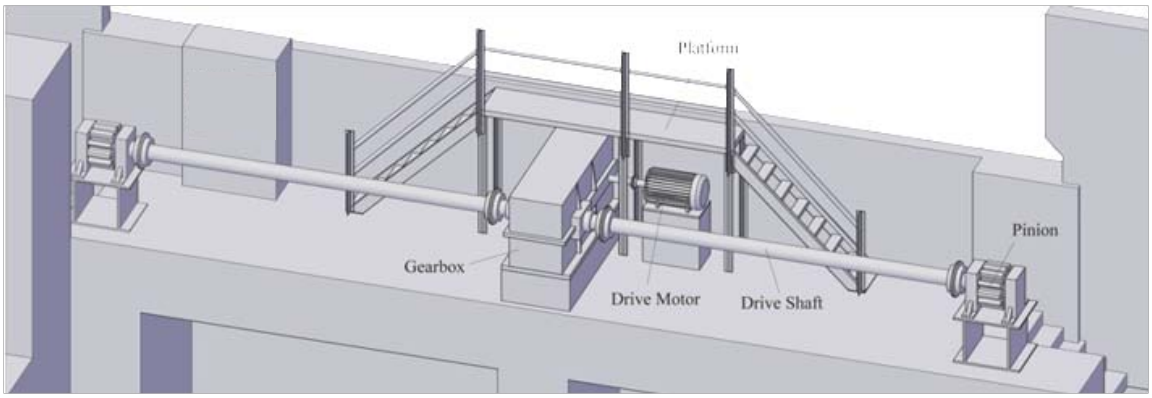

Figure 93: Mechanical Room

The motor was instrumented with four accelerometers. Two of them were installed at the front of the motor (drive shaft side) and the remaining two were installed at the back of the motor in horizontal and vertical directions. Figure 94 (Left) shows the motor with the accelerometer at the drive shaft. Figure 94 (Right) shows the acceleration data which was recorded in the vertical direction during an opening and closing. In this figure, the

first ~50 seconds corresponds to the time when the bridge is opening. Afterwards, the vibration level is almost zero, since the motor stops working when the bridge is fully open. The last part of the figure shows the level of vibration recorded during the closing.

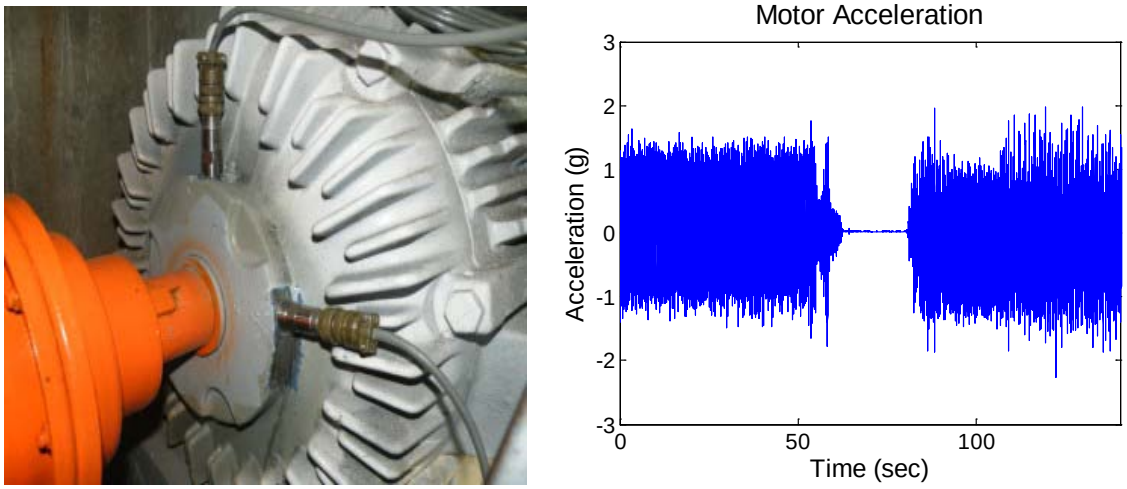

Figure 94: Electrical Motor and the Horizontal and Vertical Acccelerometers on the Drive Shaft Side (Left) and Sample Data from the Accelerometer (Right)

The electrical current that the motor needs to work is recorded with an ampmeter. Three ampmeters were installed in the electrical box shown in Figure 95. Sample data from one of the ampmeters is shown in Figure 95. This figure shows the difference in the current level when the motor was working and when it was stopped.

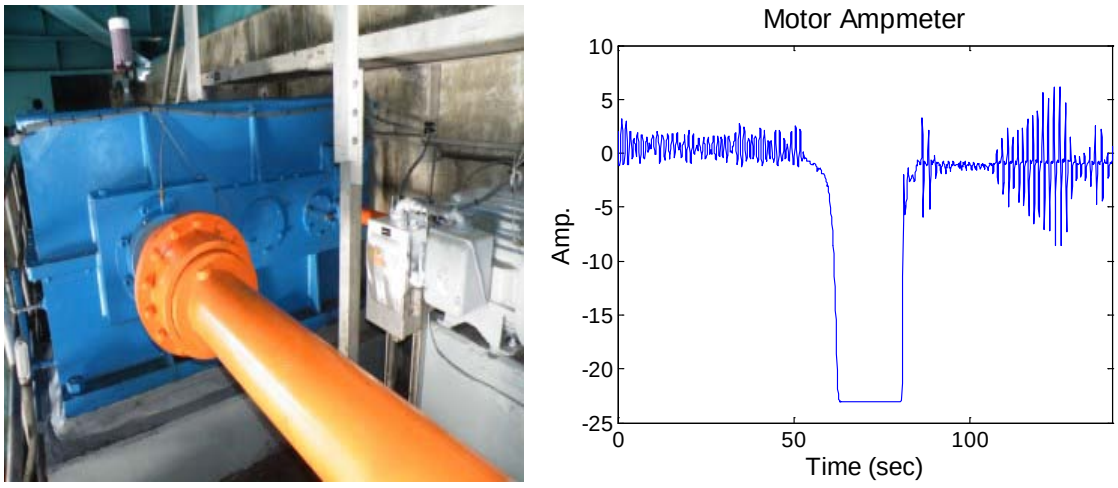

Figure 95: Motor Ampmeter (Left) and Sample Data from the Ampmeter (Right)

The gearbox was instrumented with six accelerometers at different locations in the horizontal and vertical direction. The locations of the sensors were finalized after the discussions with the FDOT engineers and consultants. Figure 96 (Left) shows one of these locations on the gearbox. Figure 96 (Right) shows the acceleration data which was taken in the vertical direction as the bridge opens and closes. Comparing Figure 96 (Right) and Figure 94 (Right), it is clearly observed that the vibration levels in the gear box were considerably less than that of the electrical motor.

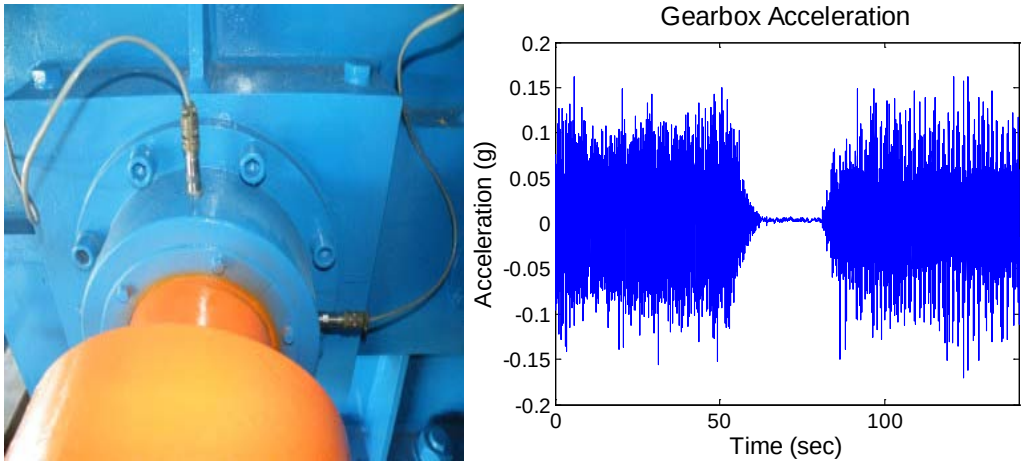

Figure 96: Gearbox and Accelerometer Installed (Left) and Sample Data from One of the Accelerometers (Right)

The sound of the gearbox during opening and closing was also recorded by microphones. The location of the microphones and sample data from one of the opening and closing are shown in Figure 97.

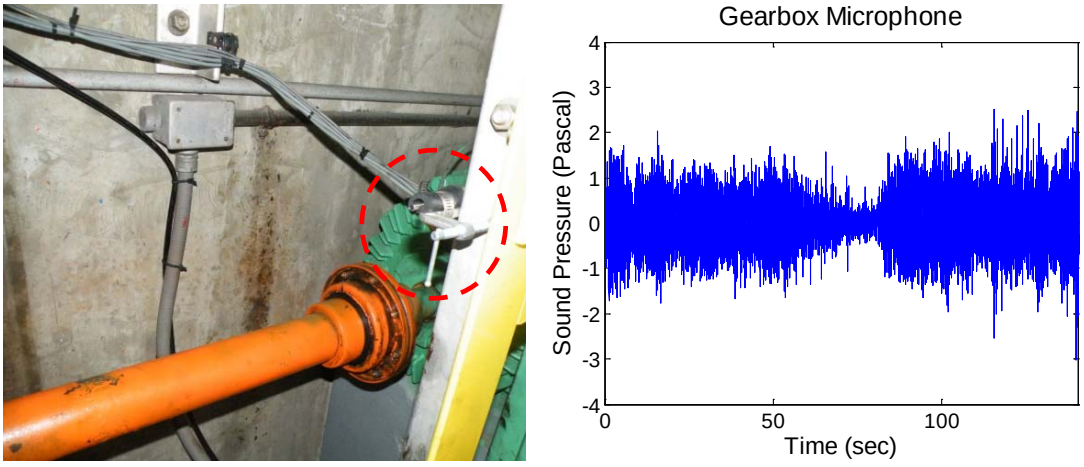

Figure 97: Gearbox Microphone (Left) and Sample Data from the Microphone (Right)

The Rack and Pinnion was only instrumented with one accelerometer in the horizontal direction. Figure 98 (Left) shows the Rack and Pinnion with the accelerometer Figure 98 (Right) shows sample data from this sensor as the bridge opens and closes.

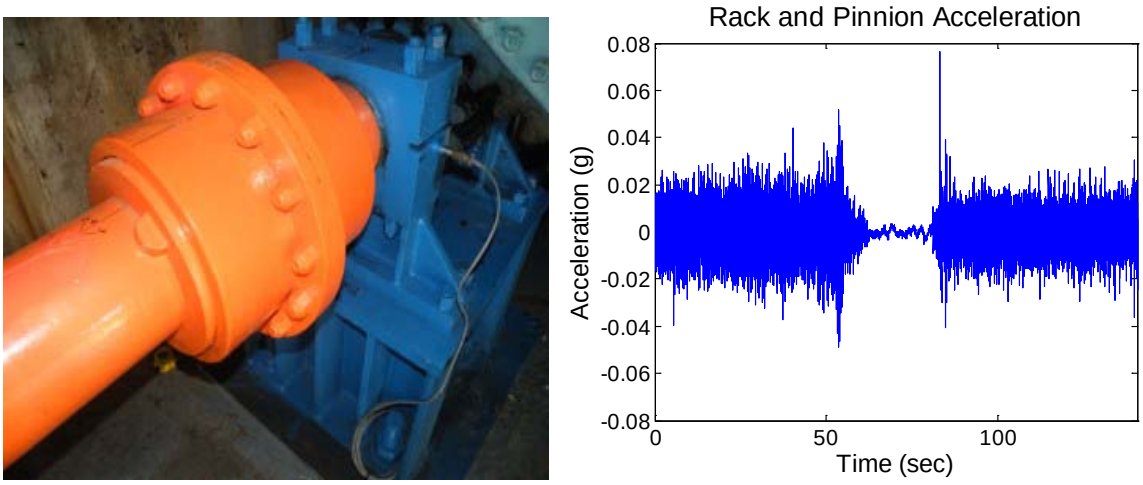

Figure 98: Rack and Pinnion and the Accelerometer on it (Left) Sample Data from the Accelerometer (Right)

The Shaft is the component between the gearbox and rack and pinion. This component is being monitored by four strain rosettes at the top and bottom at its ends. Figure 99 (Left) shows the end connected to the rack and pinnion, with the strain rosette at the top. Figure 99 (Right) shows sample data from this sensor as the bridge opens and closes.

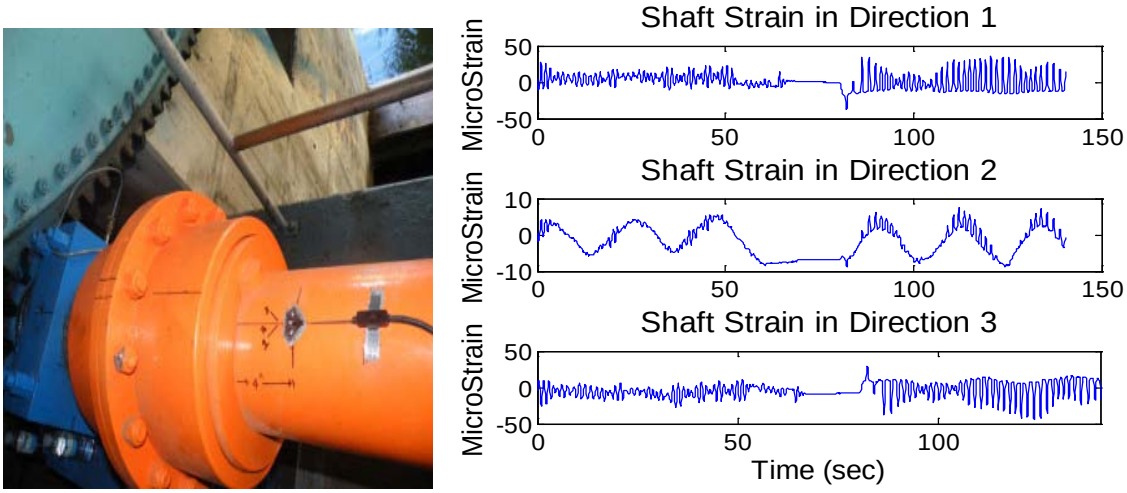

Figure 99: Shaft and Rosette on it (Left) and Sample Data from the Rosette (Right)

The Trunnion is another component around which the superstructure rotates. These parts are monitored by tiltmeters. Figure 100 (Left) shows one of the trunnions with the tiltmeter installed at the side. Figure 100 (Right) shows a sample data from this sensor as the bridge opens and closes.

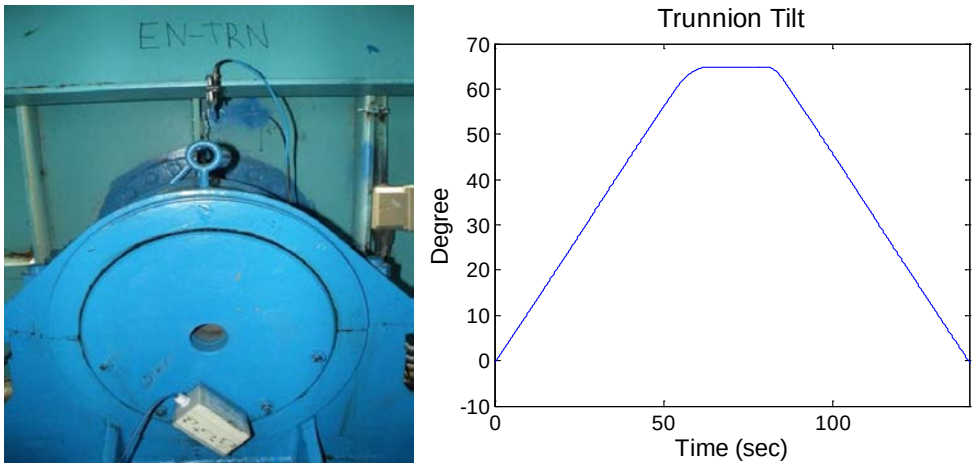

Figure 100: Trunnion and Tiltmeter on it (Left) and Sample Data from the Tiltmeter (Right)

The Span Lock is not within the mechanical room, but it is also one of the important mechanical components of movable bridges. Span lock oil pressure is monitored with two pressure gages. Figure 101 (Left) shows the span lock with installed pressure gages. Figure 101 (Right) shows sample data as the bridge opens and closes.

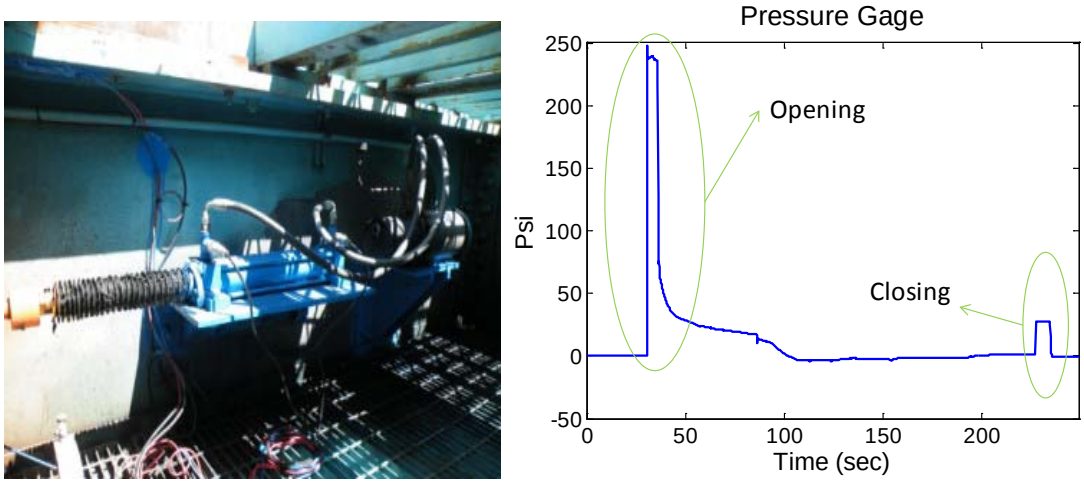

Figure 101: Span Lock and Pressure Gages on it (Left) and Sample Data from the Pressure Gage (Right)

6.2.2. Structural

In this section, sample data from various sensors at different structural elements will be shown. The important boundary and continuity elements for the movable bridge are the Live Load Shoes (LLS) and the Span-Locks (SL). Live load shoes are support blocks that the girders rest on while in the closed position. The live load shoes can be located forward of the trunnions, holding the main girder up, or behind the trunnions resisting the upward movement of the counterweight. The former type is the most common type, and is the type used for the Sunrise Blvd. Bridge. This location was instrumented with accelerometers to see the impact loading due to pounding and with strain gages to observe the excessive strains on the cross section and strain rosettes to see the shear effects of the traffic loading. Sample data for acceleration (Figure 102), sample data from strain rosette legs (Figure 103), and sample data from strain gages (Figure 104) can be seen in the following figures. In Figure 105, the corresponding real time video image at t=70 seconds is shown.

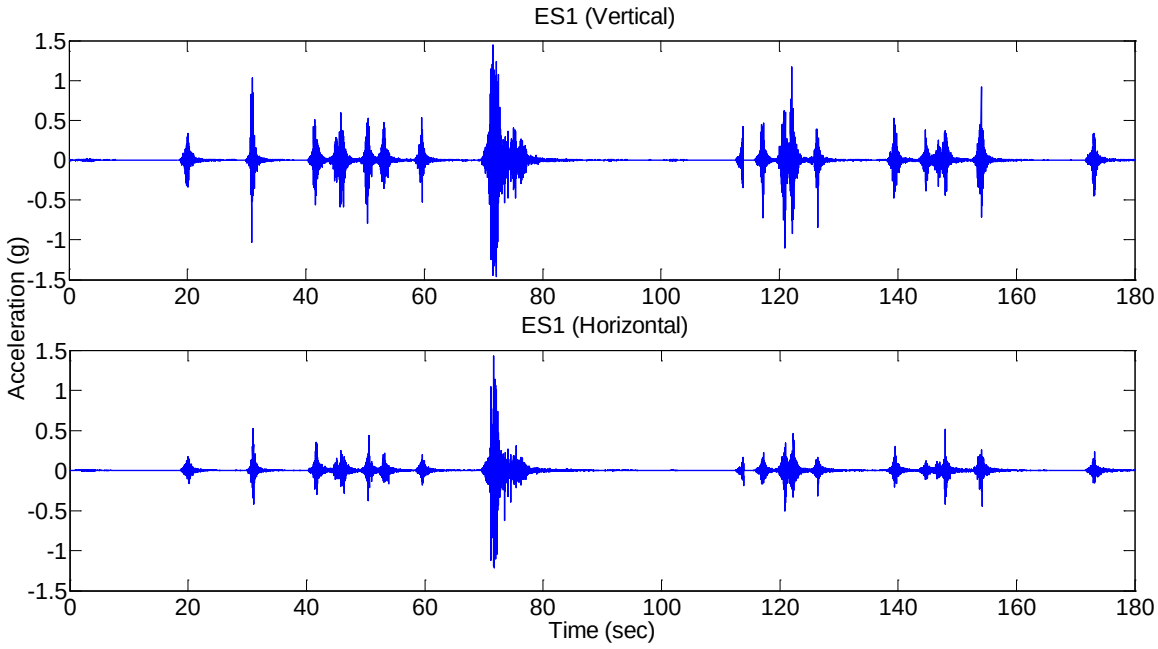

Figure 102: Sample Data from East South Main Girder Accelerometers

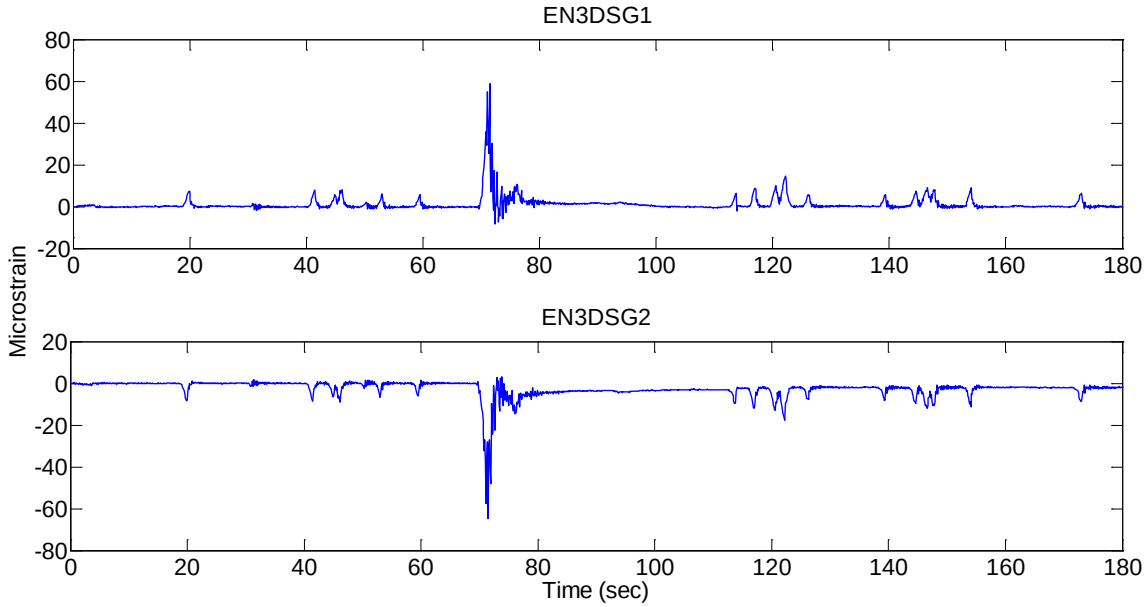

Figure 103: Sample Data from East South Main Girder LLS Strain Rosettes

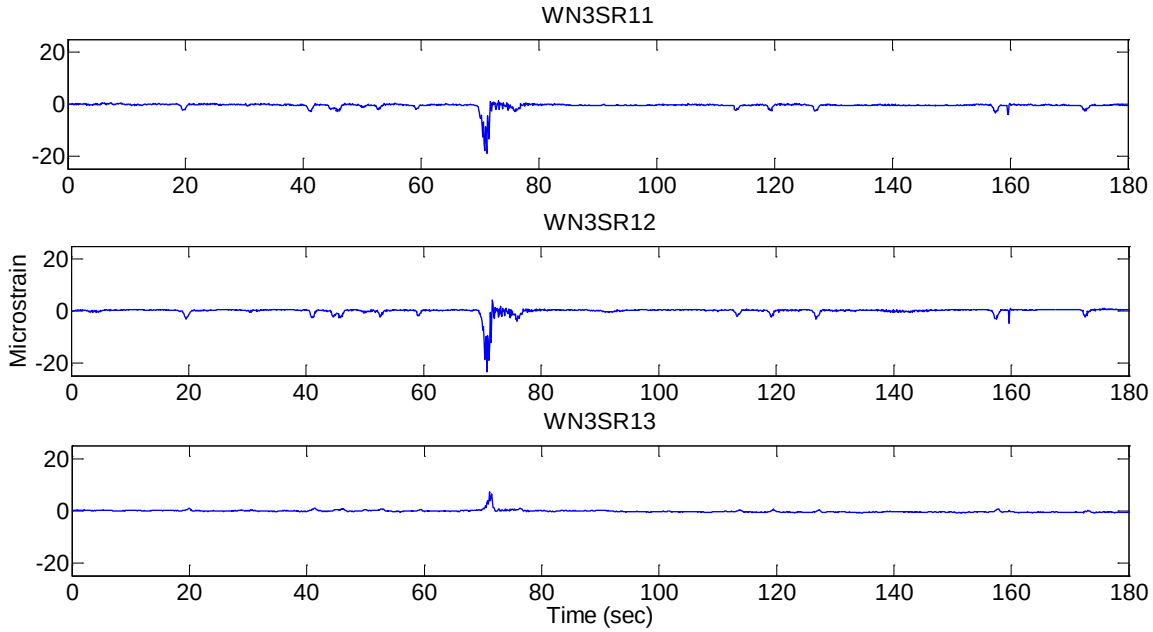

Figure 104: Sample Data from East North Main Girder LLS Strain Gages

Figure 105: Real Time Video Image Around t=70 Seconds

The other boundary elements are the Span Locks which tie the tip ends of the two cantilevered bascule leaves together, force the leaves to deflect equally, and prevent a discontinuity in the deck as traffic crosses the span. Most span locks consist of a rectangular lock bar supported by a pair of guides on one leaf that engages a single receiver on the opposite leaf. Strain gages and accelerometers at the tip of the girders can indicate continuity between two leaves as a result of span lock connectivity. Sample data for these sensors are shown in Figure 102 and Figure 106. The strain values for the tip location and the LLS location were not in the same range. Due to the fire truck in the center lane, the maximum strain from the tip location was around 20 microstrains, whereas the maximum strain from the LLS was around 50 microstrains. This comparison shows that the effect of traffic induced strains is higher at the LLS location.

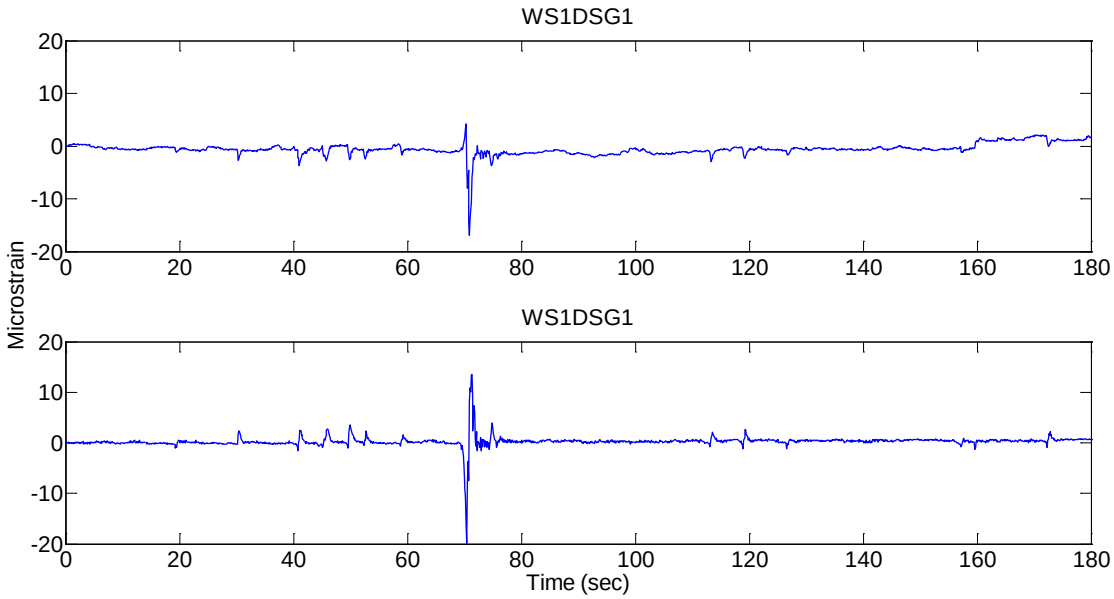

Figure 106: Sample Data from West South Main Girder Tip Strain Gages

During operation, the lock bar slides across bronze shoes mounted in the rectangular guide and receiver housings, while tiltmeters provide monitoring of the angle of rotation at the tip of the span. The tiltmeter readings (Figure 107) serve two functions: checking the leveling between girders on both sides for alignment during opening/closing and ensuring that the tips are in correct position for the locking mechanism. In addition to these tiltmeters, tiltmeters were also installed in the trunnion area.

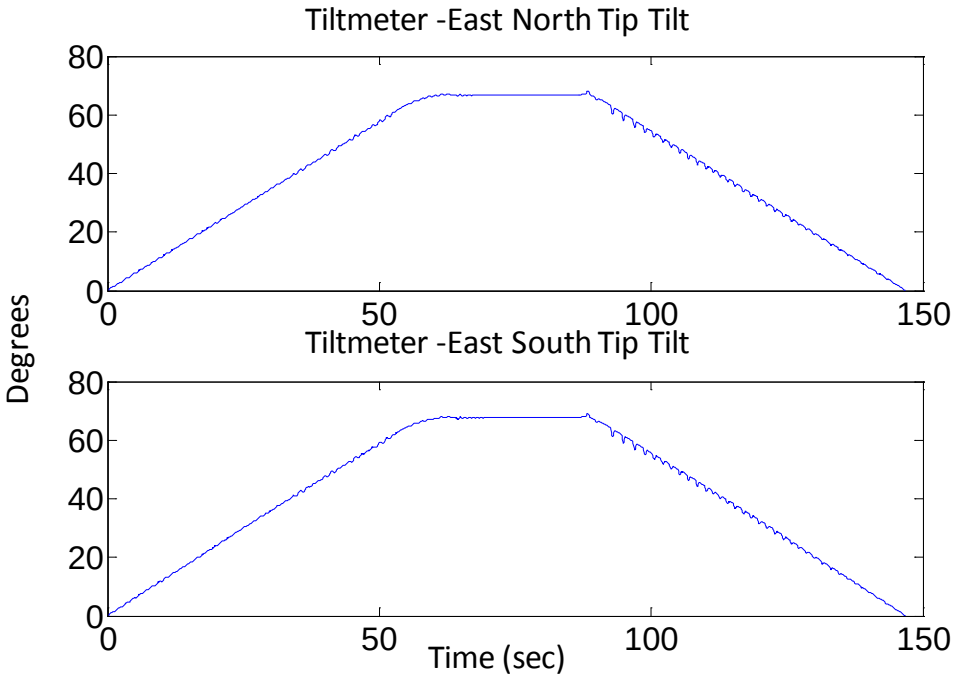

Figure 107: Sample Data from West Main Girder Tip Tiltmeters

Beyond the boundary elements, the girders and the beams are the other structural components. Main girders and floor beams form the main frame of the spans. They are made from both rolled and built-up sections with welded plates. Corrosion, misalignment, bending, or deformation can cause a change in the strain and acceleration distribution of the structure. A typical floor beam and stringer strain gage data is shown in Figure 108 and Figure 109.

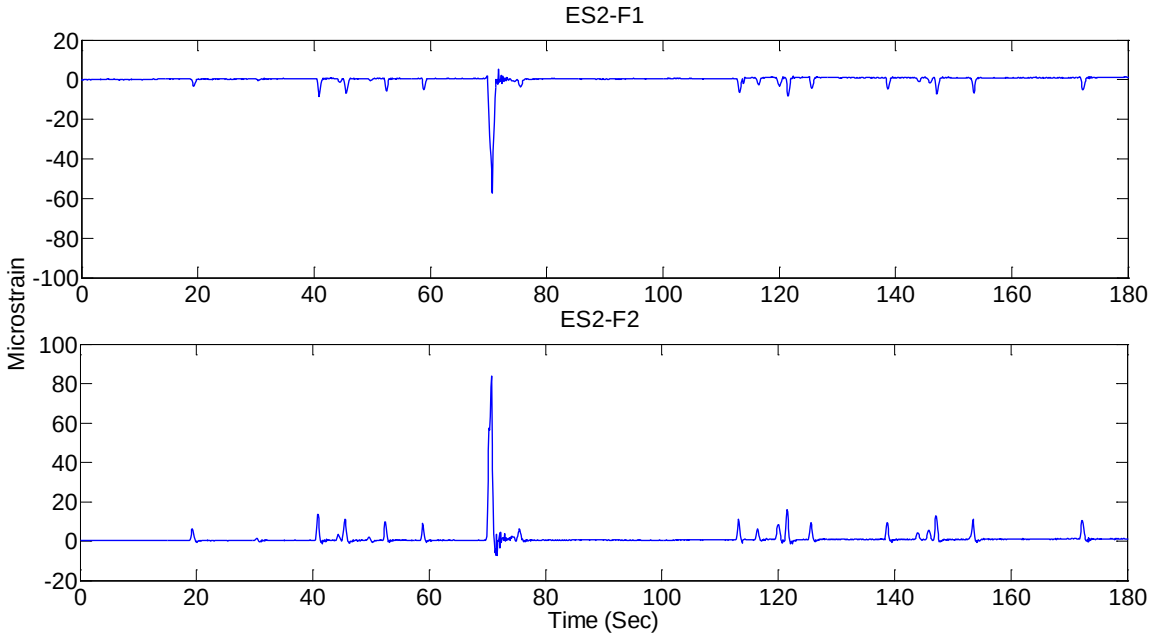

Figure 108: Sample Data from East South Middle Floor Beam

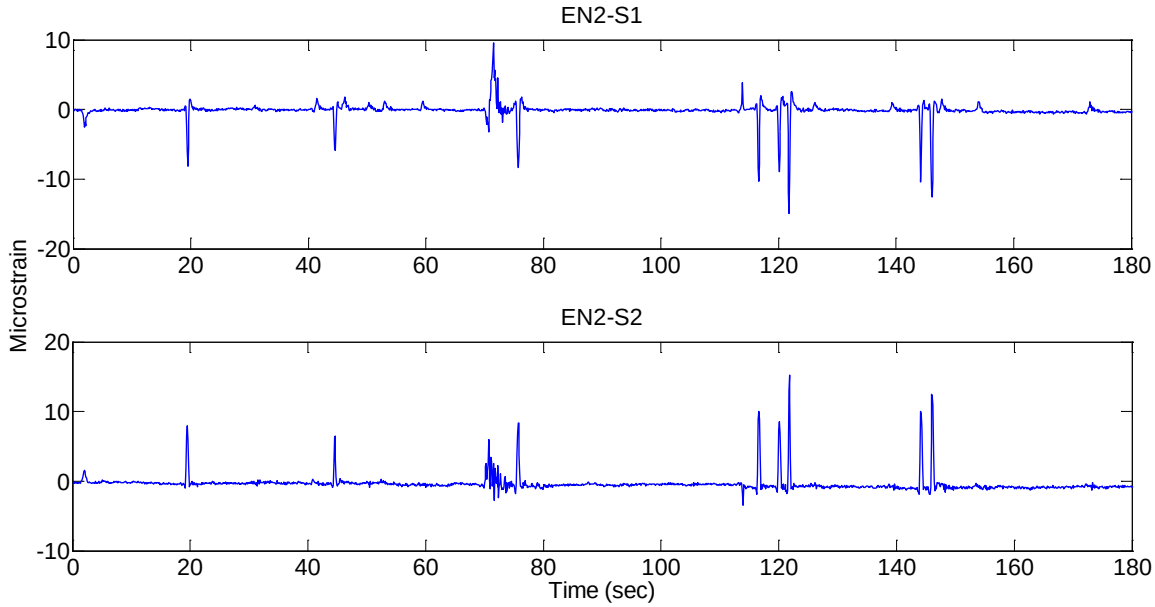

Figure 109: Sample Data from East North Middle Stringer

Additionally, environmental sensors were installed on the movable bridge to track the effects of wind speed, wind direction, humidity and barometric pressure. Wind monitoring can be used for determining the input load on the structure caused by air

currents. Bascule bridges are slender and lightweight, and are significantly affected by strong wind forces, especially when they are open. Measured wind speed and direction may also be useful during hurricane-strength winds, indicating excessive force on the girders. The following figure shows typical weather station data (Figure 110).

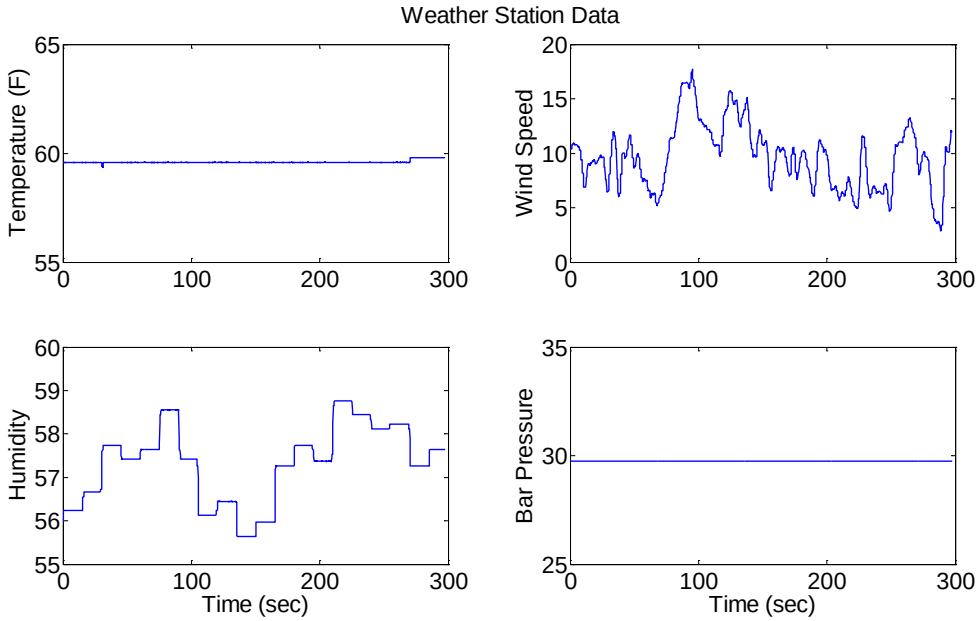

Figure 110: Sample Data from Wind Speed, Wind Direction, Humidity and Barometric Pressure

In addition to wind, ambient temperature and structural member temperatures need to be monitored. Past studies have shown that temperature differentials can cause considerably higher stresses than stresses induced by vehicular traffic (Catbas and Aktan 2002). To obtain the temperature distributions and temperature effects on the structure, vibrating wire gages were installed and ample data from vibrating wire strain and temperature readings can be seen in Figure 111.

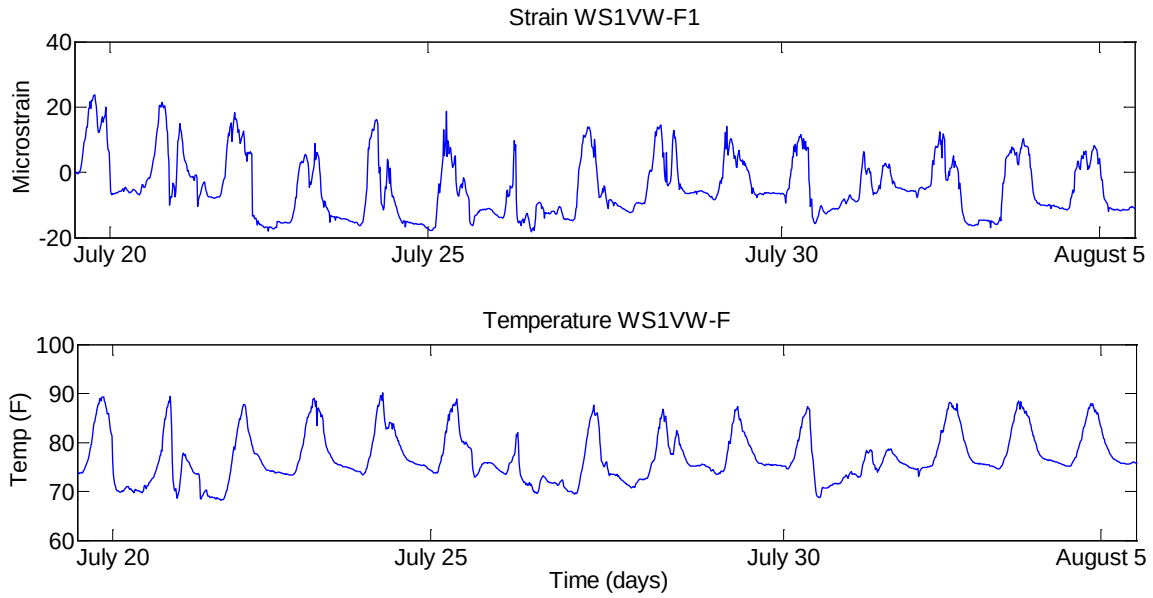

Figure 111: Sample Data from Vibrating Wire Strain and Temperature Readings

Finally, a video camera can be a complementary element as providing vehicular traffic data to be correlated with other sensor readings, informing bridge owners about accidents and suspicious activities (Figure 105).

6.3. Data Quality Control

Data quality is one of the most important factors affecting the effectiveness of the SHM applications. The analysis results obviously depend on the quality and accuracy of the data (along with other factors such as the data analysis methodology etc.) and thus different checks should be conducted for data cleansing to select or reject the data sets for data analysis process. In the following sections, some of the data quality checks employed in this study are discussed.

6.3.1. Visual Checks

Visual checking of the data is the most basic of all data quality control methods, yet its usefulness in detecting non-working and malfunctioning sensors is tremendous. Visual checking of the data consists of viewing a graphical representation of real-time or archived data from a sensor channel and inferring from the predicted behavior of that sensor, whether or not that sensor channel is working properly. The predicted behavior of

a sensor is dependent on the type of sensor and knowledge of the external stimulus during the data collection. Often times, even a general understanding of the external stimulus combined with heuristics, is adequate for inferring whether or not a sensor is working properly. For example, Figure 111 shows a graphical representation of 15 minutes of data collected from a dynamic strain gage located on the main girder. It can be reasonably assumed that during a 15 minute timeframe, at least one vehicle crossed the bridge. This external stimulus is expected to register some response in a strain gage; however, the data collected shows a flat-line, or no response. From this visual inspection, this sensor can be identified as non-working, at least for the timeframe analyzed.

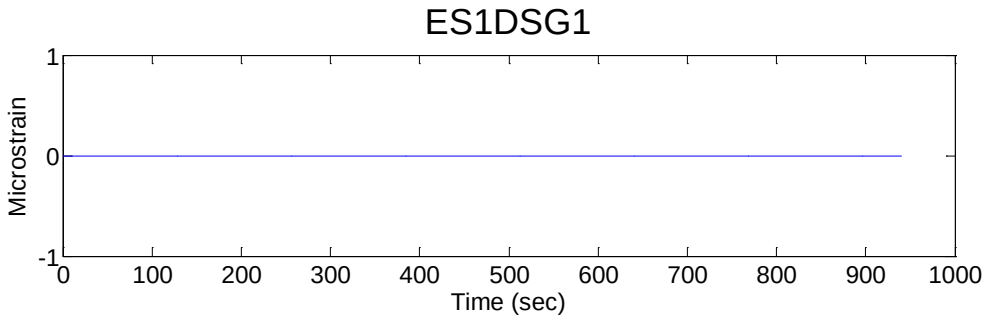

Figure 112: Example of a Non-working or "Dead" Sensor

In the above example, non-working meant zero registered response, which corresponds to a "dead" sensor or a broken electrical connection. However, non-working can also mean a drifting sensor or a sensor that is registering "noise". For identification of these later two classifications, it is often easier to combining the above procedure with comparison of data from other similar sensors installed on the bridge. Figure 113 shows the comparison of data from two accelerometers located at different positions along the main girder. From inspection of the data, it is apparent that the second sensor, although registering some response, is not properly functioning.

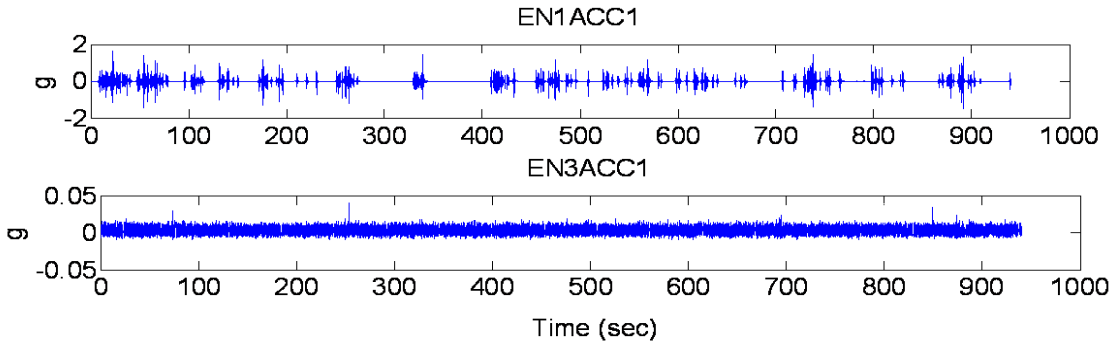

Figure 113: Example of a Non-working Sensor Registering Noise

Sensor drift is another indication of a non-working sensor. Sensor drift can be identified as general trend of the data to shift to higher or lower readings during the collection. This trend can be shown in Figure 114.

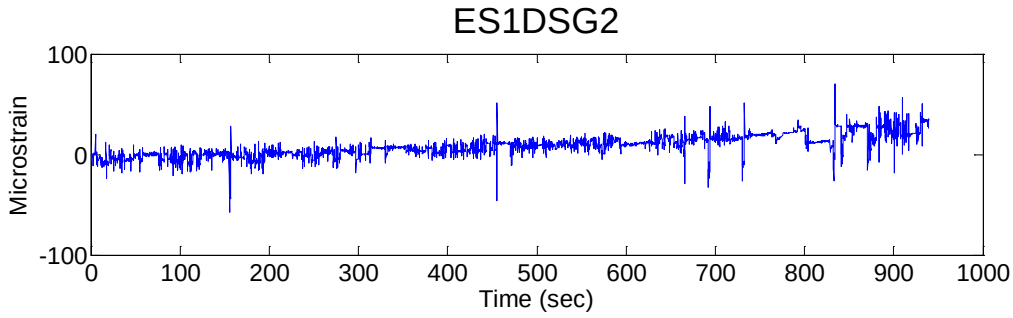

Figure 114: Example of a Non-working Sensor Drifting

The visual checking procedure is a continuous method for data quality control. Visual checks are often the first step for checking data quality. From identification of non-working sensors, trouble-shooting can be used to identify and correct hardware problems. When hardware problems cannot be addressed, due to inaccessibility, particular sensor channels may be labeled as non-working and not used in data analysis techniques. It is important to note that the condition of a sensor is not a constant. For example, a once working sensor may become a non-working sensor if it encounters some sort of trauma. For this reason, visual checking of data should be integral to the data analysis process and during implementation of the other data quality control methods.

6.3.2. Sensor Cross Correlation

Another subject related to health monitoring is the functionality of the monitoring system. For long term monitoring, sensors should have a longer life time than the

structure being monitored, however, this is often not the case. Depending on the malfunctioning errors of sensors, the damage identification results may be affected. When the sensor fails, the damage identification gives a false alarm and the structure will be incorrectly classified as damaged. For this reason, dynamic strain gages and vibrating wire strain gages were used in this study for quality control by taking their cross correlation into account. Cross correlation is a measure of similarity of two data sets in vector form. Having similar behavior in data sets gives higher correlation while low correlation indicates either no correlated response or change in correlated response due to structural changes or sensor malfunction.

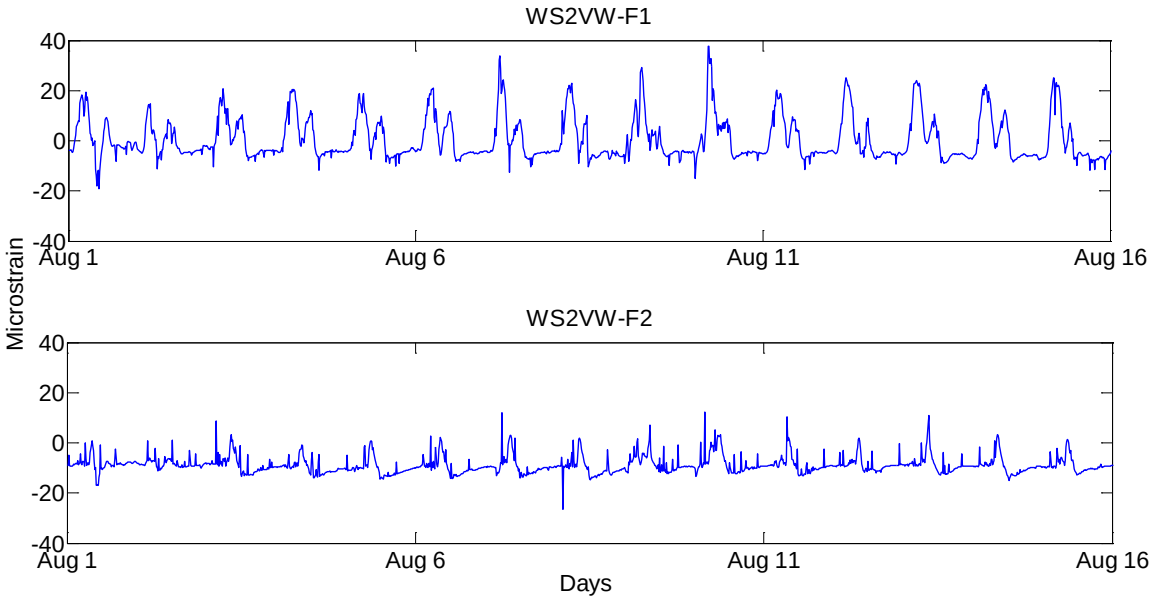

Figure 115: West Leaf Middle Span Floor Beam Top-Bottom Strain Correlation

Vibrating wire strain gages include stress-induced strain readings and temperature readings together. For the correlation study of vibrating wires, two main applications were used, which are top-bottom strain measurement correlations and strain-temperature correlations. Past studies show that the daily or seasonal temperature effects may create critical stress levels, even higher than traffic induced stresses. Therefore, the strain temperature relationship should be investigated carefully. Figure 115 shows top and bottom vibrating wire sensors at the West leaf mid span floor beam, for a two-week duration. The figure below shows that top and bottom vibrating wire sensors correlated well and exhibited the same behavior at the same time (Figure 115).

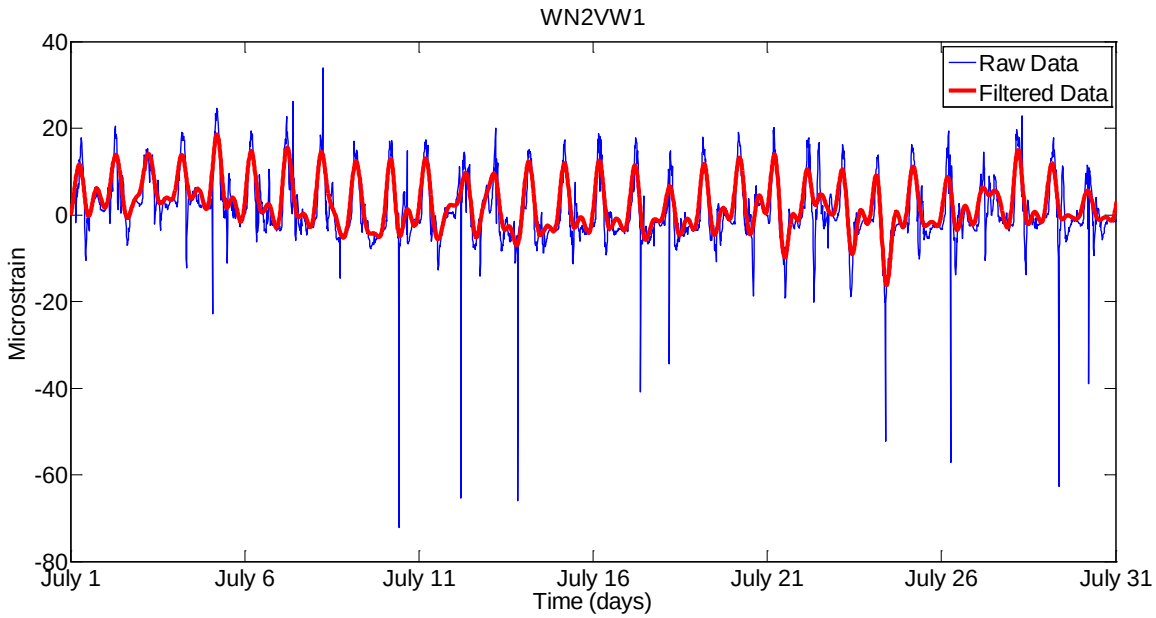

Figure 116: North West Middle Span Main Girder Top Sensor Raw and Filtered Data

This correlation study was also applied to the dynamic strain gages. The main idea behind this was to check whether or not the sensors were working based on top and bottom flange strain gage correlations, and also to identify damage by checking neighbor or symmetrically located sensors on the bridge. More discussion about this can be found in following chapters.

When the long term data from vibrating wires was observed, it was seen that there were some spikes in the data. In a fixed bridge, these can be attributed to vehicular traffic; however, in this case, opening and closing of the bridge can also be captured. These effects were not created due environmental effects; therefore, filtering these spikes out of the data enabled a better correlation of the temperature and structural response (Figure 116). A special low pass filter was designed to eliminate the effects of traffic and opening-closings. These outliers were eliminated to see only the effects due to environment inputs to the bridge. One main issue for the special filter was peak matching for the raw data, that is capturing the responses without inducing too much artificial phase. This peak matching was crucial to see the real time strain temperature correlations, otherwise, the peaks would be removed and catching the true correlation would not have been very accurate.

After filtering the data, the correlation between the temperature and strain was more clearly observed. In Figure 117, filtered vibrating wire strain data is shown to correlate better with temperature.

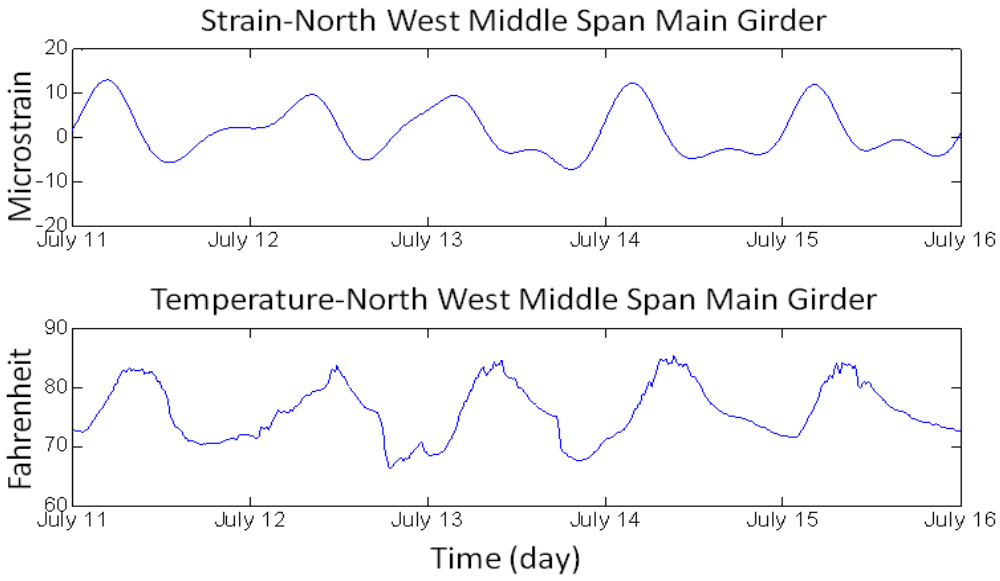

Figure 117: Close View North West Middle Span Main Girder Top Sensor Filtered Data

6.3.3. Finite Element Model (FEM)-based Verification

Another method of checking the data quality and accuracy is to make use of a FEM when such a model is available. Although the experimental results usually differ from that of the FEM results (especially when the model is not calibrated), it is still an effective way of assessing the accuracy of the experimental data. For this application, several checks were conducted, and the experimental results were compared to the FEM results. These results are presented in the previous chapter and it was seen that the sensor data was correlating well with the FEM results.

6.4. Possible Methods for Data Analysis in this Study

6.4.1. Statistical Methods

Use of statistical pattern recognition methods offers promise for handling large amounts of data, while taking into account variations in the data. Farrar and Sohn (2000) further describe SHM as the observation of a system over time using periodically sampled dynamic response measurements from an array of sensors, the extraction of damage sensitive features from these measurements, and the statistical analysis of these

features to determine the current state of system health. Most of the studies focusing on statistical pattern recognition applications on SHM use a combination of time series modeling with a statistical novelty detection methodology (e.g. outlier detection). One of the main advantages of such methodologies is that they require only the data from the undamaged structure in the training phase (i.e. unsupervised learning) as opposed to supervised learning where data from both undamaged and damaged conditions is required to train the model. The premise of the statistical pattern recognition approach is that as the model is trained for the baseline case, new data coming from the damaged structure will likely be classified as outliers in the data.

Most of these statistical models are used to identify the novelty in the data by analyzing the feature vectors, which include the damage sensitive features. For example, Sohn et al. (2000) used a statistical process control technique for damage detection. Coefficients of Auto-Regressive (AR) models were used as damage-sensitive features and they were analyzed by using X-bar control charts. Different levels of damage in a concrete column were identified by using the methodology. Worden et al. (2000) and Sohn et al. (2000) used Mahalanobis distance-based outlier detection for identifying structural changes in numerical models and in different structures. Worden et al. (2000) used transmissibility function as damage sensitive features, whereas Sohn et al. (2000) used the coefficients of the AR models. Manson et al. (2003) also used similar methodologies to analyze data coming from different test specimens including aerospace structures.

6.4.2. Image and Video Analysis

Very recently, some investigators have explored the possibility of incorporating imaging and optical devices and combining them with sensing technology. It should be noted that there are only a few and limited attempts of real life testing and implementations of these ideas (Wahbeh et al, 2003, Lee and Shinozuka, 2006).

Computer-vision is the processing of acquired images in order to detect and track certain features. Recently, computer vision applications have gained attention for SHM. This approach has been implemented and tested at the UCF Structures and Systems Research Laboratory (Catbas and Zaurin, 2008).

Most of the previous work presented in the literature search was based on studies using mainly ambient vibration data and could not differentiate ambient from traffic readings, unless testing was scheduled by closing the bridge. An effective system should include the following closely interrelated components: the vision module, the distributed sensors network array, the analytical model, the database, and the diagnostic module as shown in Figure 118.

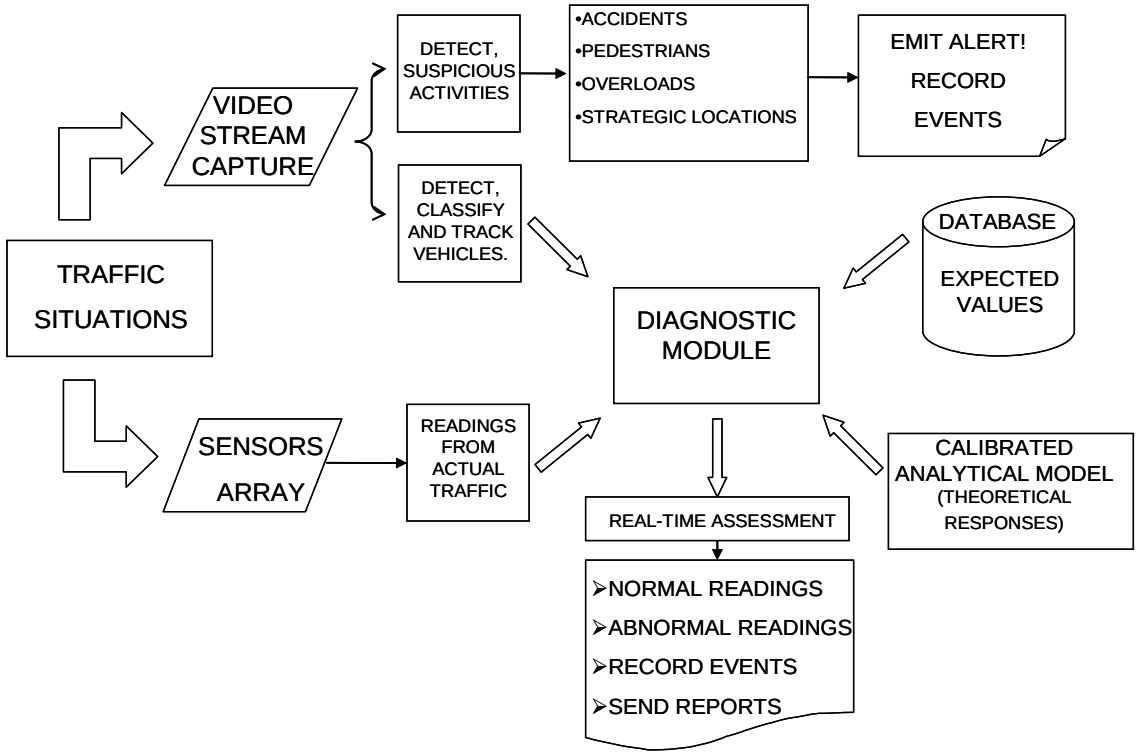

Figure 118: The Components of a Monitoring Framework with Computer Vision

Traffic is monitored and captured by a firewire camera, while sensors collect traditional data. A video stream is used in conjunction with computer vision techniques to determine the class, speed, and location of vehicles moving over the bridge, and this information is synchronized with data from the sensors. Unit Influence Line (UIL) feature vectors are extracted for assessment and damage diagnostic. Additionally, video can be also used to detect suspicious activities, i.e. the presence of persons, vehicles and/or objects in critical or prohibited, predetermined locations.

6.4.3. Time Domain Analysis

Descriptive statistics are useful for describing the basic features of data in a study. They are used as the first place to get a feel for the data, used in the statistical tests

themselves, and finally used to indicate the error associated with results and graphical output. In a research study with large data, descriptive statistics may help us to manage the data and present it in a clear and understandable way. For example, a large quantity of data was collected in this project from different sensors on the structure and mechanical components. When we consider one of the acceleration data sets from one sensor on gearbox, representing this data with meaningful metrics becomes a critical issue. In that case, for example, using the descriptive statistics such as mean, standard deviation etc. can be very useful. These parameters can then be used with other methods such as Artificial Neural Networks (ANN) for condition monitoring.

6.4.4. Frequency Domain Analysis

Frequency domain methods transform the time histories to frequency domain and extract the modal parameters in the frequency domain. These methodologies use FRFs (Frequency Response Functions) to compute the modal parameters. One of the main advantages of frequency domain methodologies is that less computational modes (noise modes) are obtained in comparison with time domain algorithms. Some of the disadvantages of these methodologies are due to the restrictions of the FFT (Fast Fourier Transform). For example, leakage is one of the commonly encountered problems because FFT assumes the signal is periodic within the observation time. The effect of leakage can be reduced by using windowing functions, but it cannot be avoided completely.

One of the simplest frequency domain methods is the Peak Picking method, where the modes are selected from the peaks of the FRF plots. If the system is lightly damped and if the modes are well separated, the natural frequencies (eigenfrequencies) can be estimated from the FRF plots. The damping ratios can be determined by using the half power method.

Another method called Complex Mode Indicator Function (CMIF) has also been used for frequency domain analysis in the context of SHM. Recently, Catbas et al. (1997, 2004) modified and further extended CMIF to identify all of the modal parameters, including the modal scaling factors from MIMO test data. In these studies, it was shown that CMIF is able to identify physically meaningful modal parameters from the test data, even if some level of nonlinearity and time variance were observed. Figure 119 shows the basic steps of the methodology.

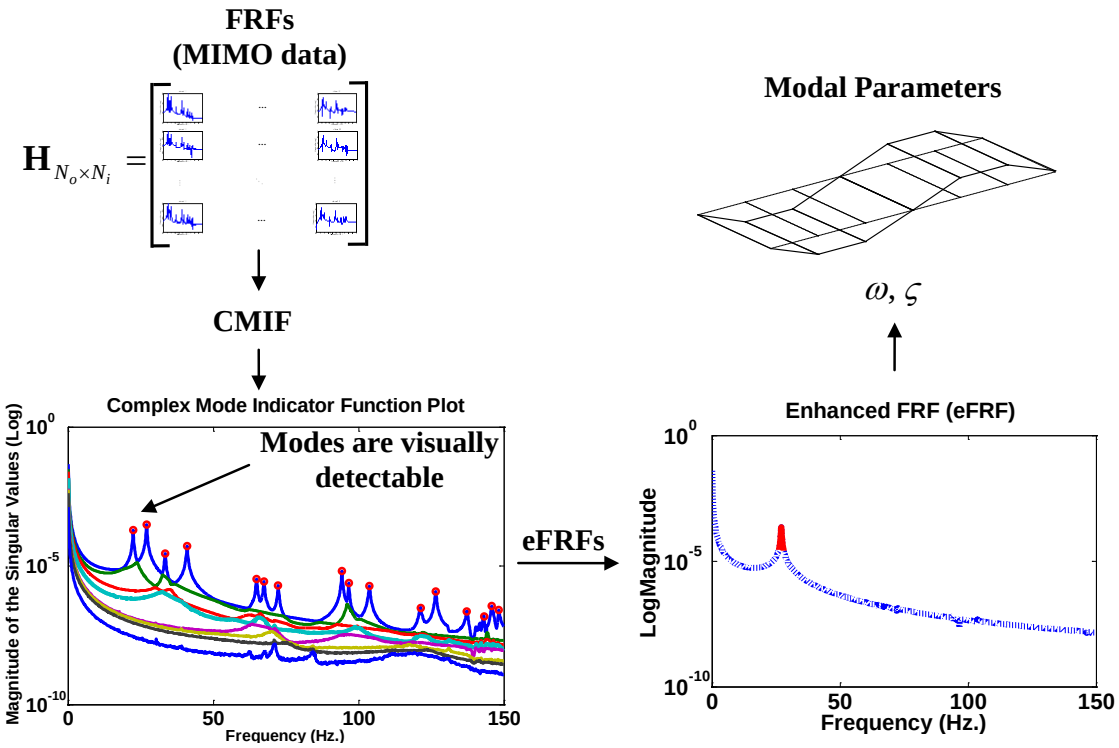

Figure 119: Summary of CMIF Method

6.4.5. Artificial Neural Networks

An Artificial Neural Network (ANN) is a network of many nodes with local memories. These nodes are connected to each other to carry and process numerical data. Multi-layered feed-forward neural networks are currently the most commonly used neural networks in structural engineering applications and have demonstrated a notable degree of success. An ANN learns from the existing patterns, capturing the subtle functional relationships among the patterns, and then makes a prediction for the patterns which were not considered during learning. A multi-layered feed-forward neural network consists of multiple layers of computational units (nodes) interconnected in a feed-forward way (Figure 120).

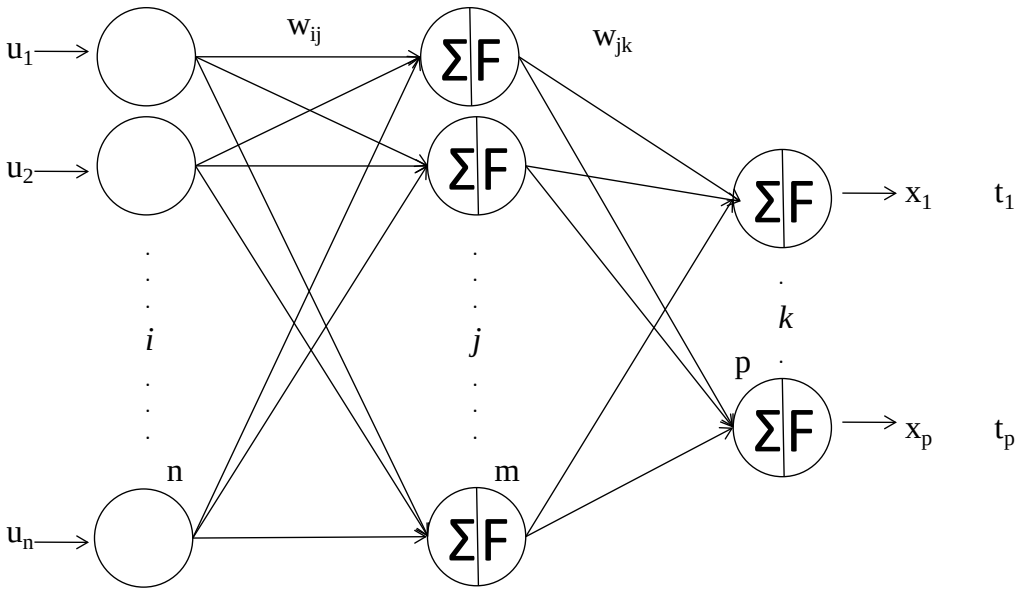

Figure 120: Single Hidden Layer Feedforward Neural Networks

The input vector distributes the inputs to the input layer. There is no processing in input layer; rather it can be conceived as a sensory layer, where each neuron receives a sole component of the input vector **U**. The last layer is the output layer, which outputs the processed data. The output of each neuron in this layer corresponds to a component of the output vector **X**. The layers between the input and output are referred to as hidden layers. Hidden layer(s) may have any number of neurons; however, they should be chosen carefully as the results may be directly affected in some cases.

Each neuron in a layer is connected to all the neurons of the previous and next layers by weighted connections. Except for the first sensory layer, the outputs of all neurons from the previous layer are received as an input to each neuron. Each neuron performs a nonlinear transformation of the weighted sum of the incoming inputs to produce the output of the neuron, which is given to other neurons or outside the network.

The basic algebraic equation for each layer can be written as:

where is the output of neuron j; represents the weight from neuron i to neuron j; is the input signal generated for neuron i; is the bias term associated with neuron j; and the nonlinear activation function is assumed to be a sigmoid function as.

The success of a network is measured by its generalization performance. If the difference between the actual (**T**) and computed (**X**) output by ANN is within the acceptable level, then the network can be used for prediction in the similar domain which exhibits certain common characteristics with the existing patterns. This objective is achieved by learning techniques, the most popular being back-propagation (BP). In the back-propagation, the output values are compared with the desired answer to compute the value of some predefined error-function. Then, the error is fed back through the network by various techniques. The back-propagation neural networks are basically a gradient descent method, and two parameters called as the learning rate and the momentum factor ; are usually introduced in the iterative calculation process as the following equation

where is the error signal for neuron j; denotes the adjusting weights between neurons *i* and *j*; meanwhile the symbols (n + 1) and n are the current and the most recent training step, respectively. BP algorithm adjusts the weights of each connection in order to reduce the value of the error function by using this information. After repeating this process for a sufficiently large number of training cycles, the network will usually converge to some state where the error of the calculations is small, which indicates that learning is completed. Furthermore, to evaluate the effectiveness of neural networks model, the coefficient of correlation (R) may be used and defined as follows

where and are the theoretical results and its averaged values, respectively, and are the estimated and its averaged values, respectively, and s denotes the number of data in the analysis.

The prediction performance of a network usually depends on the network parameters, the training process, the complexity of the underlying process represented in the training data set and the topology chosen. The best performance is generally achieved by extensive parametric study on the different network using trial and error approach. In each trial, performance of network is evaluated. This process is repeated until the best architecture with the right network parameters is arrived.

6.5. Application of Data Analysis Methods for Main Components

6.5.1. Mechanical and Electrical Components

The mechanical and electrical parts of the bridge were investigated by using the data from different mechanical and electrical component acceleration sensors. The critical characteristics and distinct behavior change in dynamic response behavior can be tracked over time by means of collected data. Using different analysis techniques, the information hidden in the collected data can be revealed for the owners to easily monitor their structures over its life time. ANN is one of those techniques which was very effective in capturing the underlying behavior of Structural Health Monitoring Data. During the SHM process, a large number of data sets from the healthy condition and several data sets from the unhealthy condition of monitored parts were collected. A thorough understanding of damage-sensitive features from these measurements was needed in order to obtain accurate damage prediction. Here, statistical methods were used to identify certain features of the SHM data. The statistical analysis of these features to determine the current state of system health and any change in the features can be attributed to damage. Statistical significance of these changes in the extracted features was evaluated in neural networks. A neural network-based method was developed here, for an efficient and practical determination of the current state of system health. An Artificial neural network (ANN) was trained to learn the pattern between the statistical parameters and damage cases. Statistical parameters were used as the input data to train the network. The outputs introduced in the training session were the existence or absence of damage. The bridge data acquired was divided into three sets; the training set, the cross validation set, and the

test set. The training set was used to establish intrinsic relationships between the statistical parameters and damage. The cross validation set was used to avoid over-fitting, which is the case of poor generalization. The test set was used to evaluate the performance of the network. Several network designs were examined to determine one with a reasonable performance. Once trained successfully, the network can confidently be used to accurately predict the current state of system health for new input data.

6.5.2. Structural Components

In this study, the monitored structural component elements were the main girders, floor beams, stringers, live load shoes and the span locks. These locations were instrumented with strain gages, strain rosettes, tiltmeters and accelerometers. The live load shoe and the span lock locations can be considered as boundary conditions of the movable bridge; therefore, the damage scenarios were applied to these locations. More discussion regarding the damage scenarios can be found in Chapter 7. In this section, detailed structural data analysis applications will be discussed.

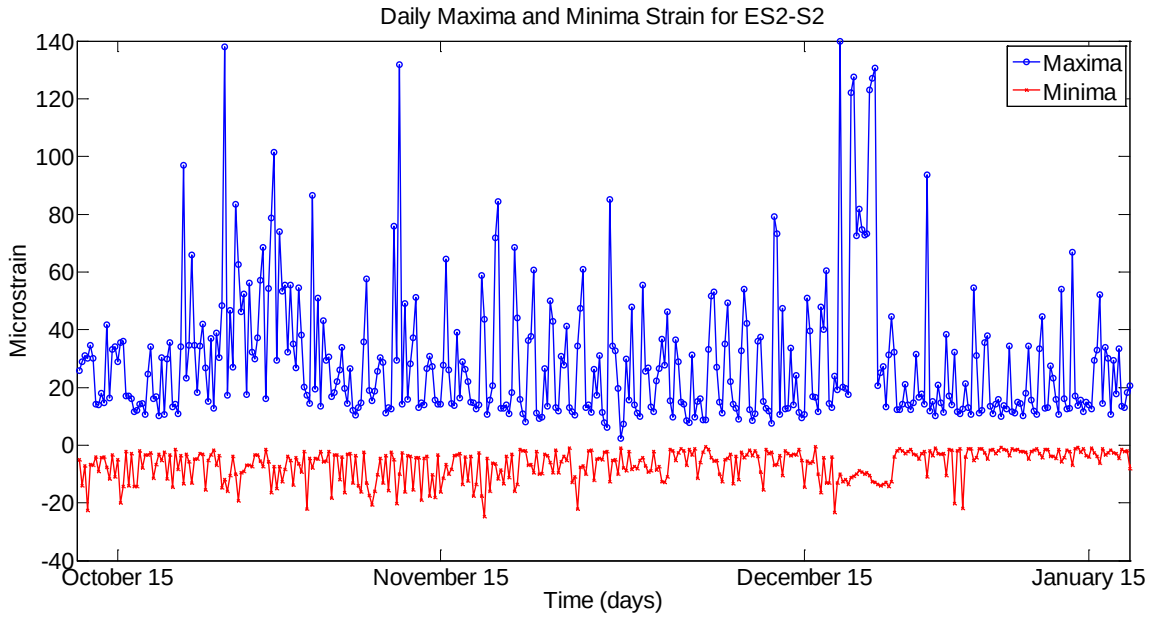

Figure 121: Daily Maximum and Minimum Strain for Each Data Set from Bottom Flange of East South Stringer

Statistical information, such as maximum, minimum, mean, standard deviation, correlation and root mean square, is a crucial part of data analysis because it helps the

engineer, not only to understand the data behavior, but also to interpret the data. In addition to these advantages, statistics also help for identification of behavior. Figure 121 shows the daily maximum and minimum strains coming from the bottom flange of the East South stringer from the period of October 15 to January 15. Since the stringers are the starting point of the load distribution and have smaller cross-sections, higher strain values at stringers are observed compared to some of the other component such as floor beams and main girders From the plot, it is clear that the strain levels of these elements are changing between 20 microstrains and 140 microstrains. Higher strain values were not observed in all the data sets because for each day, three data sets (coming from the rush hour times) were collected during traffic. The same procedure can also be applied to accelerometer data. In this case, beside the maximum and minimum values, mean of the accelerometers can be checked over the time to see whether the sensor is not working or not. For instance, the mean of accelerometer data should give zero in our application. If the mean is not zero, the data and sensor should be checked for a possible malfunction.

After collecting the basic statistical information from each sensor channel for each data set, some data analysis methods were used for structural damage identification. These methods were the correlation and root mean square (RMS) analysis.

As discussed in the previous sections, correlation is the measure of the dependence, or similarity, of the data sets in vector form. A correlation constant can also be calculated from these vectors. Ideally, the strain channels should have a correlation with the neighbor, or symmetric locations, and the outcome of this correlation will show consistency in the strain levels.

The objective of scatter plotting is to see the correlation between two strain channels. If the scatter can be bounded closely, then this indicates a good correlation, whereas the opposite means a low correlation. Moreover, the correlation coefficient can also be computed from these graphs by fitting a line to the plot, and the tangent of this line will give the correlation coefficient of these channels. Figure 122 and Figure 123 show the scatter plots of neighbor (West South main girder live load shoe area and middle area) and symmetrical locations (West North main girder live load shoe area and East North main girder live load shoe area). From these figures, it can be easily seen that the scatters are distributed on a line, which means there was a reasonably good correlation between

the neighbor and symmetric locations. On the other hand, when Figure 124 is closely checked, a low correlation can be observed, because the East North main girder middle location strain sensor and West South live load shoe area strain sensor are not excited with a given loading. This means there is very small structural relation between these two locations.

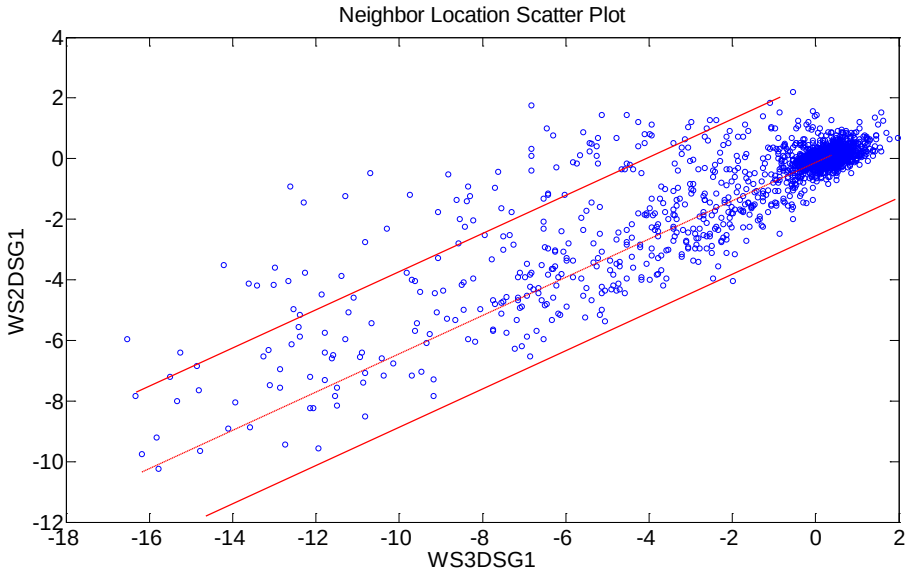

Figure 122: West South Main Girder Neighbor Location Scatter Plot

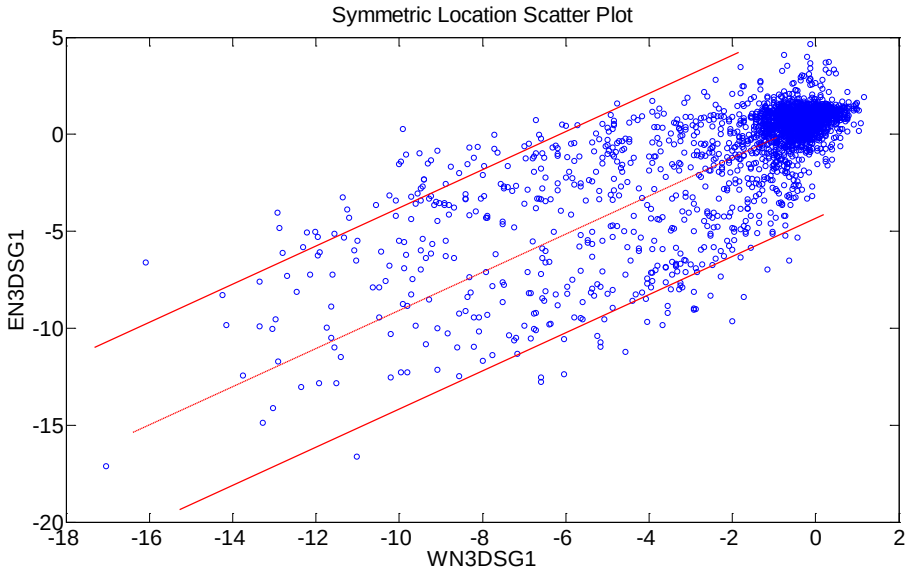

Figure 123: Symmetric Location Scatter Plot

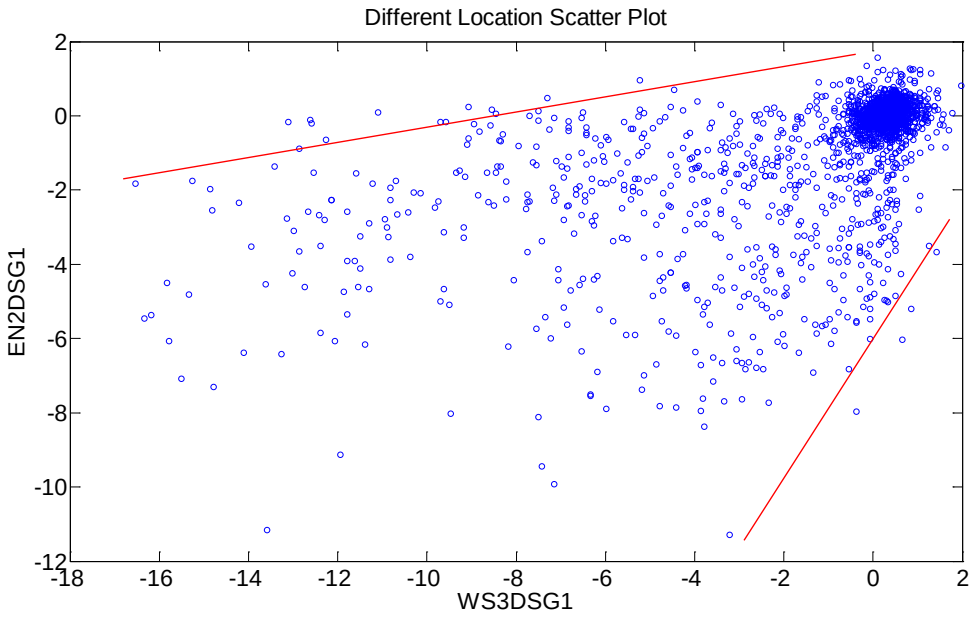

Figure 124: Different Location Scatter Plot

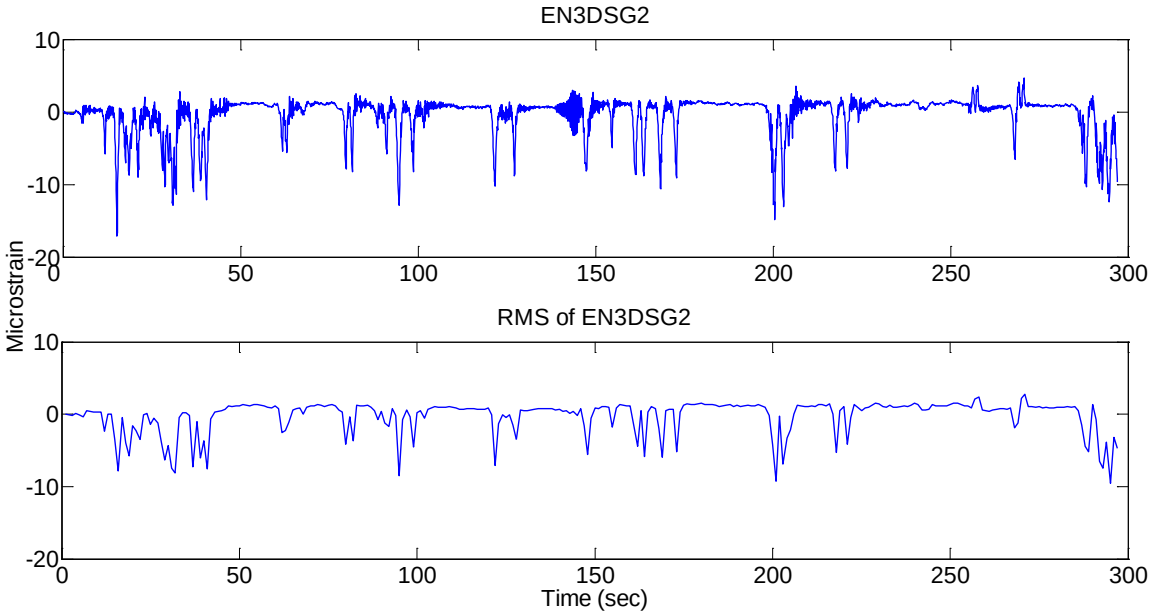

Figure 125: Strain Comparison After RMS

Another data analysis application is the root mean square (RMS), which is also a statistical measure that shows the magnitude of varying quantity. Basically, as a powerful signal processing tool, RMS is the square root of the mean of the squares of the values for each window in the data set. This can be employed to eliminate the dynamic effects on

the strain data, but as it is seen from Figure 125, RMS application decreases the strain values, eliminating some valuable information.

In this study, the researchers implemented a number of different techniques, as described in the sections above, and also some others that are not reported here (e.g. time-frequency analysis). Based on extensive preliminary work, some of the most promising techniques were employed, as they can be considered robust, easy to interpret, and practical for automation, while reducing the size of the data. The implementation of these techniques with real data for structural and mechanical conditions will be presented in the following chapter.

7. FIELD TESTS WITH ARTIFICIALLY INDUCED DAMAGE AND LONG TERM MONITORING

7.1. Objectives of the Tests and Monitoring

One of the important objectives of this monitoring study was to collect data that would serve two purposes: to better understand the operation environment of a movable bridge, and to establish criteria for system-wide monitoring of a bridge population. Long term monitoring of the bridge was conducted to determine the operating conditions of the critical structural, mechanical and electrical components. The following are to be monitored for a sufficiently long period of time: the traffic induced stresses, the impact of temperature induced effects, the opening and closing of the leaves, and activation of mechanical and electrical components. Monitoring serves to increase the understanding of the behavior of the bridge and the causes of this behavior. The comprehensive monitoring system, with different sensor types installed at different locations, is discussed in the previous chapters. Data analysis methods were also discussed in the previous chapter. In this chapter of the report, the application of those methodologies will be presented for both structural and mechanical components. Field tests were conducted to establish thresholds for conditions that are critical for the maintenance and operation of the bridge. These conditions will be referred to as "damage." In collaboration with FDOT engineers, some of the most common structural maintenance problems are identified and subsequently implemented on the movable bridge to simulate such damage conditions.

7.2. Damage Scenarios

7.2.1. Structural Alterations and Simulated Damage

7.2.1.1. Live Load Shoe (LLS) Shim Removal

The two main structural damage scenarios for this study are live load shoe shim removal and span lock shim removal. A combined damage scenario was also applied to the structure. First, the West South LLS shims were removed (Case-1), then the West South SL shims were removed for the combined damage scenario (Case-2), and finally the LLS shims were installed again to see only the SL effect on the structure (Case-3).

The Live Load Shoes (LLS) are the support locations of the main girders when the bridge is in closed position (Figure 126). For the Sunrise Blvd. Bridge the LLS is located forward of the trunnions. Cracking and wear are rarely seen on the live load shoe,

but mainly, operational problems, such as loss of contact, are of concern. If misaligned or improperly balanced, the bridge may not fully sit on the LLS. In that case, the dead load and traffic load are transferred to the gears and shafts, which cause damage to mechanical assemblies. Small gaps also lead the girders to pound on the live load shoes, which results in further misalignment, additional stresses, fatigue damage, and excessive wear.

Figure 126: Live Load Shoe (LLS) and the Shim Removal Operation by FDOT Contractors (sketch adapted from Christa McAuliffe Bridge construction plans)

Case-1 is the creation of a gap (around 1/8" up to 3/16") between the West South LLS and resting support pads, which corresponds to non-fully seated LLS (Figure 127). This will cause misalignment and problems for proper opening and closing of the leaves. Moreover, because of the inadequate support conditions, bouncing may occur in the girders, creating additional stresses due to impact, as well as stress redistribution, possibly subjecting the structure to different internal forces.

Figure 127: LLS with Shims and Without Shims

7.2.1.2. Span Lock (SL) Shims Removal

In double leaf bascule bridges, Span Locks (SL) are used to connect the tip ends of two cantilever bascule leaves; therefore, both leaves are forced to deflect equally (Figure 128). Consequently, this situation prevents a discontinuity in the deck during the operational traffic. In most of the span locks, there are two main components: the receiver and the rectangular lock bar. These elements are located in different leaves. During operation, the lock bar slides across bronze shoes, mounted in the rectangular guide and receiver housings.

Figure 128: Typical Span Lock (SL)

The main concern for the span locks is that the coupling has to be loose enough to allow a proper opening operation, but at the same time, the gap between the bar and the receiver has to be small enough to ensure the adequate connection with minimal bouncing while vehicles cross from one leaf to the other. This is achieved by placing metallic sheets (or shims) to adjust the spacing. The housings are usually mounted to the side of the bascule girders, or in the webs of the floor beams. Lock bars are typically driven or retracted directly, using a linear actuator that can be electric, hydraulic or mechanical (Figure 129). Span locks are some of the members that fail the most due to deterioration or incorrect operation. For the SL shims removal case, some of the shims were removed to create a gap of approximately 1/8” up to 3/16” on the West South SL (Figure 130).

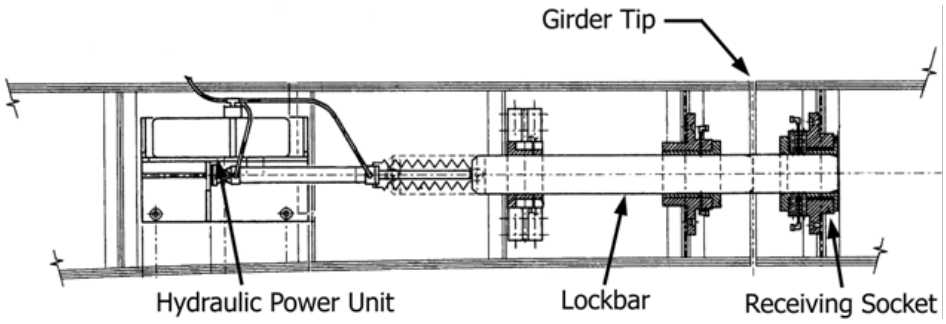

Figure 129: Lock Bar, Receiver and Hydraulic Unit (sketch adapted from Christa McAuliffe Bridge construction plans)

Figure 130: FDOT Contractors Removing Some of the Shims from the SL

7.2.2. Mechanical Alterations and Simulated Damage

7.2.2.1. Gear Box Oil Removal

A gear box, also called the transmission, uses gears to provide speed and torque conversions from a rotating power source to another device. The gear box is equipped to provide the necessary amount of oil to the various gear meshes and bearings, thereby resulting in smooth and trouble free operation. The gear box should be regularly checked for any leaks to see if the gear box has adequate oil. In this project, the oil in the gear box

was partially removed to provide data corresponding to such an undesirable condition. Figure 131 shows the removal of the oil from the gear box. Only 25% of the oil was removed, and the effect of the oil reduction was monitored by six accelerometers attached to the gear box during a few openings.

Figure 131: Removal of the Oil from the Gearbox

7.2.2.2. Open Gear Lubrication Removal

The open gear is situated where the superstructure and the mechanical parts meet (Figure 132a). The shaft delivers the force to Rack and Pinnion (RP), while the RP gear delivers the force to the open gear shown in the Figure 132a. For smooth operation, the open gear and RP gear should be properly lubricated. In order to observe the effect of lack of lubrication at these gears, grease was removed, and the response was monitored by the horizontal accelerometer on Rack and Pinnion. Figure 132c and d show the open gear with and without the grease.

a) Open Gear

b) Gear on Rack and Pinion

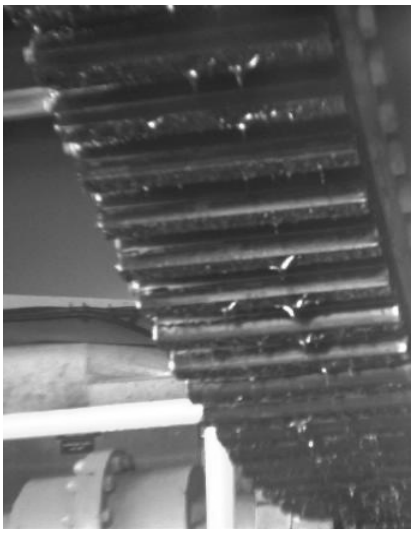

b) Open Gear with Grease

c) Open Gear without Grease

Figure 132: Removal of Open Gear Grease

7.2.2.3. Rack and Pinnion Bolt Removal

The Rack and Pinnion is located between the shaft and the open gear; therefore, it can be considered a transmission zone for opening and closing operation forces. Therefore, it should be free from defects to ensure safe operation of the bridge. Here, the removal of bolts was the simulated damage scenario, and the effect of the absence of these bolts was monitored by one horizontal accelerometer. Figure 133 shows the Rack and Pinnion with the removal of the bolts.

Figure 133: Rack and Pinnion Bolt Removal

7.2.2.4. Shaft Bolt Removal

Another important mechanical component is the shaft between the gearbox and RP, which is used for transmitting torque and rotation. Since the shafts are subjected to torsion and shear stress, they should be strong enough to bear these forces. In this study, the effect of loosening the bolts at the location where the shaft is connected to the Gearbox was monitored. Figure 134 shows the removal of the bolts from the shaft.

Figure 134: Removal of the bolts

7.3. Data Analysis to Detect Damage and Establish Triggers

7.3.1. Identification of Structural Alterations at Live Load Shoe and Span Lock

Three different damage cases were considered and implemented with the collaboration of FDOT engineers. In Case-1, the girder was not fully seated on the LLS. Case-2 was the combined damage scenario with the LLS, and involved slightly increasing the gap between the SL bar and the receiver conditions. Case-3 was only SL damage. All damage scenarios were induced as follows: first, some of the LLS shims were removed and the bridge was monitored during normal traffic operation; second, the shims of the SL housing were removed in addition to the first case, and vehicles were allowed to cross the bridge while the system monitored the structural responses; lastly, the shims of the LLS were installed again to see only the SL effect during traffic operation.

Detection of damage or malfunction at an early stage is one of the main goals of any structural monitoring system. Possible methodologies, which use strain data to identify structural damage, were discussed in previous chapters. In Figure 135, the strain locations are shown. It should be noted that a 3rd order, zero phasing, low-pass filter, with a 2 Hz cutoff frequency, was applied to the strain data to eliminate the dynamic effects of the traffic. The order and cutoff frequency of the filter was determined after detailed investigations. The main consideration for the cutoff frequency was the first vertical mode frequency of the bridge. Computational efficiency was another consideration for the order of the filter.

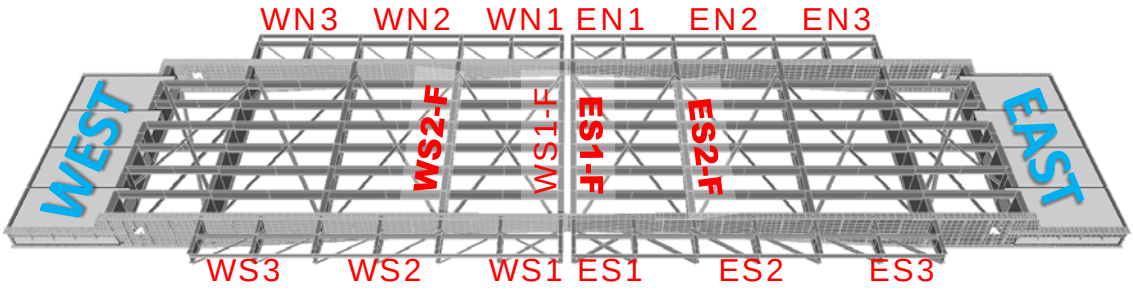

Figure 135: Strain Gage Locations on the Bridge

As mentioned in the previous chapters, cross correlation is a measure of the similarity between two data sets; having similar behavior gives higher correlation,

whereas having dissimilar behavior gives lower correlation. For this section, data sets were analyzed between the period of 10/15/2009–10/31/2009. This period was selected because the damage scenarios were applied to the bridge on 10/21/2009, and therefore, one week before and after this date was used for the undamaged cases. In this period, 80 data sets were investigated. It should be noted that 25 of these data sets came from the damage day and the rest came from the undamaged days.

In order to demonstrate this approach, first, the correlation between the top flange and bottom flange strain correlations was computed. In Figure 136, the West North main girder LLS location is shown, and in Figure 137, the East North main girder middle location top flange and bottom flange strain correlations can be seen. With the outliers excluded, the average correlation coefficient was over 0.9, with very low variation. Another aspect of inspecting the top and bottom flange correlations is tocheck data quality, since it is expected to have a high correlation with low variation from measurements characterizing a particular response especially from the same cross section.

It should be noted that the correlation between different, remote measurement locations may not necessarily be high, due to different loading conditions and response of the bridge at different locations. However, it is reasonable to expect a somewhat consistent level of correlation under regular operating conditions; deviation from which can indicate a change or damage in the structure.

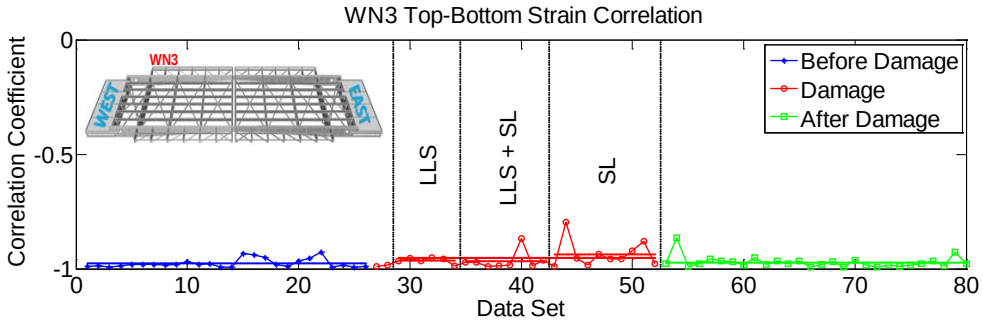

Figure 136: WN3 Top & Bottom Strain Correlations

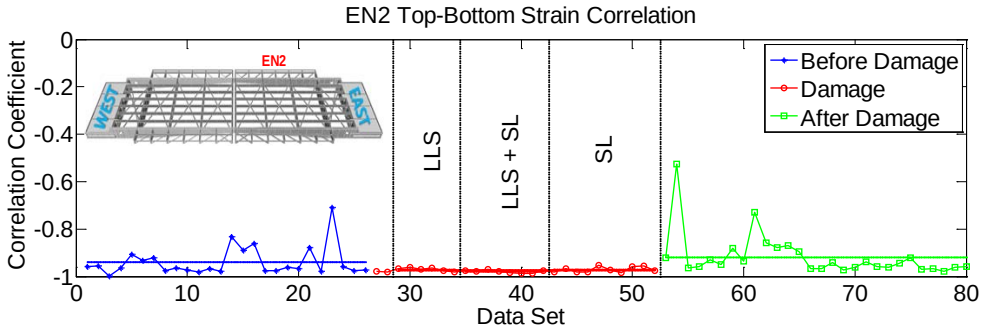

Figure 137: EN2 Top & Bottom Strain Correlations

After checking the data quality, cross correlation analyses were conducted for damage identification. In this manner, data sets were separated as: before damage; damage; and after damage, which can be seen in the following plots. The average correlation coefficients for each part are shown to illustrate how damage impacts the correlation of sensors. Moreover, damage data sets were also separated into three subgroups, which correspond to: Case-1 (LLS shims removal), Case-2 (combined effect), and Case-3 (SL shims removal). For this investigation, four analysis groups were defined as follows: Damage Location-1 (LLS), Damage Location-2 (SL), Corner Locations, and Floor Beams.

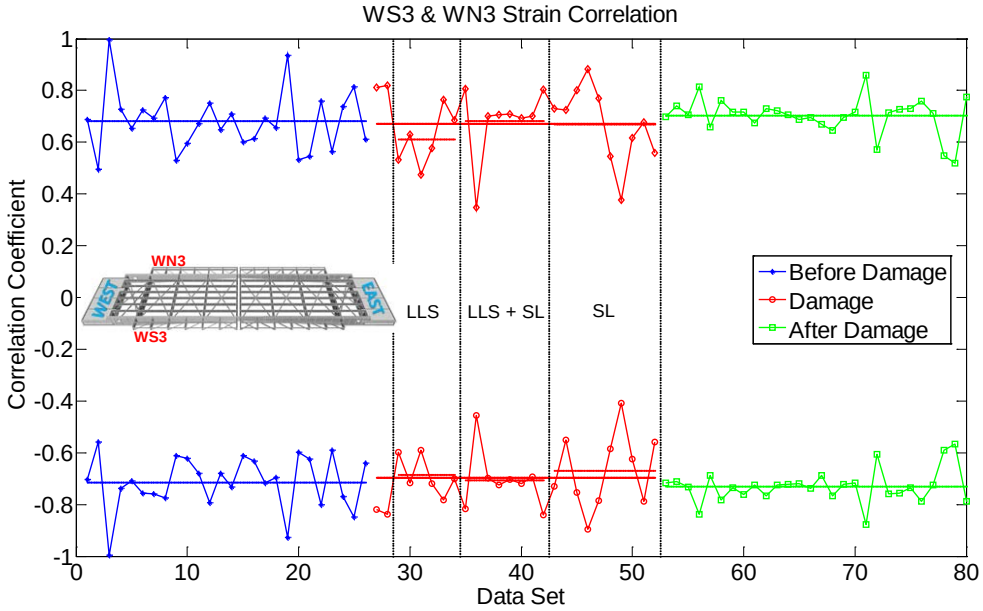

Figure 138: WS3 & WN3 Strain Correlations

In the first analysis group, “Damage Location-1”, the correlation between the West South main girder LLS location (WS3) and other LLS locations (WN3, EN3 and ES3) were investigated. Change in support conditions can be expected to impact the load distribution; consequently, there exists a correlation between the LLS at WS3. For these sets of correlations from the WS3 location, bottom flange strain was used constantly and compared with the other LLS locations both top and bottom flanges. Figure 138 shows the cross correlation coefficients of each data set between WS3 and West North main girder LLS (WN3). The top part of Figure 138 shows the correlation of the WS3 bottom flange and WN3 bottom flange strains. Since both sensors are at the bottom flange, a positive correlation was seen. On the other hand, the bottom part of Figure 138 is showing a negative correlation between WS3 bottom flange and WN3 top flange strains. The correlation was negative because when there was tensile strain at the upper flange, the strain at the lower flange was compressive. It should be noted that the following plots in this section will be in the same manner, along with the top-bottom flange correlations, for checking the data quality and detecting malfunctioning sensors.

From the damage identification point of view, Figure 138 does not show a significant change in the correlation coefficients, whereas Figure 139 and Figure 140 are showing a considerable deviation in the cross correlation coefficients -- a change that can be attributed to damage or structural change at the boundary conditions. The common point between these two plots (Figure 139 and Figure 140) is that both are showing correlation coefficients from two different leaves. Additionally, the trend of the coefficients from the healthy cases (±0.6) and the coefficients during damage simulations (±0.3) show a major difference. It is observed that the mean of the coefficients, before and after damage, is almost equal, demonstrating that the damage was repaired effectively. The behavior of the bridge after damage was similar to the baseline condition.

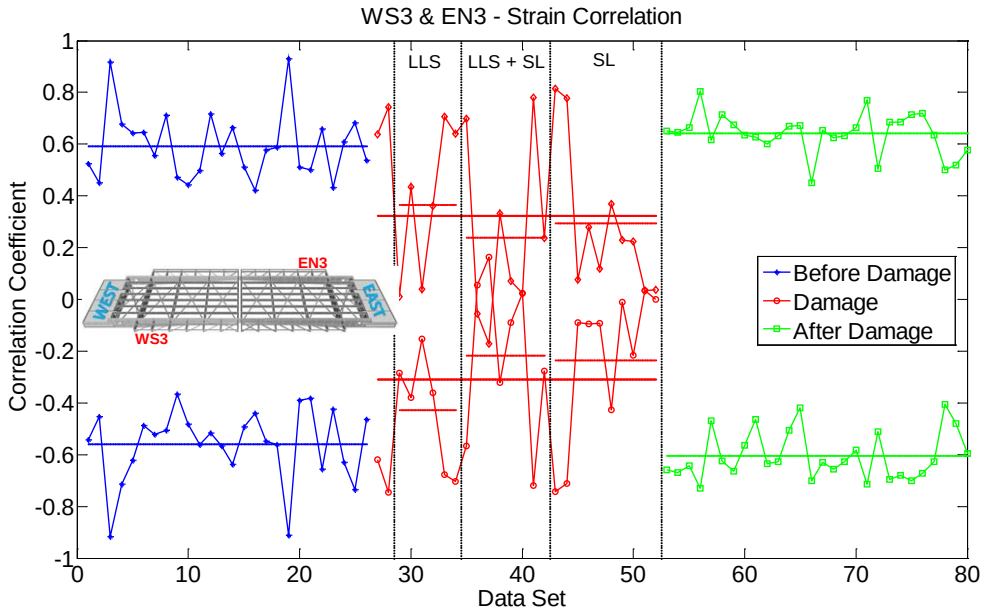

Figure 139: WS3 & EN3 Strain Correlations

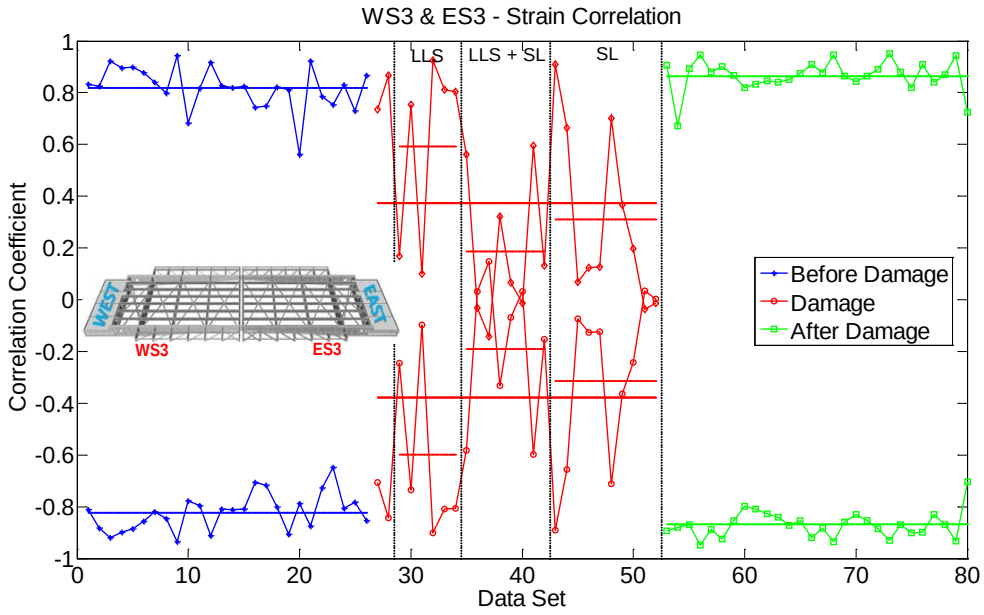

Figure 140: WS3 & ES3 Strain Correlations

Besides Damage Location-1 (LLS) group, when the Damage Location-2 (SL) group was checked, the same results were also seen. The trend of the strain correlation coefficients from same leaf did not change; however, when locations from different leaves were checked, the change was easily observed. For instance, Figure 141 shows the correlation coefficients of WS1 and EN1 strain gages. It should be noted that WS1 and

EN1 are the tip locations, and the lowest strain measurements were seen in these locations. Another important note here is that the correlation of top and bottom strain values was not too high; therefore, the tip locations can have some variability (especially at the bottom flange) in the strain measurements. Nonetheless, these locations also showed the damage in the LLS and SL locations.

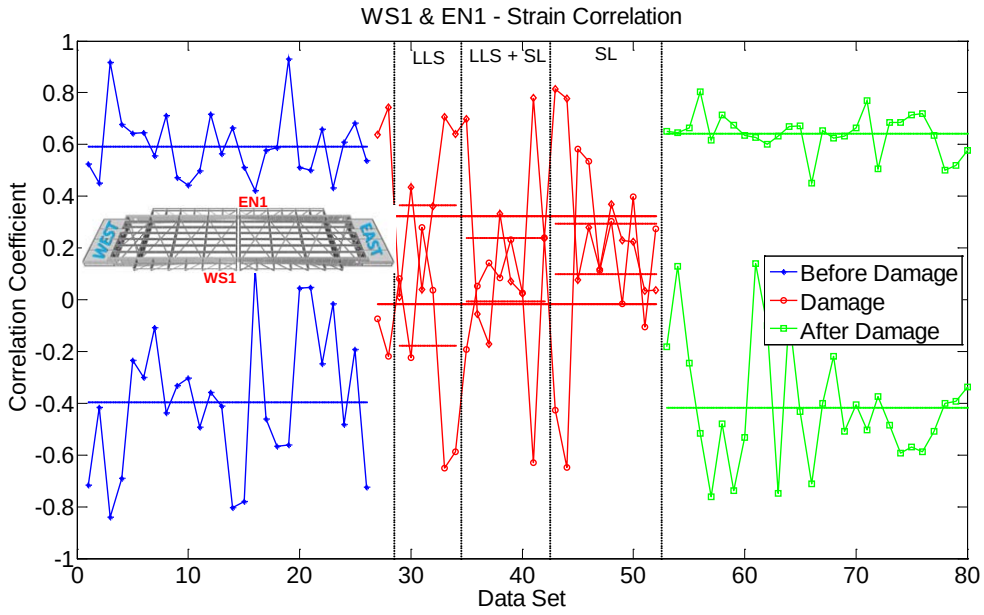

Figure 141: WS1 & EN1 Strain Correlations

After evaluating the correlations of damage locations, corner location correlations were also checked to show that it is not necessary to install a sensor around the damage location. For this reason, corner locations (WN3, EN3 and ES3), except damage location (WS3), correlations were investigated.

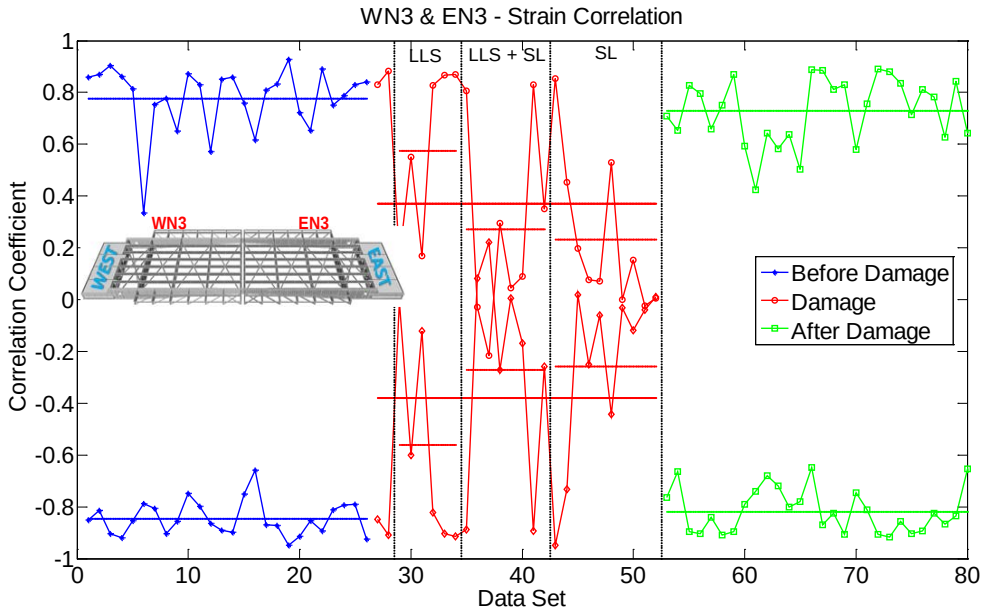

Figure 142: WN3 & EN3 Strain Correlations

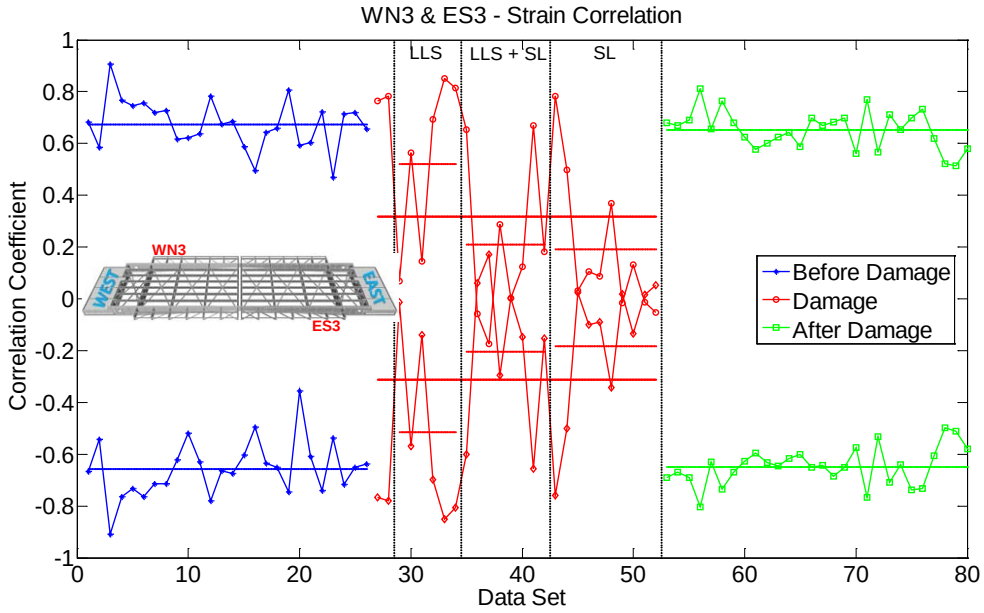

Figure 143: WN3 & ES3 Strain Correlations

Figure 142 and Figure 143 show the correlations of WN3 & EN3 and WN3 & ES3, while Figure 144 shows the correlations of EN3 & ES3. The same observation that damage can be identified from the correlation of different leaf strains was also made from these plots. Again, it should be noted that the damage location strains were not used in Figure 142, Figure 143, and Figure 144.

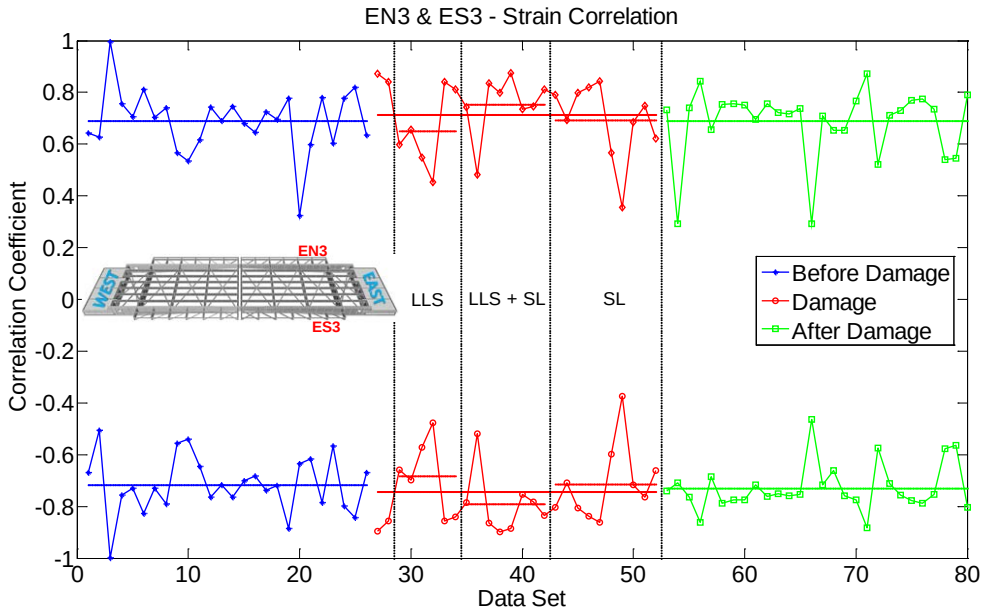

Figure 144: EN3 & ES3 Strain Correlations

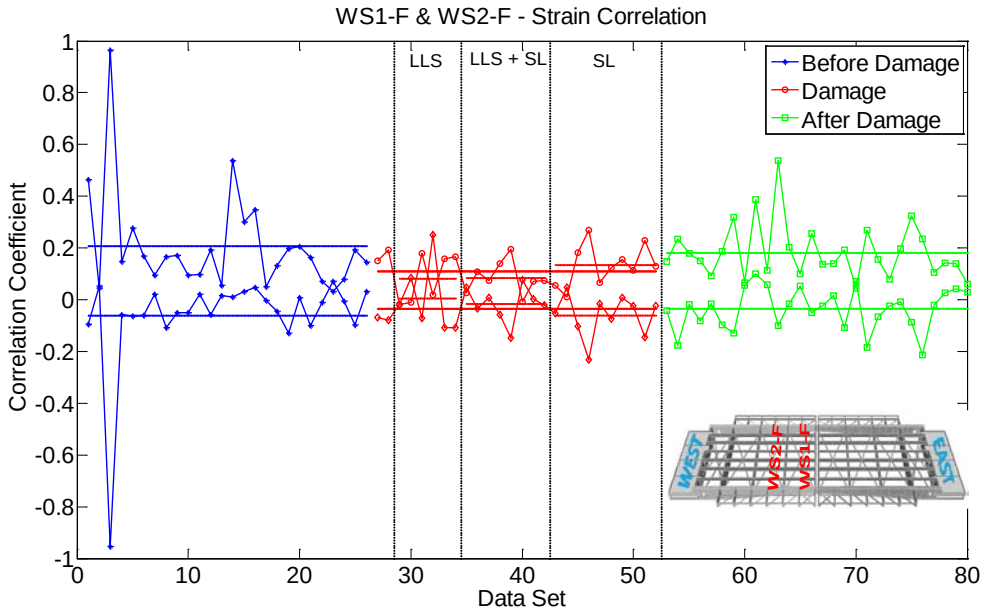

Figure 145: WS1-F & WS2-F Strain Correlations

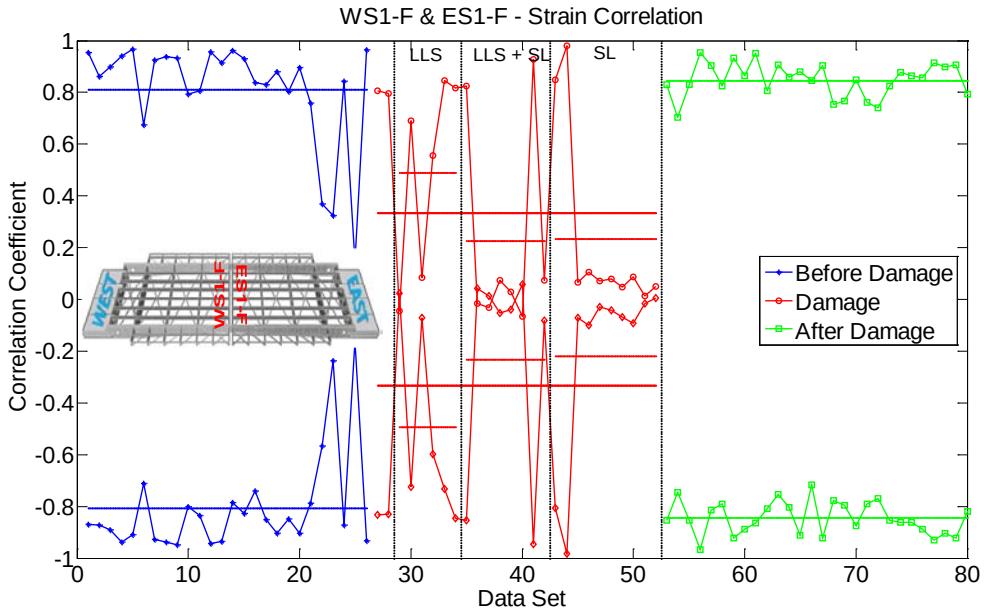

Figure 146: WS1-F & ES1-F Strain Correlations

The last group for correlation analysis was the floor beam correlations. The floor beams can be considered as the second most critical part of the structural components after the main girders. Their role in the structure is to transfer loads to the main girders; and thus, investigating the floor beam correlation was also important. As discussed before, damage could not be detected from the same side sensors, as shown in the correlation trend of WS1-F & WS2-F, Figure 145. On the other hand, damage can be detected from different leaves, such as from WS1-F & ES1-F, as shown in Figure 146.

7.3.2. Review of Results for Structural Alterations at Live Load Shoe and Span Lock

Based on the findings summarized above, it was seen that change (or simulated damage) can be detected by means of strain measurements, and more specifically, strain correlations of strain monitoring under any traffic loading. Individual strain measurements can be analyzed and checked; however, these measurements will vary due to loading magnitude and placement. Although maximum measurement can be an indicator for the stress levels due to traffic, any change of structural configuration due to damage cannot be easily extracted by just looking at the strain levels. Cross correlations of the measurements, however, indicate a level of correlation when monitored over long term. This trend can be tracked and evaluated to detect any permanent change, as shown

in the previous sections. The cross correlation approach is also helpful in detecting malfunctioning sensors especially for automated detection. This approach indicates that it is possible to reduce the number of sensors needed to detect the change induced to LLS and SL based on the measurements from a large sensor suite from the main girders, floor beams and stringers. Finally, this approach could indicate the effectiveness of maintenance procedures, as it was shown that the level of correlation was brought to its original level prior to damage, and more significantly, the level of variation is reduced.

7.3.3. Mechanical Alterations - Gearbox Oil and Open Gear Grease Removal

In this section, the removal of the gearbox oil and open gear grease are investigated by using the data from accelerometers installed on these components. The critical characteristics and distinct behavior change in dynamic response can be tracked over time by means of structural monitoring. Two recurrent types of damage were identified for bridge components namely, leakage from the gear box and inadequate lubrication of the open gear. The detection and diagnosis of damage in these parts are of great practical significance and importance in the sense that an early detection of these faults may help to avoid performance degradation and major damage to the machinery. The gearbox (Figure 147-a) was instrumented with six accelerometers at different locations in both the horizontal and vertical directions. The Rack and Pinions (Figure 147-b) was instrumented with one horizontal sensor to monitor the open gear. A large number of data sets from the healthy condition of these parts were collected (Figure 147-c and Figure 147-d). In order to see the effect of leakage from gear box, 25% of oil from the gearbox was removed. In addition, to simulate inadequate lubrication of open gear, large portion of the grease on the open gear was removed. Under these damage conditions, the gearbox and the rack and pinion were monitored during the opening and closing of the leaves of the bridge. Using healthy (baseline, undamaged) and unhealthy (altered, damaged) data sets, an artificial neural network-based framework was developed for detecting the mechanical alterations at the gearbox and the rack and pinion.

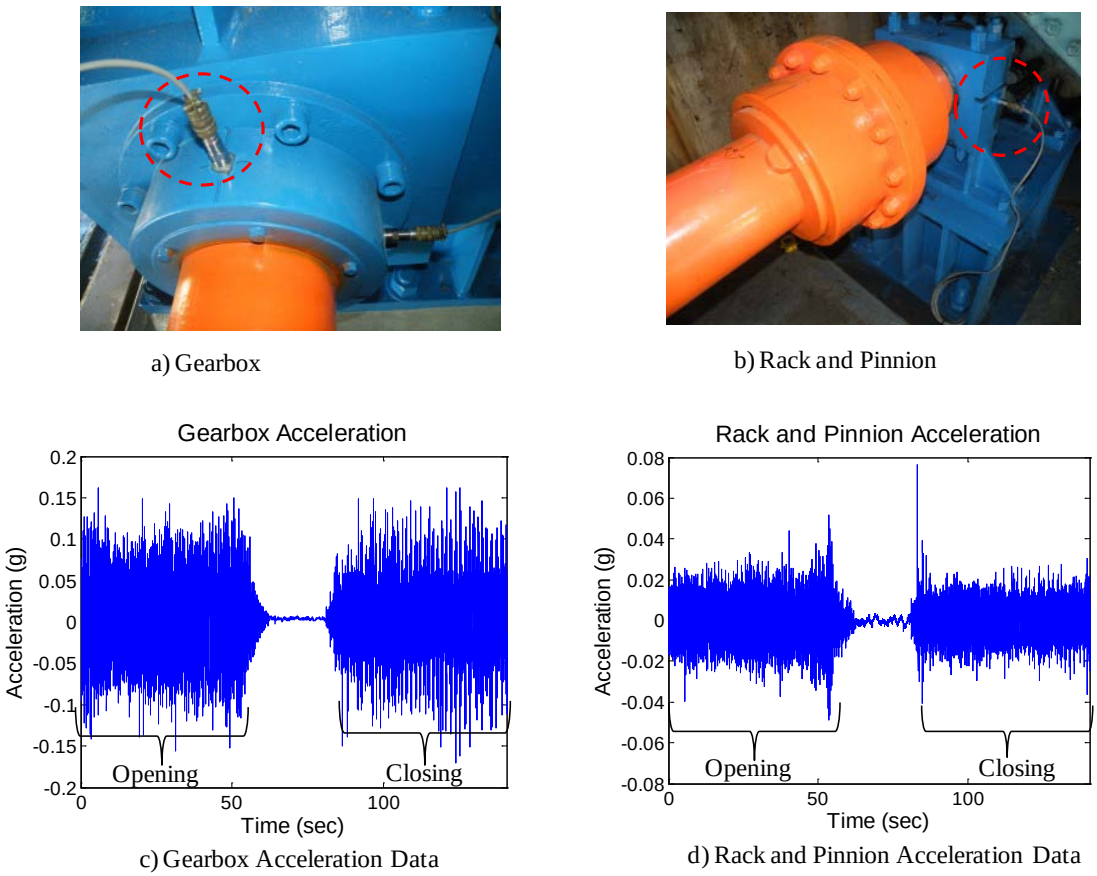

Figure 147: Sensors on Gearbox and Rack and Pinion with Corresponding Sample Acceleration Data

7.3.3.1. Artificial Neural Network (ANN) Framework

ANN learns from the existing patterns and then makes a prediction for the patterns which are not considered during learning. Therefore, the success of a network is measured by its generalization performance. If the difference between the actual and computed output by ANN is within the acceptable level, then the network can be used for prediction in the similar domain, which exhibits certain common characteristics with the existing patterns. The prediction performance of a network usually depends on the network parameters and the topology chosen. The best performance is generally achieved by extensive parametric study of the different networks using a trial and error approach. In each trial, performance of the network is evaluated. This process is repeated until the best architecture, with the right network parameters, is arrived.

As mentioned before, a large number of data sets from the healthy condition and several data sets from the unhealthy condition of monitored parts were collected. A thorough understanding of damage-sensitive features from these measurements was needed in order to obtain accurate damage prediction. Here, statistical methods were used to identify the certain features of opening and closing part of acceleration data. The statistical analysis of these features can be used to determine the current state of system health and any change in the features. The statistical significance of these changes in the extracted features was evaluated in neural networks. The identified features in this study were the maximum vibration (average of the ten largest to avoid extreme values) and minimum vibration (average of the ten smallest values) of opening and closing data sets, along with the standard deviation of these dynamic signals from the accelerometers. Considering these as input to the ANN and no damage/damage indication (as 0 and 1) as output from the ANN, a total of 172 input-output patterns (pairs) were generated and were divided into three sets, namely, the training set, the cross-validation set and the test set. The training set contained 125 patterns and was used to detect any relationship between the statistical parameters and damage. Out of 125 patterns, two (2) patterns indicated the damage due to removal of 25% oil from the gearbox, three (3) patterns indicated the damage due to inadequate lubrication of the open gear. The remaining patterns indicated no damage, in other words, representing the healthy condition of the components. The cross-validation set contained 40 patterns and was used to avoid an overfitting problem. The test set consisted of seven (7) patterns that were not used in the training phase, and it was used to evaluate the performance of the networks. Out of 7 patterns, one (1) pattern was used to identify the removal of 25% of oil from the gearbox, 3 patterns were used to identify the damage due to inadequate lubrication of open gear, and the remaining 3 patterns were used to identify the no damage. In this study, the Levenberg-Marquardt algorithm (Rao and Kumar, 2007) was used for ANN learning rule, and the sigmoid function was used for activation function. Since Levenberg-Marquardt requires less time and iterations to converge, it performs more efficiently compared to other learning rules, which in turn makes it ideal for trial of different networks. The use of sigmoid function requires that the input and output data be scaled to the range [0-1]. In the present study, the input and output data were scaled to a somewhat

narrower range, between 0.2 and 0.8, resulting in a considerable improvement in learning speed due to increased sensitivity of the sigmoid function within this range. Based on defined network parameters, the effect of the number of hidden layers and number of processing elements in hidden layers, as well as in output layer, were observed using several architectures. After completion of training of each network design, the performance of the network was tested using the test patterns that were not used during the training. The performance was measured by the average maximum error in the testing set and mean square error (MSE). This process was repeated for each network design. In this way, many networks which were capable of generalization at different levels were obtained. Among them, the best network was selected.

7.3.3.2. Best Neural Network Model

The learning and prediction performance of the network vary depending on the number of hidden layers and the number of nodes in the hidden layers. Based on preliminary studies, it was seen that the number of hidden layer and hidden nodes had effect on mean square error (MSE), consequently on the predictive ability of the ANN. All the trained networks here in this study were able to predict the existence and location of damage for all the testing patterns. Our studies showed that for this particular machinery monitoring, networks with two and three hidden layer nodes had the lowest MSE and lowest prediction difference. Hence, a single or two hidden layer with two or three number of neurons was sufficient for modeling of this problem with a great accuracy. The best MSE and prediction performance was achieved by a network architecture with two hidden layers and 2 nodes per layer which was denoted as 6-(2-2)-2.

As discussed, the best performance in predicting was achieved by using two hidden layers, each having two nodes with the defined network parameters. To make sure that the network training has been satisfactorily completed and the network is capable of generalization, a set of unused patterns must be selected and the network should be tested with these patterns. For this purpose, a total of 7 testing patterns were used to observe the prediction performance of all the architectures considered in the study. As discussed before, out of 7 patterns, 1 pattern was used to identify the removal of 25% of oil from

the gearbox, 3 patterns were used to identify the damage due to the inadequate lubrication of open gear, and the remaining 3 patterns were used to identify the no damage.

Table 11: Testing set with Actual Outputs and Best Network (6-(2-2)-2) Outputs

INPUTS						ACTUAL OUTPUTS		NN OUTPUTS	
GB Max	GB Min	GB Stdev	RP Max	RP Min	RP Stdev	GB	RP	GB	RP
0.1650	-0.1682	0.0495	0.0276	-0.0321	0.0093	1	0	1.000054	0.000053
0.1332	-0.1398	0.0360	0.1585	-0.1442	0.0118	0	1	-0.000010	1.000018
0.1392	-0.1348	0.0358	0.1299	-0.1863	0.0125	0	1	0.000038	1.000020
0.1417	-0.1523	0.0364	0.1236	-0.1563	0.0114	0	1	0.000038	1.000020
0.1437	-0.1524	0.0416	0.0337	-0.0286	0.0094	0	0	-0.000025	0.000016
0.1481	-0.1484	0.0397	0.0313	-0.0295	0.0092	0	0	-0.000026	0.000016
0.1356	-0.1475	0.0404	0.0302	-0.0329	0.0092	0	0	-0.000025	0.000016

Table 11 shows the actual outputs (known healthy/unhealthy cases) and best network outputs for all testing patterns. It is clear that the prediction of the best networks for 7 unseen patterns was quite satisfactory. The best network yielded a maximum difference of 0.007% for the gearbox and yielded a maximum difference of 0.005% for the rack and pinion, under the defined network parameters. This indicates that the networks trained successfully, established a relationship between the statistical parameters and unhealthy cases, and interpolated this relationship for other unseen data with a great accuracy. In addition, the coefficient of correlation between actual and predicted outputs was 0.999 for the gearbox and 1.000 for the rack and pinion, indicating that the generalization performance of the network was very good and it was able to generalize within the range of the data used for training.

7.3.4. Mechanical Alterations - Open Gear Lubrication Removal

The lack of lubrication and corrosion of the open gear is one of the mechanical alterations, which was previously discussed. Surface mounted sensors cannot be applied in the case of an open gear. As a result, a non-contact method using cost-effective cameras was considered to detect lack of lubrication to avoid possible corrosion. This section will briefly discuss a methodology that was developed and demonstrated using

cost effective cameras and computer vision based methods to detect this undesirable condition.

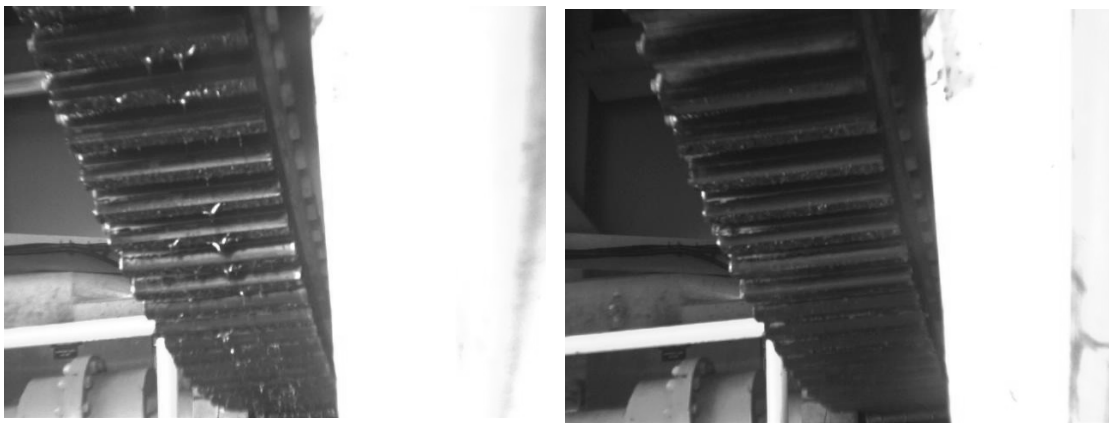

Figure 148: Open Gear with Proper Lubrication and with Lack of Lubrication

By visual inspection, the proper lubrication can be observed (Figure 148). Now, it is important to define some type of computer vision algorithm to detect and differentiation these two cases. In order to do that, first the area of interest should be defined, and this area should be analyzed using computer vision techniques (Figure 149).

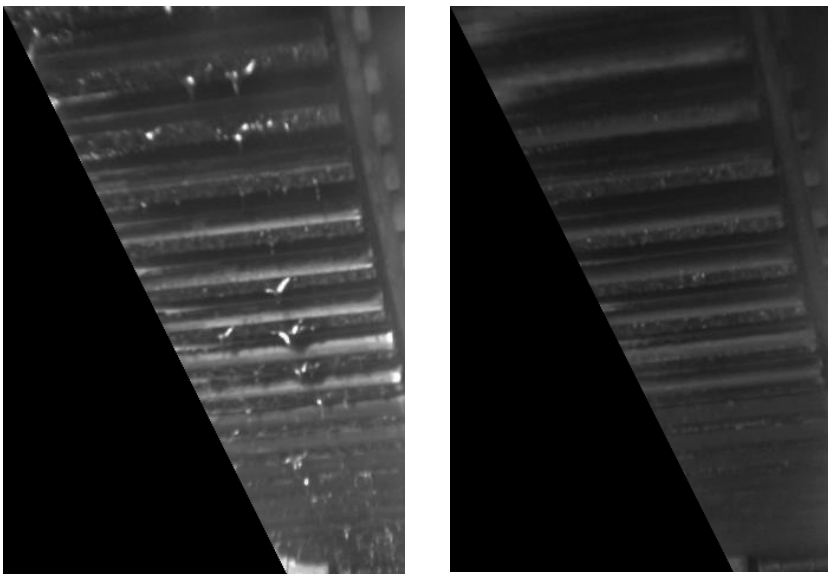

Figure 149: Selecting the Area of Interest for Detection Purposes

After the area of interest was defined, the image was analyzed using edge detection techniques to identify the areas of grease, first for the baseline case, which is the

desirable condition. This case indicated that the grease chunks are visible, hence, observed using the edge detection technique as shown in Figure 150. It is also seen in the same figure that edge detection identified a totally different number of grease areas. An index comparing the two areas would be an indicator for the change in proper lubrication.

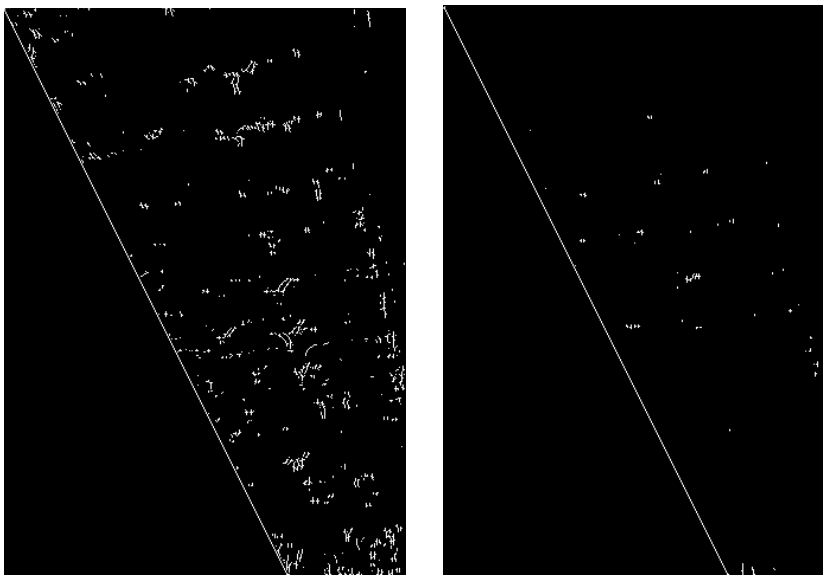

Figure 150: Implementation of Edge Detection Techniques for Detection Grease for with and without Proper Lubrication

The next step for demonstrating the use and implementation of this technique was to analyze data from long term measurements. For this reason, a time span of approximately a month was considered before the implementation alteration (grease removal). The index, *LI*, was computed for this time window. When the grease was removed, this condition could be detected from the *LI*, and tracked over a period of time until the next maintenance where is can be seen that the average *LI* was improved. The results from approximately three month window are shown in Figure 151. This method is showing an excellent promise to detect the lubrication of the open gear based on the data collected as part of the mechanical alterations.

Figure 151: Monitoring and Tracking Lubrication Index (LI) Over Long Term

7.3.5. Review of Results for Mechanical Alterations

As presented above, different methodologies were employed for detecting mechanical problems. Gearbox oil reduction and rack-pinion grease removal were monitored with accelerometers using the data when the bridge was opened and closed. The high speed vibration data was collected and analyzed using an Artificial Neural Network (ANN). Once established with the long term data and the damage threshold data, this method offers an easy tracking method by indicating a healthy case with an ANN output of “0” and unhealthy case with “1.” This method is easy to interpret for maintenance and operation purposes. Another critical condition that was considered for the mechanical alterations was grease removal from the open gear. In this case, the researchers developed a methodology using computer vision, with an index to monitor and track the change in the lubrication state of the open gear. By tracking the average value of the Lubrication Index (LI), it was also possible to determine the change in the lubrication, as demonstrated with a 3-month monitoring data where the grease was removed as part of the mechanical alterations Such a method with an index provides the

engineers with actionable information, as well as data for evaluating the state of maintenance.

7.4. Long Term Monitoring of Critical Components

7.4.1. Friction Number

The friction number of a movable bascule bridge is a value determined from an operation known as balance testing. Balance testing is a method for determining whether a bridge is in proper balance. For the Sunrise Bridge, like most bascule bridges, the ideal balance condition is slight leaf heaviness, and it is the condition for which the bridge and mechanical components were designed. Operation under balance conditions other than this may place excessive wear on the bridge's structural and mechanical components, leading to costly repairs or possible safety concerns. The friction number is commonly used as an indicator of a change in balance conditions.

In this project, the Handbook of Bascule Bridge Balance Procedures (1982) was used as a guideline for calculation of the balance test parameters, including the friction number. In general, the friction number, AVTF, is defined as:

---

where $T_{opening}$ and $T_{closing}$ are the opening and closing torques, respectively. Strain rosettes located on each main shaft record axial strains.

These recorded strain values are transformed to obtain an engineering shear strain on the surface of the shaft, which is further adjusted based on mechanical factors specific to the bridge of study to obtain the total leaf opening and closing torques. For trunnion-type bascule bridge's the equation for the total torque is given by:

—

where γ is the shear strain on the surface of the shaft in microstrain.

The following values where used for the Sunrise Bridge: Radius of instrumented shaft, r = 3.995 inches; Radius of Rack, R = 102 inches; Pitch radius of pinion gear, C_1 = 6.963 inches; and Gear Ratio between instrumented shaft and final shaft, GR = 1.0 (Shaft Design Plan). Employing mechanics of materials concepts along with Eqn.-18, the

following equation was derived to calculate total opening/closing operation torque from the installed strain rosette measured axial strain values:

where ε_3 = axial strain measured from strain rosette leg 3 (microstrain) and ε_1 = axial strain measured from strain rosette leg 1 (Figure 152).

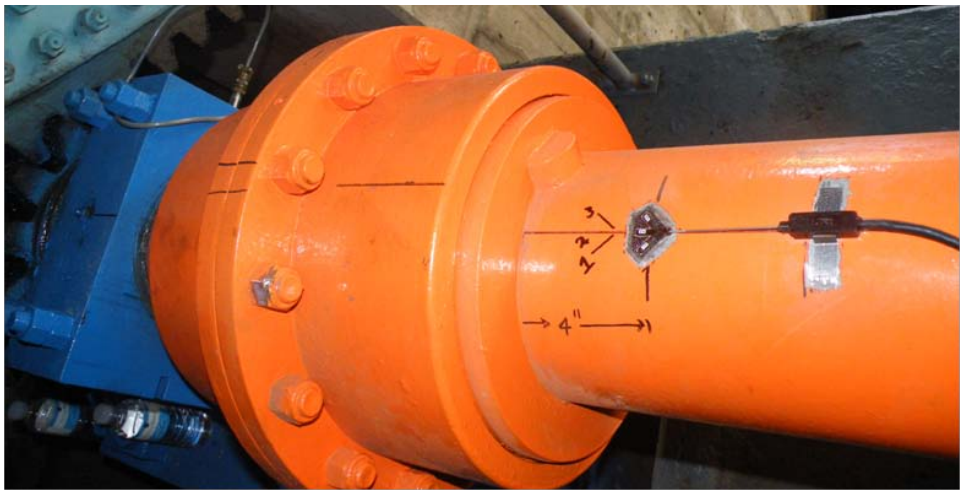

Figure 152: Strain Rosette on the Drive Shaft

In this report, the opening and closing operation data collected from 10/15/09 to 11/15/09 from the West leaf was analyzed and the results are presented. It should be noted that typical balance testing conducted by FDOT field engineers only analyzes the data from one of the two shafts from each leaf. However, in this study both shafts for each leaf were instrumented with two strain rosettes for calculation redundancy and consistency purposes. Comparison of the opening and closing torque curves vs. angle and calculated AVTF for each of strain rosettes indicated consistency between one another and with prior FDOT collected data (Figure 153).

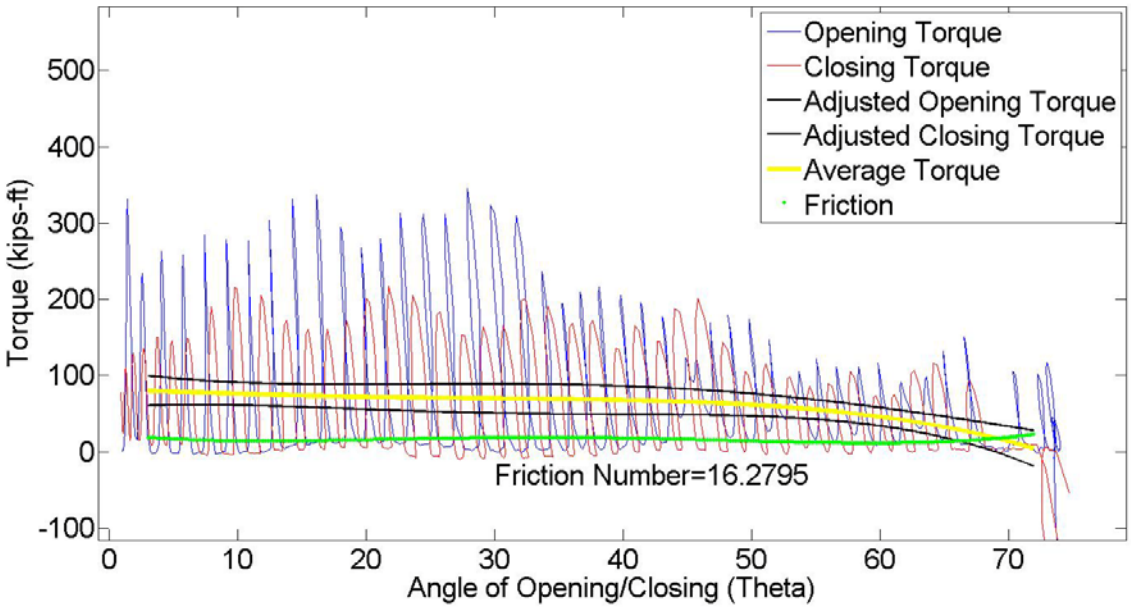

Figure 153: West Leaf North Shaft SR2 Open/Closing Torque 10/22/2009 4:30PM

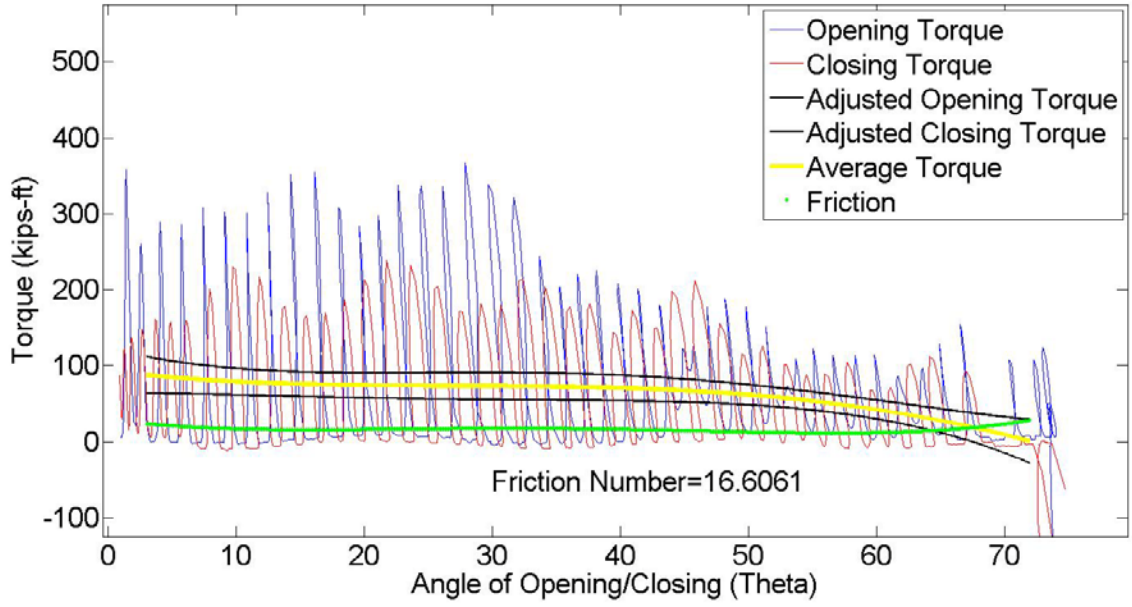

Figure 154: West Leaf South Shaft SR2 Open/Closing Torque 10/22/2009 4:30PM

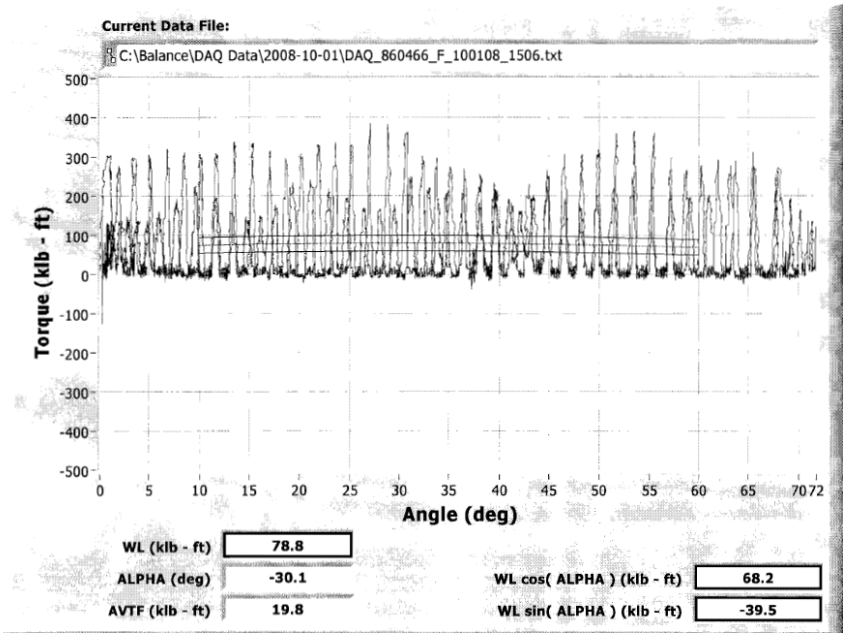

Figure 155: West Leaf FDOT Archived Open/Closing Torque 10/01/2008

The calculated friction number values were within the FDOT recorded range of values from 2003-2008. It should be also be noted that this study used a different test setup, DAQ, and post processing procedure from the FDOT, yet, yielded very similar results. An important issue of the balance test configuration was the location of the strain rosettes along the shafts. The common rule of thumb for balance testing configuration calls for a 6 inch buffer between installed strain rosette and shaft end, especially for mitigating possible stress concentrations and fluctuations near the connection at the shaft ends. Correspondence with Mr. Duane Robertson, FDOT Movable Bridge Specialist, indicated that this rule of thumb, based on past recommendations, accounts for the possibility of material discontinuities, or hardening near the shaft ends as a result of the manufacturing process. In addition, Mr. Robertson reported that this 6 in. tolerance was not followed in a few of the other monitored Florida bridges, and no inconsistencies or problems have been observed as a result of these strain rosette placements. The strain rosettes at Sunrise Bridge were about 4 in from the end of the shafts. The data analysis results obtained using data from different locations on the shafts showed that the data were consistent. Therefore, given the consistency of friction number results with adjacent

sensor friction number results, and archived FDOT recorded values, the current testing configuration and location of the strain rosettes did suggest any problems.

A major difference and advantage in this project was the determination of the friction number for every opening/closing operation, which allows for the analysis of the friction number trend with respect to time. The friction number for each operation (465 operations) from 10/15/09 to 11/15/09 for the West leaf was plotted using an average of the friction number values from the 3 West leaf sensors.

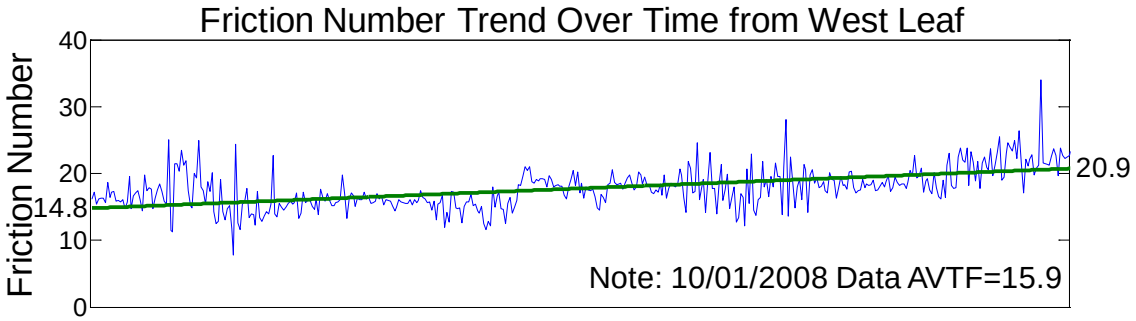

Figure 156 – Friction Number Trend from 10/15/09 to 11/15/09

From this figure a gradual increasing trend in the friction number can be seen. Examination of the mean temperature measurements recorded for every operation show a similar, but inverse, trend (Figure 157).

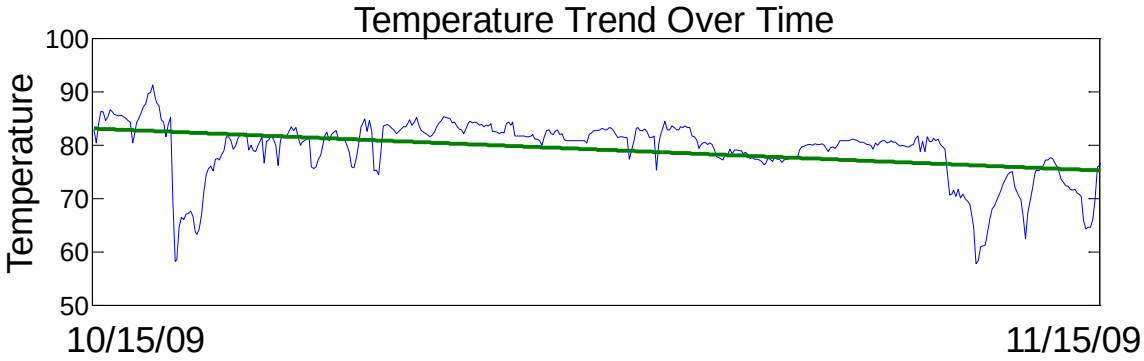

Figure 157 – West Leaf Open/Closing Operation Corresponding Temperature Trend 10/15/09 to 11/15/09

Further analysis reveals that the friction number showed a meaningful correlation with both temperature and humidity, as shown in the Table below. Both mean wind speed and barometric pressure did not show any significant correlation with friction number.

However, further examination of select large wind speed events may show significant correlation. A more reliable analysis for understanding the correlation of environmental effects to friction numbers can be carried out by monitoring the friction numbers over a longer period of time with different environmental conditions.

Table 12: Friction Number Correlation Coefficients with Temperature, Humidity, Wind Speed and Barometric Pressure

Friction Number Correlation Coefficients				
Friction Number	**Temperature Mean**	**Humidity Mean**	**Wind Speed Mean**	**Barometric Pressure Mean**
WNSR1	-0.4110	-0.3394	-0.0173	-0.0943
WNSR2	-0.4987	-0.3308	0.0563	-0.0684
WSSR2	-0.3317	-0.3416	-0.0591	-0.1152
Averaged	-0.4566	-0.3874	0.0018	-0.0946

FDOT personnel have indicated that balance adjustment decisions are generally based on the history of friction numbers. Review of balance testing records indicated that balance testing of the Sunrise Bridge is not under a regular schedule and testing has been conducted at various times throughout the year. Therefore, due to the apparent correlation between friction number and temperature, temperature effects should be considered as a source of fluctuation.

7.5. Structural Response due to Environmental Traffic Induced Effects

Long term monitoring is a crucial part for Bridge Maintenance Monitoring System (BMMS), since the environmental and traffic effects on the structure can be characterized over the long term with a better understanding. In addition, the root causes of certain types of behavior can be established with this approach. In this section, both of these environmental and traffic effects over long term monitoring will be discussed.

For investigating the temperature effects, vibrating wire gages were installed on the main girders, as well as other elements such as floor beams. These gages are very reliable for collecting strain and temperature data in every 15 minutes. On the other hand, for monitoring effects due traffic, high speed strains and acceleration data were collected three times a day. These times (9:10 am, 1:10 pm and 5:10 pm) were selected to capture the extreme loading events on the structure due to rush hour traffic.

7.5.1. Temperature Effects

The temperature induced effect on a structure is best observed through the long term monitoring. Seasonal and daily temperature induces changes, as well as sudden temperature shocks need to be captured to establish the effects on different components of the bridge. Depending on the material type and boundary conditions temperature induced stresses will vary. Since vibrating wire strain gages are made of steel, their readings are better adjusted on similar steel material, and they respond to temperature changes in the same way steel structural members respond.

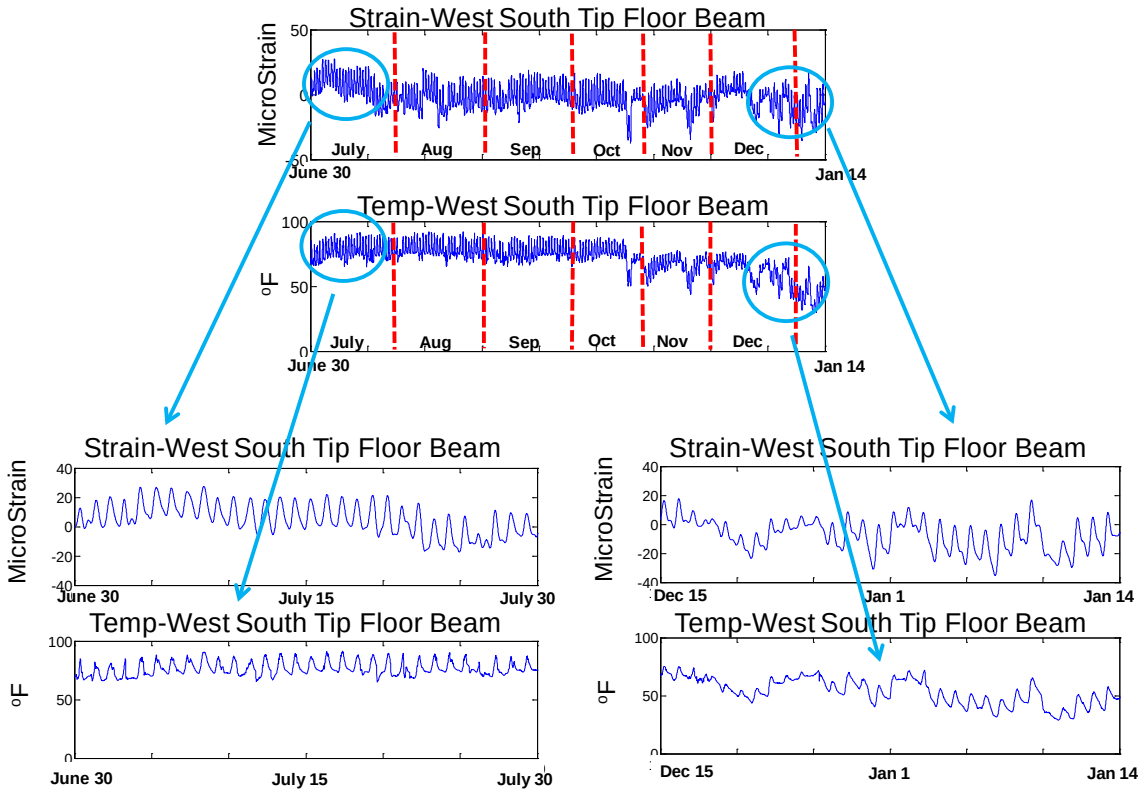

Figure 158: Strain–Temperature Relation for Tip Location

In order to explore the effects of temperature, an approximate seven month time window, from early July to mid-January, was considered. It was seen that temperature differential during the summer months was about 20 degrees between day and night, which caused a stress fluctuation in the range of 20 microstrain, (Figure 158). It is also noted that during this period seasonal variation was quite low. When the winter season data was investigated, sharp temperature drops were identified due to cold weather, especially from the relatively cold season in 2009-2010. When the winter temperatures

were investigated, it was observed that those sharp drops in temperature created a temperature differential of 40 microstrain, which was the double the strain created during the summer season. The importance of these levels become more clear when the car or the bus effect on the bridge is investigated such that a regular single car creates around 5 microstrain in the tip location of bridge and a bus creates around 20 microstrain at the same location, which means regular daily change of temperature creates close to the effect of a bus and sharp drops creates double that effect. These observations were also seen in main girder of live load shoe location of the bridge (Figure 159).

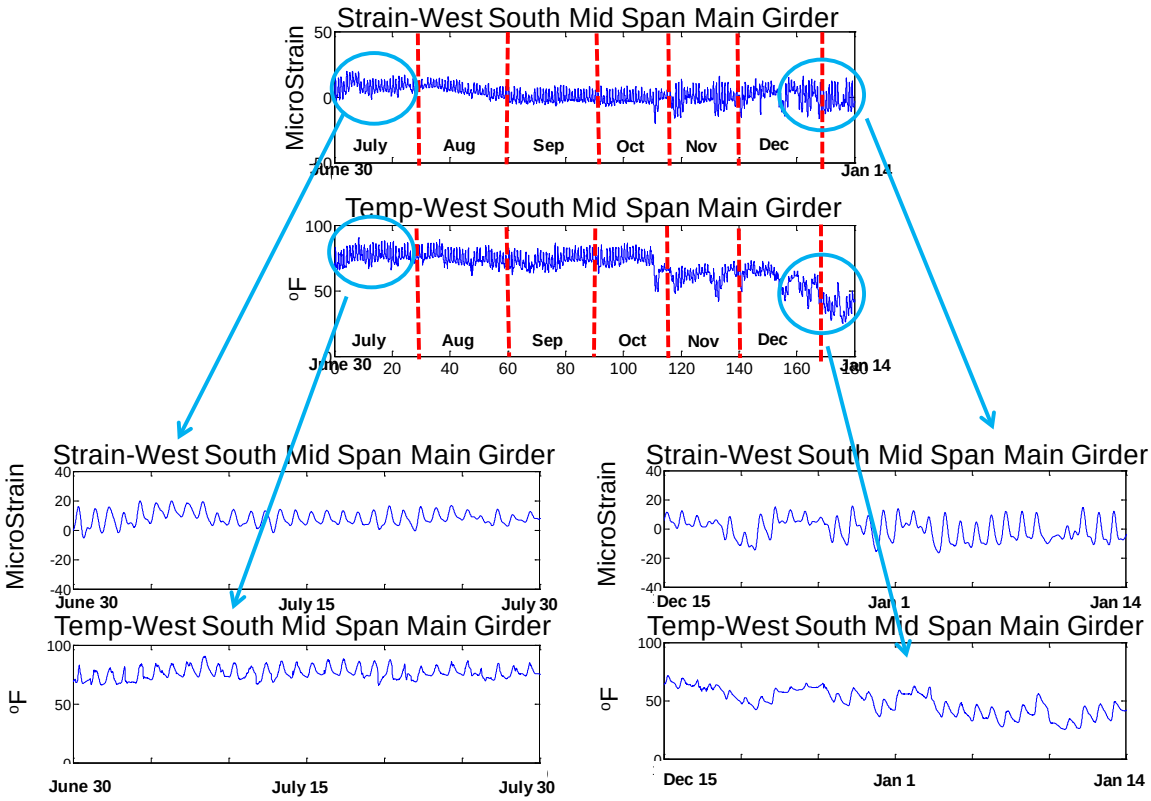

Figure 159: Strain–Temperature Relation for Main Girder Location

7.5.2. Traffic Effects

Traffic effects are the other important component of long term monitoring. This will not only help to predict the average daily traffic (ADT) and stress ranges, but also help to monitor the changes in the structural configurations due to conditions such as partially seated live load shoes. In addition, statistical data can be employed for structural reliability estimation and prediction of the future behavior. This advanced analysis can be

conducted with the data generated over long term. The reliability assessment concept deals with the failure probability of structures by using the statistical parameters of resistance and loading effects. Reliability is the probability that a component or a structural system performs within specified condition limits over a specified time span, which can be the expected lifetime of the structure. To collect these statistical parameters, long term traffic monitoring is a valuable source because monitoring data will reduce the uncertainty in the structural assessment.

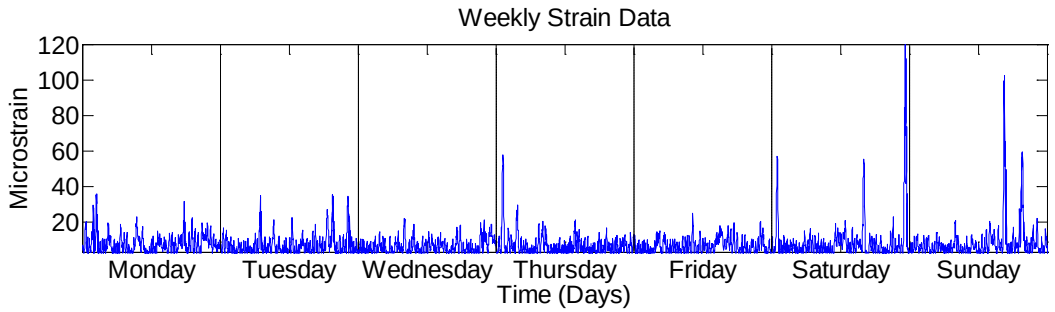

Figure 160: Weekly Strain Data from Live Load Shoe Location

Long term traffic monitoring is very important to collect statistical parameters. Therefore traffic induced strain data over week was employed for demonstration. In Figure 160, weekly traffic induced strain data between the period of 10/15/2009 - 10/21/2009 can be seen. As seen in Figure 160, the strain data is not very representative and the maximum strain that is observed in this window is about 120 microstrain. When a longer window of about 3 months was considered, it was possible to obtain a better distribution, thus a better characterization of the ADT, stress ranges, and statistics of the traffic induced stresses. The histogram that corresponds to three months (10/15/2009-1/15/2010) provided extreme strains in the range of 230 microstrain (Figure 161), almost twice the value that was observed in a week monitoring data.

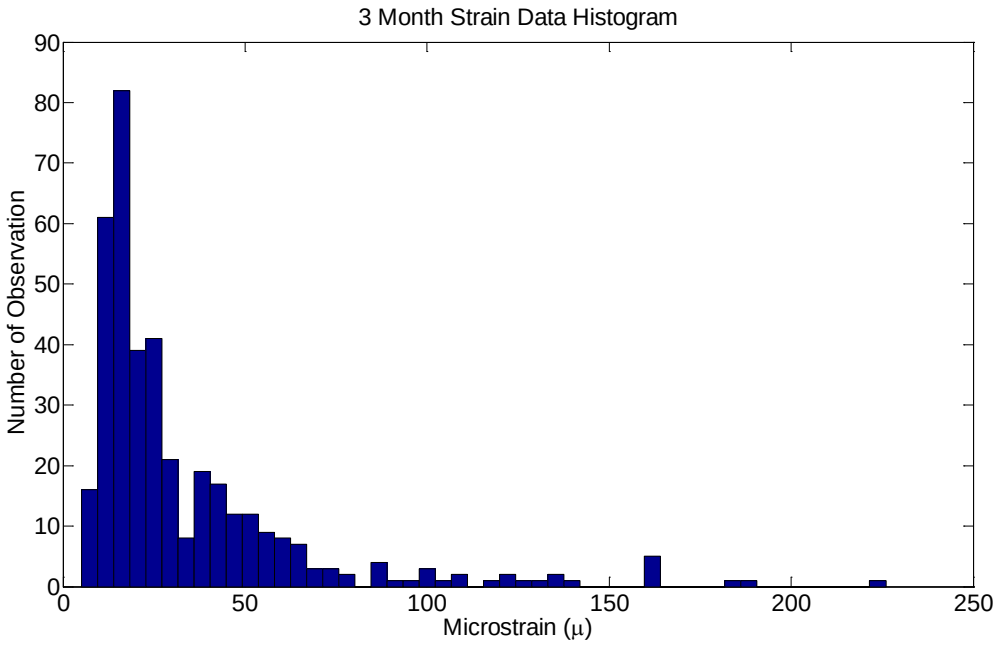

Figure 161: Three Months Daily Maximum Strain Histogram

The main concern for long-term strain monitoring is the peak values, since the maximum effects govern the structural capacity; however, all the maximum values were not critical in this histogram. Therefore, strain less than 30 microstrain were filtered out, and an extreme value histogram was created (Figure 162). This histogram shows the observed heavy traffic that the bridge was subjected to during a three month time period. In Figure 162, lognormal distribution was fitted to the histogram which had a mean of 67 microstrains and a standard deviation of 22 microstrains. These statistical studies will help to predict the probability of failure, but more data will improve this prediction. Such data and further analysis can be employed for remaining fatigue life of the bridge. This study is beyond the scope of the current project.

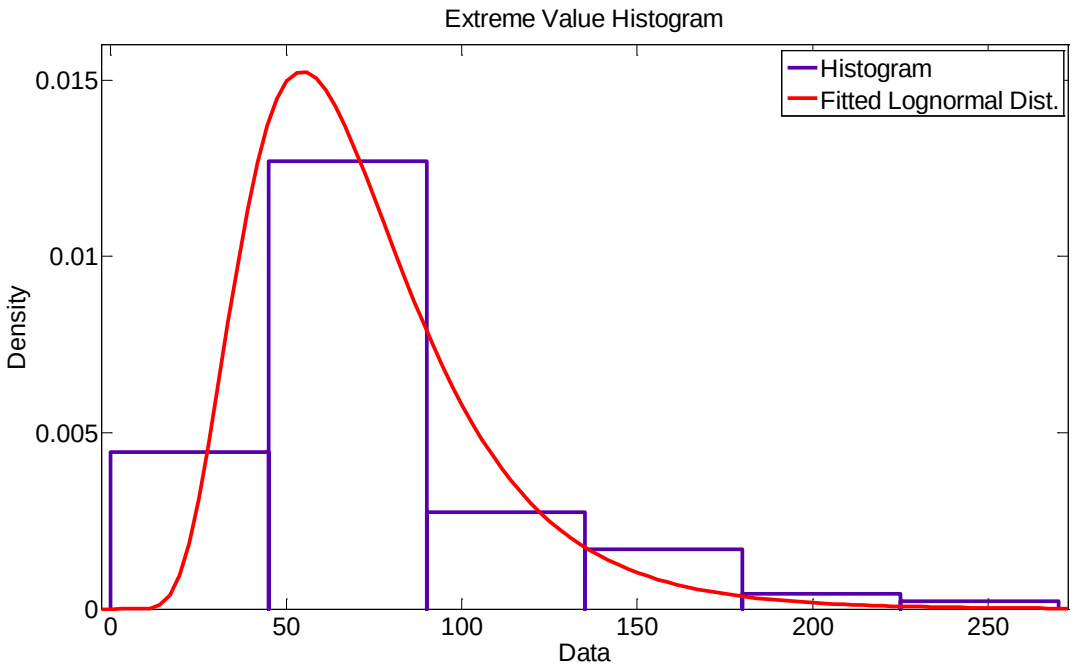

Figure 162: Extreme Values Histogram with Fitted Distribution

8. SUMMARY, CONCLUSIONS AND RECOMMENDATIONS

8.1. Brief Summary

This study aims to provide a general Structural Health Monitoring (SHM) framework, which includes design, development and implementation, to be applied for improved decision making for maintenance and management of movable bridges. For this study, the monitoring system was designed and implemented on a representative bridge in District 4 in Ft. Lauderdale, Florida. The selected representative movable span is the west-bound span of two parallel spans on Sunrise Boulevard in Ft. Lauderdale. This span was constructed in 1989. It has double bascule leaves with a total span length of 117 ft and a width of 53.5 ft, carrying three traffic lanes. Each leaf is 70-ft long and 40-ft wide. The bridge opens 10 to 15 times a day.

After the decision of the representative bridge was made in collaboration with District 4 engineers, the next task was the design of the monitoring system. For this task, first the most common types of structural, mechanical and electrical component problems were investigated with the help of FDOT officials, bridge engineers and consultants. Therefore, a series of group meetings and site visits were arranged to identify and finalize the critical components for monitoring. Finally, the design considerations and components were finalized for the structural, mechanical and electrical components, which include: electrical motors, gear boxes, drive shafts, open gears/racks, trunnions, live load shoes, span locks, main girders, floor beams and stringers. Following completion of the design considerations, the appropriate technology needs, such as sensors and data acquisition systems were identified; parallel to these needs the instrumentation plan was prepared. Another important challenge of the design phase was the wireless connection between the two leaves. Since a permanent physical connection does not exist between the two leaves, using one data acquisition was not possible. Therefore, a wireless connection and GPS synchronization system were established between the two leaves.

The next task was the laboratory preparations and field work. After defining all the sensors and data acquisition systems, the necessary equipment was purchased, and laboratory preparations began. These preparations were mainly for the cables, connectors,

and cabinets. The cable preparation process included quality control measures and was completed in a systematic manner. At the same time, the junction boxes and cabinets were designed and constructed. These preparations were tested by performing sensor, noise level, and complete system checks. Each sensor type was tested in the laboratory, and corresponding readings were collected to understand the noise levels for each sensor. After these component checks, the complete system, which includes two data acquisitions, sensors, GPS synchronization and a wireless connection, was checked. The field work involved sensor, cabinet, traffic camera, and weather station installations. A snooper truck was used for the sensor, cable, and cabinet installations to reach underneath locations of the bridge, and to lower the cabinets to the mechanical rooms. The traffic camera and wind station were installed with the help of lift trucks. After completing the structural sensor installation, the mechanical room sensors were installed, and the cables were connected to the side junction boxes and data acquisitions. Lastly, the wireless connection and GPS antenna were installed. Upon completion of this task, the system was ready for data collection.

As part of the long-term monitoring, data was collected continuously on every single opening and during rush hours. It should be noted here that the monitoring system is still collecting data at the time of writing this report. The data collected from the monitoring system through routine monitoring, as well as from the damage scenarios, were employed for developing and demonstrating methodologies to identify mechanical and structural alterations. The researchers first developed methods and tools to efficiently analyze the data in order to have valuable information to be extracted in a timely manner and interpreted easily by engineers. Various algorithms were investigated by the researchers and then the most effective ones were employed to provide meaningful information about the condition of the structure. Excellent results were obtained using the methodologies developed for structural and mechanical monitoring of critical components of the movable bridge. This task also allows refining the extensive monitoring system for a practical and cost-effective monitoring design (e.g. fewer sensors than what was considered for this research project) for system-wide implementation to the movable bridge population.

Following the completion of the field work and collection of data, numerical studies, consisting of the development and verification of a FE model, were performed. Construction plans of the Sunrise Boulevard Bridge were closely investigated, and one of the main girders was created using shell elements. This girder was divided into various numbers of shells in a mesh sensitivity analysis. Tip deflections were compared and an efficient mesh size was selected. After this selection, four main girders were created and connected to each other with the floor beam and stringer frame elements. Finally the FE model was completed and the verification process began. For this step, the model was verified both locally and globally. Local verification consisted of comparing FE model and SHM data strain values from the opening and closing operation and traffic. These comparisons showed that the FE model is in good agreement with the monitoring data. Global verification of the FE model was conducted by using the modal frequencies, which were also in good agreement.

8.2. Conclusions and Findings

Bridge records, inspection reports and site visits showed that the movable bridge population has certain deterioration of structural components and high maintenance cost for mechanical components. Structural components are subject to corrosion and adverse effects due to misalignments and operational wear, whereas the mechanical and electrical components are subject to frequent problems or breakdowns even if they are continuously inspected and maintained. For these reasons, a comprehensive monitoring system with hardware and software was designed, developed and implemented. This monitoring system will serve not only the FDOT officials, but also the researchers for future applications. To conclude the report, a summary of the findings are presented below.

For this project, a detailed FE model was created for in depth analysis and verification studies. This model was also used for load rating calculations. Truck load tests were employed on the bridge to better understand the load carrying capacity of the bridge. These test results were combined with the FE model studies to obtain the load rating of the bridge under AASHTO HL-93 design truck. For the Sunrise Boulevard Bridge, for all lanes three loaded case, inventory load rating was found to be 1.17, whereas the operating load rating was found to be 1.52. This model indicates that Sunrise Bridge, as a representative bridge of the population, has adequate load carrying capacity.

In addition, the FE model can be further employed for different scenarios for gradual deterioration, repair and permit truck simulations.

In this project, effective and unique data analysis methods were developed. One of these was the cross correlation based method for structural assessment. In this methodology, basically, the strain correlations from different strain locations (main girders and floor beams) were investigated before, during and after the structural damage scenarios. Live Load Shoe and Span Lock damage scenarios could be easily identified with this new methodology. This approach is expected to help the bridge engineers and maintenance personnel to reduce the number of maintenance visits for shim replacement at these locations. Because it is highly unlikely to have the same traffic effects each day, this method is advantageous because it is independent for each data set. This method can also be used to evaluate the effectiveness of maintenance by checking the correlation levels of the baseline (well-maintained, proper operations) conditions to conditions with no maintenance or new maintenance.

For the mechanical assessment, two new methods were developed. One method was the image based analysis for the open gear. For this method, computer vision edge detection techniques were used to identify whether the open gear was lubricated well or not. In a well lubricated open gear, it was very easy to see the grease chunks on the gear, and in this methodology, this was tracked by a lubrication index before, during and after damage scenarios. This tracking was very important since the lubrication was directly affecting the friction numbers and balance of the leaves. The other mechanical assessment method was identification of the oil level change in the gear box and the rack and pinion bolts removal. For identification of these damage scenarios, Artificial Neural Networks (ANN) techniques were used. In this methodology, first the training sets were prepared by including undamaged and damaged data. Cross validation sets were then prepared. For effective decision making these data sets were analyzed and the data was reduced to “0 and 1” values, corresponding to a healthy (undamaged) or unhealthy (damaged) state.

For the long term analysis, preliminary studies, such as environmental effects on structural and mechanical components, were executed. For the interaction of structural components and environmental effects, slow speed vibrating wire gages were used, and

daily temperature cycles were identified. During the summer season, daily strain variation was between day and night was 20 microstrain, but this variation became 40 microstrain during the winter season. The strain cycle due to temperature was below truck induced strains under regular traffic and therefore, the observed temperature strains were within acceptable range. It should be mentioned that it is important to monitor this behavior over long term, especially for temperature effects on span locks when the bridge is to be opened. The total monitoring duration for this project was less a year after the design and implementation of the monitoring system where it would be desirable to establish at least a yearly cycle due to environmental effects. Moreover, long term monitoring can also provide important information about the effects of the temperature variations on the bridge balance and seating of different girders. For the mechanical components, the long term monitoring studies showed that there was an interaction between the mechanical friction and environmental effects. The most critical environmental effect was due to temperature. Humidity also showed a meaningful correlation, but the correlation was lower than the temperature correlation. Lastly, the effects of wind speed and barometric pressure on the mechanical friction were also analyzed, however, these environmental effects were not as effectual as temperature and humidity. It should be noted that friction numbers and plots were obtained for average torque calculations. As for the bridge operation, change in mechanical friction may be an indicator of a need for maintenance. With better understanding the causes of the changes, maintenance can be done more effectively and timely.

All in all, these effective and unique methodologies can be employed for proactive maintenance, operation and safety. For instance, a refined monitoring system with such data analysis capabilities is expected to help to reduce the costs, to better understand the root causes and improve new designs.

8.3. Recommendations

Since the cost of maintaining movable bridges is approximately one hundred times higher than the cost of fixed bridges, monitoring of a movable bridge provides an excellent opportunity to reduce such costs once this system is refined, data analysis methods are fully established, and automated programs are developed with appropriate thresholds. This type of objective information allows for condition based maintenance as

well as tracking the effectiveness of maintenance. A sufficiently long period (1-1.5 years) of monitoring would be ideal for several reasons with long term data. For calibration, fine tuning the methodologies, and investigation of cause and effects on the structure, long term monitoring data is needed to capture and analyze these cycles. A continuous monitoring system, with relatively little investment, can help track the bridge degradation, and preventative maintenance work can be better scheduled. Moreover, these new methodologies show promise for detecting changes thus reducing unexpected breakdowns by providing instant warnings to maintenance personnel. Costs associated with traffic delays can also be reduced. Another benefit of long term monitoring, which includes ADT and stress cycles, is the fatigue evaluation of the steel bridge.

For a complete monitoring system, integration of different aspects of monitoring is necessary. Improved remote monitoring, communication and integrated data archival methods should also be investigated in detail to make the maximum and most efficient use of the collected data. On the other hand, further explorations for some sensor types such as microphones and pressure sensors are necessary.

The findings of this monitoring project have excellent potential for developing improved knowledge on performance and degradation, better design methods and performance predictive models, and advanced management decision making tools for maintenance and operation. Continued monitoring and collection of data from a sufficiently long cycle would allow for calibrating and fine tuning methods and investigation of cause-and-effect. Further exploration of sensor data and damage cases, improvement to programming and communication systems and monitoring based fatigue evaluation methodologies can be carried out by taking advantage of the existing system. Continued research will also allow for the design and implementation of a compact monitoring system for system-wide application. Further studies and pilot applications are recommended to design and implement a compact monitoring system for system-wide SHM applications. This way, the approach can be further improved and customized according to user needs and other challenges that can only be discovered through real-life applications.

It should be noted that the existing system has been developed in parallel to efforts of the Federal Highway Administration (FHWA) Advanced Exploratory Research Program, therefore, has a potential to have a broader impact.

9. REFERENCES

"AASHTO LRFD Bridge Design Specifications" Washington, DC., American Association of State Highway and Transportation Officials (AASHTO), 2002.

"Bridge Analysis and Rating Program - BAR7, V7.10" PennDOT Bureau of Information Systems Application Development Division, PennDOT, 2001.

"Bridge Inspector's Reference Manual" Publication No. FHWA NHI 03-001, FHWA Report, 2002.

"Bridge Study Analyzes Accuracy of Visual Inspections" http://www.tfhrc.gov/focus/jan01/bridge_study.htm, Turner-Fairbank Highway Research Center, 2005.

"Bridge Study Analyzes Accuracy of Visual Inspections" http://www.tfhrc.gov/focus/jan01/bridge_study.htm, Turner-Fairbanks Highway Research Center, 2005.

"Development of a Model Health Monitoring Guide for Major Bridges" Drexel Intelligent Infrastructure and Transportation Safety Institute, Aktan, A. E., Catbas, F. N., Grimmelsman, K. A. and Pervizpour, M., 2003.

"Guide Manual for Condition Evaluation and Load and Resistance Factor Rating (LRFR) of Highway Bridges, 1st Edition", AASHTO, 2003a.

"Handbook of Bascule Bridge Balance Procedures" Report submitted to Florida Department of Transportation, Malvern, L. E., Lu, S. Y. and Jenkins, D. A., 1982.

"Manual for Condition Evaluation and Load and Resistance Factor Rating (LRFR) of Highway Bridges" American Association of State Highway and Transportation Officials, AASHTO, 2003b.

"Manual for Maintenance Inspection of Bridges", AASHTO, 1983.

"Parametric Finite Element Modeling and Full-Scale Testing of Trunnion-Hub-Girder Assemblies for Bascule Bridges" A Report on a Research Project Spnsored by the Florida Department of Transportation, Besterfield, G., Kaw, A. and Crane, R., 2001.

"Recording and Coding Guide for the Structural Inventory and Appraisal of the Nation's Bridges" FHwA, Federal Highway Administration (FHWA), 1995.

"Remote Global Monitoring of the Michigan Street Bridge, Sturgeon Bay, Wisconsin" ITI technical report no. 19, Prine, D. W. and Fish, P. E., 1996.

"Structures Design Guidelines" Florida Department of Transportation, FDOT, 2004.

"Transportation Asset Management Case Studies, Bridge Management: Experiences of California, Florida and South Dakota", FHWA, 2003.

"Transportation Asset Management Case Studies, FHWA-IF-05-040: Bridge Management Experiences of California, Florida, and South Dakota" Office of Asset Management, Federal Highway Administration (FHWA), 2005.

Aktan, A. E., Chase, S., Inman, D. and Pines, D. (2001a). "Monitoring and Managing the Health of Infrastructure Systems". Proceedings of the 2001 SPIE Conference on Health Monitoring of Highway Transportation Infrastructure, Irvine, CA, March 6-8.

Aktan, A. E., Pervizpour, M., Catbas, F. N., Grimmelsman, K. A., Barrish, R. A., Curtis, J. and Qin, X. (2001b). "Information Technology Research for Health Monitoring of Bridge Systems". Proceedings of the Structural Faults & Repair 2001 Conference, London, UK, July 4-6, 2001.

Aktan, A.E., et al. Information Technology Research for Health Monitoring of Bridge Systems. in Proceedings of the Structural Faults & Repair 2001 Conference. 2001. London, UK.

Aktan, A.E., et al., Issues in Infrastructure Health Monitoring for Management. Journal of Engineering Mechanics, ASCE, 2000. 126(7): p. 711-724.

Anderson, O. D. (1976). "Time Series Analysis and Forecasting the Box-Jenkins Approach." Butterworth & Co, UK.

Asmussen, J. C. (1997). "Modal Analysis Based on the Random Decrement Technique - Application to Civil Engineering Structures." Doctoral Dissertation, University of Aalborg, Aalborg.

Bell, E.S., et al. Instrumentation, Modeling, and Monitoring of a Concrete Bridge from Construction Through Service. in Transportation Research Board 89th Annual Meeting. 2010. Washington, DC.

Box, G. E., Jenkins, G. M. and Reinsel, G. C. (1994). "Time Series Analysis: Forecasting and Control". Prentice-Hall, New Jersey.

Burkett, J. L. (2005). "Benchmark Studies for Structural Health Monitoring using Analytical and Experimental Models." MS Thesis, Department of Civil and Environmental Engineering, University of Central Florida, Orlando, FL.

Buxton-Tetteh, B. (2004). "Development of User Cost Model for Movable Bridge Openings in Florida." MS Thesis, Civil Engineering, Florida State University, Tallahassee, FL.

Castro, T., D.V. Jauregui, and S. Maberry. A Collaborative Approach for Load Rating of State-Owned Bridges. in Transportation Research Board 89th Annual Meeting. 2010. Washington, DC

Catbas, F.N., et al. (1997) Modal Analysis of Multi-Reference Impact Test Data for Steel Stringer Bridges. in Proceedings of the 15th International Modal Analysis Conference. 1997. Orlando, FL.

Catbas, F. N. and Aktan, A. E. (2002). "Condition and Damage Assessment: Issues and Some Promising Indices." Journal of Structural Engineering, ASCE, 128(8): 1026-1036.

Catbas, F. N., Shah, M., Burkett, J. and Basharat, A. (2004). "Challenges in Structural Health Monitoring". Proceedings of the 4th International Workshop on Structural Control, 195-202, Columbia University, New York, June 10-11.

Catbas, F.N., D.L. Brown, and A.E. Aktan (2004), Parameter Estimation for Multiple-Input Multiple-Output Modal Analysis of Large Structures. Journal of Engineering Mechanics ASCE 2004. 130(8): p. 921-930.

Catbas, F.N., et al. (2004) Challenges in Structural Health Monitoring. in Proceedings of the 4th International Workshop on Structural Control. 2004. Columbia University, New York.

Catbas, F. N., Ciloglu, S. K. and Aktan, A. E. (2005). "Strategies for Condition Assessment of Infrastructure Populations: A Case Study on T-beam Bridges." Structure and Infrastructure Engineering Journal, SIE, 1(3): 221-238.

Catbas, F. N., Brown, D. L. and Aktan, A. E. (2006). "Use of Modal Flexibility for Damage Detection and Condition Assessment: Case Studies and Demonstrations on Large Structures." Journal of Structural Engineering, ASCE, 132(11): 1699-1712.

Catbas, F.N., Zaurin, R., Susoy, M., and Gul, M. (2007) “Integrative Information System Design for Florida Department of Transportation – A Framework for Structural Health Monitoring of Movable Bridges,” Final Report to Florida Department of Transportation, Contract No. BD548-RPWO#11, 231 pages.

Catbas, F.N. (2010) Structural Health Monitoring Case Study on a Movable Bridge. in Transportation Research Board 89th Annual Meeting. 2010. Washington, DC.

Chen, H. M., Qi, G. Z., Yang, J. C. S. and Amini, F. (1995). "Neural Network for Structural Dynamic Model Identification." Journal of Engineering Mechanics, ASCE, 121(12): 1377-1381.

Ditlevsen, O. and Madsen, H. O. (1996). "Structural reliability methods". Wiley, Chichester ; New York.

Doo Kie, K., et al. Active Vibration Control of a Structure Using Neural Network Techniques. in Transportation Research Board 86th Annual Meeting. 2007. Washington, DC.

Dunn, P. F. (2005). "Measurement and Data Analysis for Engineering and Science". McGraw-Hill, New York, NY.

Farrar, C.R. and H. Sohn. Pattern Recognition for Structural Health Monitoring. in Workshop on Mitigation of Earthquake by Advanced Technologies. 2000. Las Vegas, NV.

Farrar, C.R., et al. A Statistical Pattern Recognition Paradigm for Vibration-Based Structural Health Monitoring. in 2nd International Workshop on Structural Health Monitoring. 1999. Stanford, CA.

Feng, M.Q., et al., Baseline Models for Bridge Performance Monitoring. Journal of Engineering Mechanics, 2004. 130(5): p. 562-569.

Francoforte, K., Gul, M. and Catbas, F. N. (2007). "Parameter Estimation Using Sensor Fusion and Model Updating". Proceedings of the 25th International Modal Analysis Conference (IMAC), Orlando, FL, February 19 - 22.

Giraldo, D. and Dyke, S. J. (2004). "Damage Localization in Benchmark Structure Considering Temperature Effects". 7th International Conference on Motion and Vibration Control.

Gul, M. and Catbas, F. N. (2006). "An Integrated System Identification Framework for Structural Condition Assessment Using Ambient Vibration Data." Journal of Engineering Mechanics, ASCE, under review.

Gul, M., Catbas, F. N. and Georgiopoulos, M. (2007). "Application of Pattern Recognition Techniques to Identify Structural Change in a Laboratory Speciment". Proceedings of the SPIE Smart Structures and Materials & Nondestructive Evaluation and Health Monitoring Conference San Diego, CA, March 18 - 22.

Iranmanesh, A., S.A. Bassam, and F. Ansari. Damage Evaluation of a 4-Span Concrete Bridge Subjected to Near Source Ground Motions using Nonlinear Finite Element Method. in Concrete Bridge Conference. 2008. St. Louis, MO.

Jain, A. K., Duin, R. P. W. and Mao, J. (2000). "Statistical Pattern Recognition: A Review." IEEE Transactions on Pattern Analysis and Machine Intelligence, 22(1): 4-37.

Jain, A. K., Murty, M. N. and Flynn, P. J. (1999). "Data Clustering: A Review." ACM Computing Surveys, 31(3): 264-323.

Kao, C. Y. and Hung, S.-L. (2003). "Detection of Structural Damage via Free Vibration Responses Generated by Approximating Artificial Neural Networks." Computers and Structures, 81: 2631-2644.

Kim, J.-T., H.-J. Jung, and I.-W. Lee, Optimal Structural Control Using Neural Networks. Journal of Engineering Mechanics, 2000. 126(2): p. 201-205.

Koglin, T. L. (2003). "Movable Bridge Engineering". John Wiley and Sons.

Lee, J. and M. Shinozuka, “Real-Time Displacement Measurement of a Flexible Bridge Using Digital Image Processing Techniques” Experimental Mechanics, 2006(46): p. 05-114

Lynch, J. P. and Loh, K. (2005). "A Summary Review of Wireless Sensors and Sensor Networks for Structural Health Monitoring." Shock and Vibration Digest, Sage Publications, 38(2): 91-128.

Manson, G., K. Worden, and D. Allman, Experimental Validation of a Structural Health Monitoring Methodology. Part II. Novelty Detection on a GNAT Aircraft. Journal of Sound and Vibration, 2003. 259(2): p. pp. 345-363.

Masri, S. F., Nakamura, M., Chassiakos, A. G. and Caughey, T. K. (1996). "Neural Network Approach to Detection of Changes in Structural Parameters." Journal of Engineering Mechanics, ASCE, 122(4): 350-360.

Matta, F., et al., Distributed Strain Measurement in Steel Bridge with Fiber Optic Sensors: Validation through Diagnostic Load Test. Journal of Performance of Constructed Facilities, 2008. 22(4): p. 264-273.

Melchers, R. E. (1999). "Structural Reliability Analysis and Prediction". John Wiley & Sons.

Moghimi, H. and H.R. Ronagh, Impact factors for a composite steel bridge using non-linear dynamic simulation. International Journal of Impact Engineering, 2008. 35(11): p. 1228-1243.

Nair, K. K. and Kiremidjian, A. S. (2005). "A Comparison of Local Damage Detection Algorithms Based on Statistical Processing of Vibration Measurements". Proceedings of the 2nd International Conference on Structural Health Monitoring and Intelligent Infrastructure (SHMII), Shenzen, China.

Nowak, A. S. (1995). "Calibration of LRFD Bridge Code." ASCE Journal of Structural Engineering, 121(8): 1245-1251.

Nowak, A. S. and Collins, K. R. (2000). "Reliability of Structures". McGraw-Hill.

Omega Engineering Inc. (1995). WMS-22A and WMS-22 Current Loop Wind Stations: Operator's Manual.

Owen, J.S., et al., Classification of Damaged and Modified Bridge Beams with Vibration Signatures. Transportation Research Record, 2002: p. p. 135-144.

Patton, G. C. (2006). "Bascule Leaf Fabrication and Erection Tolerances: Where Structure Meets Machine". Heavy Movable Structures, Inc. Eleventh Biennial Symposium, Orlando, FL.

Pumma, R. and P. Suwanvitaya. Bridge Load Test and Load Rating of Reinforced-Concrete Slab Bridges. in Transportation Research Board 89th Annual Meeting. 2010. Washington, DC.

Rackwitz, R. and Fiessler, B. (1978). "Structural Reliability under Combined Random Load Sequences." Computers and Structures, 9: 489-494.

Rajasekaran, S., Functional Networks in Structural Engineering. Journal of Computing in Civil Engineering, 2004. 18(2): p. 172-181.

Rao, A.R., Kumar, B., (2007), "Predicting Re-aeration Rates Using Artificial Neural Networks in Surface Aerators", International Journal of Applied Environmental Sciences, Vol. 2, No. 1, pp. 155-166.

Shalkoff, R. J. (1992). "Pattern Recognition: Statistical and Neural Approaches". John Wiley & Sons, US.

Sohn, H. and Farrar, C. R. (2001). "Damage Diagnosis Using Time Series Analysis of Vibration Signals." Smart Materials and Structures, 10: 1-6.

Sohn, H., et al., Structural Health Monitoring Using Statistical Pattern Recognition Techniques. Journal of Dynamic Systems, Measurement, and Control, ASME, 2001. 123: p. 706-711.

Sohn, H., Farrar, C. R., Hunter, N. F. and Worden, K. (2001). "Structural Health Monitoring Using Statistical Pattern Recognition Techniques." Journal of Dynamic Systems, Measurement, and Control, 123: 706-711.

Sohn, H., J.A. Czarnecki, and C.R. Farrar, Structural Health Monitoring Using Statistical Process Control. Journal of Structural Engineering, ASCE, 2000. 126(11): p. pp. 1356-1363.

Soyoz, S. and M.Q. Feng, Long-Term Monitoring and Identification of Bridge Structural Parameters. Computer-Aided Civil and Infrastructure Engineering, 2009. 24: p. pp 82-92.

Susoy, M., Catbas, F. N. and Frangopol, D. M. (2006a). "Implementation of Structural Reliability Concepts for Structural Health Monitoring". Proceedings of the 4th World Conference on Structural Control and Monitoring, San Diego, CA, July 11-13.

Susoy, M., Catbas, F. N. and Frangopol, D. M. (2006b). "Reliability-Based SHM of a Long-Span Bridge." Journal of Engineering Structures, Elsevier (submitted).

Susoy, M., Catbas, F. N. and Frangopol, D. M. (2007). "Structural Health Monitoring Development using System Reliability". Proceedings of the 10th International Conference on Applications of Statistics and Probability in Civil Engineering (ICASP10), University of Tokyo, Japan, July 31 - August 3.

Susoy, M., R. Zaurin, and F.N. Catbas, Development of a Structural Health Monitoring Framework for the Movable Bridges in Florida, in Transportation Research Board 86th Annual Meeting. 2007: Washington D.C.

Thompson, P. D., Sobanjo, J. O. and Kerr, R. (2003). "Florida DOT Project-Level Bridge Management Models." Journal of Bridge Engineering, ASCE, 8(6).

Turner-Fairbanks Highway Research Center, Bridge Study Analyzes Accuracy of Visual Inspections. 2005, http://www.tfhrc.gov/focus/jan01/bridge_study.htm.

Wahbeh, A.M., J.P. Caffrey, and S.F. Masri, A vision-based approach for the direct measurement of displacements in vibrating systems. Smart Materials and Structures, 2003. 12(5): p. 785-794.

Wang, X., et al., Development of Dynamic-Response-Based Objective Functions for Finite-Element Modeling of Bridges. Journal of Bridge Engineering, 2007. 12(5): p. 552-559.

Webb, A. (1999). "Statistical Pattern Recognition". Oxford University Press, New York, NY.

Wong, K.-Y. (2005). "Design of Structural Health Monitoring System for Long-Span Bridges." Structure and Infrastructure Engineering, 3(2): 169-185.

Worden, K. (1997). "Structural Fault Detection Using a Novelty Measure." Journal of Sound and Vibration, 201(1): 85-101.

Worden, K., G. Manson, and N.R.J. Fieller, Damage Detection Using Outlier Analysis. Journal of Sound and Vibration, 2000. 229(3): p. pp. 647-667.

Worden, K., Sohn, H. and Farrar, C. R. (2000). "Damage Detection Using Outlier Analysis." Journal of Sound and Vibration, 229(3): 647-667.

Worden, K., Sohn, H. and Farrar, C. R. (2002). "Novelty Detection in a Changing Environment: Regression and Interpolation Approaches." Journal of Sound and Vibration, 229(3): 647-667.

Xu, H. and J. Humar, Damage Detection in a Girder Bridge by Artificial Neural Network Technique. Computer-Aided Civil and Infrastructure Engineering, 2006. 21: p. pp 450-464.

Xu, R. and Wunsch, D. (2005). "Survey of Clustering Algorithms." IEEE Transactions on Neural Networks, 16(3): 645-678.

Yan, A.-M., Kerschen, G., De Boe, P. and Golinval, J.-C. (2005). "Structural Damage Diagnosis under Varying Conditions - Part I: A Linear Analysis." Mechanical Systems and Signal Processing, 19: 847-864.

Yetilmezsoy, K., Demirel, S., (2008), “Artificial neural network (ANN) approach for modeling of Pb(II) adsorption from aqueous solution by Antep pistachio (Pistacia Vera L.) Shells”, Journal of Hazardous Materials, Vol. 153, pp. 1288–1300.

Zang, C., M.I. Friswell, and M. Imregun, Structural Health Monitoring and Damage Assessment Using Frequency Response Correlation Criteria. Journal of Engineering Mechanics, 2007. 133(9): p. 981-993.

Zaurin, R. and Catbas, F. N. (2007). "Computer Vision Oriented Framework for Structural Health Monitoring of Bridges". Proceedings of the 25th International Modal Analysis Conference (IMAC), Orlando, FL, February 19 - 22.

Zaurin, R. and F.N. Catbas, Computer Vision and Sensor Fusion Structural Health Monitoring Framework, with Emphasis in Unit Influence Line Analysis, for Condition Assessment.UCF 4-Span Bridge, in ociety for Experimental Mechanics. IMAC XXVII. 2009: Orlando, Florida.

Zaurin, R. and F.N. Catbas. Benchmark Studies for Structural Health Monitoring using Computer Vision in The Fourth International Conference on Bridge Maintenance. Safety, and Management. 2008. Seoul, Korea: IABMAS'08.

Zaurin, R. and F.N. Catbas. Demonstration of a Computer Vision and Sensor Fusion Structural Health Monitoring Framework on UCF 4-Span Bridge. in Internationam Modal Analysis Conference- Technologies for Civil Structures. 2008. Orlando, Florida.

Zaurin, R. and F.N. Catbas. Integration of Computer Imaging and Sensor Networks for Structural Health Monitoring: Case Study for Load Rating. in Transportation Research Board 89th Annual Meeting. 2010. Washington, DC.

Zhou, L., C.-C. Chang, and B. Spencer, Intelligent technology-based control of motion and vibration using MR dampers. Earthquake Engineering and Engineering Vibration, 2002. 1(1): p. 100-110.

10. APPENDIX

10.1. Sensor Characteristics Definitions

Sensitivity: Sensitivity is defined as the ratio of output to input, and is an important characteristic related with the precision and accuracy of the measurement.

Resolution: Resolution defines how small a change in the measurand can be detected by the sensor.

Discrimination: Also referred to as the limit of detection, this is the smallest increment of a measurement that can be discerned.

Range: The maximum and minimum values of the measured occurrence that can be measured with the sensor define the range property.

Hysteresis: The maximum deviation between the measurement obtained by increasing and decreasing values of the measurement.

Accuracy: This is the closeness of a measurement to the value defined to be the true value of the measurand.

Linearity: Linearity defines the deviation of measurements from the linear calibration line.

Repeatability: Obtaining the same output value for repeated measurements of the same quantity specifies the repeatability of the instrument.

Stability: This refers to the ability of a sensor to maintain its calibration value over an extended time period. Drift is the continuous upward or downward change of measurements mostly due to environmental effects.

10.2. File Name Structure

The file names are automatically generated using the convention outlined below:

1. The body of the file names are created according the following pattern:
   DiskDrive:\Directory\Date_Time_TriggeringEvent_
2. For each component, a particular name is added to the previous pattern and the following data files are saved:

   Weather Station:
   DiskDrive:\Directory\Date_Time_TriggeringEvent_WEATHER.lvm
   - This data file contains all data corresponding to the weather station.

   Trunnion

DiskDrive:\Directory\Date_Time_TriggeringEvent_TRUNNION.lvm

- This data file contains the responses from each one of the legs for the two strain rosettes located at each trunnion.

Structural Strain

DiskDrive:\Directory\Date_Time_TriggeringEvent_STRAIN.lvm

- All the structural strain gages and rosettes on girders and spanlocks.

Shaft

DiskDrive:\Directory\Date_Time_TriggeringEvent_SHAFT.lvm

- All strain rosettes on the shaft as well as tilt from bridge openings/closings

Rack and Pinnion

DiskDrive:\Directory\Date_Time_TriggeringEvent_RACKANDPINNION.lvm

- Two Accelerometers located at the base of the rack and pinion structure.

Spanlock

DiskDrive:\Directory\Date_Time_TriggeringEvent_SPANLOCK.lvm

- Data from the 4 pressure gages (two at each spanlock)

Gearbox

DiskDrive:\Directory\Date_Time_TriggeringEvent_GEARBOX.lvm

- All 6 gear box accelerometers as well as the microphones (including the trunnion)

Open Gear

DiskDrive:\Directory\Date_Time_TriggeringEvent_\OpenGear\

- In this folder are stored all images from the open gear during the opening/closing operation as well as a file name TimeFrame.lvm which contains the time corresponding to each one of the video frames.

Traffic Video

DiskDrive:\Directory\Date_Time_TriggeringEvent_\VideoTraffic\

- In this folder all images from the operational traffic are stored as well as a file name TimeFrame.lvm which contains the time corresponding to each one of the video frames.

10.3. Cabling Design Alternatives

Several alternatives were considered and studied for selection of the cabling types:

Individual 1-2 Pair Shielded/Grounded Cables

As previously stated, the use of individual one or two pair shielded/ground cable were studied but deemed to be impractical due to the quantity of sensors and their distances from the DAQ.

Multiconductor Twisted Pair

Selection of multiconductor cables results in the transmittal of several different types of signals through the twisted pairs; including various DC voltages. Due to the fact that

this cable was not individually shielded, some signals were causing noise to each other. In addition, the protective coating was not suggested for use in harsh environments, and therefore also made it unsuitable for our long-term study.

Multiconductor Twisted Pair Individually Shielded

Finally, a twisted pair multiconductor cable that was individually shielded and featured a PVC outer jacket was tested. Signal quality was better as a result of the pairs being individually shielded and grounded. The PVC outer jacket was rated for outdoor use and both sunlight and oil resistive; providing confidence for long-term use in a harsh environment. This was the selected product.

(a)

(b)

(c)

Figure 163: Cable Alternatives, a) Individual 1-2 Pair Shielded, b) Multiconductor Twisted Pair, c) Multiconductor Twisted Pair Individually Shielded

10.4. Cable Segment Labels

The following provides a summary of the main cable segments installed on each leaf. Each main cable carries the data from a group of installed sensors to the junction box on either leaf. Please refer to the instrumentation plan (Figure XX and Figure XX) for location information.

16-Pair Cables

East Leaf: ES3, ES4, ES5, EN3, ES.RP, EN.RP EN.TRN, ES.TRN

West Leaf: WS3, WS4, WS5, WN1, WN3, WS.RP, WN.RP WN.TRN, WS.TRN

24-Pair Cables

East Leaf: ES1, ES2, EN1, EN2, E.GB

West Leaf: WS1, WS2, WN2, W.GB

10.5. Connector Design Alternatives

The following design options for this connection were analyzed:

- **Pre-Connect sensors to cable in Lab**
  - *Pros:* Provides best quality control, secure hardwired connection, lower cost
  - *Cons:* Extremely difficult installation procedure due to securing of main cable prior to sensor installation, very difficult to repair
- **Fixed Junction Box Enclosures**
  - *Pros:* Scaled down version of side junction boxes, easy to repair
  - *Cons:* Higher cost, requires robust attachment to girders to prevent detachment during openings, time consuming at time of installation
- **Military Style Connectors ()**
  - *Pros:* Low cost alternative connector, quick field installation
  - *Cons:* Poor design requires soldering each individual wire in lab, extremely time consuming, poor quality control

Figure 164: Military Style Connector (Not Selected for Use)

- **Harting Han Industrial Connectors ()**

- *Pros:* Quick field installation, quality control and reduced lab prep time, watertight seal, robust design
- *Cons:* Higher cost, variance in products

10.6. Connector Individual Components

The Harting Han Industrial Connectors used have both Male and Female parts, with each of these actually composed of four (4) distinct components: the outer weather-proof housing, the internal electrical connector, the opening reducer, and the cable gland. A summary of the components contained in each complete connection (both halves) and associated product names is provided (Sub Bullets represent different configurations):

Male Connector Side	**Part No.(s)**
• Male Outer Housing	
o 32-M Size	19 30 032 0427
o 40-M Size	19 30 032 0428
• Male Connector	
o 32 Contact (cage-clamp)	09 33 016 2616, 09 33 016 2626
o 64 Contact (crimp terminal)	09 32 032 3001, 09 32 032 3011
▪ Reqd. Male Crimp Contacts	09 33 000 6122
• Opening Reducers	
o M32 to M25	73 00 000 5347
o M40 to M32	73 00 000 5348
• Cable Glands	
o M25	19 00 000 5090
o M32	19 00 000 5094
o M32x	19 00 000 5096
o M40	19 00 000 5097
o M40x	19 00 000 5098
Female Connector Side	**Part No.(s)**
• Female Outer Housing	
o 40-M Size	19 30 032 0728
• Female Connector	
o 32 Contact (cage-clamp)	09 33 016 2716, 09 33 016 2726
o 64 Contact (crimp terminal)	09 32 032 3101, 09 32 032 3111
▪ Reqd. Female Crimp Contacts	09 33 000 6122
• Opening Reducers: Same Products as for Male side	
• Cable Glands: Same Products as for Male side	

10.7. Internal Components of Side Junction Boxes

Side Junction Box Fastener

Hoffman Steel Mounting Panel Product: A30P30

- Bolt mountable to inside enclosure
- Provides surface to mount DIN rails and cable sorters

DIN Rails

TS 15 DIN Rail with slotsProduct: 117500000

- Attached to mounting panel
- Securely holds individual terminal blocks

Terminal Blocks & Accesories

Weidmuller AKZ 2.5 Beige Terminal Blocks (with Spigots) Product: 0318580000

- Attaches to DIN rails'

Weidmuller Blue Partition Product: 318580000

- Provides visual separation between groups of terminal blocks

Weidmuller End Bracket ZEW 15 for TS 15 Product: 382860000

- Prevents terminal blocks from sliding

Weidmuller Blank DEK 5/5 Tags Product: 473360000

- Labeling Tags

Cable Sorters

SPC Technology High-density wiring duct (1.5" x 1.5") Product: 97N9474
SPC Technology High-density wiring duct (1" x 1") Product: 97N9468
SPC Technology Wiring Duct Cover 1.5" Product: 51N2368
SPC Technology Wiring Duct Cover 1" Product: 51N2367

Figure 165: Strain Relief for Main Cables

	Sensitivity	Resolution	Range	Hysteresis	Accuracy	Linearity	Repeatability	Stability
Hitec HBW High Speed Strain Gage	2.100 ± 0.5%		3% strain		based on 6με/°F			
Hitec HBWR Strain Rosette Gage	2.105 ± 1.0%		3% strain		based on 6με/°F			
Geokon 4150 Vibrating Wire Strain Gage		0.4με	3000με		±0.5% FS	<0.5% FS		
Applied Geomechanics 801-W/L Uniaxial Tiltmeter		0.01°	50°			0.5% of full span	0.02°	
The Imaging Source DFK 21AF04 Firewire Camera	0.5 lx at 1/30s, gain 20 dB	640x480 (HxV)	10 bit, output: 8 bit (Dynamic)					
The Imaging Source DFK 21AF04-Z Firewire Camera	0.5 lx at 1/30s, gain 20 dB	640x480 (HxV)	11 bit, output: 8 bit (Dynamic)					
PCB 603C01 Acclerometer	100mV/g	350μg	50g			-0.01		

PCB 130D20 Microphone	45mV/Pa		>122 dB (Dynamic)					
STS Passive Pressure Transmitter			1-15,000 psi	Typical	≤ ±0.25% FS BSL	±2%	±0.02%	0.1 %/year
Omega Infrared Transmitter			0-400°F		3% of rdg or 8℃		1% of rdg	
Columbia Orion Weatherstation Pressure		0.01 in Hg	17.5-32.5 inHg		0.03 inHg			
Columbia Orion Weatherstation Wind Speed		1mph	0-135mph		0.7mph			
Columbia Orion Weatherstation Wind Direction			0-360°		2°			
Columbia Orion Weatherstation Temperature		0.1°F	-60 to 140°		0.5°			
Columbia Orion Weatherstation Humidity		1%RH	0-100%RH					

Columbia Orion Weatherstation Rainfall		0.01in	cumulative		5%			

10.8. Oil Sample Test

An oil sample was acquired from the West Leaf gearbox on October 21, 2009 by the University of Central Florida researchers after FDOT personnel and contractors stopped the operation of the bridge and collected oil samples for analysis. The sample was collected after a normal operation cycle, on the same day as the field experiments for damage threshold identification. Analysis of the oil sample was conducted by the Phoenix, Arizona company, FINA Lubricants, upon the recommendation by FDOT engineers in District 5. The sample results are summarized on the following page. These results were intended to be used for long term comparison of the gearbox oil condition. Only one sample could be collected during the duration of the project and future oil sample collections need to be carried out by coordinating with FDOT and contractors. The results provided in this report serve as a benchmark to be compared if more oil samples are collected and tested for comparative analysis. Results of the analysis revealed that the oil parameters are within acceptable limits.

FINA LUBRICANTS -
"Keep Things Moving"

UIN: 01E4C88

Oil

Unit No. Open Gear

Unit:
Make
Model
Serial No.
Site FDOT Sunrise Blvd Bridge

Compartment:
Name Oil
Make
Model
Serial No.
Capacity

Customer:

DIAGNOSIS

All wear levels appear within acceptable limits for first sample. Silicon level (dirt/sealant material) satisfactory. Water content acceptable. Viscosity within specified operating range.

Action: Resample at next recommended interval to monitor and establish wear trend.

ANALYST: Troy.Evey

NORMAL

LEGEND
STOP SEVERE ABNORMAL CAUTION NORMAL

FINA CHECK

DATE SAMPLED	21-Oct-09
DATE RECEIVED	15-Jul-10
DATE REPORTED	20-Jul-10

LAB NO.	44020109729
SIF NO.	102418380010
TIME ON UNIT	
TIME ON OIL	
OIL BRAND	Fina
OIL TYPE	Unidentified
OIL GRADE	220
OIL ADDED	
FILTER	Not Applicable
OIL CHANGED	Not Changed
WO NUMBER	

Metals (ppm)	
Iron (Fe)	13
Chromium (Cr)	<1
Lead (Pb)	<1
Copper (Cu)	2
Tin (Sn)	<1
Aluminium (Al)	<1
Nickel (Ni)	<1
Silver (Ag)	<1
Titanium (Ti)	<1
Vanadium (V)	<1
Contaminants (ppm)	
Silicon (Si)	5
Sodium (Na)	<1
Potassium (K)	<5
Water (%)	<0.05
Additives (ppm)	
Magnesium (Mg)	1
Calcium (Ca)	6
Barium (Ba)	1
Phosphorus (P)	162
Zinc (Zn)	10
Molybdenum (Mo)	<1
Boron (B)	<5
Physical Tests	
Viscosity (cSt 40C)	225.4
Solids	<0.1

10.9. CR1000 Code

CRBASIC Code: Program sent to East Leaf CR1000

```
'CR1000 AVW200 Template using Com 1

'Declare Variables and Units
Public BattV
Public PTemp_C
Public StrainES(10), TempES(10), StrainEN(8), TempEN(8)
Public FreqES(10), ThermES(10), FreqEN(8), ThermEN(8), I

'This is a summary of 6 elements of an AVW200 measurement
                '(1) =  Frequency in Hertz
                '(2) = SignalStrength in mV_RMS
                '(3) = Signal/Noise Ratio (unitless)
                '(4) = Noise Frequency Hz
                '(5) = DecayRatio (unitless)
                '(6) = Thermistor output in Ohms of resistance (see Section 2.2)

'Public Temp_C
Public Data1, Data2
Public Mux1_ES(10,6), Mux2_EN(8,6)
Units BattV=Volts
Units PTemp_C=Deg C

Const A=.00145051
Const B=.0002369
Const C=.0000001019

'Define Data Tables
DataTable(VWData_East,True,-1)
        DataInterval(0,900,Sec,10)
        Sample (60,Mux1_ES(),IEEE4)
        Sample (48,Mux2_EN(),IEEE4)
        Minimum(1,BattV,FP2,False,False)
EndTable
DataTable(VWStrain_East,True,-1)
        DataInterval(0,900,Sec,10)
        Sample (10,StrainES(),IEEE4)
        Sample (10,ThermES(),IEEE4)
        Sample (8,StrainEN(),IEEE4)
        Sample (8,ThermEN(),IEEE4)
        Minimum(1,BattV,FP2,False,False)
EndTable
'Main Program
BeginProg
        SerialOpen (Com1,38400,0,0,10000)
                Scan(900,Sec,1,0)
                        AVW200(Data1(),Com1, 200, 200, Mux1_ES(1,1),1,1,10,1000,4000,2,_60HZ,1,0)
                        AVW200(Data2(),Com1, 200, 200, Mux2_EN(1,1),2,1,8,1000,4000,2,_60HZ,1,0)
                                Battery(BattV)
                                PanelTemp(PTemp_C,_60Hz)
                                CallTable(VWData_East)
                For I = 1 To 10
                        FreqES(I) = Mux1_ES(1,1)
                        StrainES(I)=(FreqES(I)^2/1000)*0.391
                        ThermES(I) = Mux1_ES(1,6)
                        TempES(I)=1/(A+B*LN(ThermES(I))+C*(LN(ThermES(I)))^3)-273.15
                Next I
                For I = 1 To 8
                        FreqEN(I) = Mux2_EN(1,1)
                        StrainEN(I)=(FreqEN(I)^2/1000)*0.391
                        ThermEN(I) = Mux2_EN(1,6)
                        TempEN(I)=1/(A+B*LN(ThermEN(I))+C*(LN(ThermEN(I)))^3)-273.15
                Next I
                CallTable(VWStrain_East)
                NextScan
EndProg
```

CRBASIC Code: Program sent to West Leaf CR1000

```
'CR1000 AVW200 Template using Com 1

'Declare Variables and Units
Public BattV
Public PTemp_C
Public StrainWS(10), TempWS(10), StrainWN(8), TempWN(8)
Public FreqWS(10), ThermWS(10), FreqWN(8), ThermWN(8), I

'This is a summary of 6 elements of an AVW200 measurement
                        '(1) =  Frequency in Hertz
                        '(2) = SignalStrength in mV_RMS
                        '(3) = Signal/Noise Ratio (unitless)
                        '(4) = Noise Frequency Hz
                        '(5) = DecayRatio (unitless)
                        '(6) = Thermistor output in Ohms of resistance (see Section 2.2)

'Public Temp_C
Public Data1, Data2
Public Mux1_WS(10,6), Mux2_WN(8,6)
Units BattV=Volts
Units PTemp_C=Deg C

Const A=.00145051
Const B=.0002369
Const C=.0000001019

'Define Data Tables
DataTable(VWData_West,True,-1)
        DataInterval(0,900,Sec,10)
        Sample (60,Mux1_WS(),IEEE4)
        Sample (48,Mux2_WN(),IEEE4)
        Minimum(1,BattV,FP2,False,False)
EndTable
DataTable(VWStrain_West,True,-1)
        DataInterval(0,900,Sec,10)
        Sample (10,StrainWS(),IEEE4)
        Sample (10,ThermWS(),IEEE4)
        Sample (8,StrainWN(),IEEE4)
        Sample (8,ThermWN(),IEEE4)
        Minimum(1,BattV,FP2,False,False)
EndTable
'Main Program
BeginProg
        SerialOpen (Com1,38400,0,0,10000)
                Scan(900,Sec,1,0)
                        AVW200(Data1(),Com1, 200, 200, Mux1_WS(1,1),1,1,10,1000,4000,2,_60HZ,1,0)
                        AVW200(Data2(),Com1, 200, 200, Mux2_WN(1,1),2,1,8,1000,4000,2,_60HZ,1,0)
                                Battery(BattV)
                                PanelTemp(PTemp_C,_60Hz)
                                CallTable(VWData_West)
                For I = 1 To 10
                        FreqWS(I) = Mux1_WS(1,1)
                        StrainWS(I)=(FreqWS(I)^2/1000)*0.391
                        ThermWS(I) = Mux1_WS(1,6)
                        TempWS(I)=1/(A+B*LN(ThermWS(I))+C*(LN(ThermWS(I)))^3)-273.15
                Next I
                For I = 1 To 8
                        FreqWN(I) = Mux2_WN(1,1)
                        StrainWN(I)=(FreqWN(I)^2/1000)*0.391
                        ThermWN(I) = Mux2_WN(1,6)
                        TempWN(I)=1/(A+B*LN(ThermWN(I))+C*(LN(ThermWN(I)))^3)-273.15
                Next I
                CallTable(VWStrain_West)
                NextScan
EndProg
```